

A seismic reflection study of salt tectonics and incipient continent-continent-collision in the easternmost Mediterranean Sea

Dissertation

zur Erlangung des Doktorgrades an der Fakultät für
Mathematik, Informatik und Naturwissenschaften

Fachbereich Geowissenschaften
der Universität Hamburg

vorgelegt von

Sönke Reiche

Hamburg

2015

Tag der Disputation: 08.04.2015

Folgende Gutachter empfehlen die Annahme der Dissertation:

Prof. Dr. Christian Hübscher

Prof. Dr. Dirk Gajewski

Zusammenfassung

Das Forschungsgebiet der vorliegenden Arbeit befindet sich im östlichen Mittelmeer und umfasst neben dem Levante Becken auch die Kollisionszone zwischen Zypern und dem Eratosthenes Seeberg. Im Zuge der Messinischen Salinitätskrise (ca. 5.96-5.33 myr) wurden dort zunächst etwa 1.5 km mächtige Evaporite und nachfolgend pliozäne-quartäre hemipelagische Sedimente abgelagert. Während diese Sedimente entlang der Zypern-Eratosthenes Seeberg Kollisionszone tektonisch überprägt wurden, dominierten salztektonische Prozesse die strukturelle Entwicklung der pliozänen-quartären Schichten in Richtung Zentrum des Levante Beckens. Untersuchungsgegenstand der vorliegenden Arbeit ist die Erforschung der Einflüsse salz- und plattentektonischer Prozesse auf die messinische und post-messinische Sedimentdecke. In diesem Zusammenhang konnten auf der Grundlage eines umfangreichen Datensatzes reflexionsseismischer Profile und bathymetrischer Daten sowohl Rückschlüsse auf die tektonische Entwicklung des Untersuchungsgebietes als auch neue Einblicke in salztektonische Deformationsprozesse gewonnen werden.

Lange wurde das Einsetzen von Salzbewegungen im Untergrund anhand einer Dichteinversion zwischen Salz und Suprasalzsedimenten erklärt. Neuere Erklärungsansätze gehen davon aus, dass einsetzende Salzdeformation eher durch differentielle Suprasalz-Sedimentauflast oder durch eine Verkipfung von Subsalzschichten bedingt ist: Zwei Mechanismen, welche von bisherigen Studien vorrangig zur Erklärung beobachteter Salzdeformation im Levante Becken herangezogen wurden. Die Ergebnisse dieser Arbeit zeigen, dass Salzdeformation im Levante Becken zusätzlich durch Deformationsprozesse im Subsalzbereich bedingt ist. Das lässt sich anhand der tiefenmigrierten industrieseismischen Profilen der vorliegenden Arbeit zeigen, welche die interne Geometrie des messinischen Salzkörpers hervorragend abbilden. So kann ein räumlicher Zusammenhang zwischen Subsalzstörungen und dem Auftreten von Falten und Störungen innerhalb des Salzkörpers beobachtet werden. Daran zeigt sich, dass die Entstehung der salzinternen Strukturen in besonderem Ausmaß durch Deformationsprozesse im Subsalzbereich bedingt ist. Unter Berücksichtigung dieser Ergebnisse wird in der vorliegenden Arbeit ein neues Modell zur Beschreibung der beckenweiten räumlichen und zeitlichen Variabilität salztektonischer Deformationsmechanismen gezeigt. Während synsedimentäre, durch Störungen im Subsalzbereich bedingte Salzdeformation den nördlichen Teil des Levante Beckens charakterisiert, wurde Salz im südlichen Teil des Beckens primär postsedimentär und gravitativ verformt. Die im Rahmen dieser Arbeit gewonnen Erkenntnisse geben somit einen umfassenden Überblick zu bereits bekannten und neubeschriebenen salztektonischen Deformationsprozessen im Levante Becken. Darüber hinaus tragen sie zum besseren Verständnis von komplexen Salzstrukturen außerhalb des Untersuchungsgebietes bei.

Das Gebiet zwischen Zypern und dem Eratosthenes Seeberg bietet die Möglichkeit, salztektonische Prozesse in einer aktiven Kollisions- und Subduktionszone zu untersuchen. Die Ergebnisse zeigen einen tektonisch verdickten, autochthonen Salzkörper im östlichen Bereich des Untersuchungsgebietes sowie akkretierte Sub- und Suprasalzsedimente nahe der Plattengrenze. Im Gegensatz dazu hat sich im westlichen Bereich ein allochthoner Salzkörper ausgebildet. Unter Mitnahme einer intakten Suprasalz-Sedimentschicht hat sich dieser allochthone Salzkörper über pliozäne-quartäre Ablagerungen hinwegbewegt und wurde damit samt Suprasalzsedimenten dem Akkretions- und Subduktionszyklus entzogen. Diese Beobachtungen zeigen neben grundlegenden Erkenntnissen zum Verhalten von Salz in einer aktiven Kollisionszone auch eine stärkere tektonische Verkürzung des westlichen Untersuchungsgebietes und deuten damit auf eine primär nord-nordwestlich orientierte post-messinische Konvergenzrichtung zwischen der Afrikanischen und Anatolischen Platte hin. Anders als bisher postuliert, lässt sich vor diesem Hintergrund ein späteres Einsetzen der heutigen nordostwärts gerichteten Konvergenzrichtung annehmen, vermutlich um den Zeitpunkt der Plio-/Pleistozän-Grenze.

Eine entsprechende post-messinische Reorganisation der plattentektonischen Bewegungsrichtung lässt sich auch aufgrund von Beobachtungen im Gebiet des Hecataeus Rückens – einer plateauförmigen bathymetrischen Erhebung südlich von Zypern – vermuten. Es handelt sich dabei um eine wenig erforschte Struktur, welcher durch ihre Nähe zur Zypern-Eratosthenes Kollisionszone eine Schlüsselrolle zum besseren Verständnis der regionalen tektonischen Entwicklung zukommt. Die Untersuchungen der vorliegenden Arbeit zeigen eine markante Winkeldiskordanz innerhalb der pliozänen-quartären Sedimentschicht im nordwestlichen Plateaubereich, deren Entstehung zeitlich mit einem Ablagerungswechsel von flachlagernden zu wellenförmig abgelagerten Sedimenten korreliert. Zusätzlich lässt sich ein zeitlicher Zusammenhang zwischen der Entstehung der Winkeldiskordanz und dem Einsetzen hangabwärtsgerichteter Sedimentation entlang einer submarinen Canyonstruktur direkt südlich von Zypern feststellen. Diese Ablagerungsgeometrie kann durch einsetzende Kontinent-Kontinent-Kollision zwischen Zypern und dem Eratosthenes Seeberg um die Plio-/Pleistozän-Grenze und einer daraus entstandenen Hebung Zyperns erklärt werden: Eine differentielle Anhebung zwischen Zypern und dem Hecataeus Rücken führte zur Ausbildung einer Winkeldiskordanz und verursachte einen Wechsel zu einem vermehrt hangabwärtsgerichteten Ablagerungsmilieu. Diese Interpretation ist konsistent mit Beobachtungen im Gebiet der Zypern-Eratosthenes Kollisionszone und schließt entscheidende Lücken im Puzzle zur tektonischen Entwicklung des östlichen Mittelmeers.

Abstract

The study area of the present thesis is located in the easternmost Mediterranean Sea and extends from the Levant Basin into the collision zone between Cyprus and Eratosthenes Seamount. The post-Messinian sedimentary succession within the study area is composed of averagely 1.5 km thick Messinian evaporites which were precipitated during the Messinian Salinity Crisis (approximately 5.96-5.33 Ma) and subsequently overlain by Pliocene-Quaternary hemipelagic deposits. While these deposits are structurally affected by African-Anatolian convergence near the plate boundary, sediment deformation is largely driven by salt tectonics towards the basin center. In this study, the structural imprint of salt tectonics and plate tectonic convergence on Messinian and post-Messinian strata is investigated by means of a comprehensive set of reflection seismic profiles and multibeam bathymetric data. Conclusions are drawn on the tectonic evolution of the Cyprus-Eratosthenes collision zone and new mechanisms driving salt deformation in the Levant Basin are shown.

The onset of subsurface salt deformation was long explained by density inversion between salt and supra-salt deposits. However, newly developed salt tectonic concepts have shown that incipient salt deformation is rather driven by differential supra-salt sediment loading or inclination of sub-salt strata. These two mechanisms were primarily considered in previous studies for explaining salt deformation in the Levant Basin. However, results of this study suggest that Messinian evaporites in the Levant Basin have also deformed in response to sub-salt faulting. Depth-migrated industry seismic lines are shown which image the internal geometry of the Messinian evaporite layer particularly well. Sub-salt faults are observed to spatially coincide with the presence of intra-evaporite faults and folds, suggesting a relation between sub-salt faulting and internal evaporite deformation. Together with previously considered salt tectonic processes, this newly described fault-controlled deformation mechanism is incorporated into a new model of the geographic and temporal variability of evaporite deformation mechanisms in the Levant Basin. While syn-depositional fault-controlled evaporite deformation dominates within the northern part of the Levant Basin, post-depositional evaporite deformation is mainly driven by gravity further south. Results of this study thus provide a comprehensive overview of salt tectonic deformation mechanisms in the Levant Basin which may also contribute to a better understanding of the development of complex salt structures outside the study area.

The area between Cyprus and Eratosthenes Seamount provides the unique opportunity to investigate the behavior of salt within an active collision and subduction setting. Results show that the collision zone may be subdivided into an eastern and a western domain. While plate convergence drives inflation of autochthonous salt and accretion of sub- and supra-salt sediments in the eastern

part of the convergence zone, a stage of allochthonous salt tectonics is reached further west. There, Messinian evaporites have evidently begun to advance across Pliocene-Quaternary strata, carrying an intact roof of supra-salt sediments along. Messinian evaporites and supra-salt deposits have thus efficiently escaped subduction and accretion, bearing important implications for the general understanding of the behavior of salt within an active collision zone. The apparent difference in the magnitude of salt tectonic shortening between the eastern and western domain of the Cyprus-Eratosthenes collision zone suggests a mainly north- to northwestward oriented post-Messinian plate convergence direction, implying a later, possibly Late Pliocene-Early Pleistocene, change to the present northeastward directed convergence regime than previously thought.

A post-Messinian plate tectonic re-organization is also inferred from observations across the Hecataeus Rise – a plateau-like feature directly south of Cyprus. Owing to its proximity to the Cyprus-Eratosthenes collision zone, this yet underexplored structure represents a key site for understanding the regional tectonic evolution. An intra-Pliocene-Quaternary angular unconformity is identified in the northwestern part of the Hecataeus Rise. The formation of this prominent unconformity is interpreted to temporarily coincide with a change from horizontal to wavy sediment deposition and initial downslope sediment transport along a large submarine canyon at the southern Cyprus slope. The observed depositional and structural changes are related to incipient continent-continent-collision between Cyprus and Eratosthenes Seamount around the Pliocene-Pleistocene transition and subsequent uplift of Cyprus: vertical separation between Cyprus and the Hecataeus Rise led to development of a prominent angular unconformity and caused a change to more energetic, downslope sediment transport. Finally, this interpretation is consistent with observations along the Cyprus-Eratosthenes collision zone and closes yet another gap within the Eastern Mediterranean tectonic puzzle.

Contents

1	Introduction	1
1.1	Study area.....	5
1.2	A brief overview of the geological evolution of the Levant region.....	5
1.3	Structure of the thesis and resulting publications	8
1.4	Contributions of co-authors.....	9
2	Data	11
2.1	Multibeam bathymetric data.....	11
2.2	Multichannel seismic data.....	11
3	Fault-controlled evaporite deformation in the Levant Basin	19
	Abstract.....	19
3.1	Introduction	20
3.2	Geological background	21
3.2.1	Tectonic setting	21
3.2.2	Stratigraphy of the Messinian evaporites.....	22
3.2.3	Salt tectonics.....	23
3.3	Methods	25
3.3.1	Seismic data.....	25
3.3.2	Model-based processing	25
3.4	Results	26
3.4.1	Stratigraphy.....	26
3.4.2	Extensional faults	29
3.4.3	Evaporite deformation	30
3.4.3.1	Fault-controlled evaporite deformation	30
3.4.3.2	Evaporite deformation independent of sub-salt faults	31
3.4.4	Amplitude anomalies.....	34
3.4.5	Intra-evaporite velocities	35
3.5	Discussion.....	36
3.5.1	Origin of extensional faults in the Levant Basin.....	36

3.5.2	The composition of the Messinian evaporites.....	37
3.5.3	Fluid migration.....	39
3.5.4	Evaporite deformation in the Levant Basin	40
3.5.4.1	Tectonically driven evaporite deformation	41
3.5.4.2	Gravity-driven evaporite deformation.....	44
3.5.4.3	Synthesis of salt deformation in the Levant Basin	46
3.6	Conclusions	48
4	The fate of salt in the Cyprus subduction zone.....	51
	Abstract.....	51
4.1	Introduction	52
4.2	Geological background	54
4.2.1	Present-day geodynamic situation.....	54
4.2.2	Miocene to recent evolution	55
4.3	Data and methods	58
4.3.1	Multibeam bathymetric data	58
4.3.2	Multichannel seismic data.....	59
4.3.2.1	Seismic data acquisition.....	59
4.3.2.2	Seismic data processing	60
4.3.2.3	Industry seismic data	60
4.4	Results	60
4.4.1	Physiography	60
4.4.2	Seismic stratigraphy.....	63
4.4.2.1	Unit 5.....	65
4.4.2.2	Unit 4.....	67
4.4.2.3	Unit 3.....	67
4.4.2.4	Unit 2.....	68
4.4.2.5	Unit 1a.....	69
4.4.2.6	Unit 1b.....	69
4.4.2.7	Unit 1c.....	70
4.4.3	Structural architecture.....	81
4.4.3.1	Southern Domain	81
4.4.3.2	Central Domain	82
4.4.3.3	Northern Domain.....	83
4.5	Discussion.....	84
4.5.1	Convergence direction and location of the plate boundary.....	84
4.5.2	Structural evolution – previous models and new interpretation	86
4.5.3	Salt tectonic concepts applied to evaporites in the Cyprus subduction zone	87
4.5.4	The impact of salt on the structural evolution of the Cyprus subduction zone	89
4.5.5	The enigmatic circum-Eratosthenes depression – enigma solved?	92
4.5.6	Salt tectonic and sea level controlled Lago Mare deposition.....	93
4.5.7	Pliocene-Quaternary tectonostratigraphic evolution	95
4.6	Conclusions	97

5	The Miocene-Quaternary tectonic evolution of the Hecataeus Rise	101
	Abstract.....	101
5.1	Introduction	102
5.2	Geological background	104
5.2.1	Geodynamic setting and crustal composition	104
5.2.2	Tectonostratigraphic evolution	105
5.3	Data acquisition and processing.....	107
5.3.1	Multibeam bathymetric data.....	107
5.3.2	Multichannel seismic data.....	107
5.4	Results	109
5.4.1	Physiography	109
5.4.2	Seismic stratigraphy.....	111
5.4.2.1	Approach to stratigraphic interpretation.....	111
5.4.2.2	Unit 5.....	114
5.4.2.3	Unit 4.....	117
5.4.2.4	Unit 3.....	120
5.4.2.5	Unit 1	121
5.4.3	Structural interpretation.....	126
5.4.3.1	Pre-Messinian deformation	126
5.4.3.2	Post-Messinian deformation	128
5.5	Discussion.....	130
5.5.1	Structural and stratigraphic link to Cyprus	130
5.5.2	Pre-Messinian tectonostratigraphic evolution of the Hecataeus Rise	133
5.5.3	Messinian-Quaternary tectonostratigraphic evolution of the Hecataeus Rise	134
5.5.4	On the origin of the Hecataeus Rise	137
5.6	Conclusions	138
6	Conclusions and outlook	141
6.1	Conclusions	141
6.2	Outlook.....	144
	Bibliography.....	147
	Acknowledgements	161

1 Introduction

Salt giants occupy several sedimentary basins on Earth, profoundly affecting structural basin evolution owing to their distinct mechanical properties. Unlike clastic or carbonate rocks, evaporites deform in a viscous, fluid-like manner and low strain rates are sufficient to initiate salt deformation. These unique mechanical properties of evaporites are presently reflected by salt structures of variable shapes and often quite remarkable sizes (Hudec and Jackson, 2007; Warren, 2010). When it comes to driving forces responsible for initiating salt deformation a paradigm change occurred in the late 1980s (Jackson, 1995). The concept of buoyancy as the main driving mechanism shrank in importance and other mechanisms, such as differential supra-salt sediment loading and basement inclination were increasingly considered (Jackson, 1995; Brun and Fort, 2011; Rowan et al., 2012). However, deciphering individual driving mechanisms responsible for the present-day shape of large salt structures in Earth's sedimentary basins is not an easy task. These structures have often experienced a long-lasting and complex deformation history and their present-day shape spectacularly deviates from its initial, depositional state.

Earth's youngest salt giant was precipitated during the Messinian Salinity Crisis in the Mediterranean realm (Warren, 2010). Tectonic closure of the strait of Gibraltar reduced Atlantic-Mediterranean water exchange and ultimately led to desiccation and wide spread precipitation of the Messinian evaporites (Hsü et al., 1973; Krijgsman et al., 1999). An averagely 1.5 km thick evaporite sequence occupies the Levant Basin, easternmost Mediterranean Sea (Fig. 1.1) (Netzeband et al., 2006b). Unlike most evaporite basins on Earth, such as the Central European Basin, where Zechstein evaporites have suffered long-lasting deformation (e.g. Mohr et al., 2005), Messinian evaporites in the central part of the Levant Basin are yet fairly undeformed (Netzeband et al., 2006b; Hübscher et al., 2007), making this basin a natural laboratory for investigating deformation of a salt giant in its initial stage. However, despite the near horizontal upper boundary of the Messinian salt layer, the presence of internal evaporite deformation was reported from multiple locations (Gradmann et al., 2005; Netzeband et al., 2006b; Hübscher et al., 2007;

Dümmong and Hübscher, 2011; Gvirtzman et al., 2013). Detection of internal evaporite deformation by means of reflection seismic imaging would not be possible without the multi-layered nature of the Levant Basin evaporites. Seismic images have shown that these deposits locally consist of up to six layers of alternating reflective and transparent acoustic properties (Bertoni and Cartwright, 2005; Hübscher et al., 2007).

Until now, incipient evaporite deformation in the Levant Basin was mainly explained by gravity-driven processes only. In this regard, two main mechanisms were frequently considered, being differential sediment loading at marginal areas (e.g. Loncke et al., 2006) and basinward inclination of sub-salt strata (e.g. Gradmann et al., 2005). While the former mechanism causes spreading of evaporites away from the center of supra-salt loading, the latter mechanism is associated with gliding of evaporites towards the basin center (Rowan et al., 2004). It becomes increasingly clear, that incipient evaporite deformation in the Levant Basin is more complex than previously thought with several deformation mechanisms acting on different time scales and likely also in combination. While differential sediment loading in the vicinity of the Nile deep-sea fan has caused post-depositional spreading of Messinian evaporites (Loncke et al., 2006), structural uplift near the Israeli coast is believed to have initiated syn-depositional gliding of the salt layer (Gvirtzman et al., 2013).

Few authors have locally observed faults which create displacements in sub-salt sediments and also structurally affect the Messinian evaporites (Gradmann et al., 2005; Netzeband et al., 2006b). The question about a more frequent relation between faulting and evaporite deformation in the Levant Basin has never been systematically addressed. If applicable, such a deformation mechanism would add additional complexity to the internal deformation history of the Levant Basin evaporites and should be considered in future numerical and experimental modelling studies. It is therefore the first principal aim of this thesis to investigate whether evaporites in the Levant Basin have also deformed in response to sub-salt sediment deformation. Additionally, the Levant Basin evaporites will be revisited on a basin-wide scale with the objective to draw an up-to date picture of the spatial and temporal variability of various mechanisms responsible for driving salt deformation.

An entirely different situation of salt tectonics can be studied where the Levant Basin passes into a narrow, trench-like zone bordered by Cyprus to the north and the Eratosthenes Seamount further south (Fig. 1.1). This area is believed to be characterized by ongoing subduction which is changing towards incipient continent-continent-collision as Eratosthenes Seamount has entered the subduction zone since post-Messinian times (Robertson, 1998d). While our present-day understanding of the tectonic history in this area is significantly based on results obtained in the course of Ocean Drilling Program (ODP) Leg 160,

evaporites were long considered absent between Cyprus and Eratosthenes Seamount (Robertson, 1998d). This misconception arose from insufficient penetration of pre-site survey seismic data and was not contradicted by the drilling results as thick Messinian evaporites could not be reached (Limonov et al., 1994; Robertson et al., 1995b; Robertson, 1998d; Galindo-Zaldívar et al., 2001). Only recently published reflection seismic lines have initially shown that evaporites laterally continue from the Levant Basin into the area bordered by Cyprus and Eratosthenes Seamount (Klimke and Ehrhardt, 2014; Montadert et al., 2014). Consequently, kilometer-thick evaporites occupy an active subduction/collision setting, enabling the rare opportunity to study the fate of salt in a subduction zone.

Studying the behavior of salt in this geologically complex area is not only of interest from a salt tectonic point of view. Incipient collision between Cyprus and Eratosthenes was previously regarded as the main trigger for initiating Eastern Mediterranean wide tectonic changes at the time of the Pliocene-Pleistocene transition (Schattner, 2010). Deducing the post-Messinian structural evolution of this area from the structural record of deformed salt, sub-salt and supra-salt deposits is therefore of significant relevance. A second principal goal of this thesis is thus to investigate the structural evolution of the area between Cyprus and Eratosthenes Seamount focusing on the behavior of salt in an active subduction setting and its impact on the post-Messinian evolution of the collision zone.

Deciphering the structural evolution of the African-Anatolian collision zone offshore Cyprus is complicated by the presence of the Hecataeus Rise, an elevated, plateau-like feature attached to the southern Cyprus margin (Fig. 1.1). Little is known about the origin of this feature – disagreement even exists whether the African-Anatolian plate boundary would run along its northern (Klimke and Ehrhardt, 2014) or southern (Ben-Avraham et al., 1995; Vidal et al., 2000b) edge. Previous authors interpreted the Hecataeus Rise as an offshore continuation of the Cyprus ophiolite (Robertson, 1998c) or as an accreted crustal unit (Rotstein and Ben-Avraham, 1985; Ben-Avraham et al., 1988).

Importantly, the Hecataeus Rise is located in direct vicinity to the presently ongoing Cyprus-Eratosthenes collision and should thus bear a structural record of the area's most recent tectonic history. If the Cyprus-Eratosthenes collision at the Pliocene-Pleistocene transition was able to trigger an Eastern Mediterranean tectonic re-organization (Schattner, 2010), this event should also be structurally reflected in the sedimentary record of the Hecataeus Rise. Yet, few seismic lines were published from this structure (McCallum et al., 1993; Vidal et al., 2000b) and except for its northernmost edge, the stratigraphy and structural evolution of the Hecataeus Rise are virtually unknown. Unraveling the structural evolution of the Hecataeus Rise with special emphasize on its Pliocene-Quaternary tectonic history is therefore the third principal goal of this thesis.

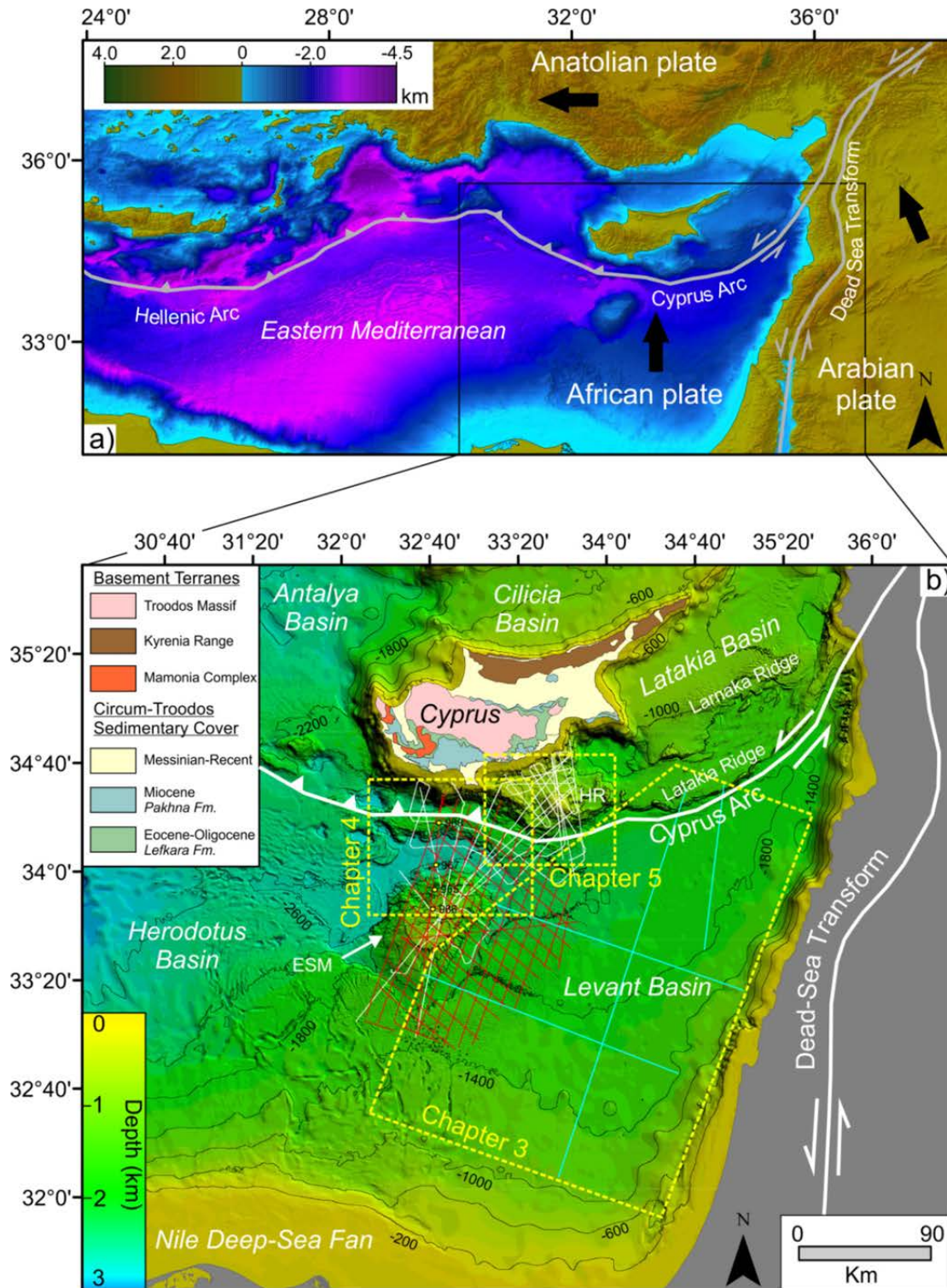


Figure 1.1 a) Overview map of the Eastern Mediterranean Sea. Black arrows indicate the direction of plate motion drawn after Schattner (2010). The large-scale tectonic configuration is based on Hall et al. (2014) and Schattner (2010). Topography and bathymetry data were retrieved from GeoMapApp® (<http://www.geomapapp.org>) (Ryan et al., 2009). **b)** Location map and database. The main study areas of the present thesis are indicated by stippled yellow boxes/polygons. Red lines represent seismic data acquired during RV MARIA S. MERIAN (MSM) cruise MSM 14/2, white lines were acquired during MSM 14/3. Light blue lines represent industry seismic data provided by Spectrum. A simplified geological map of Cyprus was drawn after Kinnaird and Robertson (2012). The bold white line represents the inferred location of the Cyprus Arc. Small yellow dots represent ODP Leg 160 Sites. ESM=Eratosthenes Seamount, HR=Hecataeus Rise. Data used in compiling this map is specified in Chapter 2.1.

1.1 Study area

The easternmost Mediterranean Sea represents a tectonically complicated region, being affected by differential motion along the boundaries of three major tectonic plates (Fig. 1.1) (Robertson, 1998c; Aksu et al., 2005). The African and Anatolian plates converge along the Cyprus Arc while differential motion between Africa and Arabia is accommodated along the Dead-Sea Transform. The Levant Basin occupies the northern part of the African Plate and is confined by the Cyprus Arc to the north and by the Levant and Egyptian coasts to the east and south. Further west, the Levant Basin extends to the Eratosthenes Seamount – a topographically elevated feature directly south of Cyprus. The Eratosthenes Seamount is separated from the Anatolian side of the collision front by a narrow, trench-like zone which is bordered by Cyprus and the plateau-shaped Hecataeus Rise to the north (Fig. 1.1).

1.2 A brief overview of the geological evolution of the Levant region

The evolution of the Levant Basin was closely associated with opening of the Neotethyan Ocean during several rifting stages from Late Permian to Mid-Jurassic times (Robertson, 1998c; Gardosh and Druckman, 2006; Gardosh et al., 2010). The basin opened along a north-northeast to south-southwest oriented axis, separating the Eratosthenes Seamount from its conjugate margin further east (Fig. 1.2) (Gardosh and Druckman, 2006; Montadert et al., 2014).

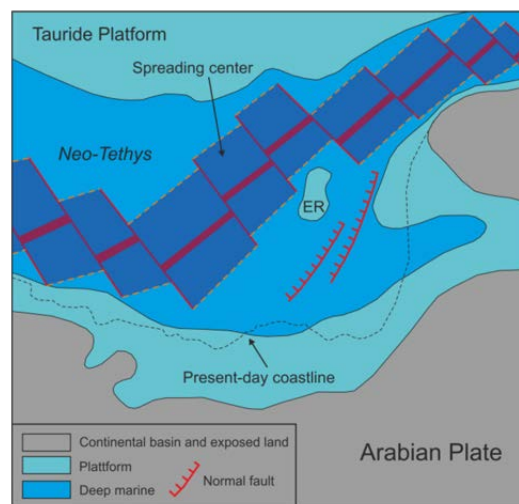


Figure 1.2 Paleotectonic map of the easternmost Mediterranean area at Mid-Jurassic times modified after de Lamotte et al. (2011). ER=Eratosthenes block.

While the crust beneath Eratosthenes Seamount is generally agreed to be of continental origin, the crustal nature of the Levant Basin was subject to debate (Makris et al., 1983; Ben-Avraham et al., 2002; Netzeband et al., 2006a; Welford et al., 2015). Refraction seismic lines published by Netzeband et al. (2006a) extend from offshore Israel across the Levant Basin to the Eratosthenes Seamount and suggest the presence of stretched continental crust beneath the Levant Basin. A stage of seafloor-spreading was only reached north and west of Eratosthenes (Fig. 1.2) and oceanic crust generated at that time is believed to have later been subducted along the Cyprus Arc (Netzeband et al., 2006a; Gardosh et al., 2010). The northern limit of Eratosthenes was interpreted as a transform fault, separating the Eratosthenes continental block to the south from ancient oceanic Tethyan crust further north (Fig. 1.2) (Longacre et al., 2007; de Lamotte et al., 2011). Possible remnants of such Tethyan oceanic crust were recently imaged by refraction seismic profiles along the northern edge of the Eratosthenes block (Welford et al., 2015).

Following rifting, the passive Levant margin experienced post-rift thermal subsidence and sedimentation for a period of more than 100 Ma (Gvirtzman and Garfunkel, 1998; Robertson, 1998c). Subsequently, Late Cretaceous African-Eurasian convergence was accommodated along a northward-dipping intra-oceanic subduction zone at the present-day locations of Cyprus and southern Turkey (Robertson, 1998c). Slab-roll back of cold and dense Triassic oceanic crust facilitated asthenospheric upwelling and ultimately led to the formation of supra-subduction zone ophiolites, now widely present in the Eastern Mediterranean realm (Moores et al., 1984; Robertson, 1998c). The Troodos ophiolite represents the main basement block of Cyprus and is an example of ophiolites formed during that time (Robertson, 1998c).

Subduction related far-field stresses initiated formation of inversion structures along the Levant margin, commonly known as the Syrian Arc (Bosworth et al., 2008). This event lasted from Late Cretaceous to Miocene times and was characterized by several pulses of tectonic compression (Gardosh and Druckman, 2006). Eocene-Miocene compressional pulses also affected the area around the present-day Cyprus Arc and led to development of a linked system of southward verging large-scale thrusts which are expressed as the Larnaka and Latakia Ridges in the present-day bathymetry (Fig. 1.1) (Calon et al., 2005; Hall et al., 2005). Magnetic and seismic reflection data suggest that the Larnaka Ridge is cored by the eastward continuation of the Troodos ophiolite (Rybakov et al., 1997; Calon et al., 2005). From the Late Eocene onwards, the Levant Basin was subject to massive sediment input and more than half of the basins overall 12 km sedimentary infill accumulated within the last 37 Ma (Steinberg et al., 2011).

A phase of Early Miocene tectonic compression was reported from onshore southern Cyprus and along the Latakia Ridge (Robertson, 1998c; Hall et al.,

2005). Robertson (1998c) related this compressional event to subduction zone migration from a position north of Cyprus to its present-day location. Early-Middle Miocene tectonic changes of regional significance also affected the Levant margin where initial slip along the Dead-Sea Transform occurred, linking the Bitlis-Zargos convergence zone with the Red Sea further south (Bosworth et al., 2005).

Late Miocene closure of the marine gateway between the Atlantic Ocean and the Mediterranean Sea resulted in wide-spread desiccation within the Mediterranean realm (Hsü et al., 1973). This comparably short period in geologic time is known as the Messinian Salinity Crisis and lasted from 5.96 to 5.33 Ma (Krijgsman et al., 1999). In the Levant Basin, an averagely 1.5 km thick evaporite layer was precipitated in the course of the Messinian Salinity Crisis (Netzeband et al., 2006b). Absence of evaporites on top of Eratosthenes Seamount indicates the seamount's elevation above Messinian sea level during this time (Robertson, 1998c). A period of rapid Early Pliocene reflooding at 5.33 Ma terminated the Messinian Salinity Crisis and all ODP Leg 160 drilling Sites, north of the Eratosthenes Seamount (Fig. 1.1), revealed a change to deep-marine conditions (Robertson, 1998d).

Westward motion of Anatolia with respect to Eurasia was initiated in Early Pliocene times (Bozkurt, 2001). Based on tomographic images and experimental modelling, Faccenna et al. (2006) related the onset of motion along the North Anatolian Fault to slab break-off in the Bitlis area. According to these authors, slab break-off caused an increase in convergence rate towards the east (Bitlis area), whereas slab roll-back accelerated further west (Hellenic Arc). Ultimately, this newly created stress regime initiated the westward motion of Anatolia along the present-day North Anatolian Fault (Faccenna et al., 2006). The onset of westward Anatolian escape is also evident along the Cyprus Arc. Based on reflection seismic profiles across the Latakia Ridge, Hall et al. (2005) report a post-Messinian change from northwest-directed compression to sinistral transpression at the plate boundary.

Rapid Early Pliocene subsidence of Eratosthenes Seamount in the order of 2 km preceded Pliocene-Quaternary uplift of Cyprus of similar magnitude (Robertson, 1998d; Whiting, 1998; Kinnaird et al., 2011). While these events are likely related to incipient collision between Cyprus and Eratosthenes Seamount, the time difference remains to be understood. Based on a comprehensive literature review, Schattner (2010) related incipient collision between Cyprus and Eratosthenes Seamount to subduction interruption and associated Eastern-Mediterranean-wide tectonic changes.

1.3 Structure of the thesis and resulting publications

The present thesis is subdivided into six main chapters:

- Chapter 1** provides an introduction and motivates the main scientific questions to be addressed in Chapters 3-5. Furthermore, the study area is introduced together with a brief overview of its geological evolution.
- Chapter 2** introduces the data used in the present thesis. Additionally, the seismic processing workflow is described.
- Chapter 3** is based on a manuscript published in *Marine Geology*: Reiche, S., Hübscher, C., Beitz, M., 2014. *Fault-controlled evaporite deformation in the Levant Basin, Eastern Mediterranean. Marine Geology 354, 53-68*. In this chapter, evaporite deformation in the Levant Basin is investigated by means of four regional, high-quality and deeply penetrating industry seismic lines. The existence of a new evaporite deformation mechanism in the Levant Basin is shown, where salt was deformed in response to sub-salt faulting.
- Chapter 4** is based on a manuscript submitted to *Basin Research*: Reiche, S., Hübscher, C., Ehrhardt, A., 2015. *The impact of salt on the late Messinian to recent tectonostratigraphic evolution of the Cyprus subduction zone*. In this chapter, a dense grid of reflection seismic lines is used to show how Messinian salt is structurally affected by incipient collision between Cyprus and Eratosthenes Seamount. Observation of lateral differences in the style of salt tectonic deformation along this collision zone bears important implications for the Cyprus-Eratosthenes collision history.
- Chapter 5** is based on a manuscript submitted to *Marine and Petroleum Geology*: Reiche S., Hübscher C., 2015. *The Hecataeus Rise, easternmost Mediterranean: A structural record of Miocene-Quaternary convergence and incipient continent-continent-collision at the African-Anatolian plate boundary*. Interpretation of reflection seismic profiles across the Hecataeus Rise shows offshore continuation of onshore Cyprus structural lineaments, indicating long-term proximity (pre-Miocene) of these two structural entities. A significant intra-Pliocene-Pleistocene tectonic event is identified across the Hecataeus Rise and related to incipient continent-continent-collision between Cyprus / the northwestern corner of the Hecataeus Rise to the north and Eratosthenes Seamount further south.
- Chapter 6** draws the overall conclusions of the present thesis and states some major unresolved scientific questions to be possibly addressed by future research initiatives.

1.4 Contributions of co-authors

Chapters 3-5 are based on manuscripts submitted to or published in scientific journals. Co-authors have contributed to each manuscript and these contributions are stated below.

Chapter 3 Manuel Beitz developed the velocity model shown in figure 3.9. As my main doctoral advisor, Christian Hübscher contributed to the ongoing discussion throughout the preparation phase of the manuscript.

Chapter 4 Axel Ehrhardt provided processed seismic data acquired during RV MARIA S. MERIAN (MSM) cruise MSM 14/2. He also wrote the first paragraph of Chapter 4.3.2.2, describing the processing workflow of the MSM 14/2 data. As my main doctoral advisor, Christian Hübscher contributed to the ongoing discussion throughout the preparation phase of the manuscript.

Chapter 5 As my main doctoral advisor, Christian Hübscher contributed to the ongoing discussion throughout the preparation phase of the manuscript.

2 Data

2.1 Multibeam bathymetric data

This thesis is based on a comprehensive set of high-resolution multibeam bathymetric data covering an area which extends from offshore southwestern Cyprus across the Eratosthenes Seamount and the Hecataeus Rise further west along the Latakia and Larnaka Ridges to the Levant coast (Fig. 1.1). Bathymetric data presented in Chapters 4 and 5 were mainly acquired in the course of RV MARIA S. MERIAN cruises MSM 14/2 and MSM 14/3 using a SIMRAD EM120 echo sounder system (Ehrhardt, 2011; Hübscher, 2012). For the easternmost study area introduced in Chapter 5, multibeam data acquired during the BLAC survey was additionally utilized (Benkhelil et al., 2005; Maillard et al., 2011). Continuous bathymetric coverage was obtained by filling gaps within the high-resolution bathymetric dataset with data retrieved from the ETOPO2 bathymetry (U.S. Department of Commerce, NOAA/NGDC, 2006).

2.2 Multichannel seismic data

Reflection seismic data shown in the present thesis consist of three datasets (Fig. 1.1):

1. *Industry seismic data.* Data presented in Chapter 3 were provided fully processed and depth-migrated by Spectrum. Data were acquired using a 7200 m cable, 50 m shot point interval, 12.5 m hydrophone group interval and 12 s record length.
2. *MSM 14/2 data.* Processed seismic data representing parts of the dataset shown in Chapter 4 were provided by Axel Ehrhardt (2013, personal commun.) and were acquired in 2010 during RV MARIA S. MERIAN cruise MSM 14/2. Seismic energy was released by two G-Gun arrays at time intervals of 18, 13 or 10 s and recorded by a 3900 m long, 312-channel digital streamer (Ehrhardt, 2011).

3. *MSM 14/3 data.* The main seismic dataset of this thesis is presented in Chapters 4 and 5, comprising seismic profiles acquired in 2010 during RV MARIA S. MERIAN cruise MSM 14/3 (Hübscher, 2012). Data were acquired with two GI-Guns, releasing energy at constant time intervals of 6-9 s and a 24-channel analogue streamer with an active length of 600 m as a seismic receiver.

While the first two datasets were provided fully processed and ready for interpretation, processing of data acquired during MSM 14/3 is part of the present thesis and briefly described below.

Pre-stack seismic data processing included bandpass filtering, geometry-setup and common mid-point (CMP) binning with a CMP-distance of 12.5 m. As data were acquired at a constant ship's speed of 5 kn over ground, the resulting approximate shot distance of 20 m led to an average CMP-fold of around 15. An apparent streamer dip during data acquisition was corrected by application of an offset-dependent static correction.

As previous studies on seismic reflection imaging have reported significant signal-to-noise ratio improvements by generating common reflection surface (CRS) stacks (Menyoli et al., 2004; Yoon et al., 2008; Baykulov et al., 2009), this method was also applied to the present dataset. For details on the CRS-workflow, the reader is referred to Mann et al. (1999) and Jäger et al. (2001). Here the approach described by these authors was followed, where the search for the three CRS-parameters is split into three one-parameter searches with the first one representing an automatic, coherency-based search for a stacking-velocity equivalent parameter. For the present dataset, low offset-to-target ratios complicate reliable determination of stacking velocities. Therefore, the automatic search for this stacking velocity-equivalent parameter was constrained by assigning the stacking velocity to a constant value of 1500 m/s. The remaining CRS parameters were determined following the search strategy of Jäger et al. (2001), resulting in the final CRS stack. Selection of appropriate CMP- and midpoint apertures is crucial for the quality of the resulting CRS-stack (Hertweck et al., 2007). The CMP-aperture is defined in the time-offset plane and was – given the low offset-to-target ratios – always chosen to comprise the full offset range of around 660 m (approximately 60 m initial offset + 600 m active section of the streamer). The mid-point aperture is defined in the time-midpoint plane. Various tests were performed on this value in order to effectively increase the signal-to-noise ratio while avoiding loss in lateral resolution which could prevent imaging of small-scale structures such as low-offset faults in the Pliocene-Quaternary section (e.g. Fig. 5.8d). This criterion was most satisfactorily met by choosing a midpoint aperture radius which linearly increases from 60 m at 0 s (TWT) to 220 m at 6 s (TWT).

For some profiles, the image quality was improved by exclusively using the ten nearest offset channels for stacking. Finally, the stacked seismic profiles were time migrated with a constant velocity of either 1500 m/s or 1600 m/s.

In order to specifically target deeper (i.e. sub-salt) reflections and to efficiently eliminate diffractions generated at the highly deformed top of salt boundary, I additionally applied an alternative processing workflow to selected seismic profiles located within the study area of Chapter 4 (profiles are specified in Chapter 4.3.2.2). I followed the approach described by Dell et al. (2012) who introduced a processing workflow, where partly time-migrated gathers were subsequently used for CRS-stacking. In combination, these methods have performed well in enhancing the signal-to-noise ratio and producing high-quality images in geologically complex areas (Dell et al., 2012). As mentioned above, stacking velocities and thus initial time-migration velocities could not be determined from the MSM 14/3 data itself. Therefore, our approach differs from Dell et al. (2012) by the fact that a velocity model was constructed by geological interpretation instead of being determined automatically.

As a starting point for velocity model building, an interval velocity model provided by Axel Ehrhardt (2013, personal commun.) was used. This model was constructed from the MSM 14/2 data for depth-migration of seismic data published by Klimke and Ehrhardt (2014). Within the model, the presence of distinct units of characteristic seismic velocities can be observed (VelU1-5 in Fig. 2.1a). In a next step, these velocity units were identified within the seismic data as units of similar acoustic properties. This was initially carried out along the profile corresponding to the MSM 14/2 velocity model (Fig. 2.1b) and all identified seismic units were subsequently correlated throughout the MSM 14/3 dataset (Fig. 2.1c).

It should be noted that velocity unit 5 within the MSM 14/2 velocity model represents largely undeformed Miocene clastics of the Levant Basin (Fig. 2.1b) (Klimke and Ehrhardt, 2014). Such deposits are only locally present within the study area of Chapter 4. Most of these deposits were presumably accreted to the Cyprus margin in the course of continuous convergence between Cyprus and Eratosthenes Seamount (see Chapter 4.5.4) and are now comprised within an acoustically chaotic to transparent seismic unit directly south of Cyprus and the Hecataeus Rise (Fig. 2.1c). For simplicity, this seismic unit was correlated with velocity unit 5 of the MSM 14/2 model.

All units correlated to the MSM 14/3 data were assigned to a top velocity and a velocity gradient extracted from the MSM 14/2 model, resulting in the final velocity model which was built individually for selected MSM 14/3 profiles (Fig. 2.1d). It should be noted that the resulting velocity models clearly represent a simplification. For instance, no discrimination was made between salt velocities and sub-salt velocities (Figs. 2.1c,d).

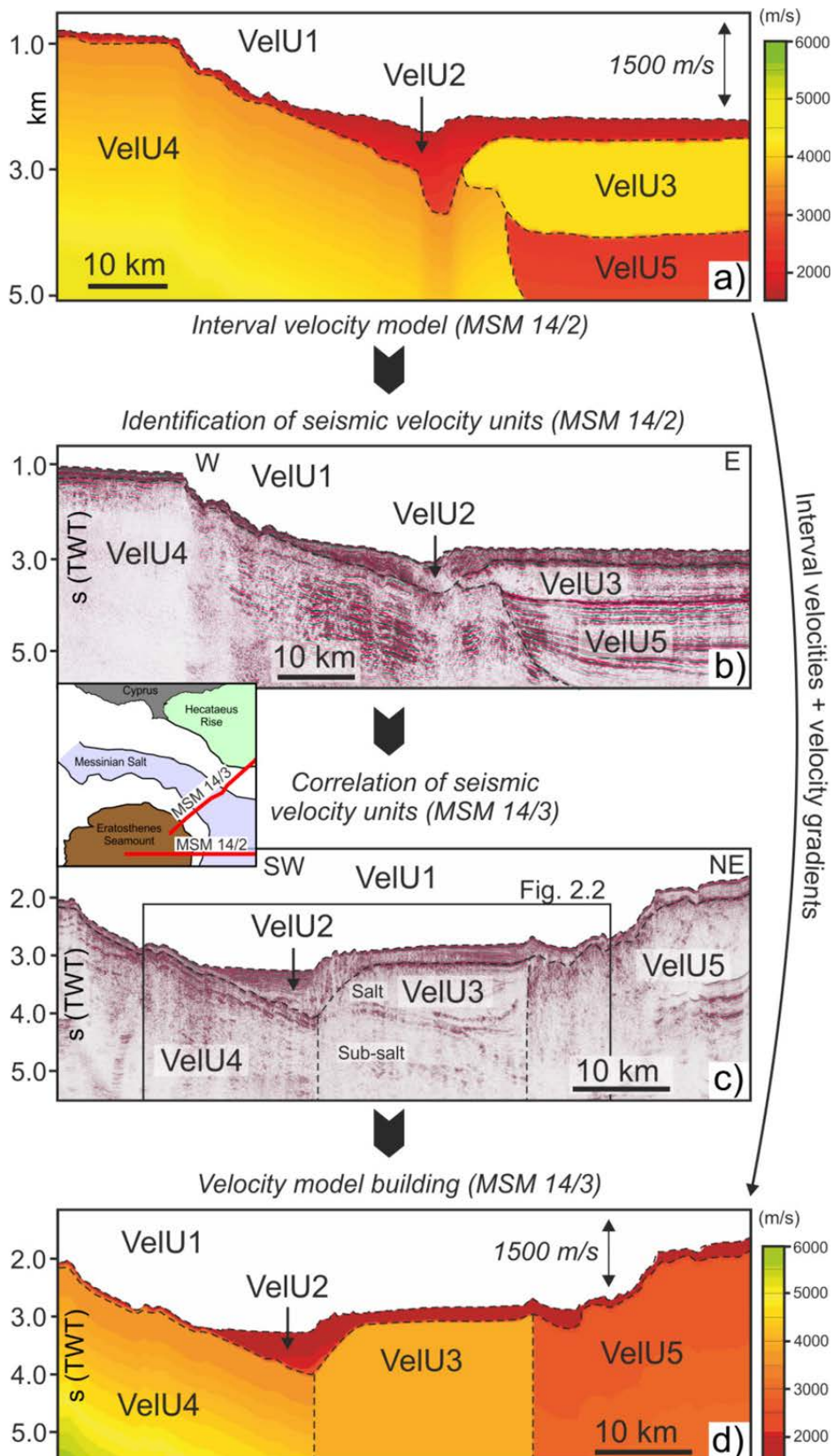


Figure 2.1 Approach to velocity model building. **a)** Interval velocity model used for MSM 14/2 data processing by Klimke and Ehrhardt (2014). Seismic velocity units were defined and **b)** identified within the corresponding seismic profile. **c)** In a next step, these velocity units were identified in and correlated throughout the MSM 14/3 dataset. **d)** Finally, each velocity unit within the MSM 14/3 data was assigned a top velocity and a velocity gradient extracted from the initial velocity model.

Table 1.1 provides an overview of the interval velocities and velocity gradients assigned to each velocity unit and a correlation between velocity units and seismostratigraphic units identified in Chapter 4 together with the interpreted composition of each unit.

Table 1.1 Overview of velocity units defined for processing MSM 14/3 seismic data. A correlation to seismostratigraphic units described in Chapter 4 is shown for each velocity unit.

Velocity unit	Top velocity (m/s)	Velocity gradient ($\text{ms}^{-1} / \text{m}$)	Correlation to stratigraphy of Chap. 4	Composition
VelU1	1500	0.0	No seismic unit	Water
VelU2	1600	0.8	Units 1a, 1b, 2	Post-Messinian clastics
VelU3	4000	0.0	Unit 3 (+ sub-salt Units)	Evaporites
VelU4	3500	0.3	Unit 5	Carbonates
VelU5	2600	0.1	No seismic unit	Mioc. accreted material

The final velocity model was converted to RMS-velocities and included into the partial time migration and CRS-processing workflow. Tests on the resulting image quality at various migration apertures have yielded good results with an aperture radius of 300 m at 0 s (TWT) and 900 m at 6 s (TWT). Partially time-migrated gathers were subsequently stacked with the CRS-routine which was constrained with the same velocity model used for migration. Overall, this processing workflow performed particularly well for imaging deeper and sub-salt reflections and efficiently eliminated diffracted and/or out-of-plane energy. The resulting images allowed for a meaningful seismic interpretation in places where standard processing techniques turned out to be insufficient.

Results of the processing workflows described above are shown in figure 2.2, where a) a constant-velocity, post-stack migrated CMP-stack is compared to b) a constant-velocity, post-stack migrated CRS-stack and c) a pre-stack partly time migrated CRS-stack.

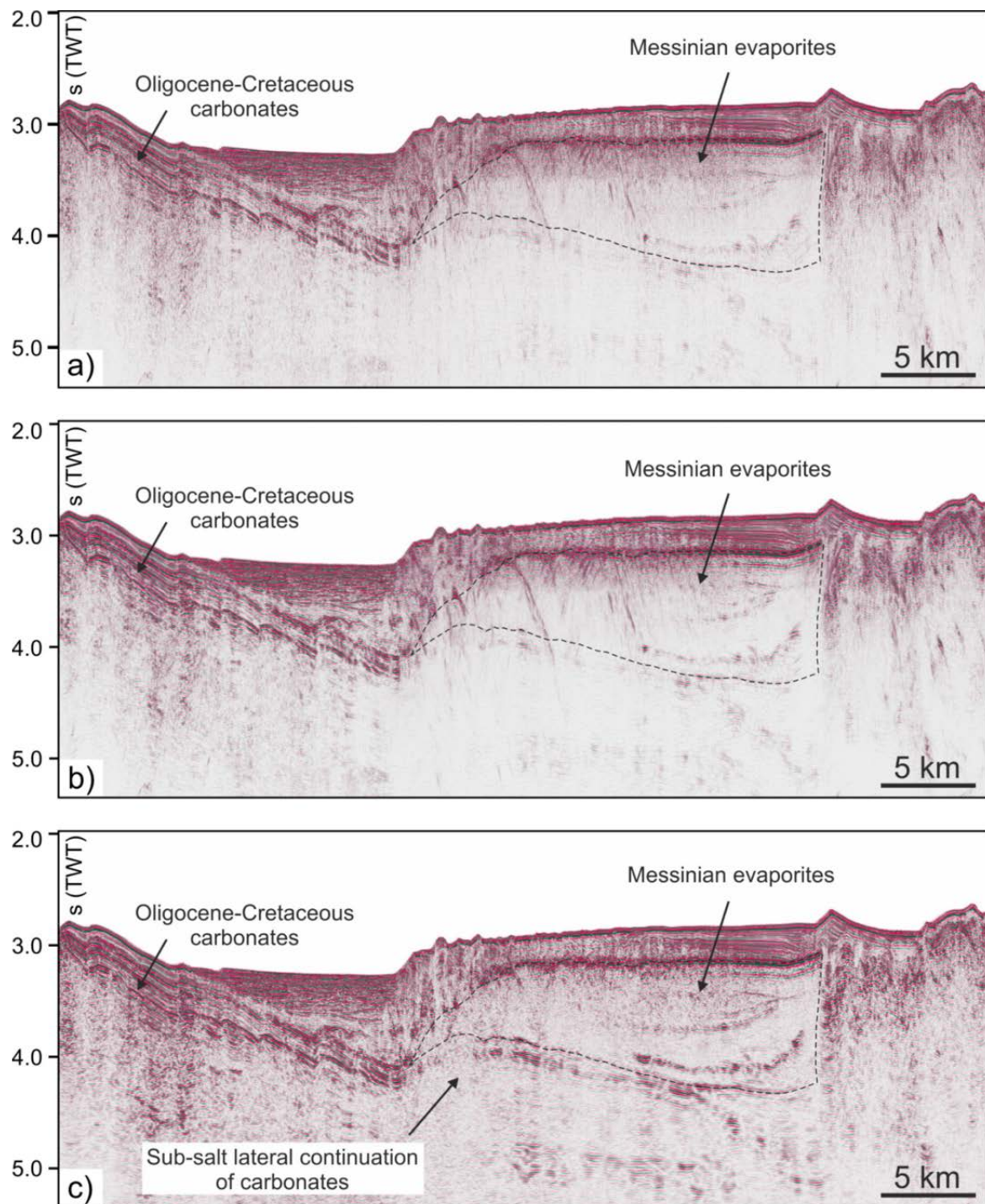


Figure 2.2 a) Constant-velocity CMP-stack, migrated with a post-stack time migration. b) Post-stack time migrated CRS-stack. The signal-to-noise ratio was generally improved. c) Pre-stack partly time-migrated CRS-stack showing significant improvements in sub-salt imaging. Additionally, diffracted and/or out-of-plane energy was efficiently eliminated. For location see figure 2.1c.

3 Fault-controlled evaporite deformation in the Levant Basin

Abstract

During the Messinian Salinity Crisis, a multi-layered salt giant of 1.5 km thickness was precipitated in the Levant Basin, easternmost Mediterranean Sea. Incipient deformation of this geologically young salt layer was commonly explained by gravity-driven processes only. Based on high-quality depth-migrated seismic data, I show for the first time, how sub-salt extensional faults influence the internal deformation pattern of the Messinian evaporites in the Levant Basin. Extensional faulting started in the Middle Miocene and lasted until late Messinian times. Faulting is suggested to have caused the development of fault-propagation folds within the evaporite unit. Subsequently, folds may have accommodated tectonic shortening at the Latakia Ridge and evolved into the presently observed complex intra-evaporite fold pattern. While fault-controlled evaporite deformation is evident in the northern part of the Levant Basin only, evaporites are increasingly influenced by Nile-derived differential sediment loading towards the south. Locally, zones of reduced amplitudes in the sub-salt domain terminate into phase-reversed bright spots within the lower part of the evaporites, indicating active fluid migration and potentially evaporite dissolution. Finally, a high-resolution velocity model of the Messinian evaporites is presented, based on model-based processing and residual moveout analysis. Relatively high interval velocities of acoustically transparent evaporites (3850-4240 km/s) are consistent with halite, whereas lower velocities of reflective layers (3650-4030 km/s) may point towards the presence of low-velocity evaporite facies like gypsum.

3.1 Introduction

Massive evaporite accumulations cover numerous basins around the globe, effectively destabilizing overlying sediments by their nature to easily deform (Warren, 2010; Brun and Fort, 2011). Low differential stresses are sufficient to cause evaporites to flow and long-lasting deformation commonly alters their original shape dramatically (Quirk et al., 2012; Strozyk et al., 2012). Despite being located within an active plate tectonic setting, the geologically young Messinian evaporites in the Eastern Mediterranean Sea are yet fairly undeformed, representing an excellent site to study deformation of a salt giant in its initial stage (Hübscher et al., 2007).

The Levant Basin, located in the easternmost Mediterranean, has been targeted by several studies, addressing early evaporite destabilization as a consequence of differential sediment loading, uplift or tilting of surrounding margins (Gradmann et al., 2005; Loncke et al., 2006; Netzeband et al., 2006b; Hübscher and Netzeband, 2007; Cartwright and Jackson, 2008). Multiple driving mechanisms have thus influenced the present-day shape of Messinian salt in the Levant Basin. While most of intra-salt deformation was suggested to occur post-depositionally (Cartwright et al., 2012), recent investigations demonstrate earlier, syn-depositional stages of salt contraction (Gvirtzman et al., 2013). Hence the basin-wide history of salt deformation is not easily understood and even new deformation mechanisms may need to be considered. Yet, faults and folds within supra-salt deposits have clearly been linked to salt tectonics below (e.g. Gradmann et al., 2005), but limited evidence exists as to what extent evaporite deformation itself is influenced by structures in the sub-salt domain.

Newly acquired industry seismic data from the northern part of the Levant Basin have recently shown the presence of such sub-salt structures by imaging a large set of Miocene extensional faults, clearly offsetting the base of the evaporites (Kosi et al., 2012; Skiple et al., 2012). Tracing the impact of faulting on intra-salt deformation represents a challenge to seismic data quality. Deformation may have occurred syn-depositionally and could thus be structurally absent within supra-salt deposits. With evaporites in the Levant Basin being composed of alternating transparent and reflective sequences (Netzeband et al., 2006b; Bertoni and Cartwright, 2007a; Hübscher and Netzeband, 2007), these layers may, however, reflect such deformation internally. In order to image intra-salt structures optimally, an accurate velocity model of the evaporite succession is required. Since basinal evaporites in the Eastern Mediterranean have not been penetrated by drilling yet, velocity information are limited to refraction velocities of the uppermost salt unit (Dümmong and Hübscher, 2011) and models derived from pre-stack stereotomography (Dümmong et al., 2008). By now, tomography has yielded

rather coarse velocity models, insufficient to accurately distinguish velocities of individual evaporite layers.

In this study, I use high-quality pre-stack depth-migrated industry seismic data crossing the Levant Basin in east-southeast to west-northwest and north-northeast to south-southwest direction (Fig. 3.1). Based on the reasoning above, the following objectives are defined: i) to investigate the influence of Miocene extensional faults on evaporite deformation, ii) to integrate new findings and previous results into a basin-wide concept of spatially and temporarily variable evaporite deformation within the Levant Basin and iii) to use a model-based approach for velocity model building in order to present a high-resolution velocity model of the Messinian salt and provide further constraints on the lithological interpretation of individual evaporite sequences.

3.2 Geological background

3.2.1 Tectonic setting

The evolution of the Levant Basin dates back to the Mid-Permian and was closely associated with the opening of the Neotethys Ocean (Garfunkel, 1998; Robertson, 1998c). Refraction seismic velocities across the Levant Basin suggest the presence of continental crust beneath approximately 12-14 km of sedimentary basin fill deposits (Ben-Avraham et al., 2002; Netzeband et al., 2006a). Closure of the southern Neotethyan Ocean was initiated by Late Cretaceous convergence of the Eurasian and Afro-Arabian plates (Robertson, 1998c). Subduction-related far field stresses caused the development of anticlines and synclines throughout the Levant region known as the Syrian Arc fold belt, extending from northern Egypt and continuing parallel to the Levant coastline (Walley, 1998; Gardosh and Druckman, 2006). The Levant Ramp stretches from the Lebanese coast into the central Levant Basin and represents a prominent anticlinal feature that has presumably formed during this inversion period (Fig. 3.1) (Hodgson, 2012). In Miocene times, the Eastern Mediterranean realm experienced considerable tectonic changes. To the north, subduction of the African plate moved to its present location south of Cyprus followed by the onset of slip along the Dead Sea Transform in Middle Miocene times (Robertson, 1998c; Bosworth et al., 2005). Subsequently, westward escape and counterclockwise motion of Anatolia was caused by a combination of north-northwest directed push of Arabia and basal drag at the Hellenic subduction zone in the Late Miocene-Early Pliocene (Reilinger et al., 1997). At the Cyprus Arc, the onset of Anatolian motion is manifested by a change from southeast directed compression to strike-slip movement since Early-Middle Pliocene times (Hall et al., 2005).

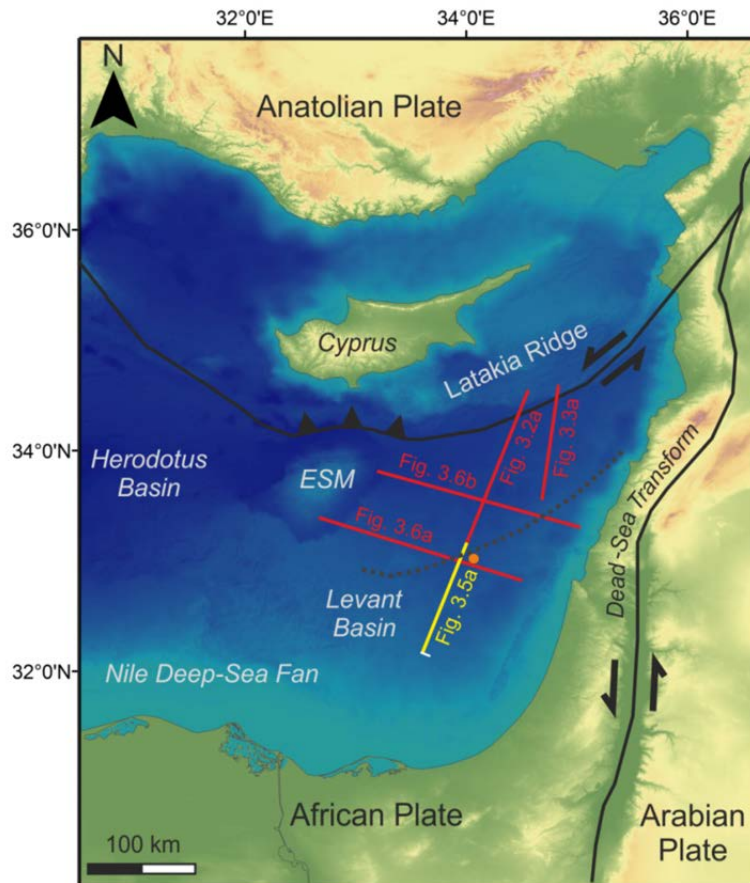


Figure 3.1 Location map of the study area. Red and yellow lines represent seismic profiles shown in this study. Tectonic elements were drawn after Aksu et al. (2005). Black stippled line indicates the location of the Levant Ramp after Hodgson (2012). Orange dot shows the approximate location of the Tamar 1 well. ESM=Eratosthenes Seamount.

3.2.2 Stratigraphy of the Messinian evaporites

Late Miocene reduction in water exchange between the Atlantic Ocean and the Mediterranean Sea caused Mediterranean water shortage, evaporation and ultimately initiated the Messinian Salinity Crisis at 5.96 Ma (Hsü et al., 1973; 1978; Krijgsman et al., 1999). During this period, up to 2 km of evaporites were deposited in the Levant Basin, until the Messinian Salinity Crisis was terminated by a short period of rapid Early Pliocene reflooding at 5.33 Ma (Krijgsman et al., 1999; Netzeband et al., 2006b; CIESM, 2008). Evaporites in the Levant Basin are bound by two high-amplitude reflections. Their base is defined by a reflection termed BES/BS (base erosion surface/base surface), where BES and BS are differentiated depending on the presence of erosional truncation. Similarly, the top of the evaporites is delineated by the TES/TS reflection (top erosion surface/ top surface) (Lofi et al., 2011). The erosive nature of the top-evaporite reflection is generally accepted in the Levant Basin based on the discordant termination of intra-evaporite reflections at the TES (Bertoni and Cartwright, 2007a; Dümmer and Hübscher, 2011). Netzeband et al. (2006b) observed internal evaporite reflections to toplap against the TES, providing further evidence for a Late Messinian

basin-wide erosion event. In contrast, erosion at the BES was only locally observed by canyon incision off the Israeli coast (Bertoni and Cartwright, 2006).

Most of the present knowledge on basinal evaporite stratigraphy is based on seismic data only (Bertoni and Cartwright, 2005; 2006; Netzeband et al., 2006b; Hübscher et al., 2007; Hübscher and Netzeband, 2007; Dümmong and Hübscher, 2011). In this regard, major advances were made during the last decades where newly collected academic and industry seismic data allowed discrimination between six evaporite sequences, termed ME-I to ME-VI and separated by horizons labeled ME20-ME60 (Bertoni and Cartwright, 2005; 2006; Hübscher et al., 2007; Hübscher and Netzeband, 2007; Dümmong and Hübscher, 2011). Seismic profiles crossing the Levant Basin from Cyprus to the Nile deep-sea fan and from the Israeli shelf to the Eratosthenes Seamount show most of these evaporite sequences to be present basin-wide (Netzeband et al., 2006b). Four sequences (ME-I, ME-II, ME-IV and ME-VI) are seismically transparent and consist presumably of halite (Bertoni and Cartwright, 2007a; Hübscher and Netzeband, 2007). The occurrence of two reflective intervals (ME-III and ME-V) was related to the presence of interbedded clastics or variations in evaporite facies (Garfunkel, 1984; Gradmann et al., 2005). Information on seismic velocities of individual evaporite layers may provide further insight into their composition. The uppermost, transparent sequence ME-VI reveals refraction velocities between 4.4 and 4.6 km/s consistent with halite, whereas velocities of reflective sequence ME-V (4.2-4.5 km/s) are reduced relative to ME-VI (Dümmong and Hübscher, 2011).

3.2.3 Salt tectonics

The influence of buoyancy in driving salt tectonics has long been overestimated (Hudec and Jackson, 2007). Instead, in many settings, evaporite deformation is primarily related to gravitational forces, either causing salt to flow in response to differential sediment loading (spreading) or as a consequence of basement tilt (gliding) (Hudec and Jackson, 2007; Brun and Fort, 2011). With the Levant Basin being part of an active plate tectonic setting (Ben-Avraham, 1978; Vidal et al., 2000a), evaporites may additionally deform tectonically (e.g. Netzeband et al., 2006b), adding another potential mechanism to drive salt tectonics in this area.

Several studies have focused on salt tectonics in the vicinity of the Nile Cone by means of swath bathymetry, seismic data and analogue modelling (Gaullier et al., 2000; Mascle et al., 2001; Loncke et al., 2004; 2006; 2010; Netzeband et al., 2006b). Results clearly show the impact of salt tectonics on the Pliocene-Quaternary overburden. Proximal to the Nile deep-sea fan, this can be observed by the presence of growth faults and minibasins, whereas in more distal regions, evaporite contraction is evident by numerous salt ridges and buckle folds which clearly shape the present-day seabed morphology (Gaullier et al., 2000; Loncke et

al., 2006). Such observations are best explained by gravity spreading of evaporites in response to Nile-derived sediment loading, implying salt deformation to have occurred post-depositionally (Loncke et al., 2006; 2010).

The Levant margin represents another prominent site where evaporite deformation was intensively studied (Mart and Ben Gai, 1982; Tibor and Ben-Avraham, 1992; Bertoni and Cartwright, 2005; 2006; 2007a; Gradmann et al., 2005; Netzeband et al., 2006b; Hübscher et al., 2007; Hübscher and Netzeband, 2007a; Carton et al., 2009; Gvirtzman et al., 2015). Here, gliding of Messinian salt is suggested to occur in response to basement tilt caused by a combination of Pliocene marginal uplift and basin subsidence (Gradmann et al., 2005; Cartwright and Jackson, 2008). In the marginal domain, basinward salt flow caused the development of extensional faults in the overburden (e.g. Mart and Ben Gai, 1982; Almagor, 1984; Garfunkel and Almagor, 1985) and the formation of well pronounced salt rollers and salt welds (Gradmann et al., 2005; Hübscher and Netzeband, 2007). Further basinward, evaporites are subject to compression, manifested in a complex pattern of intra-evaporite folds and faults and associated reverse faults and pop-up structures in the Pliocene-Quaternary overburden (Gradmann et al., 2005; Cartwright and Jackson, 2008). In a recent study off the southernmost Levant margin, Gvirtzman et al. (2015) have shown that evaporites, spreading basinward under the weight of the Nile Cone, have locally climbed up the Levant slope, creating compressional displacements within Pliocene-Quaternary strata.

Whereas salt tectonics in response to gravitational forces (gliding and spreading) was frequently observed in the Levant Basin, only sparse evidence of tectonically-controlled evaporite deformation exists. Examples include observations off the Israeli coast by Gradmann et al. (2005), where deep rooted faults appear to extend through the evaporite succession towards the seabed. Few tens of kilometers further north, Schattner et al. (2006) reported recent motion on the marine extension of the Camel Fault, cutting through the evaporites.

The existence of a syn-depositional, Messinian period of evaporite deformation is currently debated (Cartwright et al., 2012; Gvirtzman et al., 2013). A single, post-depositional phase of salt deformation was suggested by Cartwright et al. (2012), investigating the timing of salt tectonics offshore Israel. These authors used analogue modelling to support the idea that mechanical differences between salt and supra-salt sediments lead to strain partitioning during deformation. Consequently, supra-salt clastics may only moderately deform while evaporites accommodate significant post-depositional gravity-driven shortening. In contrast, a syn-depositional phase of evaporite deformation is strongly supported by recent 3D seismic findings off the Israeli coast (Gvirtzman et al., 2013), close to the study area investigated by Cartwright et al. (2012). In this study, Gvirtzman et al. (2013) showed reflections associated with intra-salt unit ME-IV to onlap against unit

ME-III folds. Such observations clearly point towards an intra-Messinian deformation event, creating folds within evaporite unit ME-III which subsequently became buried underneath deposits associated with unit ME-IV.

Fluids seem to play an important part in salt dynamics (Hübscher and Dümmong, 2011). Several pockmarks and mud volcanoes were observed in the vicinity of the Nile deep-sea fan, linked to the presence of salt tectonic faults (Loncke et al., 2004; Dupré et al., 2010). Off the southern Levant margin, fluids have escaped from the sub-salt domain towards the seabed. Ascending fluids remobilized sediments and caused the formation of meter thick mud pies (Gradmann et al., 2005; Netzeband et al., 2006b). Fluids migrating through evaporites may cause salt dissolution and create up to 1 km wide circular collapse structures in the Pliocene-Quaternary overburden (Bertoni and Cartwright, 2005). Offshore Israel, numerous pockmarks were recently observed to perforate the base of the evaporites. Their formation was linked to a short episode of vigorous gas escape caused by initial sea level drop at the onset of the Messinian Salinity Crisis (Lazar et al., 2012; Bertoni et al., 2013).

3.3 Methods

3.3.1 Seismic data

Seismic profiles of this study were selected from a large regional survey covering the Eastern Mediterranean (Fig. 3.1). The data were acquired using a 7200 m streamer, 50 m shot point interval, 12.5 m hydrophone group interval and 12 s record length. The data were reprocessed through Kirchhoff pre-stack depth migration. The key to depth imaging was a geological understanding of the survey area and, in particular, the Messinian salt. Details on the processing workflow applied to the present dataset are described by Peace et al. (2012).

3.3.2 Model-based processing

The seismic data used for velocity model building were acquired with a streamer consisting of 544 channels and an active length of 7200 m. In order to allow for high accuracy velocity model building, only a small (2.3 km) section was extracted from the original seismic profile, located approximately 80 km west of the salt pinchout off the Israeli coast. The entire seismic profile was published by Dümmong and Hübscher (2011) (Fig. 10.5 in Dümmong and Hübscher, 2011). In order to calculate reliable interval velocities for the individual Messinian sequences, a model-based approach is applied as described by Fagin (1998). First, the data were normal moveout (NMO)-corrected and stacked with an initial velocity model derived from semblance analysis. The time domain stack was iteratively improved by residual moveout analysis. Based on the final NMO-

corrected section, the model for interval velocity estimation was build. Interval velocities were derived for each model-layer by ray-tracing, starting with the uppermost water layer. Pre-stack depth migration of each individual layer yielded the layer thickness necessary for performing ray-tracing on the next layer boundary. After depth migration of the entire section, interval velocities were iteratively refined by residual moveout analysis on common image gathers and repeated depth migration.

3.4 Results

3.4.1 Stratigraphy

In order to adapt a seismostratigraphic framework, I follow the stratigraphic interpretations by Skiple et al. (2012) and Steinberg et al. (2011) which are supported by recent drilling results of the Tamar-1 well (Fig. 3.1). The lowermost identified stratigraphic unit is bound by the Senonian and Eocene Unconformities followed by a unit of Oligocene age. Both units are characterized by acoustically transparent to low-amplitude parallel reflections (Fig. 3.2a). Above, sediments assigned to the Early Miocene unit are characterized by parallel high-amplitude reflections and are heavily dissected by numerous normal faults (Figs. 3.2a, 3.3a). The uppermost sub-salt unit is assigned to a Middle-Late Miocene age, being similarly composed of parallel medium-amplitude reflections and offset by several normal faults (Figs. 3.2a, 3.3a). The approximately 1.5 km thick Messinian evaporite unit can easily be recognized, being composed of alternating acoustically transparent and more reflective sequences (Figs. 3.2, 3.3, 3.5-3.8). The latest internal stratigraphy of the evaporite unit was established by Hübscher et al. (2007), subdividing the Levant Basin evaporites into six sequences. The lowermost two sequences (ME-I and ME-II) are characterized by acoustic transparency, separated by a high-amplitude reflection event which is broadly concordant to the base of the evaporites (Fig. 3.2b). Despite previous studies referred to this reflection as a boundary instead of an individual evaporite sequence, this prominent reflection will be included into the stratigraphy of this study, termed ME-20 according to Bertoni and Cartwright (2005). Sequence ME-III is composed of a set of continuous moderate to high-amplitude reflections which are followed by another transparent sequence, ME-IV (Fig. 3.2b). Above, ME-V is characterized by several reflections of moderate amplitude and continuity, being overlain by the uppermost evaporite sequence (ME-VI) which appears acoustically transparent and is restricted to the southwestern part of the Levant Basin (Fig. 3.5b). On top of Messinian evaporites, the uppermost unit comprises sediments of Pliocene to Quaternary age. These deposits are thickest in the southernmost part of the study area (900 m), gradually thinning to approximately 300 m in the vicinity of the Latakia Ridge (Figs. 3.2a, 3.5a).

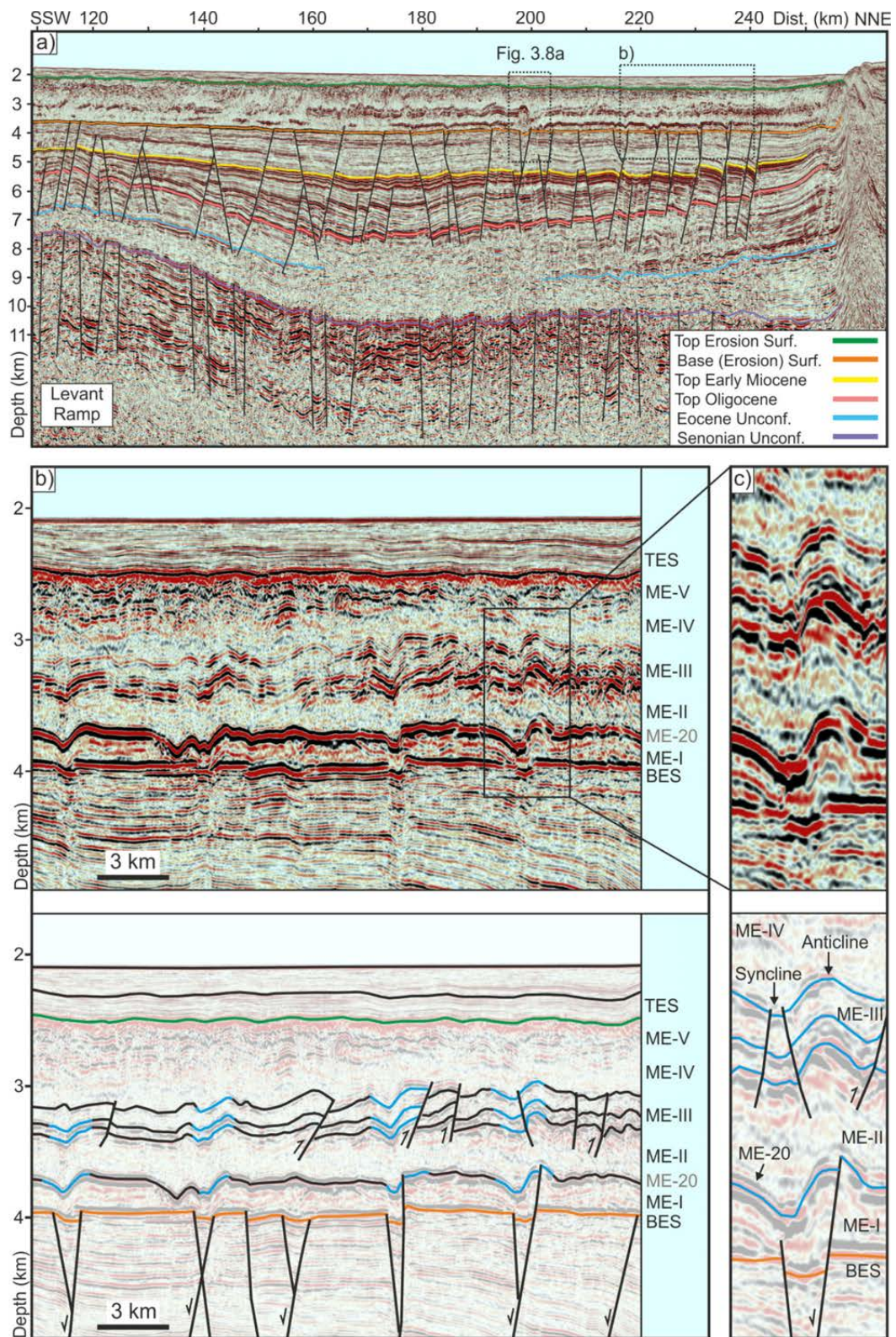


Figure 3.2 a) Seismic profile, crossing the Levant Basin in north-northeast to south-southwest direction. Note the presence of several Miocene extensional faults cutting through up to 3.7 km thick Miocene deposits. For location see figure 3.1. **b)** Extraction from the seismic profile shown in figure 3.2a and associated line drawing, displaying intra-evaporite folds which clearly coincide with sub-salt extensional faults. Blue segments along the interpreted reflections highlight the presence of folds following the pattern described in Chapter 3.4.3.1. **c)** Detailed section showing the intra-salt deformation pattern above a sub-salt extensional fault.

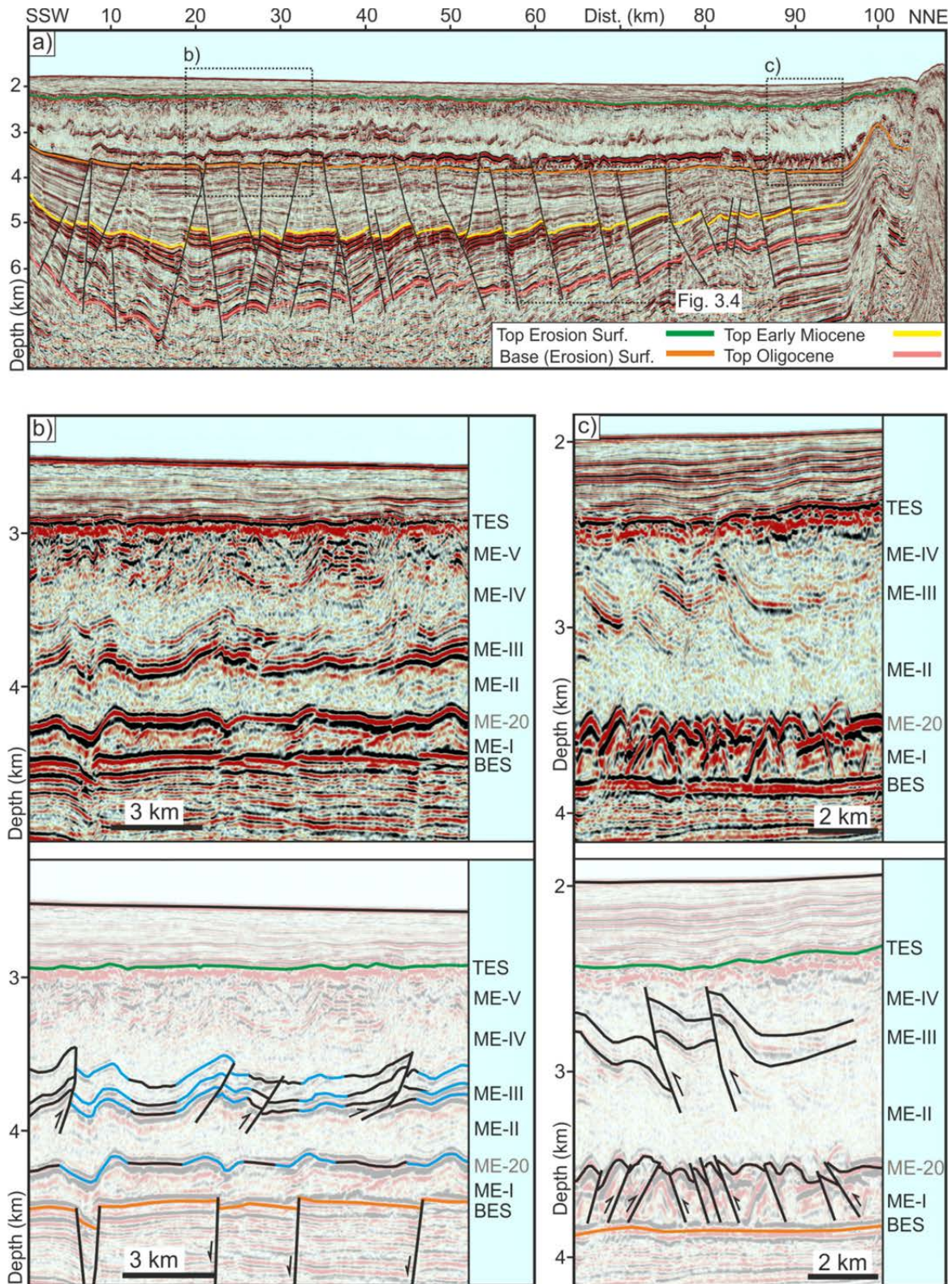


Figure 3.3 a) Seismic profile showing several normal faults which dissect Miocene deposits. For location see figure 3.1. b) Uninterpreted and interpreted enlarged seismic sections from figure 3.3a. Blue segments along the interpreted reflections highlight the presence of folds following the pattern described in Chapter 3.4.3.1. c) Enlarged seismic section and the corresponding line drawing from figure 3.3a, directly south of the Latakia Ridge. Note how ME-20 and reflections associated with ME-III are intensively faulted in this area.

3.4.2 Extensional faults

Miocene deposits are heavily dissected by numerous normal faults (Figs. 3.2a, 3.3a). Faults are predominantly observed in the northern Levant Basin, with few faults being present south of the Levant Ramp (Figs. 3.2a, 3.5a). Based on 3D-seismic data, Kosi et al. (2012) reported a northwest-southeast strike direction of this fault system. Fault throw was measured in profiles shown in figures 3.2a and 3.3a. Maximum and constant throw is observed between the Top-Oligocene and Top-Early Miocene reflections, with a maximum of 600 m and an average of 160 m. Dip angles are relatively uniform, averaging to 45° (Figs. 3.2a, 3.3a, 3.4).

In order to assess the timing of faulting, standard techniques were utilized. The onset of faulting is defined by the reflection delineating the base of syn-kinematic deposition (i.e. stratal divergence), represented by the Top-Early Miocene reflection (corresponding to approximately 16 Ma according to the stratigraphic framework of Steinberg et al., 2011) (Fig. 3.4). Faulting has continued throughout the stratigraphic interval associated with diverging reflections, represented by sediments between the Top-Early Miocene and the BES reflections, i.e. throughout the Middle-Late Miocene period (Fig. 3.4). Syn-kinematic deposition of Middle-Late Miocene sediments is further evident by observing a progressive decrease in fault throw along this interval (Fig. 3.4).

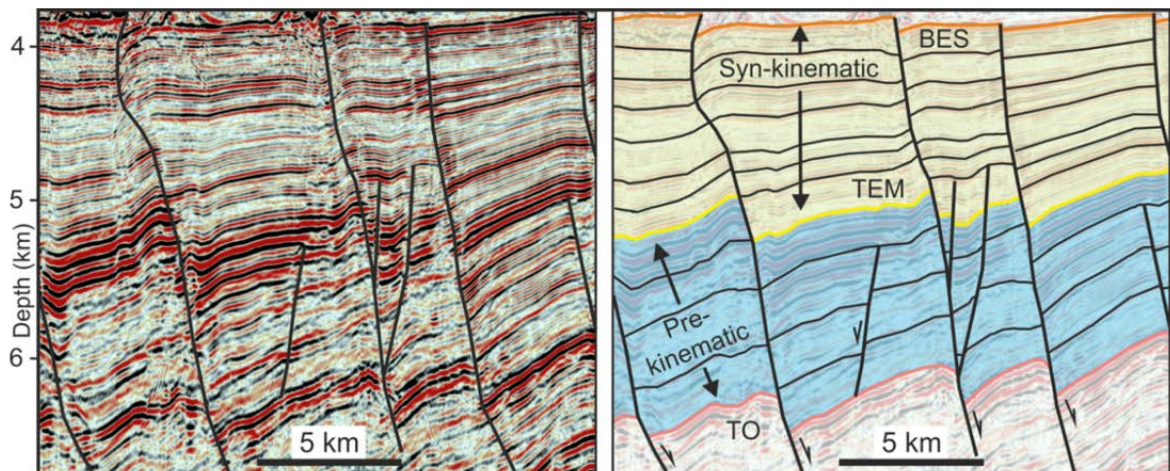


Figure 3.4 Enlarged seismic section and the corresponding line drawing, showing extensional faults within the Miocene succession. While sediments between TO (Top-Oligocene) and TEM (Top-Early-Miocene) strata are equally thick and thus faulted post-depositionally, syn-kinematic deposition is marked by stratal divergence between the TEM and BES (Base Erosion Surface) reflections. For location see figure 3.3a.

Towards the top of the Middle-Late Miocene unit, faults frequently branch out, forming graben-like displacements at the base of the evaporites (Figs. 3.2a,b). Some of the northern- and southernmost faults can be traced into the Oligocene unit (Fig. 3.2a). None of the faults could be followed far below the Eocene Unconformity, owing to the acoustically transparent character of this unit (Fig.

3.2a). Below the Senonian Unconformity, several near vertical faults are observed, which are not obviously linked to the overlying extensional fault system (Fig. 3.2a). However, limited resolution and reflection continuity make interpretation of faults at these depths rather imprecise.

3.4.3 Evaporite deformation

3.4.3.1 Fault-controlled evaporite deformation

Northern Levant Basin: In the northern Levant Basin, between km 165 and 240 in figure 3.2a and between km 10 and 60 in figure 3.3a, a relation between intra-salt deformation and the presence of sub-salt extensional faults is recognized. This relation is most clearly observed by following the shape of intra-salt reflection ME-20, showing a typical deformation pattern: intra-salt anticlinal folds frequently coincide with the footwall cutoff of sub-salt extensional faults, turning into synclinal structures towards the hanging wall (Figs. 3.2b,c, 3.3b). Occasionally, sub-salt extensional faults extent into the lowermost evaporite unit, creating displacements of intra-salt reflection ME-20 (Fig. 3.2c). However, in most instances ME-20 appears to be folded above sub-salt extensional faults rather than faulted (Figs. 3.2b, 3.3b). It is further noted that this deformation pattern is also observed within the shape of reflections associated with sequence ME-III. Again, these reflections show anticlinal folds above the footwall cutoff of sub-salt extensional faults, whereas synclinal folds are observed above the hanging wall (Figs. 3.2b,c, 3.3b). However, unlike ME-20, reflections within ME-III are frequently offset by intra-salt thrust faults, creating a deformation pattern more complex than observed for ME-20 (Figs. 3.2b,c, 3.3b). Reflections within sequence ME-V are largely discontinuous to chaotic, inhibiting a clear correlation to the shape of underlying intra-evaporite reflections (Figs. 3.2b, 3.3b). Sediments of Pliocene-Quaternary age are rather undisturbed, except of some broad undulations in the lower part of this unit (Figs. 3.2b, 3.3b).

Latakia Ridge: Directly south of the Latakia Ridge, between km 240 and 255 in figure 3.2a and between km 85 and 105 in figure 3.3a, a distinct style of intra-salt deformation is observed. While intra-salt unit ME-V is no longer observed in this area, the remaining intra-evaporite reflections (ME-20 and reflections associated with ME-III) are strongly deformed (Figs. 3.2a, 3.3a,c). At km 100 in figure 3.3a, a significant compressional sub-salt structure offsets reflection ME-20 by almost 1 km. In close vicinity to this structure, reflection ME-20 is heavily faulted by a set of densely spaced thrust faults (Figs. 3.3a,c). In contrast, ME-III is faulted by few significantly larger thrusts, offsetting reflections within unit ME-III by up to 250 m (Fig. 3.3c). Sediments within the Pliocene-Quaternary succession are slightly elevated above the sub-salt structure, but have otherwise remained largely undisturbed (Figs. 3.3a,c).

3.4.3.2 Evaporite deformation independent of sub-salt faults

Evaporite deformation in the southern Levant Basin: In the southern part of the study area, reflection ME-20 generally follows the base of the evaporites, remaining fairly undeformed throughout figure 3.5a. In contrast, reflections within sequences ME-III and ME-V are offset by south-southwest-dipping thrust faults which are also structurally reflected by deformation within the Pliocene-Quaternary overburden (Figs. 3.5a,b). This deformation pattern can generally be observed along most of figure 3.5a, but is particularly evident between profile km 70 and 90 (Figs. 3.5a,b). This section shows the presence of several intra-salt thrusts. Within ME-V, a backthrust developed, creating a small pop-up structure within the salt unit (Fig. 3.5b). Above, north-northeast-dipping thrust faults offset sediments within the supra-salt deposits, suggesting thrusting to have changed dip direction while propagating into the Pliocene–Quaternary succession (Fig. 3.5b).

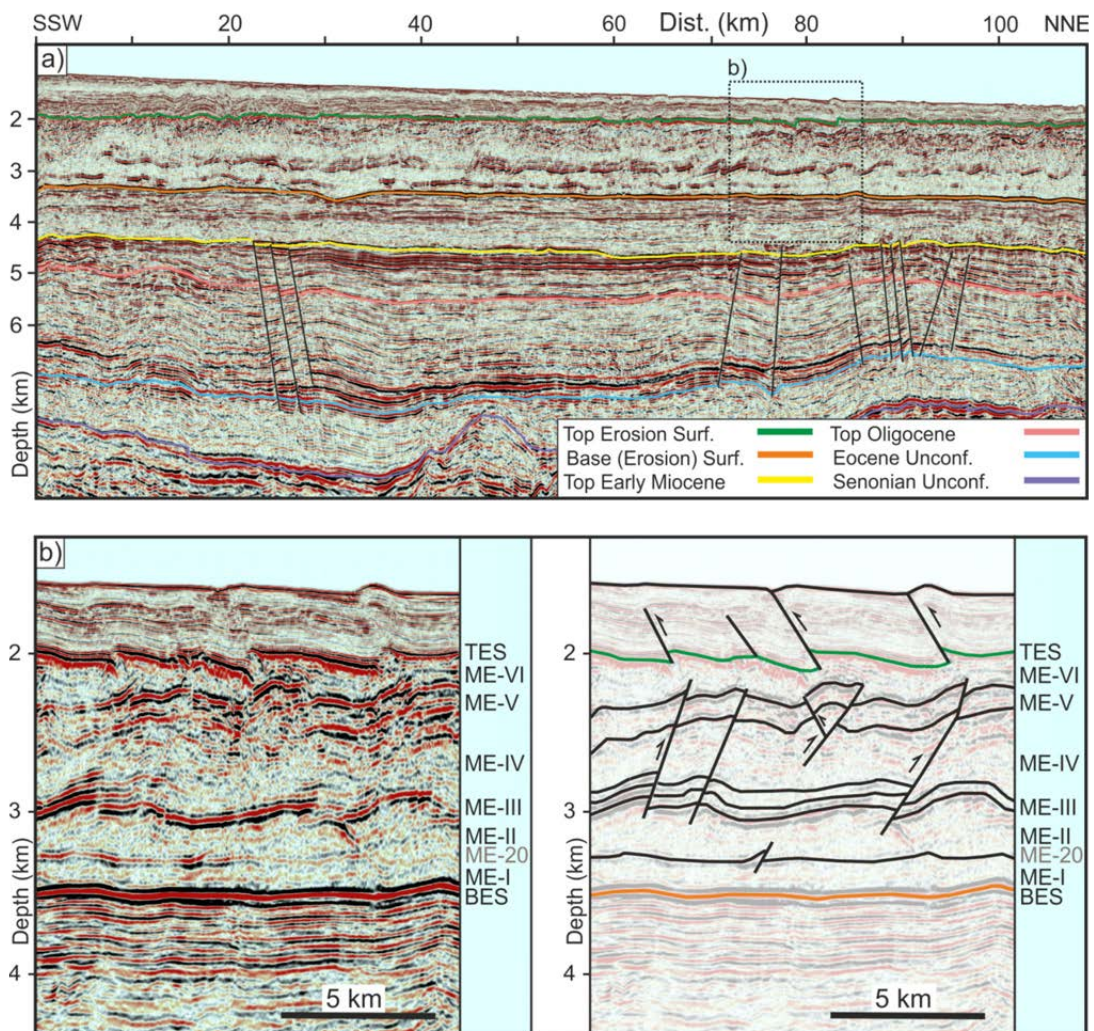


Figure 3.5 a) Seismic profile representing the southern continuation of the profile shown in figure 3.2a. In this part of the Levant Basin, only few faults are observed and none of them intersects the base of the Messinian evaporites. For location see figure 3.1. **b)** Seismic section and associated line drawing extracted from the profile shown in figure 3.5a. Reflection ME-20 remains nearly undisturbed and is followed by intra-salt faults of sequences ME-III and ME-V. Above, post-Messinian sediments are cut by reverse faults.

Evaporite deformation at the Eratosthenes Seamount: At the eastern flank of the Eratosthenes Seamount, between km 10 and 30 in figure 3.6a and between km 25 and 40 in figure 3.6b, significant intra-salt deformation is observed. While deformation is hardly evident within ME-20, reflections associated with ME-III are faulted by large thrusts, offsetting intra-salt reflections by up to 300 m (Fig. 3.7). In both profiles shown in figures 3.7a and 3.7b, intra-ME-III reflections are steeply bent upwards at a large thrust fault directly west of the seamount. A slight convergence of ME-III reflections is observed towards this structure (Fig. 3.7). Reflections associated with ME-V show thrusting at the southeastern flank of the seamount but poor resolution of this unit inhibits a detailed interpretation (Fig. 3.7a). Minor thrusts are identified within Pliocene-Quaternary sediments (Fig. 3.7).

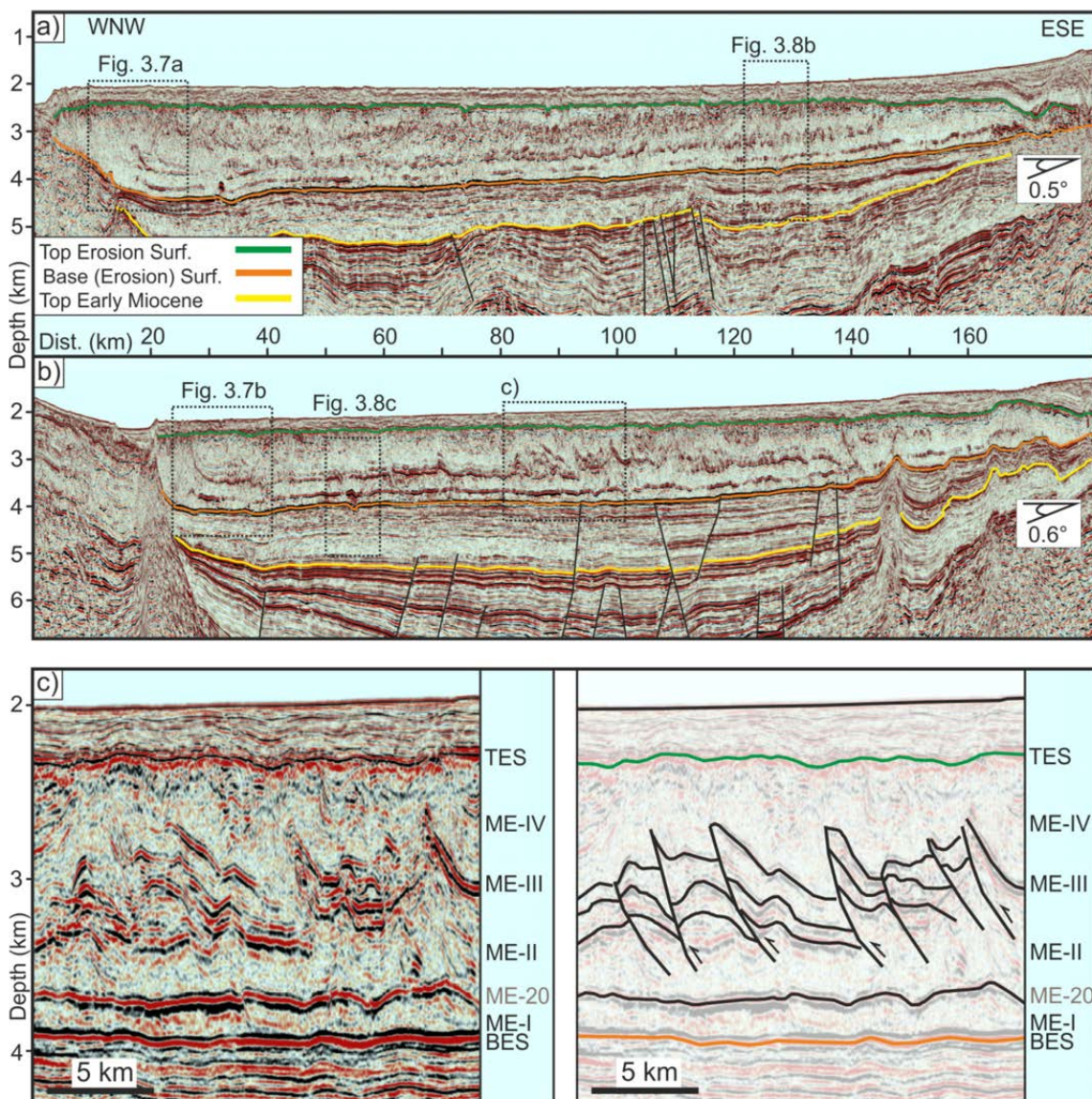


Figure 3.6 a,b) Seismic profiles crossing the Levant Basin in east-southeast to west-northwest direction. Dip angles refer to the average dip at the Base (Erosion) Surface. For locations see figure 3.1. **c)** Enlarged seismic section from the profile shown in figure 3.6b and associated interpretation. Reflection ME-20 remains largely horizontal. Heavily faulted reflections of ME-III are overlain by mostly undisturbed supra-salt deposits.

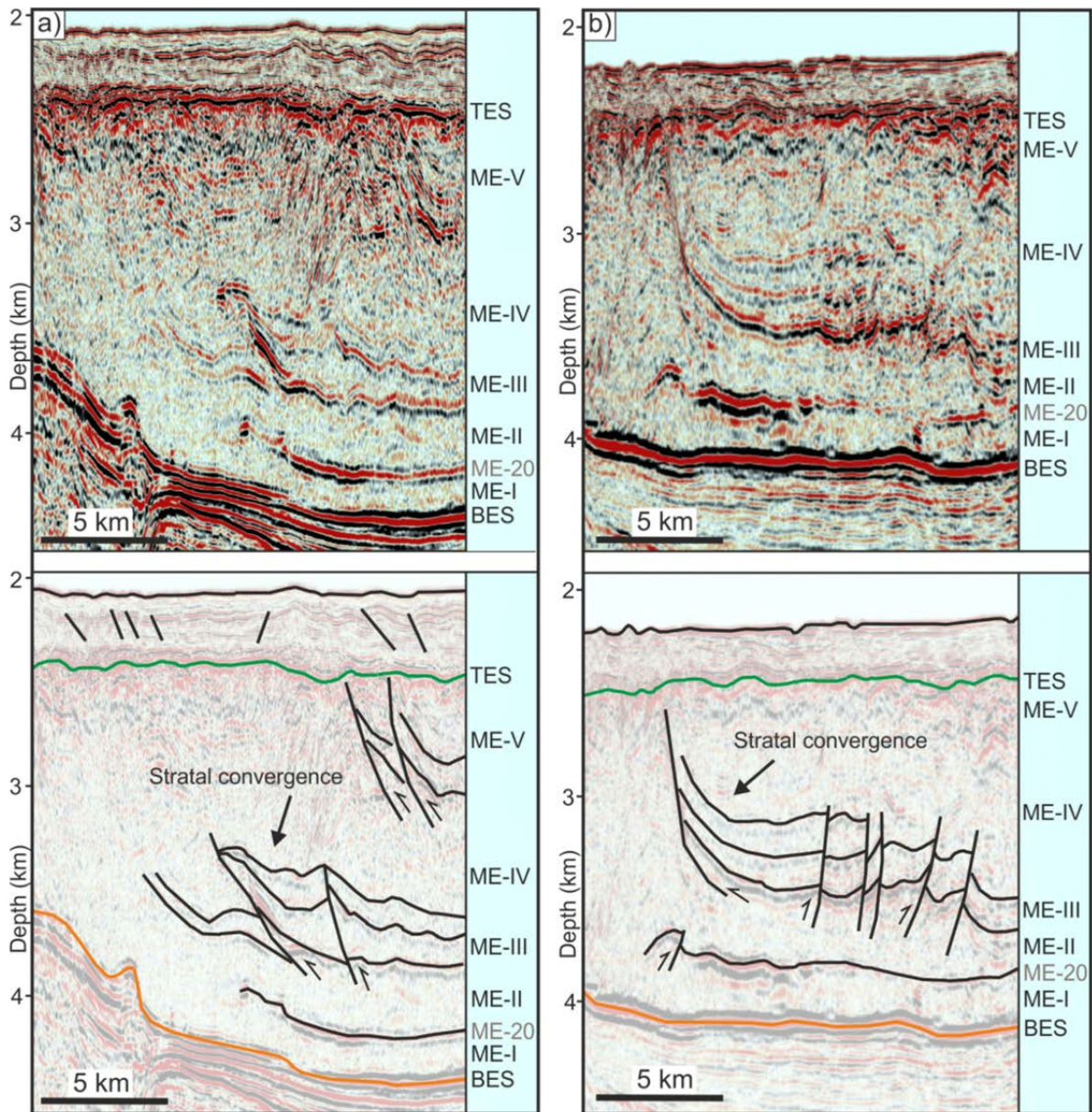


Figure 3.7 a) Seismic section zooming into the evaporite unit directly east of Eratosthenes Seamount. The interpreted version is shown below. Reflections of unit ME-III are heavily faulted at the flank of the seamount. Towards the main thrust, ME-III reflections appear to converge. For location see figure 3.6a. **b)** Seismic section and associated line drawing. Again, reflections of ME-III are significantly faulted and converge towards the main thrust. For locations see figure 3.6b.

Evaporite deformation in the central Levant Basin: Intra-salt reflection ME-20 remains fairly undeformed throughout figures 3.6a and 3.6b. In contrast, intense intra-salt deformation is locally evident within unit ME-III. In the central part of figure 3.6b (km 80-120), reflections associated with ME-III are cut by multiple large thrust faults, creating offsets as large as 450m (Fig. 3.6c). This deformation has not affected overlying Pliocene-Quaternary sediments which remained largely undisturbed above intra-salt thrusts (Fig. 3.6c).

3.4.4 Amplitude anomalies

Within sub-salt Miocene deposits, vertical zones of reduced amplitudes are occasionally observed. In the central-western part of figure 3.6b, a vertical zone of reduced amplitudes terminates into a depression at the base of the evaporites (Fig. 3.8c). This depression is followed by a high-amplitude reflection patch within intra-salt reflection ME-20 (Fig. 3.8c). A similar reflection pattern is also observed in the northern Levant Basin, where a vertical zone of reduced amplitudes extends into the lower part of the evaporites, masking the ME-20 reflection (Fig. 3.8a). This zone terminates at an intra-ME-III fold, showing a phase-reversed high-amplitude reflection patch (Fig. 3.8a). In the eastern part of the Levant Basin, a vertical zone of reduced reflection continuity passes from the sub-salt domain through a depression at the BES and continues upwards by piercing through the evaporite unit (Fig. 3.8b). At the seabed, this zone terminates into a topographically positive structure (Fig. 3.8b).

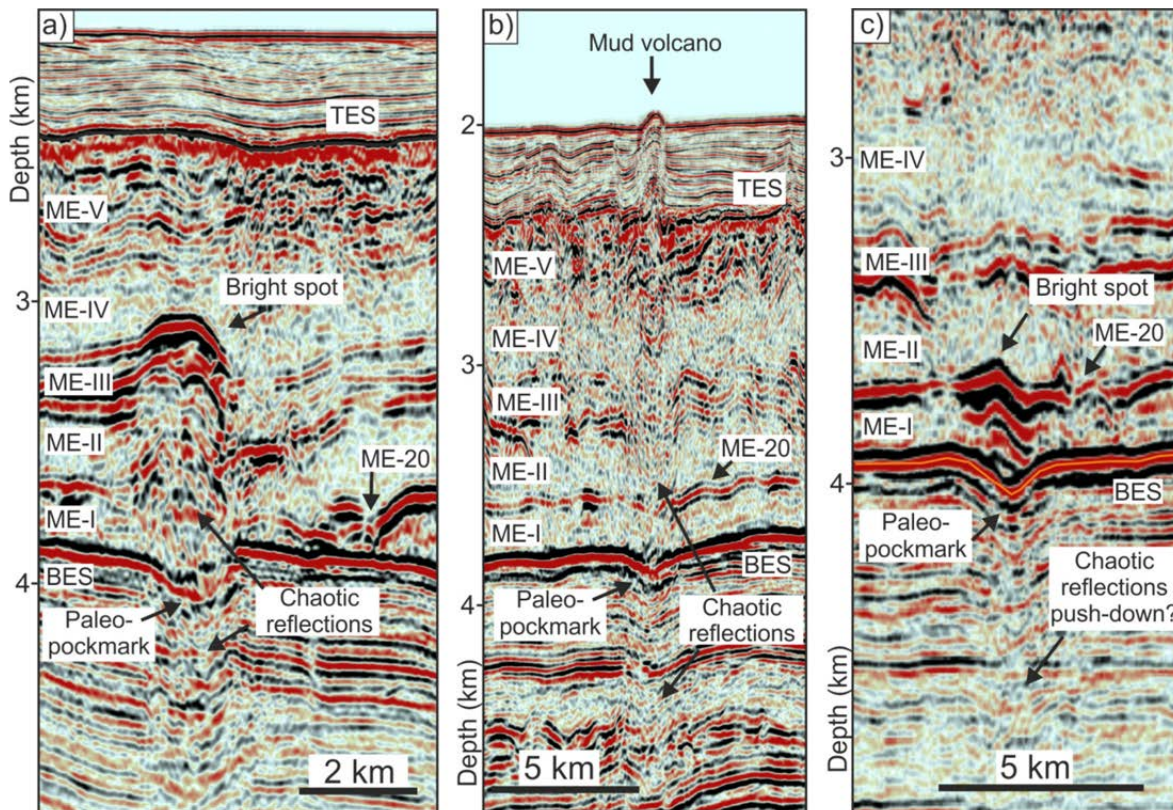


Figure 3.8 **a)** Enlarged seismic section showing a vertical zone of reduced reflection continuity in the vicinity of Miocene faults. This zone terminates into a phase-reversed bright spot within the Messinian salt. For location see figure 3.2a. **b)** Enlarged section showing a zone of chaotic reflections that extends through the Messinian evaporites and terminates within a topographically positive structure at the seafloor. For location see figure 3.6a. **c)** Enlarged seismic section showing a vertical zone of slightly reduced reflection continuity and downward-bending reflections. At the location of ME-20, this zone terminates into a high-amplitude reflection patch. For location see figure 3.6b.

3.4.5 Intra-evaporite velocities

Interval velocities of individual Messinian evaporite layers were obtained by model-based processing. For this purpose the evaporite succession was subdivided into four layers, where the upper three layers correspond to ME-IV, ME-V and ME-VI, respectively. As evaporite sequences ME-I to ME-III are too thin to be individually resolved, these sequences were modelled as a single layer (Fig. 3.9). In the light of this simplification, I note that sequences ME-I and ME-II are separated by a phase-reversed high-amplitude reflection (ME-20), implying the presence of contrasting lithologies within this layer (e.g. Fig. 3.2b).

Figure 3.9 depicts the pre-stack depth-migrated stack overlain by the final velocity model used for migration. Results show velocities of acoustically transparent evaporite sequences (ME-IV and ME-VI) to be highest with a maximum of 4240 m/s in ME-IV. In contrast, reflective sequences (ME-V and ME-I to ME-III) are characterized by lower velocities. For instance, in the lowermost layer (ME-I to ME-III), interval velocities remain below 4000 m/s with minimum values as low as 3650 m/s (Fig. 3.5). Evaporite velocities are summarized in Table 3.1.

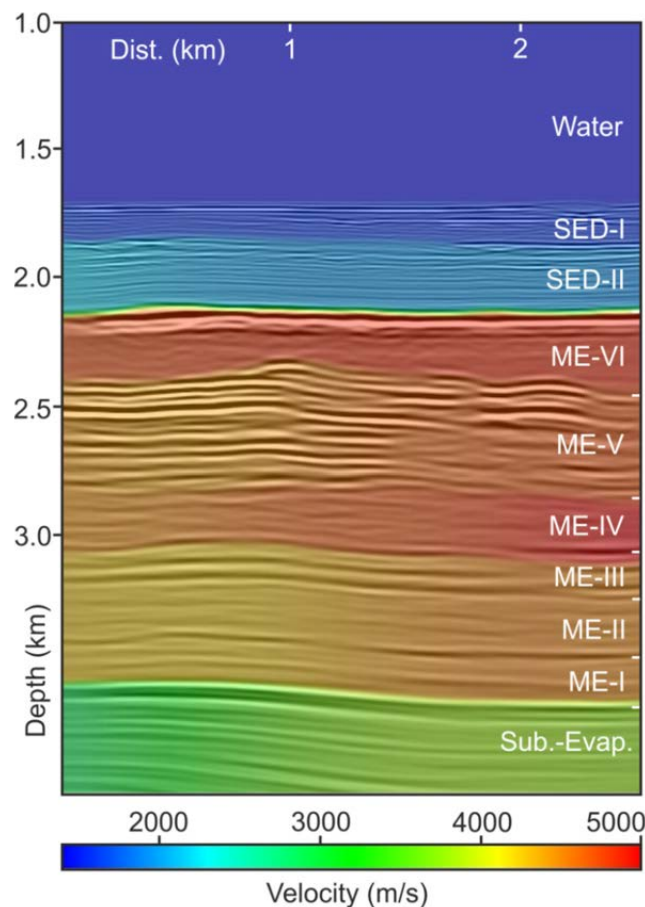


Figure 3.9 Interval velocity model of the Messinian evaporites plotted on top of the seismic profile used for velocity model building. Note that evaporite sequences ME-I to ME-III were modeled as a single layer. Velocities are found to be generally higher for acoustically transparent evaporite sequences compared to more reflective intervals.

Table 3.1 Minimum and maximum interval velocities of individual evaporite layers derived by model based processing.

Layer	Min. interval velocity (m/s)	Max. interval velocity (m/s)
Water	1500	1510
Sed-I	1660	1680
Sed-II	1900	2100
ME-VI	4030	4150
ME-V	3750	4030
ME-IV	3850	4240
ME-III to ME-I	3650	3910
Sub.-Evap.	2660	3340

3.5 Discussion

3.5.1 Origin of extensional faults in the Levant Basin

A model of the origin of sub-salt extensional faults was first described by Kosi et al. (2012) based on 3D seismic data. By analogy to extensional faults of the Canyonlands graben system in Utah, USA, these authors interpreted faults in the Levant Basin as a thin-skinned response to gravity-driven deformation of underlying Eocene ductile shales. While the observation of faults largely detaching above the Eocene Unconformity is consistent with results of this study (Fig. 3.2a), there are two points which I consider problematic with this interpretation. i) Ductile evaporite deformation and associated extensional faulting in the Canyonlands was initiated by downcutting of the Colorado River, creating a free lateral surface and thus facilitating gravity-driven flow of the evaporites. With the northern Levant Basin being bound by the Eratosthenes Seamount to the west, the Levant margin to the east, the Latakia Ridge to the north and the Levant Ramp to the south, it remains difficult to conceive into which direction ductile Eocene shales should have moved. Shale translation towards the basin center is considered unlikely, as this would imply movement towards the area of maximum overburden accumulation (Steinberg et al., 2011). ii) While Kosi et al. (2012) related the timing and cause of fault initiation to Messinian sea level drawdown, the present data show that fault activity has started in Middle Miocene times (Fig. 3.4), clearly earlier than the onset of the Messinian Salinity Crisis.

Normal faulting in the vicinity of convergent plate boundaries has previously been described in several settings (Bradley and Kidd, 1991 and references therein). Bradley and Kidd (1991) related these observations to *flexural extension* where bending due to subduction creates extensional forces within the upper and compressional forces within the lower part of the downgoing plate. The Timor Sea,

located between the Australian margin and the Timor Islands, is considered a foredeep close to the convergence zone of the Australian and Eurasian plates. In this area, normal faulting is suggested to have occurred as a thin-skinned response of a detached sedimentary layer to flexural subsidence and amplification of pre-existing basement topography. Similar to the Levant Basin-faults, these extensional structures show significant growth and die out at a certain depth (Harrofield et al., 2003; Harrofield and Keep, 2005).

Assessing the stratal architecture of the basin fill deposits offshore Lebanon, Hawie et al. (2013) reported intensification of marginal uplift and basinal subsidence in Middle Miocene times. At the same time, the formation of a new plate boundary along the Dead Sea Transform may have released pre-existing loading-induced stresses, thereby contributing to significant amplification of pre-existing topography offshore Israel (Steinberg et al., 2014). Further north, intensive convergence and thrusting has occurred at the Latakia Ridge (Hall et al., 2005). Convergence at the plate boundary together with differential vertical motion between marginal and basinal areas may have similarly caused amplification of pre-existing basement topography and thus facilitated gravitational collapse of Miocene sediments detaching at the Eocene Unconformity. This mechanism provides an explanation for extensional faulting which incorporates the correct timing of fault initiation in relation to the known geodynamic situation within the Eastern Mediterranean – tectonic compression, basinal subsidence and marginal uplift – and does not contradict the data shown by Kosi et al. (2012).

3.5.2 The composition of the Messinian evaporites

The Messinian evaporites are composed of up to six sequences of varying acoustic properties. Sequences ME-I and ME-II are separated by a high-amplitude, phase-reversed reflection event ME-20 (e.g. Fig. 3.2b). Interpreting ME-20 as a sequence boundary implies that this reflection results from a lithological contrast between ME-I and ME-II. However, both sequences are characterized by acoustic transparency, potentially indicating the presence of halite. Therefore, ME-20 could alternatively be interpreted as a distinct lithological sequence, encased between two halite layers (ME-I and ME-II). Similar intra-salt reflections were observed within the Dutch offshore Zechstein salt (called Z3 stringer), resulting from 40 to 50 m thick anhydrite and dolomite inclusions within the salt body (Van Gent et al., 2011; Strozyk et al., 2012). Hence, ME-20 could represent an analogy to the Z3 stringer, instead of being caused by impedance changes at the boundary between ME-I and ME-II.

It was shown that individual evaporite layers are characterized by different seismic velocities (Fig. 3.9), providing further evidence of their heterogeneous lithological composition. Based on previous studies, two alternative explanatory approaches

exist, either relating reflective intra-evaporite sequences to the presence of interbedded clastics (Garfunkel, 1984) or to cyclic deposition of different evaporite facies (Gradmann et al., 2005; Netzeband et al., 2006b; Bertoni and Cartwright, 2007a). Agreement exists as to the composition of acoustically transparent intra-evaporite sequences which have generally been suggested to indicate the presence of halite (Bertoni and Cartwright, 2007a). Clastic inclusions within Messinian evaporites were locally observed off the Lebanese and Israeli coasts and interpreted to represent delta and channel-lobe deposits, respectively (Bertoni and Cartwright, 2007b; Hawie et al., 2013). Such clastic inclusions are imaged as spatially limited, highly reflective bodies in seismic data which do not appear to distally merge with basinwide reflective intra-salt units ME-20, ME-III or ME-V (Bertoni and Cartwright, 2007b; Hawie et al., 2013). The presence of interbedded Messinian clastics is therefore regarded to reflect local terrigenous sediment input rather than representing the proximal termination of basin-wide clastic sediment layers. Interpreting low-velocity intra-evaporite layers to be composed of interbedded clastics, one may expect the thickness of these layers to increase towards the source areas (i.e. towards the Levant margin or the Nile deep-sea fan). However, seismic data shown in this study do not reveal significant thickness variations of intra-salt reflective units ME-20, ME-III and ME-V (Figs. 3.2a, 3.3a, 3.5a, 3.6a,b), representing a challenge to a clastic interpretation of these sequences.

Based on laboratory experiments on Mediterranean evaporite samples recovered during ODP Leg 13, Schreiber et al. (1973) reported seismic velocities to range from 4.85 to 4.91 km/s for gypsum (recovered in the Tyrrhenian Basin), 4.29 to 4.85 km/s for anhydrite (recovered on the Balearic Rise) and 3.54 to 4.05 km/s for halite (recovered from the Balearic Abyssal Plain) at a pressure of 0.5 kbar. While velocities obtained from halite are close to the range of ME-IV and ME-VI velocities shown in this study, velocities of ME-I to ME-III and ME-V are generally below 4 km/s and thus significantly lower than those reported for the Mediterranean anhydrite and gypsum samples (Table 3.1). However, well-log measurements and laboratory tests have shown gypsum velocities to vary considerably (3 km/s at Salt Valley, Utah (Daniels et al., 1980) and 4.8 km/s for gypsum-dolostones from the Triassic Evaporites from central Italy (Trippetta et al., 2010)). Hence low-velocity reflective intervals within the Messinian evaporites may still be explained by the presence of gypsum. Furthermore, also evaporites precipitated at the higher concentration end of the evaporite series (e.g. carnallite, sylvite) could cause the observed decrease in seismic velocities (Urai et al., 2008; Warren, 2010). Differentiating between these lithologies would have important implications for brine concentration and thus Messinian sea level at the time of evaporite precipitation.

In conclusion, despite having obtained accurate velocities of individual evaporite layers, the origin of these highly reflective sequences cannot conclusively be resolved. Only drilling would provide conclusive results on the lithological composition of the Messinian evaporites in the Levant Basin with widespread implications on the Messinian depositional environment.

3.5.3 Fluid migration

Vertical zones of reduced amplitudes which terminate into intra-evaporite high-amplitude reflection patches are interpreted to indicate the presence of vertically migrating fluids (Fig. 3.8). Migration pathways of gaseous fluids are commonly associated with locally reduced seismic velocities, appearing as vertical zones of push-down reflections in seismic sections (Løseth et al., 2009). If not incorporated into the velocity model used for depth migration, such velocity effects may remain within depth-migrated seismic sections. Figure 3.8c may show such push-down reflections, even though a structural cause for downward-bending reflections cannot be ruled out. Further up, these push-down reflections terminate into a depression at the base of the evaporites, potentially representing a pockmark which formed during initial sea level drop and concomitant pressure reduction at the onset of the Messinian Salinity Crisis (Fig. 3.8c). This period has previously been associated with vigorous gas escape in the Eastern Mediterranean, as shown by numerous pockmarks perforating the BES off the Israeli coast (Lazar et al., 2012; Bertoni et al., 2013). Observation of phase-reversed high-amplitude reflection patches within intra-salt reflection ME-20 and reflections associated with sequence ME-III, suggests fluids to migrate into the evaporite layer (Figs. 3.8a,c). There, fluids may become trapped or continue to migrate horizontally. Lateral fluid migration along reflective evaporite sequences has previously been suggested by Hübscher et al. (2009), observing intra-salt reflections to intersect the top of the salt and terminate into mud volcanoes at the seabed. Alternatively, fluids may continue to migrate vertically by progressive evaporite dissolution until having breached the evaporite unit and gaseous muddy fluids are drained at the seabed. Figure 3.8b may represent such a case, where a vertical zone of chaotic reflections extends from the sub-salt domain through a depression at the BES into a topographically positive structure at the seabed. This structure is interpreted as a mud volcano, where fluid migration has probably been initiated in the early Messinian by forming a pockmark at the BES with continued fluid migration until Quaternary times. Again, instances from the southern Levant Basin have shown several mud volcanoes, located off the Israeli coast or situated at the seabed close to the Nile deep-sea fan (Loncke et al., 2004; Gradmann et al., 2005; Netzeband et al., 2006b).

In conclusion, additional evidence for fluid migration below, into and out of the Messinian evaporite unit is shown (Fig. 3.8). Whereas initial fluid escape was likely

triggered by sea level lowstand at the onset of the Messinian Salinity Crisis, the process of fluid flow continues today, evidently along pathways established in early Messinian times. Even the presence of 1.5 km thick sealing evaporite deposits does not seem to represent an obstacle for fluids to reach the present-day seabed.

3.5.4 Evaporite deformation in the Levant Basin

Interpretation of various seismic sections throughout the Levant Basin reveals quite significant spatial variability in the structural style of evaporite deformation. Relating individual evaporite structures to a specific deformation mechanism is complicated by 2D seismic data lacking the third dimension, but also by several deformation mechanisms which are likely to act in combination. Neglecting small-scale complexity, I focus on the structural characteristics of evaporites on a basin-wide scale, aiming to establish a model of geographically variable evaporite deformation mechanisms, their related driving forces and associated timing within the Levant Basin. For reasons of simplicity one may attempt to group different deformation styles to either represent i) tectonically-controlled evaporite deformation or ii) gravity-controlled evaporite deformation (here I consider salt deformation in response to sub-salt faulting to represent tectonically-controlled evaporite deformation). In order to distinguish between these two mechanisms, the following observation is considered: Investigating the structural style of various examples of salt tectonics within the Levant Basin, seismic sections described in Chapter 3.4.3 either show deformation where reflection ME-20 is clearly involved or deformation where reflection ME-20 remains largely horizontal and deformation is evident within stratigraphically higher salt units only (Figs. 3.2b,c, 3.3b,c, 3.5b, 3.6c, 3.7). While the existence of several intra-salt detachment levels is quite likely (Cartwright and Jackson, 2008; Cartwright et al., 2012), the question about the cause for such structural differences remains.

Significant deformation of ME-20 is most clearly observed in the northern Levant Basin, where the lower salt units were obviously deformed by a sub-salt extensional fault system (Figs. 3.2b, 3.3b). Furthermore, deformation involving ME-20 is observed directly south of the Latakia Ridge (Fig. 3.3c), where a Messinian period of tectonic convergence is known to have shortened evaporites at the northern side of the deformation front (Hall et al., 2005; Maillard et al., 2011). Finally, ME-20 has also significantly been deformed at marginal areas beneath the extensional domain where massive loading-induced salt withdrawal has occurred. This can be observed in the easternmost part of figure 3.6a and in seismic profiles published by Bertoni and Cartwright (2007a) and Dümmling and Hübscher (2011). However, further basinward, where salt withdrawal ceases, deformation of ME-20 distinctly decreases (Fig. 3.6a or Fig.10.5 in Dümmling and Hübscher, 2011).

Thus in the absence of sub-salt faults, thrust fronts (i.e. Latakia Ridge) or areas of massive salt withdrawal, ME-20 remains largely horizontal while stratigraphically higher evaporite units are often highly deformed. Examples of this structural style are observed in the central Levant Basin, the southern Levant Basin and east of the Eratosthenes Seamount, where significant intra-salt thrusting occurred above a near horizontal ME-20 reflection (Figs. 3.5b, 3.6c, 3.7). I therefore argue that ME-20 represents a mechanically stronger unit (or the top/base of a mechanically strong unit ME-I/ME-II), experiencing little deformation in the basinal part of the Levant Basin where sub-salt faults are absent. Except of areas where massive salt withdrawal occurs, deformation of ME-20 may thus represent a proxy for tectonically-controlled, rather than gravity-controlled evaporite deformation, while deformation above a near horizontal ME-20 reflection may have rather been driven by gravity. After having previously differentiated between fault-controlled evaporite deformation (Chapter 3.4.3.1) and evaporite deformation independent of sub-salt faults (Chapter 3.4.3.2), this subdivision is now followed and discussed as gravity vs. tectonically driven evaporite deformation. For each of these deformation mechanisms the associated driving forces and their relative timing will be discussed below.

3.5.4.1 Tectonically driven evaporite deformation

Mechanisms initiating tectonic evaporite deformation in the Levant Basin: Based on high-quality seismic data, this study presents first evidence of a spatial relation between the location of intra-evaporite structures and a large system of underlying extensional faults (Figs. 3.2b,c, 3.3b). This observation suggests a causative link between sub-salt faults and the internal evaporite deformation pattern. Given the presence of a distinct mechanical contrast between a brittle and a ductile unit, analogue and kinematic modelling studies demonstrate the development of fault-propagation folds (forced folds in Withjack et al., 1990 and Withjack and Callaway, 2000) in the ductile layer while experiencing extensional faulting of an underlying brittle unit (Withjack et al., 1990; Hardy and McClay, 1999; Withjack and Callaway, 2000; Jin and Groshong, Jr., 2006). Even though these studies provide a general mechanism for evaporite deformation in response to normal faulting, such folds are usually modeled as monoclines and do not resemble the complex fold pattern observed in seismic data of the present thesis (Withjack et al., 1990; Allmendinger, 1998). In order to account for the observed fold geometry, subsequent shortening is needed, amplifying previously established folds. Adamuszek et al. (2013) calculated the evolution of fold geometry for a single viscous layer within a viscous matrix, a situation comparable to that of intra-evaporite layers. Given the presence of a step-like perturbation subject to shortening, the resulting fold geometry is remarkably similar to that observed in seismic data of the present study (compare Fig. 12 by Adamuszek et al., 2013 to Fig. 3.2c). Recognizing that shortening of pre-existing fold-propagation faults may cause the deformation pattern observed in

the northern Levant Basin, the question about the responsible mechanism remains. Potential answers may lie in the structural style observed within evaporites directly south of the Latakia Ridge: in this area, intra-salt reflections are heavily deformed in the vicinity of a significant compressional sub-salt structure (Figs. 3.3a,b), suggesting a deformation mechanism related to plate convergence at the deformation front. This assumption is supported by observing ME-20 to be highly offset by densely spaced thrust faults (Fig. 3.3c). As previously discussed, ME-20 is believed to be mechanically strong and thus not easily deformed gravitationally. The occurrence of a Messinian tectonic event at the Latakia Ridge is also consistent with results by Hall et al. (2005), reporting a Late Miocene period of active tectonic compression and thrusting which abruptly ceased and turned into a strike-slip regime by the end of Messinian times. Consequently, the presently observed complex intra-salt deformation pattern is believed to reflect a phase of sub-salt extensional faulting and subsequent shortening at the deformation front – thus having primarily been controlled tectonically.

Within the area dominated by fault-controlled evaporite deformation, shortening within ME-III is evidently larger compared to shortening within ME20 (Figs. 3.2b,c, 3.3b). This is best understood by observing ME-III being frequently offset by thrust faults which are clearly absent within ME-20 (Figs. 3.2b, 3.3b). This style of shortening may reflect differences in the rheological properties of these two layers.

Timing of tectonic evaporite deformation in the Levant Basin: While sub-salt extensional faults in the northern Levant Basin are clearly manifested within the structural style of reflection ME-20 and reflections within unit ME-III, no offsets are recognized within Pliocene-Quaternary supra-salt deposits (Figs. 3.2b, 3.3b). I therefore suggest that extensional faulting was active during the Messinian period, ceasing after deposition of unit ME-III but prior to Pliocene clastic sediment input. As discussed above, syn-depositional fault-propagation faults have most likely experienced subsequent shortening to evolve into the presently observed complex fault pattern. Again, the compressional structure directly south of the Latakia Ridge at km 100 in figure 3.3a is much more pronounced within the salt unit than within supra-salt deposits, indicating the existence of a Messinian compressional event at the Latakia Ridge, as also reported by Hall et al. (2005). The observed absence of any topography at the top of the salt unit in response to sub-salt extensional faulting and subsequent compression at the Latakia Ridge is most likely attributed to a late Messinian erosion event, responsible for the basin-wide formation of a top-salt erosion surface (Dümmong and Hübscher, 2011; Lofi et al., 2011). Subsequently, planar evaporites were draped by Pliocene-Quaternary sediments.

The onset of Middle Miocene extensional faulting and its subsequent imprint on evaporite deformation in the northern Levant Basin is summarized in the following

conceptual model: Early Miocene sediments were cut by several extensional faults in Middle Miocene times (Fig. 3.10a), with faulting, sedimentation and subsidence (Hawie et al., 2013) continuing contemporaneously throughout the Middle and Late Miocene (Fig. 3.10b). During the Messinian Salinity Crisis, 1.5 km thick evaporites were precipitated in the Levant Basin, experiencing syn-depositional extensional faulting. Extensional faulting initiated the formation of monoclinial fault-propagation folds in the evaporite unit (Fig. 3.10c). These folds acted as nucleation points which accommodated subsequent, late Messinian tectonic shortening, evolving into the presently observed complex intra-salt deformation pattern (Fig. 3.10d). Locally, faults in the sub-salt domain may act as preferential pathways for fluid migration into the evaporite unit (Figs. 3.10c,d).

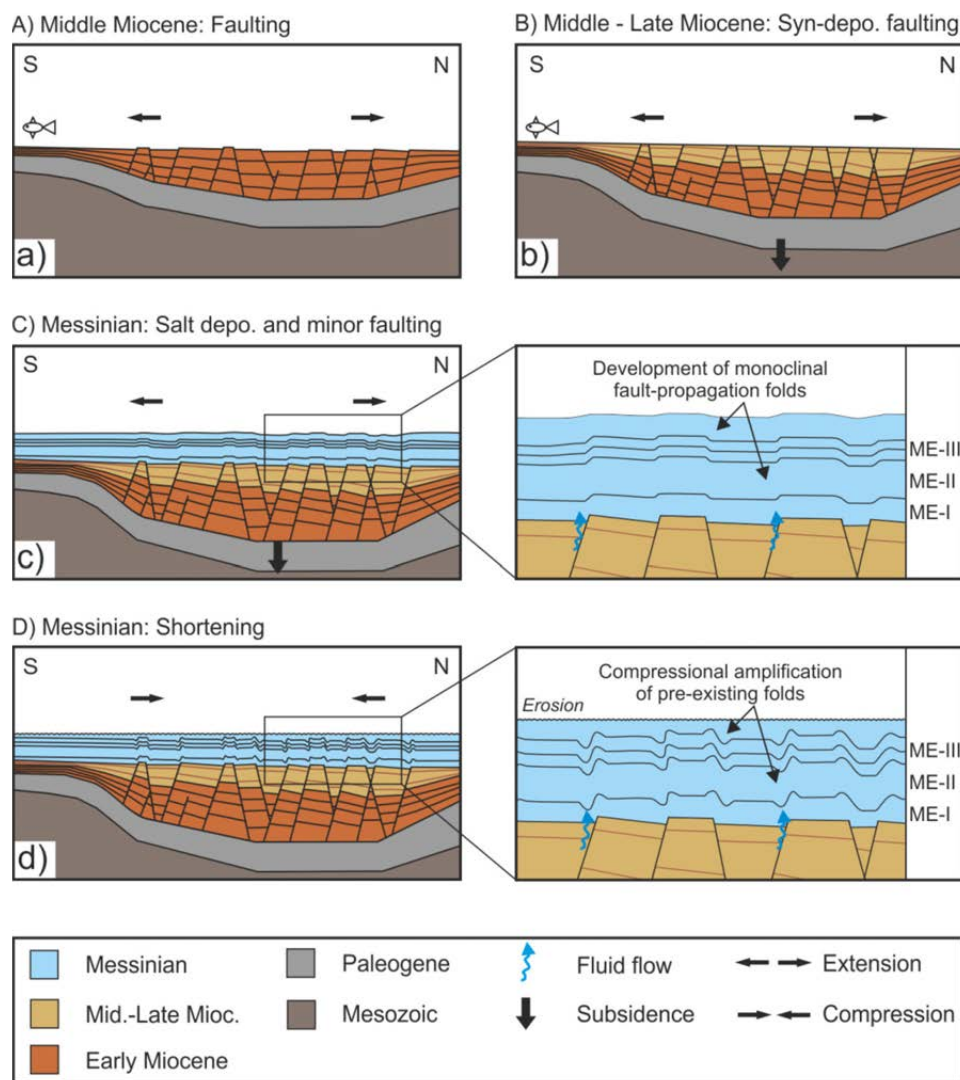


Figure 3.10 Conceptual model illustrating the timing of extensional faulting and the evolution of fault-controlled evaporite deformation in the northern Levant Basin. The location of the model cross section approximately equals the profile shown in figure 3.2a. **a)** Extensional faults developed in Middle Miocene times. **b)** Subsequently, sedimentation, subsidence and faulting continued throughout the Middle-Late Miocene, **c)** causing the formation of fault-propagation folds in the Messinian evaporite unit. **d)** Intra-evaporite folds were modified by late Messinian shortening due to plate convergence at the Latakia Ridge.

3.5.4.2 Gravity-driven evaporite deformation

Mechanisms of gravity-driven evaporite deformation in the Levant Basin: Evaporite deformation in response to gravitational forces was widely reported from the Levant Basin, and has generally been related to gravitational gliding due to inclination of sub-salt strata (Gradmann et al., 2005; Netzeband et al., 2006b; Cartwright and Jackson, 2008) or gravity spreading as a consequence of differential sediment loading (Loncke et al., 2006; 2010; Netzeband et al., 2006b; Cartwright et al., 2012; Gvirtzman et al., 2015). Inclination of sub-salt strata was previously related to northwestward tilting of the Levant Basin (Netzeband et al., 2006b), uplift of Mt. Camel (Steinberg et al., 2010; Gvirtzman et al., 2013) and uplift or tilting of the Levant Margin (Gradmann et al., 2005; Cartwright and Jackson, 2008). In contrast, load-induced spreading of Messinian salt was associated with sediment loading at the Levant coast as well as basinward sediment delivery of the Nile deep-sea fan (Gaullier et al., 2000; Loncke et al., 2006; 2010, Netzeband et al., 2006b; Cartwright et al., 2012).

Whether salt has deformed in response to loading or tilting cannot be easily differentiated based on the intra-salt deformation pattern alone. However, one diagnostic criterion may exist: while gravity gliding in response to basement inclination can have happened any time since initial evaporite deposition, gravity spreading in response to differential loading must have occurred post-depositionally. Thus, one way to differentiate between tilt- and loading-induced evaporite deformation is by assessing the timing of salt contraction. If evaporites have experienced gravity-driven syn-depositional deformation, gliding must have occurred. In contrast, both mechanisms could principally account for post-depositional evaporite deformation. However, the vast sediment delivery into the southern Levant Basin by the Nile deep-sea fan is likely to have overpowered evaporite deformation driven by tilting and loading at the Levant Margin – Nile deep-sea fan induced loading was even reported to force evaporites to creep upslope at the southern Levant margin (Gvirtzman et al., 2015). Further support for the significance of Nile derived sediment loading on evaporite deformation comes from analysis of fault and fold orientation offshore Israel and within the Levant Basin, letting Cartwright et al. (2012) and Netzeband et al. (2006b) conclude, that Nile induced evaporite spreading is clearly of greater importance in driving basinward salt contraction than loading and uplift at the Levant Margin. For simplicity, Nile-derived differential sediment loading is thus regarded as the main driving mechanism inducing post-depositional evaporite deformation in the Levant Basin.

Timing of gravity-driven evaporite deformation in the Levant Basin: Syn-depositional gravity-driven evaporite deformation (gliding): In this study, heavily faulted evaporites are observed to underlay little deformed sediments of Pliocene-

Quaternary age at the eastern flank of the Eratosthenes Seamount and in the central Levant Basin (Figs. 3.6c, 3.7). Differences in the magnitude of shortening within salt and supra-salt deposits were previously related to strain partitioning along intra- and top-salt-detachments (Cartwright et al., 2012). However, with offsets of up to 450 m, intra-salt thrusts imaged at the eastern flank of the Eratosthenes Seamount and in the central Levant Basin are significantly larger than those structures presented by Cartwright et al. (2012) (Figs. 3.6c, 3.7). Even though strain partitioning along detachments may occur, post-depositional salt deformation at marginal areas of the Levant Basin is usually also reflected by deformation within Pliocene-Quaternary supra-salt sediments (Netzeband et al., 2006b). Given the significant size of intra-salt thrusts shown here, these structures should coincide with more strongly deformed Pliocene-Quaternary sediments if faulting has occurred post-depositionally. Consequently, evaporites at the eastern flank of Eratosthenes Seamount and in the central Levant Basin have presumably experienced a phase of syn-depositional deformation.

Addressing the timing of this syn-depositional deformation event more specifically, the following observation is taken into account: At the eastern flank of Eratosthenes Seamount, ME-III reflections converge towards a large thrust fault directly west of the seamount (Fig. 3.7). This may indicate syn-depositional stratal thinning towards this structure and suggests evaporite deformation at the time of ME-III deposition. Consequently, salt deformation west of the Eratosthenes Seamount may have been largely synchronous to the intra-Messinian deformation event reported by Gvirtzman et al. (2013). In combination with previously reported results, this study thus indicates the occurrence of a Messinian phase of salt deformation on a basin-wide rather than a local scale. While uplift of Mt. Camel has initiated syn-depositional salt deformation offshore Israel (Gvirtzman et al., 2013), evaporites have additionally experienced an intra-Messinian deformation event at the Latakia Ridge (see Chapter 3.5.4.1), in the central and in the western Levant Basin – presumably reflecting a major period of plate tectonic reorganization within the Eastern Mediterranean.

Post-depositional evaporite deformation (spreading): In the southern Levant Basin (at the location of figure 3.5a), intra-salt thrusts clearly coincide with the locations of thrusts in the Pliocene-Quaternary overburden, suggesting salt and supra-salt deformation to have occurred simultaneously (Fig. 3.5b). Thus evaporites in the southern Levant Basin have deformed post-depositionally, presumably as a consequence of Nile-derived differential sediment loading. Bertoni and Cartwright (2007a) postulate Nile-induced spreading to have already been active since Messinian times, causing syn-depositional evaporite deformation off the Israeli coast. However, no significantly thick intercalated clastic sediment units were observed within the evaporites directly north of the Nile deep-sea fan (Loncke et al., 2006; 2010), contradicting a syn-depositional phase of evaporite spreading.

According to observations in this study, deformation of Pliocene-Quaternary sediments above intra-salt thrust faults is most significant in the southern Levant Basin (Figs. 3.5a,b) and decreases towards the north (Figs. 3.2b, 3.3b,c). While small northwest-southeast trending seabed folds east of the Eratosthenes Seamount are likely to be the results of Nile-induced spreading (Fig. 4 in Loncke et al., 2006), even less folding is observed within Pliocene-Quaternary sediments in the northern Levant Basin (Figs. 3.2b, 3.3b,c). A possible explanation was given by Loncke et al. (2006) by means of seismic interpretation and analogue modelling. These authors showed the Eratosthenes Seamount to have acted as a distal buttress to northeastward directed evaporite spreading. Therefore spreading induced evaporite deformation may still moderately affect Pliocene-Quaternary sediments east of the Eratosthenes Seamount, but this effect is expected to strongly decline towards the Latakia Ridge.

3.5.4.3 Synthesis of salt deformation in the Levant Basin

The discussion above is summarized in a map, showing evaporite deformation mechanisms to vary spatially (Fig. 3.11). While evaporites in the southern Levant Basin have predominantly experienced post-depositional gravity spreading due to Nile-derived differential sediment loading (Gauillier et al., 2000; Loncke et al., 2006; 2010; Netzeband et al., 2006b), the effect of loading strongly decreases towards the north. In the northern part of the basin, findings of this study demonstrate that salt has mainly deformed tectonically in response to a Messinian event of sub-salt extensional faulting and subsequent tectonic compression at the Latakia Ridge. Combining observations of this study with previous findings suggests that multiple deformation mechanisms have altered the shape of Messinian salt, particularly in the southern and central Levant Basin. During Messinian times, evaporites have experienced a phase of syn-depositional gliding in response to Mt. Camel uplift (Gvirtzman et al., 2013) and northwestward basement tilt (Netzeband et al., 2006b), followed by post-depositional deformation driven by Pliocene uplift of the Levant coast (Gradmann et al., 2005; Cartwright and Jackson, 2008) and differential sediment loading at marginal areas (Cartwright et al., 2012).

This compilation emphasizes the complexity of salt tectonics in the Levant Basin, where evaporites have deformed in response to a set of principle salt tectonic deformation mechanisms (gliding, spreading, plate tectonics) which have additionally acted syn- and/or post-depositionally. The Levant Basin thus represents a prime example for studying the influence of various driving mechanisms on incipient deformation of a geologically young salt giant.

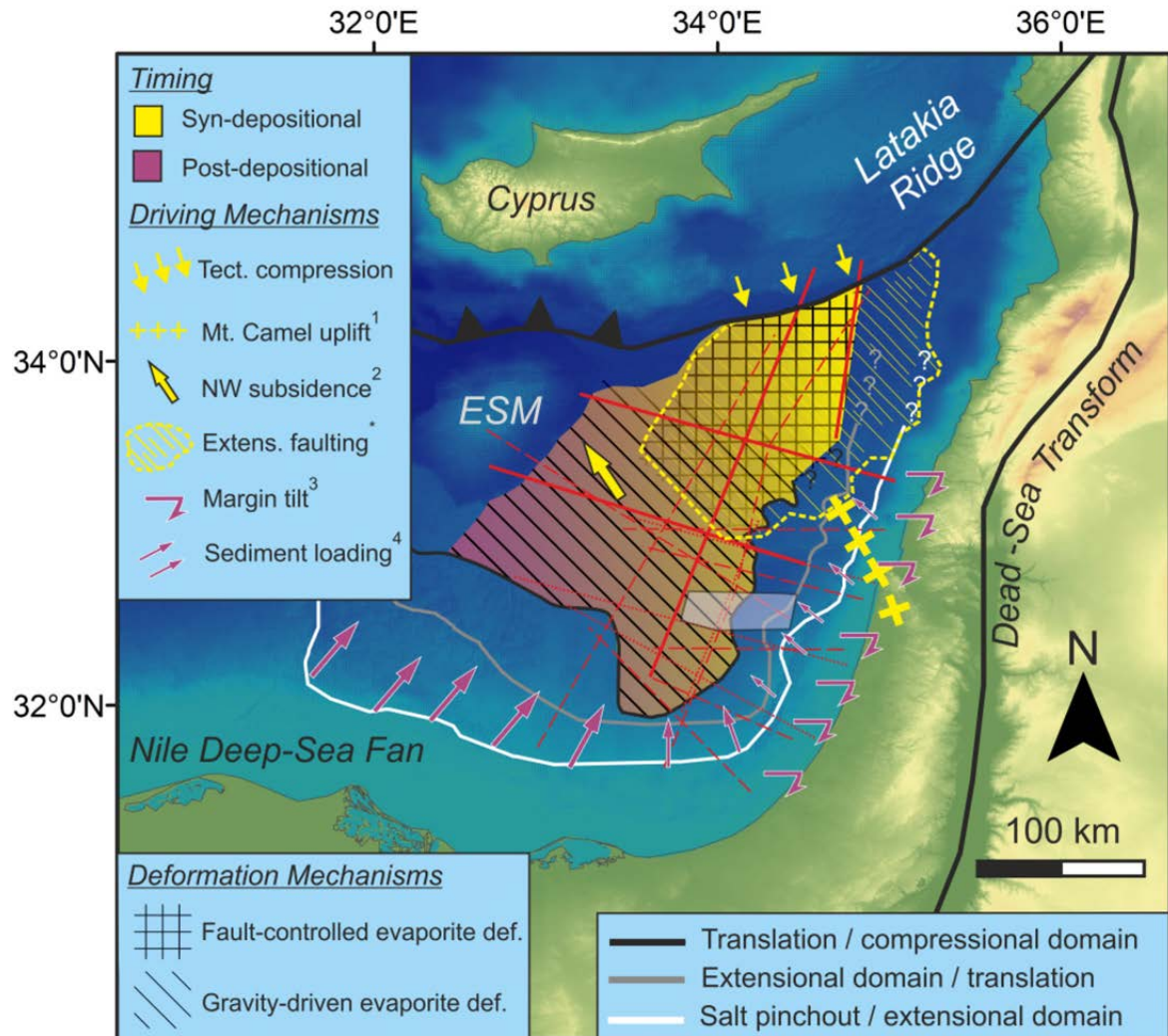


Figure 3.11. Conceptual map showing the spatial variability of salt deformation mechanisms and the spatial and temporal variability of their related driving forces. Note that I only distinguish between salt deformation mechanisms (gravity vs. tectonics) and the timing of salt deformation within the area affected by compressional salt tectonics. The areal distribution of the Messinian salt is approximated by the salt pinchout. There is no sharp boundary between syn- and post-depositional deformation but rather a large transient area being affected by both deformation phases. The same applies to evaporites being affected by gravity vs. tectonically-controlled deformation. Lines delineating the boundaries between evaporite pinchout/extension, extension/translation and translation/compression were taken from Gradmann et al. (2005); Netzeband et al. (2006b) and Cartwright and Jackson (2008). In the westernmost part of the map, these boundaries were drawn according to the presence of extensional and compressional structures at the seabed, as shown by Loncke et al. (2006). Red lines represent the seismic database used for drawing the map. Bold red lines are seismic profiles from this study. Dotted red lines represent industry seismic data, partly published by Dümmong and Hübscher (2011). Stippled red lines are published by Gradmann et al. (2005) and Netzeband et al. (2006b). The blue shaded area represents the study area of Gvirtzman et al. (2013). ESM=Eratosthenes Seamount. Mechanisms driving salt deformation according to ¹Gvirtzman et al., 2013; ²Netzeband et al., 2006b; ³Gradmann et al., 2005; Cartwright and Jackson, 2008; ⁴Loncke et al., 2006; 2010; Netzeband et al., 2006b; Cartwright et al., 2012. *The locations of extensional faults were drawn according to Kosi et al. (2012).

3.6 Conclusions

Until now, salt deformation in the basinal part of the Levant Basin was considered to result from gravity-driven processes only. In this study, I present first evidence of internal evaporite deformation in relation to a sub-salt Miocene extensional fault system. Based on interpretation of high-quality pre-stack depth migrated seismic data, the following conclusions are drawn:

- Miocene deposits in the northern Levant Basin are dissected by numerous extensional faults with maximum offsets of up to 600 m. Faulting has started in Middle Miocene times and lasted until the end of the Messinian.
- In the northern Levant Basin, intra-evaporite folds clearly coincide with the location of Miocene extensional faults. In order to explain the complex intra-evaporite fold pattern, I suggest extensional faulting to have caused the formation of intra-salt fault-propagation folds, acting as nucleation points to accommodate subsequent tectonic shortening at the Latakia Ridge.
- Different deformation mechanisms have altered the original shape of the Messinian evaporites in the Levant Basin. In the southern Levant Basin, post-depositional evaporite deformation occurred by gravity spreading as a consequence of Nile-derived differential sediment loading. The impact of differential loading appears to decline towards the north, where Pliocene-Quaternary deposits remain fairly undisturbed and significant tectonically-controlled syn-depositional evaporite deformation prevails.
- Vertical zones of reduced amplitudes and push-down reflections are locally observed near faults in the sub-salt domain. These zones terminate into phase-reversed bright spots within the lower part of the evaporites, suggesting gaseous fluids to migrate into the salt.
- A model-based processing and residual moveout analysis approach is used to develop a high-resolution velocity model of the Messinian evaporites. Velocities are higher for acoustically transparent evaporite sequences (3850-4240 m/s) compared to more reflective layers (3650-4030 m/s). Showing no significant thickness variations, reflective evaporite sequences are more likely related to variations in evaporite facies than to the presence of interbedded clastics.

Acknowledgements

I thank Spectrum for kindly providing the seismic data shown in Figs. 3.2-3.8. Benedikt Weiss is thanked for helpful discussions throughout the preparation phase of the manuscript. Constructive comments of the editor (of *Marine Geology*), Frank Strozyk and two anonymous reviewers are appreciated.

4 The fate of salt in the Cyprus subduction zone

Abstract

Messinian evaporites of locally more than 3 km thickness occupy the subduction zone between Cyprus and Eratosthenes Seamount. Based on a dense grid of reflection seismic profiles, I report on compressional salt tectonics and its impact on the Late Miocene to Quaternary structural evolution of the Cyprus subduction zone. Results show that evaporites have experienced significant post-Messinian shortening along the plate boundary. Shortening has initiated allochthonous salt advance between Cyprus and Eratosthenes Seamount, representing an excellent example of salt which efficiently escapes subduction and accretion. Further east, between Eratosthenes Seamount and the Hecataeus Rise, evaporites were compressively inflated without having advanced across post-Messinian strata. Such differences in the magnitude of salt tectonic shortening may reflect a predominately north-south oriented post-Messinian convergence direction, raising the possibility of a later coupling between the motion of Cyprus and Anatolia than previously thought. Along the area bordered by Cyprus and Eratosthenes Seamount, a prominent step in the seafloor represents the northern boundary of a controversially debated semi-circular depression. Coinciding with the southern edge of the salt sheet, this bathymetric feature is suggested to have formed as a consequence of compressional salt inflation and seamount directed salt advance. Topographic lows on top of highly deformed evaporites are locally filled by up to 700 m of late Messinian sediments. The uppermost 200 m of these sediments were drilled in the course of ODP Leg 160 and interpreted to represent Lago Mare-type deposits (Robertson, 1998d). Lago Mare deposits are spatially restricted to the western part of the subduction zone, pinching out towards the east while

presumably continuing into the Herodotus Basin further west. I suggest a sea level control on late Messinian Lago Mare sedimentation, facilitating sediment delivery into basinal areas while inhibiting Lago Mare deposition into the desiccated Levant Basin. Locally, early salt deformation is believed to have provided additional accommodation space for Lago Mare sedimentation, resulting in the presently observed minibasin-like geometry.

4.1 Introduction

The African-Anatolian plate boundary directly south of Cyprus is characterized by incipient continent-continent collision between Cyprus and Eratosthenes Seamount (Fig. 4.1) (Robertson, 1998c; Schattner, 2010). Substantial advances in understanding the nature and tectonic evolution of Eratosthenes Seamount were made in the course of ODP Leg 160 (Fig. 4.1b). The top and the northern flank of Eratosthenes were targeted at the three southernmost drilling locations (Sites 966, 965, 967), where Miocene to Cretaceous carbonates were sampled (Fig. 4.1b) (Robertson, 1998a). Drilling at the northernmost ODP location (Site 968) reached Messinian Lago Mare deposits (Robertson, 1998d), but little information on deeper strata exist owing to limited penetration of previously published seismic data (Limonov et al., 1994; Robertson et al., 1995b; Galindo-Zaldívar et al., 2001). Only recently published reflection seismic lines initially showed the presence of thick Messinian evaporites which occupy large parts of the present-day collision zone (Klimke and Ehrhardt, 2014; Montadert et al., 2014). As the existence of such a significant salt layer alters previous tectonic interpretations, the structural evolution of the Cyprus collision zone needs reinvestigation in order to account for the structural imprint of kilometer-thick tectonically shortened evaporites.

Recovery of 200 m of late Messinian Lago Mare deposits directly south of Cyprus represents an important ODP Leg 160 drilling result – given that similar deposits are absent throughout the neighboring Levant Basin (Robertson, 1998a,b,d; Netzeband et al., 2006b; Lofi et al., 2011; Roveri et al., 2014). Further investigation including mapping and structural characterization of these Lago Mare sediments is needed to understand their structural evolution and spatially limited occurrence.

In this study, I use a dense grid of reflection seismic profiles together with bathymetric data collected during RV MARIA S. MERIAN research cruises MSM 14/2 and MSM 14/3 in 2010 across the Cyprus collision zone (Ehrhardt, 2011; Hübscher, 2012) (Fig. 4.2). The following objectives are defined: i) to investigate compressional salt tectonics and the impact of salt on the style of deformation between Cyprus/Hecataeus Rise and Eratosthenes Seamount. ii) To describe the distribution and geometry of Lago Mare sediments and provide an explanation for their spatially limited occurrence. iii) To integrate these results into previous

knowledge in order to present an up-to-date picture of the Messinian to Quaternary tectonostratigraphic evolution of the Cyprus subduction zone.

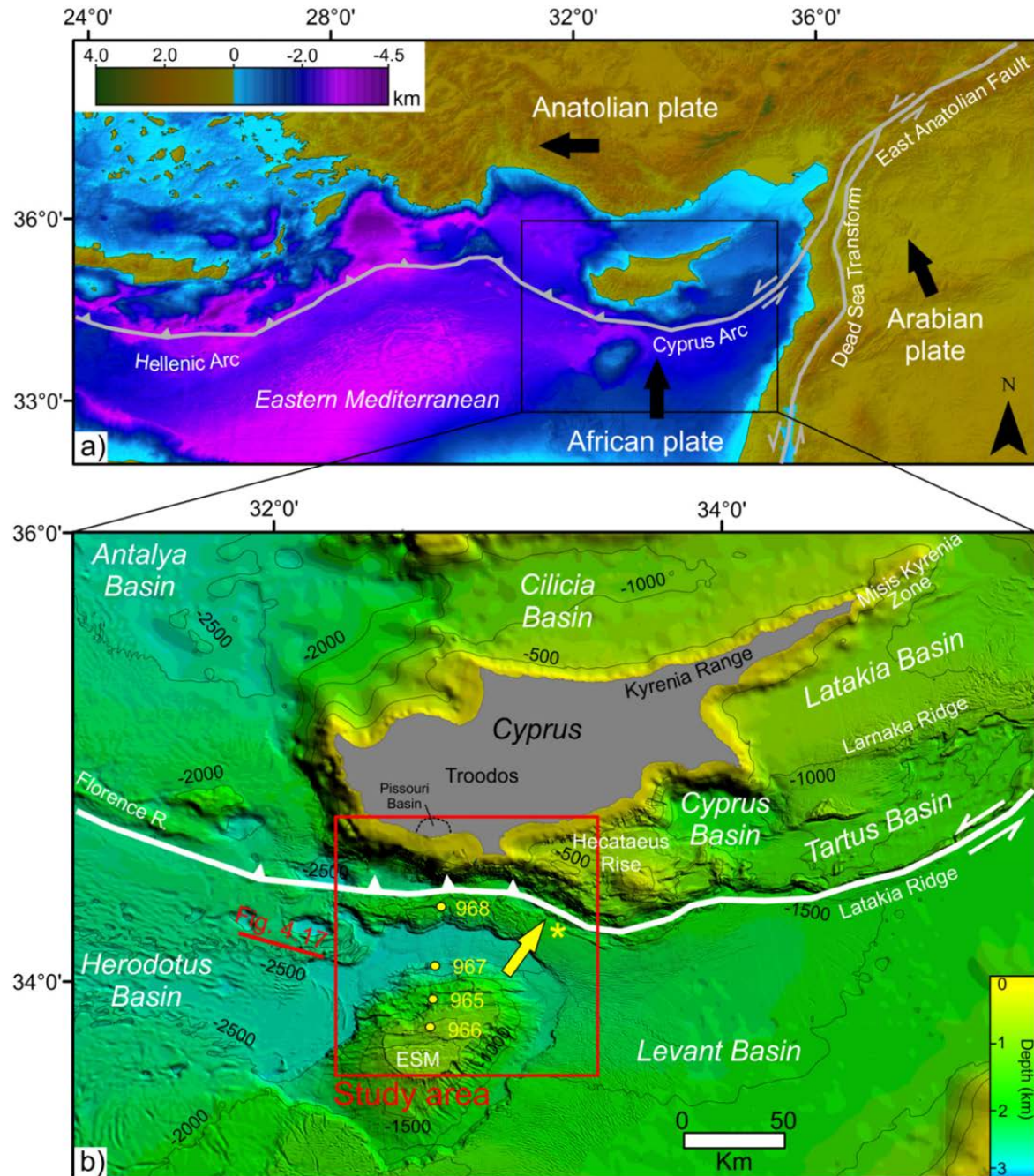


Figure 4.1 a) Simplified tectonic map of the Eastern Mediterranean. Black arrows indicate the direction of plate motion drawn after Schattner (2010). The large-scale tectonic configuration is based on Hall et al. (2014) and Schattner (2010). Topography and bathymetry data were retrieved from GeoMapApp® (<http://www.geomapapp.org>) (Ryan et al., 2009). b) Location map of the study area. Yellow dots represent ODP Leg 160 drilling locations. For references on the location of the plate boundary (bold white line) see Chapter 4.2.1. The location of the Pissouri Basin was drawn after Robertson et al. (1991). Data used in compiling this map is specified in section 4.3.1. ESM=Eratosthenes Seamount. *The yellow arrow indicates the present-day convergence direction along the central segment of the Cyprus Arc according to Wdowinski et al. (2006).

4.2 Geological background

4.2.1 Present-day geodynamic situation

The geodynamic regime of the easternmost Mediterranean is presently characterized by relative motion between the African, Anatolian and Arabian plates (Fig. 4.1a). The main plate boundaries are defined by northward motion of Arabia with respect to Africa along the Dead Sea Transform and convergence between Africa and Anatolia along two arcuate zones, the Cyprus and Hellenic Arcs (Le Pichon and Kreemer, 2010).

The eastern segment of the Cyprus Arc terminates at the East Anatolian Fault and separates the Levant Basin to the south from the Tartus and Latakia Basins further north (Fig. 4.1b). Refraction seismic velocities suggest the Levant Basin to be underlain by continental crust (Netzeband et al., 2006a). Based on deep seismic reflection data, Vidal et al. (2000a) described this segment of the Cyprus Arc as a ca. 30 km wide zone of strike-slip deformation rather than representing a sharp plate boundary. Southeast of Cyprus, the Tartus and Latakia Basins pass into the Hecataeus Rise – a topographically raised structure of presumably continental origin (Fig. 4.1b) (Welford et al., 2015). The plate boundary is generally believed to continue south of the Hecataeus Rise, where the sedimentary fill of the Levant Basin shows a near vertical termination against the Hecataeus Rise (Vidal et al., 2000a,b). Further west, the plate boundary runs along the southern margin of Cyprus, where it separates the ophiolitic terrain of Cyprus from Eratosthenes Seamount (Fig. 4.1b). This seamount represents a prominent bathymetric feature which rises 1.5 km above the surrounding seafloor (Kempler, 1998). High-resolution multibeam bathymetric data from Eratosthenes Seamount were shown by Mascle et al. (2001; 2006), Loncke et al. (2002; 2006; 2009) and Klimke and Ehrhardt (2014). Based on reflection seismic interpretation, the areal extent of the subsurface part of the Eratosthenes carbonate platform was mapped by Montadert et al. (2014) and Klimke and Ehrhardt (2014). Montadert et al. (2014) interpreted the Eratosthenes Seamount to represent the elevated part of a larger continental block which was rifted from Arabia during Triassic to Lower Cretaceous times and may thus be regarded as the conjugate margin of the Levant Margin further east.

As the Eratosthenes Seamount has entered the collision zone since Late Miocene–Early Pliocene times, this part of the convergence zone is inferred to presently be in the state of incipient continent-continent collision (Kempler, 1998; Robertson, 1998d). GPS-based studies on relative plate motion along the Cyprus Arc show a northeast-southwest convergence direction between the African and Anatolian plates (McClusky et al., 2003; Wdowinski et al., 2006). As the eastern segment of the Cyprus Arc is oriented parallel to this convergence direction, strike-slip faulting prevails. In contrast, the western segment is oriented more perpendicularly to the

direction of plate motion and thus subject to thrust faulting (Wdowinski et al., 2006).

Based on differences in seismicity along the western segment of the Cyprus Arc expressed by relatively strong and shallow earthquakes directly southwest of Cyprus vs. fairly deep earthquakes at the westernmost Cyprus Arc, Wdowinski et al. (2006) suggest these two domains to be divided by a crustal-scale tear fault, separating ongoing subduction at the westernmost Cyprus Arc from a collisional setting further east. Such a lateral change from collision to ongoing subduction is strengthened by seismic tomography, indicating the presence of a downgoing slab to cease from west to east, somewhere in the vicinity of Cyprus (Faccenna et al., 2006; Biryol et al., 2011). Gravity modelling along a profile stretching from Eratosthenes to southern Turkey supports the idea of a downgoing slab to be present underneath Cyprus (Robertson, 1998d; Ergün et al., 2005).

4.2.2 Miocene to recent evolution

Miocene: During Miocene times, compressional tectonic activity in southern Cyprus occurred along four west-northwest to east-southeast trending lineaments (Robertson et al., 1991; Eaton and Robertson, 1993). Compression related uplift of structural lineaments led to the formation of tectonically-controlled sub-basins which have subsequently been filled by carbonates of the Miocene Pakhna Formation (Robertson et al., 1991; Eaton and Robertson, 1993). Offshore Cyprus, lithological evidence from the plateau area of Eratosthenes Seamount (ODP Sites 965 and 966 in Fig. 4.1b) document a distinct change from pelagic to shallow water carbonate deposition, implying that the seamount was uplifted in the order of 1 km by Early Miocene times (Robertson, 1998a,d; Whiting, 1998). As uplift of Eratosthenes Seamount occurred coeval to tectonic activity along the Cyprus-lineaments, Robertson (1998d) related these events to the southward migration of the subduction zone to its present-day position. Miocene tectonic activity is further evident along the eastern segment of the Cyprus Arc. Based on seismic reflection data, Hall et al. (2005) reported the presence of several northeast-southwest trending anticlines north of the Latakia Ridge, where seismic imaging of Miocene growth strata indicates a Miocene phase of northwestward directed tectonic compression.

After experiencing uplift to a near sea level position, the Eratosthenes Seamount plateau area was draped by shallow water carbonates and colonized by reefs (Robertson, 1998a,d). In contrast, at ODP Site 967 (Fig. 4.1b), no Miocene deposits were recovered, except of a thin layer of Messinian gypsum inferred from borehole logging data. Being situated at the northern slope of the seamount, this site was either subject to Miocene erosion, re-sedimentation or sediment bypass to more basal levels (Robertson, 1998a,b,d). While little Miocene sediments are

evident on top of Eratosthenes Seamount, massive sediment accumulation occurred in the Levant Basin (Steinberg et al., 2011). Reflection seismic profiles south of the Latakia Ridge show that Miocene strata reach a thickness of more than 3 km (Reiche et al., 2014).

In Late Miocene times, a change from compressional to extensional faulting occurred in southern Cyprus, as evident by structural data from southern Cyprus sedimentary basins (Kinnaird and Robertson, 2012). Kinnaird and Robertson (2012) interpreted the onset of extensional faulting as a consequence of slab-rollback and associated extension within the overriding plate at a period of ongoing subduction.

Messinian: The Messinian Salinity Crisis was initiated at 5.96 Ma and a substantial drop in sea level (1.5-2.0 km) occurred (Hsü et al., 1973; Krijgsman et al., 1999; Netzeband et al., 2006b; Gargani and Rigollet, 2007). Evaporites onshore Cyprus are composed of various gypsum facies and were precipitated in small tectonically-controlled semi-enclosed sub-basins at shallow water depths (Robertson et al., 1995a). Astronomical tuning of such deposits within the Pissouri Basin (Fig. 4.1b) revealed an onset of gypsum precipitation at 5.96 Ma, coeval to evaporite deposition across the entire Mediterranean area (Krijgsman et al., 2002). Based on new sedimentological data, Manzi et al. (2014) suggested that the lowermost onshore Cyprus evaporite unit correlates with the second stage of the Messinian Salinity Crisis (5.6-5.5 Ma) while evaporites deposited during the first stage (5.96-5.60 Ma) were widely eroded and re-deposited (Manzi et al., 2014). In the Levant Basin, the Messinian salinity crisis resulted in deposition of around 1.5 km thick evaporites (Netzeband et al., 2006b). The erosive nature of the top of the salt unit is clearly evident within the Levant Basin (Netzeband et al., 2006b; Bertoni and Cartwright, 2007a), whereas only local observations point towards erosion at its base, exemplified by canyon incision off the Israeli coast (Bertoni and Cartwright, 2006). Insight into evaporite stratigraphy in the Levant Basin is based on seismic data, showing evaporites to be composed of alternating acoustically transparent and more reflective layers (Bertoni and Cartwright, 2005; 2006; Netzeband et al., 2006b; Hübscher et al., 2007; Hübscher and Netzeband, 2007; Dümmong and Hübscher, 2011; Gvirtzman et al., 2013; Reiche et al., 2014). Acoustically transparent layers were commonly related to the presence of halite while reflective intervals have either been interpreted as clastic intervals or variations in evaporite facies (Garfunkel, 1984; Gradmann et al., 2005; Reiche et al., 2014).

Lithological evidence from ODP Sites 965 and 966, drilled at the top of Eratosthenes Seamount at water depths between approximately 1.0 and 1.5 km (Fig. 4.1b), showed that the seamount was subaerially exposed during Messinian desiccation and subject to erosion, karstification and soil development (Major et

al., 1998; Robertson, 1998b). Based on reflection seismic data acquired prior to ODP Leg 160, evaporites were believed to be absent further north within the collision zone flanked by Cyprus and Eratosthenes Seamount (Limonov et al., 1994; Robertson et al., 1995b). However, recently published reflection seismic lines refute such assumptions by showing the presence of kilometer-thick evaporites within the area bordered by Cyprus and Eratosthenes Seamount (Klimke and Ehrhardt, 2014; Montadert et al., 2014).

At the northern flank of Eratosthenes Seamount, the presence of a thin layer of gypsum was inferred from borehole logging data at ODP Site 967 (Robertson, 1998a). This layer was assigned to the Lago Mare stage of the Messinian Salinity Crisis – a circum-Mediterranean period of brackish water conditions (Orszag-Sperber, 2006). Even thicker (approximately 200 m) Lago Mare deposits were drilled at the northernmost ODP Site 968 (Robertson, 1998d). These argillaceous sediments were mainly sourced from the Troodos Massif and contain intercalations of detrital gypsum and lithoclasts (Robertson, 1998a,b,d). As the isotope signature of gypsum samples at ODP Site 968 points towards precipitation under marine rather than brackish conditions, Blanc-Valleron et al. (1998) suggested that gypsum at Site 968 was initially deposited onshore Cyprus and later – during the Lago Mare stage – transported to the offshore domain. The Lago Mare stage is further evident within evaporites onshore Cyprus (Orszag-Sperber et al., 2009). In the Pissouri Basin, this interval is characterized by alternating gypsum beds and paleosols, indicating repeated subaerial exposure (Rouchy et al., 2001).

Despite the geologically short time interval of the Messinian Salinity Crisis, this period was characterized by considerable tectonic events in the Cyprus area and associated offshore domains. Based on reflection seismic investigations along the Cyprus Arc, significant Messinian tectonic activity is inferred along the plate boundary (Hall et al., 2005; Maillard et al., 2011). At the same time, tectonic activity is also believed to have affected Cyprus (Robertson et al., 1995a). Outcrop studies from western Cyprus suggested the occurrence of several tectonic pulses during Messinian times (Orszag-Sperber et al., 2009).

Pliocene-Quaternary: After termination of the Messinian Salinity Crisis, the Mediterranean experienced rapid refilling and all sites penetrated during ODP Leg 160 record a change to deep-marine sedimentation at the beginning of Pliocene times (Robertson, 1998a,d). Eratosthenes Seamount experienced rapid subsidence indicated by recovery of bathyal microfossils from the lowest part of the Early Pliocene succession (Robertson, 1998a). Subsidence was accompanied by northward tilting of the seamount and the development of several east-west trending normal faults (Limonov et al., 1994; Kopf et al., 2005). The quantitative decompacted subsidence history at Site 967 suggests that Eratosthenes

Seamount has subsided in the order of 1.8 km during post-Messinian times (Whiting, 1998). The cause of such rapid and significant subsidence was either interpreted as an isostatic response to massive circum-Eratosthenes evaporite precipitation (Major et al., 1998) or tectonic collision and subsequent underthrusting beneath the island of Cyprus (Robertson, 1998d).

Uplift of Cyprus began in Late Pliocene times. The Troodos Massif is inferred to have vertically moved as a single tectonic entity and high rates of uplift have lasted until Middle-Late Pleistocene times (Kinnaird et al., 2011). Datings of marine sediments at outcrops in eastern Cyprus provided further constraints on uplift rates during the past 40 ka, ranging from 1.8 to 4.1 mm/yr (Harrison et al., 2013).

Associated with the onset of westward Anatolian escape at 5 Ma (Bozkurt, 2001), the Cyprus Arc was suggested to have experienced a change in convergence direction from northwest-southeast to northeast-southwest directed compression (Ben-Avraham et al., 1995; Hall et al., 2005). However, recent structural investigations onshore southern Cyprus let Kinnaird and Robertson (2012) conclude that such a change did not occur prior to 3 Ma. At this time, a coupling of Cyprus to the westward motion of Anatolia may have been triggered by collision between Cyprus and Eratosthenes Seamount (Kinnaird and Robertson, 2012).

4.3 Data and methods

4.3.1 Multibeam bathymetric data

Bathymetric data were acquired during RV MARIA S. MERIAN cruises MSM 14/2 and MSM 14/3 using a SIMRAD EM120 echo sounder system (Ehrhardt, 2011; Hübscher, 2012). The hull-mounted transducer of the EM120 system periodically (12 kHz) emits a pulse and subsequently records the travel time after the signal was reflected at the seafloor. Travel times were converted to depth using information on water velocity that were measured at two locations during RV MARIA S. MERIAN cruise MSM 14/2 and range approximately from 1510 to 1550 m/s depending on the water depth (Ehrhardt, 2011). High-resolution bathymetric data shown in figure 4.1b additionally comprise data acquired during the BLAC survey in 2003 which targeted the eastern segment of the Cyprus Arc (Benkhelil et al., 2005; Maillard et al., 2011). In order to obtain continuous bathymetric data coverage, gaps within the high-resolution MSM 14/2 and the BLAC data were locally filled with data from the ETOPO2 bathymetry (U.S. Department of Commerce, NOAA/NGDC, 2006).

4.3.2 Multichannel seismic data

4.3.2.1 Seismic data acquisition

One set of seismic data shown in this study was acquired during RV MARIA S. MERIAN cruise MSM 14/2 (Fig. 4.2). Data were acquired with a 3900 m long, 312 channel digital streamer, recording energy released by two G-Gun arrays with a total volume of 3100 in³, operated at a pressure of ~150 bar (2000 PSI) and dominant frequencies centered around 40Hz. Data were acquired at a constant ship's speed over ground. Shot intervals of 18 s, 14 s and 10 s therefore correspond to shot-distances of approximately 50 m, 37.5 m and 25 m, respectively.

A second seismic dataset was acquired during the following cruise MSM 14/3 (Hübscher, 2012). For data acquisition, two GI-Guns with a total volume of 300 in³ were shot at a constant time interval of 6-9 s with dominant frequencies centered around 100 Hz. Seismic energy was recorded by a 24-channel analogue streamer with an active length of 600 m and a group spacing of 25 m.

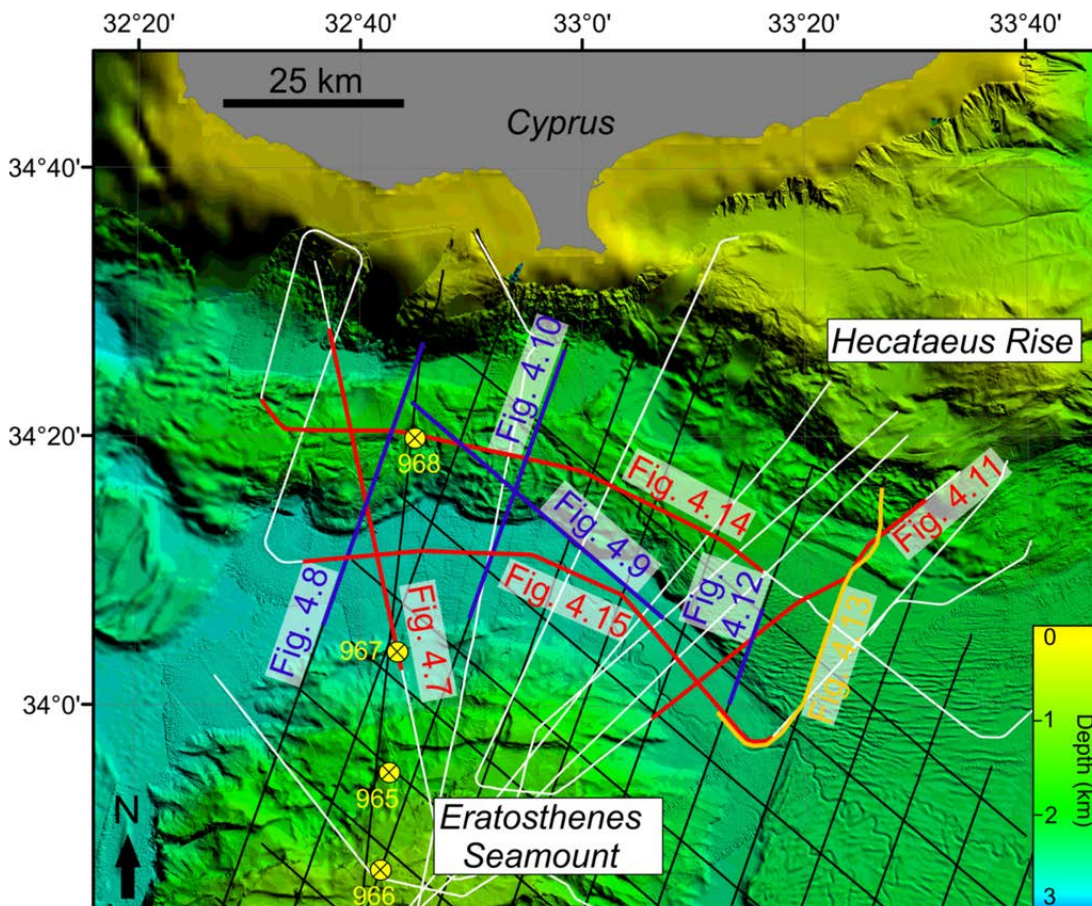


Figure 4.2 Bathymetric map of the study area, showing the locations of seismic profiles. Black profiles represent MSM 14/2 data and white profiles were acquired during MSM 14/3. Red and blue lines mark the profile locations shown in this study, differentiating between MSM 14/3 and MSM 14/2 data, respectively. The orange line indicates the location of figure 14 composed of both MSM 14/2 and MSM 14/3 data. Yellow dots indicate the locations of ODP Leg 160 drilling sites.

4.3.2.2 Seismic data processing

After geometry setup, the MSM 14/2 data were CMP-binned. The different shot-intervals of 50 m, 37.5 m and 25 m led to a nominal CMP fold of 39, 52 and 78, respectively. Source designature, bandpass filter and multiple attenuation were applied before the first semblance based velocity analysis. Multiple attenuation processes were refined by surface-related wave-equation multiple estimation techniques and complemented by a radon velocity filter. Due to the far offset and high moveout differences the radon filter worked fine and supplemented the surface-related wave-equation multiple estimation technique tool. After a second velocity analysis the data were NMO corrected, stacked and migrated using a Kirchhoff time migration algorithm (see Ehrhardt, 2011).

Processing of MSM 14/3 data involved trace geo-referencing and binning with a CMP-distance of 12.5 m, leading to an approximate fold of 15. For the main set of MSM 14/3 seismic profiles, post-stack time-migrated CRS-Stacks were produced, following the CRS processing workflow described in Chapter 2.2. This processing workflow was applied to profiles shown in figures 4.7c,d, 4.13e,f, 4.15 and 4.16.

In order to better image deeper, particularly sub-salt reflections, I additionally applied an alternative processing workflow to profiles shown in figures 4.7a,b, 4.11 and 4.14b,c. For these profiles, I first produced partly time-migrated gathers which were subsequently used for CRS-stacking, following the procedure introduced by Dell et al. (2012). Details on this processing workflow are described in Chapter 2.2. Finally, stacked profiles were exported to sgY-format and uploaded to Petrel v. 2012 for seismic interpretation. All seismic profiles are either displayed with a vertical exaggeration (VE) of 8 or 4.5. As VE was calculated using a velocity of 1500 m/s, the provided VE represents an upper boundary.

4.3.2.3 Industry seismic data

Apart from reflection seismic data acquired in the course of MSM 14/2 and MSM 14/3, one industry seismic profile is shown in this study to illustrate the stratigraphic situation west of Eratosthenes Seamount (Fig. 4.17). For details on acquisition geometry and the processing workflow applied to this dataset, the reader is referred to Peace et al. (2012) and Reiche et al. (2014).

4.4 Results

4.4.1 Physiography

Combined interpretation of MSM 14/2 and MSM 14/3 seismic and bathymetric data shows the presence of several east-northeast to west-southwest striking normal and thrust faults, offsetting the northern flank of the seamount (Fig. 4.3). The seamount is partly surrounded by an up to 25 km wide, locally more than

2.7 km deep, semi-circular trough which I define as the Southern Domain. Towards the north and northeast, this semi-circular depression is separated from relatively elevated seafloor by a prominent bathymetric step (Figs. 4.3, 4.4a). Based on seismic interpretation, this step corresponds to the southern and western limit of the Messinian evaporites and will be addressed as the Central Domain. The area directly adjacent to the southern slope of Cyprus and the Hecataeus Rise is referred to as the Northern Domain (Fig. 4.3b).

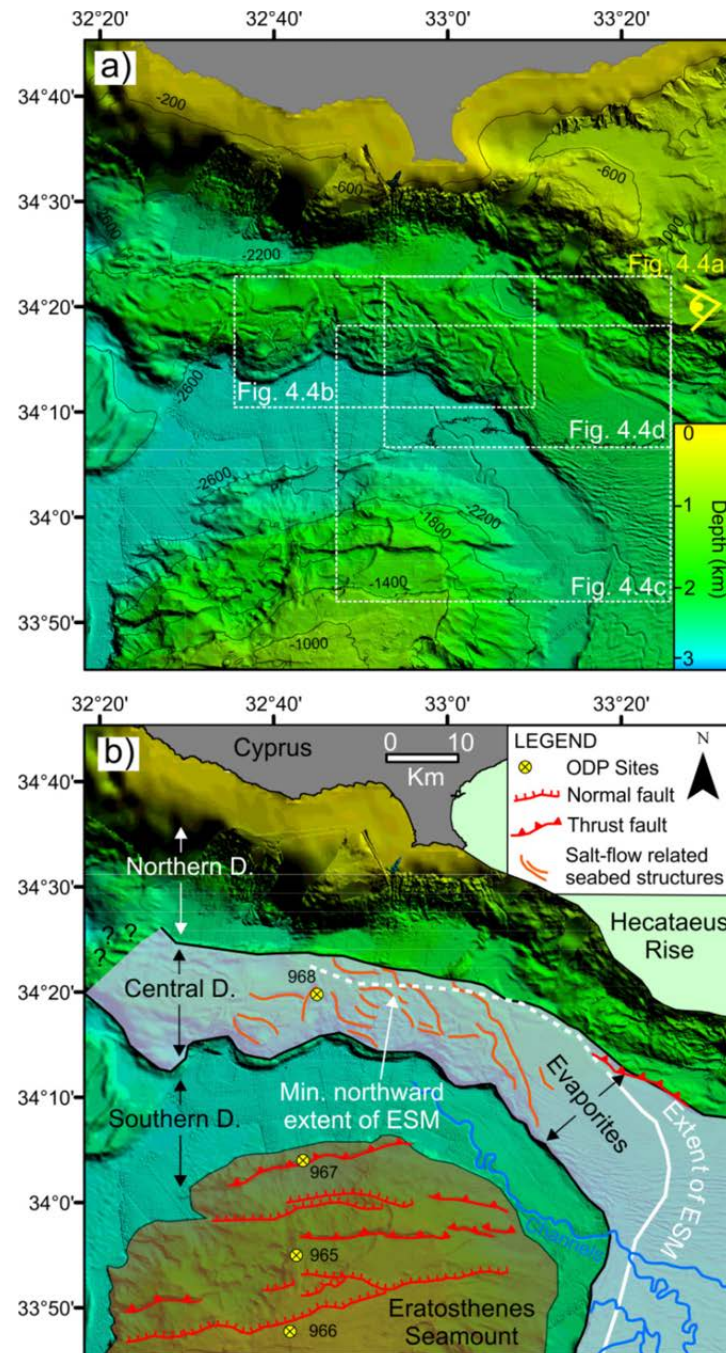


Figure 4.3 a) Bathymetric map of the study area b) with the interpreted version below. The area between Cyprus/Hecataeus Rise and the Eratosthenes Seamount (ESM) was subdivided into three semi-circular zones, termed Northern Domain, Central Domain and Southern Domain. The blue shaded area represents the mapped distribution of seismic Unit 3 (Messinian evaporites).

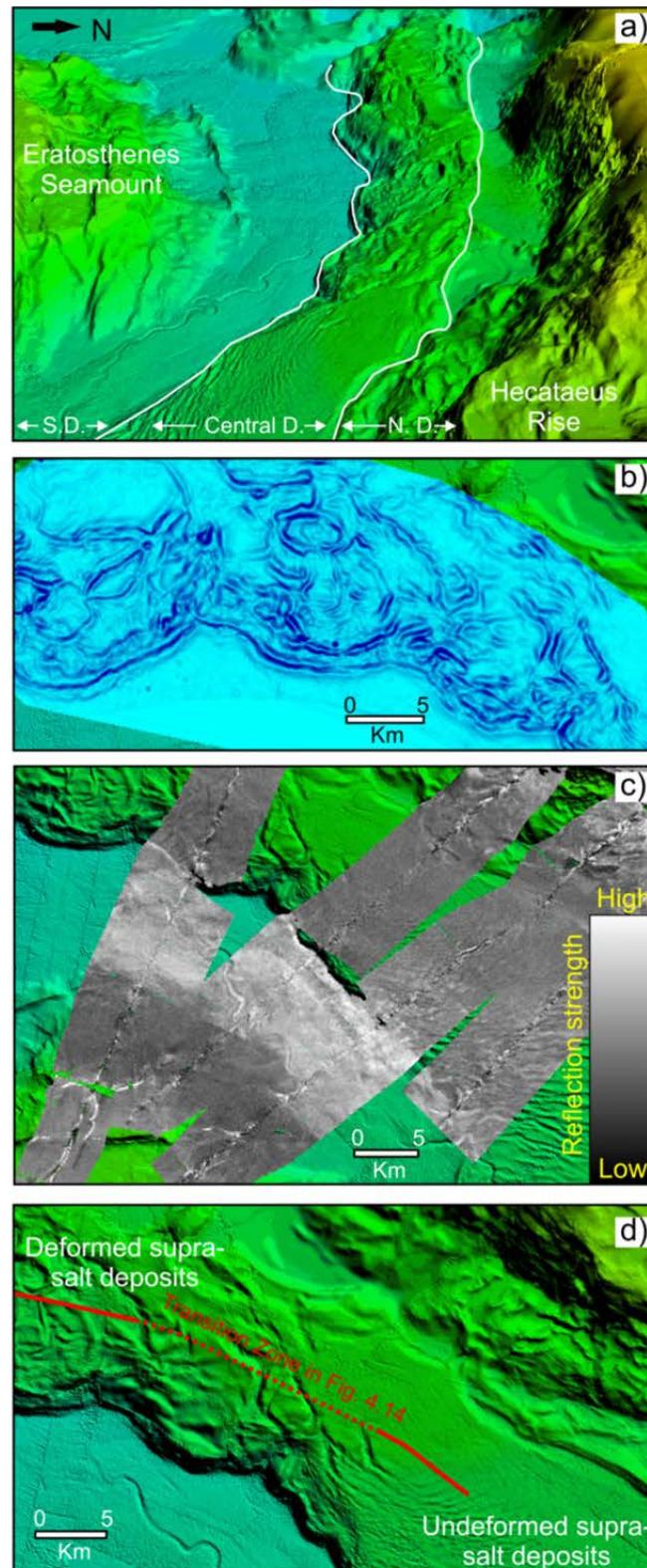


Figure 4.4 **a)** 3D view into the collision zone between Cyprus and Eratosthenes Seamount, subdivided into three domains as shown in figure 4.3b. The approximate viewing angle is indicated by the yellow eye in figure 4.3a. The vertical exaggeration is 8. **b)** Residual bathymetry of highly deformed seafloor underlain by Messinian evaporites. For location see figure 4.3a. **c)** Backscatter data across the eastern part of the study area. The area directly south of Eratosthenes (Southern Domain) is characterized by high reflectivity compared to the surrounding seafloor. For location see figure 4.3a. **d)** Enlarged section showing a significant eastward decrease in seafloor deformation above the Messinian evaporite unit. For location see figure 4.3a.

Between Cyprus and Eratosthenes, the seafloor of the Central Domain reaches a depth of 2-2.5 km and is characterized by a complex morphology (Figs. 4.3, 4.4a,b). The residual bathymetric map highlights areas which deviate from the general trend of the seafloor morphology, clearly revealing the presence of several radial ridges and graben-like structures (Fig. 4.4b). Further east, this zone of complex seafloor morphology passes into an area of fairly undisturbed seafloor, where small ripple-like structures shape the present-day seabed (Figs. 4.3, 4.4a,d). Locally, southeast-northwest oriented, meandering channels terminate at the eastern flank of Eratosthenes Seamount, with one channel continuing westwards into the bathymetric depression of the Southern Domain (Fig. 4.3).

Reaching depths between 1.9 and 2.4 km, the seafloor of the Northern Domain shows a very different morphology: there, intensive seafloor deformation is present southwest of the Hecataeus Rise while a largely undeformed seafloor is observed directly south of Cyprus (Figs. 4.3, 4.4a). Further north, the seafloor rapidly ascends towards Cyprus and the Hecataeus Rise.

Backscatter data, covering the northeastern part of the study area indicate variations in seafloor reflectivity (Fig. 4.4c). At the transition between Eratosthenes Seamount and the Southern Domain, a sharp increase in reflection intensity is observed. Within the Southern Domain, backscatter values remain comparably high before decreasing sharply at the bathymetric step towards the Central Domain.

4.4.2 Seismic stratigraphy

The sedimentary succession of the study area is subdivided into five main units with Unit 1 consisting of three sub-units termed Units 1a, 1b and 1c (Figs. 4.5, 4.6). Unlike the overall subdivision into five main units, the subdivision of Unit 1 differentiates between sediment units of limited and spatially variable extent instead of representing a chronostratigraphic subdivision. Figure 4.5 provides an overview of the seismic reflection character and inferred lithology for each unit defined in this study. Units 1a, 2 and 5 were drilled in the course of ODP Leg 160 at Sites 967 and 968. A correlation between these ODP Sites and seismic profiles crossing the core locations is shown in figure 4.6 together with an overview of the suggested stratigraphic framework and its possible correlation to the onshore Cyprus stratigraphy after Robertson et al. (1991).

Below, the acoustic characteristics, termination surfaces and, if possible, thickness distribution of each unit are described in detail, followed by a short interpretation of its corresponding age and lithology.

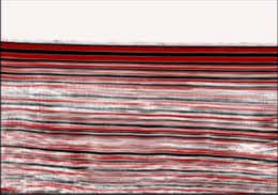
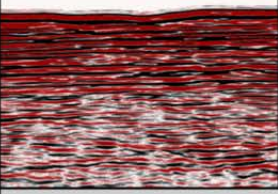

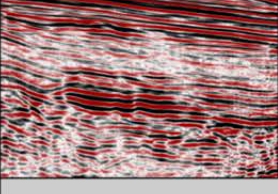
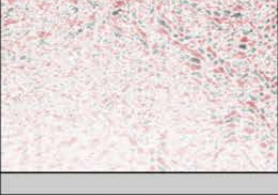

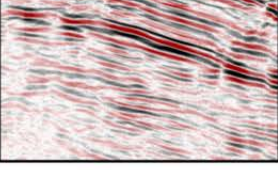
Seismic example	Seismic unit	Reflection character	Correlation to ODP leg 160	Lithology
	Unit 1a	Parallel, lateral continuous low to medium-amplitude reflections.	Entirely drilled at Sites 968*	Based on ODP Sites 967, 968*: Nannofossil ooze and clay. At Site 968 silt-turbidites in the uppermost part.
	Unit 1b	Parallel, locally wavy, continuous to semi-continuous high-amplitude reflections.	Possibly drilled at Site 967	Unknown since correlation to Site 967 is not conclusive.
	Unit 1c	Parallel to slightly divergent, lateral continuous low to medium-amplitude reflections.	Possibly drilled at Site 967	Unknown since correlation to Site 967 is not conclusive.
	Unit 2	Parallel to sub-parallel, semi-continuous high-amp.-reflections at the top and base, often separated by low-amp. reflections.	Uppermost 200 m drilled at Site 968*	Based on ODP Site 968*: Mudstone, silt turbidites and minor gypsarenite. Unknown below 200m.
	Unit 3	Acoustically transparent with local occurrence of internal high-amp. reflections.	Not drilled	Presumably halite, with local intercalations of gypsum, anhydrite etc. (see Chapter 4.4.2.3 and references therein)
	Unit 4	Parallel, lateral continuous medium-amplitude reflections.	Not drilled	Correlates to Miocene clastics of the Levant Basin see Ehrhardt and Klimke (2014).
	Unit 5	Parallel, lateral continuous high-amp. reflections at the top. Parallel, semi-continuous low-medium amp. reflections below.	Uppermost ~500 m drilled at Site 967*	Based on ODP Site 967*: ~410 m of carbonates and 90 m of tectonic breccia. Unknown below.

Figure 4.5 Overview of the defined seismostratigraphic units, their reflection characteristics and relation to ODP Leg 160 drilling locations. Each seismic example corresponds to a size of 2 km (horizontal) x 0.5 s TWT (vertical). Units 1c, 1b, 1c, 2, 3, and 5 data examples were retrieved from MSM 14/3 data while the Unit 4 data example was taken from MSM 14/2 data. *Robertson (1998d).

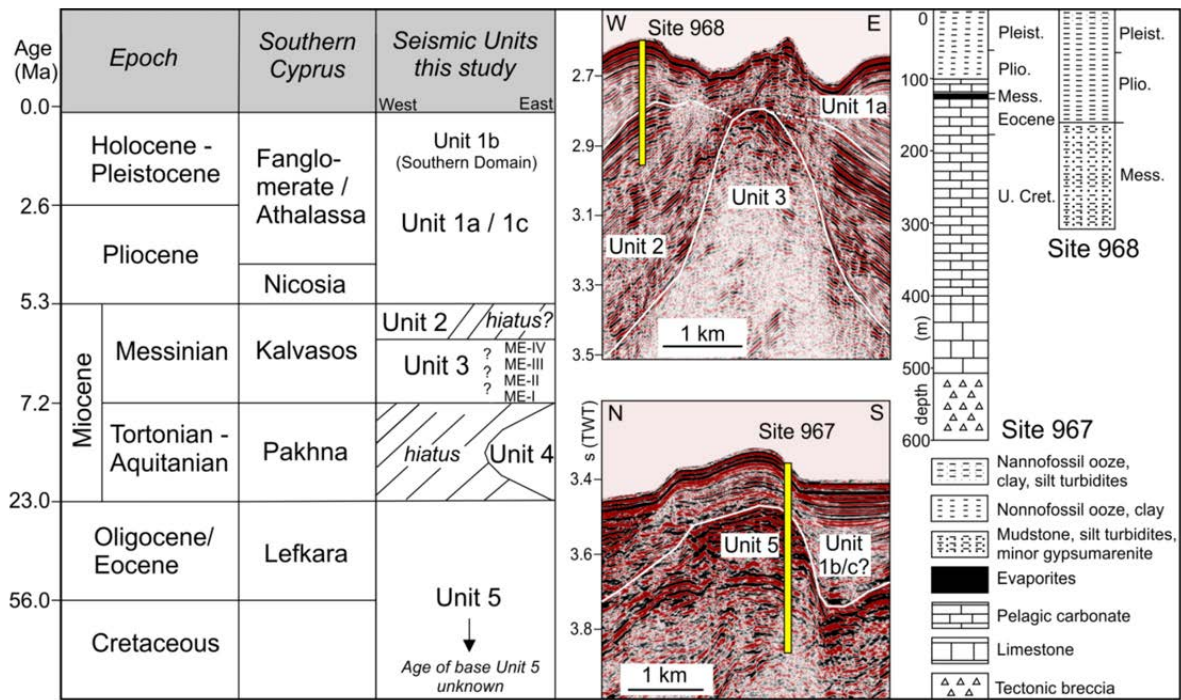


Figure 4.6 Stratigraphy of the study area and its suggested correlation to the onshore Cyprus stratigraphy (after Robertson et al., 1991). Units 1a and Unit 2 were penetrated at ODP Site 968. Units 1b/1c were possibly penetrated and Unit 5 was drilled at Site 967. Approximate location and depth of ODP cores are indicated within the seismic profiles which were acquired across the drilling Sites. The lithologic summary of successions drilled at Sites 967 and 968 was taken from Robertson (1998d).

4.4.2.1 Unit 5

Unit 5 represents the lowermost identified seismic unit. This unit is characterized by two prominent, parallel, high-amplitude reflections at its top, followed by a set of low to medium-amplitude, parallel reflections below (Figs. 4.5, 4.7a,b, 4.8a,b, 4.9-4.13, 4.14b,c). The base of Unit 5, if observable, is defined by another high-amplitude reflection event (Figs. 4.8a,b, 4.9-4.12). Reflections within Unit 5 generally dip towards the north (Figs. 4.7a,b, 4.8a,b, 4.10, 4.11) and towards the west (Figs. 4.9, 4.14b,c, 4.15), associated with a progressive north- and westward deepening of this unit. The presence of Unit 5 is easily identified within the Southern Domain (Figs. 4.7a,b, 4.8a,b, 4.9-4.12, 4.13a,b, 4.15). Tracing Unit 5 from the Southern into the Central Domain is accompanied by upward bending reflections within Unit 5 (Figs. 4.7-4.12, 4.13a,b). This transition is best observed within the least complex profiles shown in figures 4.11 and 4.12. In these profiles one can easily identify how upward bending reflections within Unit 5 closely correspond to the presence and progressive northward thickening of Messinian evaporites associated with Unit 3. With evaporites being characterized by seismic velocities easily twice as high as adjacent sedimentary strata (e.g. see Reiche et al. (2014) for velocities of the Levant Basin evaporites), the apparent upward bend of Unit 5 is attributed to velocity effects (pull-ups) caused by overlying high-velocity evaporites rather than representing true structural deformation within Unit 5. At the

structurally more complex western end of the study area, reflections within Unit 5 can occasionally be followed from the Central into the Southern Domain, similarly exhibiting upward bending reflections below the southern tip of the evaporite unit (Figs. 4.7c,d, 4.10). Occasionally, Unit 5-reflections fade out completely at the transition towards the sub-salt domain, re-appearing some km further beneath the evaporites (Unit 3), where reflections associated with Unit 5 arrive earlier in time (Figs. 4.8, 4.9). Local absence of reflections within Unit 5 across the transition zone may be related to structural complexity in the supra-salt units, causing scattering and attenuation of seismic energy. Coincidence between supra-salt faults and a reduction in Unit 5 reflectivity can similarly be observed in figure 4.12 (km 10-19), where Unit 5 remains clearly traceable beneath the salt (Unit 3), but shows a significant reduction in reflection strength where supra-salt sediments are heavily faulted. Locally, Unit 5 velocity pull-ups do not exactly coincide with the southern salt limit. For instance in figures 4.7c,d the top Unit 5-reflection appears to be bent upwards already 1 km south of the southern salt (Unit 3) termination. As described in Chapter 4.4.3.1, sediments near the southern salt limit exhibit chaotic reflections and show indications of compressional deformation. The southern salt limit is often not a sharp boundary thus leaving the possibility that evaporites may be intermingled with adjacent sediments. Therefore deformed, possibly evaporite-bearing sediments adjacent to the salt body (Unit 3) may be characterized by higher velocities than undisturbed sediments further south and thus similarly cause velocity pull-ups below.

Unit 5 is generally more difficult to follow in the Central Domain (e.g. Figs. 4.14b,c). However, along figure 4.9 the northward extent of Unit 5 is particularly well resolved. Along this profile, Unit 5 can be followed further north than the location of ODP Site 968. The minimum northward extent of Unit 5 is plotted in figure 4.3b.

Interpretation: The uppermost part of Unit 5 (approximately 500 m) is acoustically composed of parallel high-amplitude reflections and was penetrated at ODP Site 967 (Fig. 4.6, profile km 3 in Fig. 4.7b). At Site 967, Eocene to Cretaceous pelagic carbonates were recovered, being part of the Eratosthenes carbonate platform succession (Fig. 4.6) (Robertson, 1998a). The base of Unit 5 is defined by identification of the lowermost parallel-high amplitude reflection. Being located far deeper than rocks recovered at any ODP Leg 160 drilling Site, lithological constraints for the lower part of Unit 5 are missing. However, the defined base Unit 5 horizon is located well within the Eratosthenes carbonate succession interpreted by Montadert et al. (2014) who developed a stratigraphic framework for the Eratosthenes Seamount. Being not the main focus of the present study, reflections associated with Unit 5 will for simplicity be addressed as the flank of Eratosthenes Seamount below.

4.4.2.2 Unit 4

Unit 4 is exclusively observed in the easternmost study area, directly south of the Hecataeus Rise (Figs. 4.11, 4.13a-d). Acoustically, Unit 4 is composed of a set of low to medium-amplitude, parallel reflections (Fig. 4.5). The upper termination of Unit 4 is defined by the base of Unit 3. Towards the southwest, Unit 4 onlaps northeastward dipping reflections of Unit 5 (Figs. 4.13c,d). Further north, Unit 4 terminates near vertically against chaotic reflections associated with the southwestern flank of the Hecataeus Rise (Figs. 4.11, 4.13a-d).

Interpretation: Unit 4 correlates with the uppermost part of Miocene clastics, widely present in the Levant Basin (e.g. Steinberg et al., 2011; Klimke and Ehrhardt, 2014). A detailed study on the Miocene succession directly east of Eratosthenes was recently published by Klimke and Ehrhardt (2014). Based on their interpretation, Miocene sediments onlap the flank of Eratosthenes Seamount and strongly decrease in thickness towards the west until pinching out near the location of the seismic profile shown in figure 4.13c (see Fig. 11b by Klimke and Erhardt, 2014).

4.4.2.3 Unit 3

Unit 3 is observed within the entire Central Domain and generally characterized by acoustic transparency (Figs. 4.5, 4.7-4.13, 4.14b,c). Internal reflections are locally identified within this unit, particularly in the eastern part of the Central Domain (e.g. km 30-35 in Fig. 4.11). The base of Unit 3 is defined by the upper termination of Unit 5 towards the east (km 50-75 in Fig. 4.14b,c). Further west (west of approximately km 45 in Fig. 4.14), its lower boundary follows a phase-reversed reflection event, delineating the top of a reflective package below (Unit 1c) (Figs. 4.7, 4.14d-f). Unit 3 shows a near vertical termination against highly deformed sediments at the southwestern flank of the Hecataeus Rise (Fig. 4.11). South of Cyprus, the northernmost limit of Unit 3 is not clearly defined (Figs. 4.7a,b, 4.8a,b, 4.10). The southward termination of Unit 3 occurs by rapid thinning along a steep flank, corresponding to a prominent step in the bathymetry (Figs. 4.7-4.12). Deposits associated with Unit 3 reach a maximum thickness of 1600 ms (TWT) directly west of the Hecataeus Rise, approximating to 3.2 km given a salt velocity of 4000 m/s (Fig. 4.18a) (Reiche et al., 2014). In the Central Domain between Cyprus and Eratosthenes Seamount, the thickness distribution of Unit 3 becomes more complex, associated with the presence of several diapiric structures observed within Unit 3 (Figs. 4.8a,b, 4.9, 4.14b,c, 4.18a). Focusing on the general trend, however, a decrease in thickness is observed towards the west, where local thickness maxima correspond to the presence of large diapiric structures (Fig. 4.18a).

Interpretation: Unit 3 can be traced along seismic profiles towards the east, correlating to thick Messinian evaporites previously imaged in the Levant Basin

(e.g. Netzeband et al., 2006b). Similar to thick evaporites in the Levant Basin, Unit 3 is believed to be largely composed of halite (Bertoni and Cartwright 2007a; Hübscher and Netzeband, 2007). Intra-salt reflections indicate lithological changes (Figs. 4.11, 4.13c,d), previously interpreted as variations in evaporite facies (Gradmann et al., 2005; Reiche et al., 2014). These internal reflections correlate to reflections ME-20 and reflection package ME-III, based on the latest stratigraphic framework of the Levant Basin evaporites by Hübscher et al. (2007).

4.4.2.4 Unit 2

Unit 2 is exclusively observed in the Central Domain, where its areal extent closely matches the area of highly deformed seafloor topography identified in figures 4.3 and 4.4 (Figs. 4.7a,b, 4.8-4.10, 4.14b,c, 4.16). Sediments of Unit 2 are easily recognized by their distinct acoustic properties, being characterized by parallel, high-amplitude reflections that are locally separated by a less reflective interval (Figs. 4.5, 4.16). Unit 2 frequently onlaps diapiric structures of Unit 3 and rarely oversteps their crests (e.g. Figs. 4.14b,c, 4.16). The thickness of Unit 2 varies greatly along the Central Domain, with a maximum of 700 ms (TWT) in the western part (locally, a thickness of up to 800 ms (TWT) is shown in figure 4.18b but such values result from the gridding algorithm and were not directly observed in the data). Such thickness maxima are only locally observed, generally related to depressions surrounded by salt diapirs of Unit 3. The thickness of Unit 2 strongly decreases towards the east, until completely pinching out at km 67 in figures 4.14b,c. In contrast to its eastern termination, the western limit of Unit 2 cannot be resolved owing to limited data coverage. However, a seismic profile located outside the main survey area of this study, west of Eratosthenes Seamount, shows an acoustically and geometrically similar unit (Fig. 4.17). Even though the base of Unit 2 could not be mapped with certainty in this profile, its upper part is well imaged and similarly characterized by parallel, high-amplitude reflections. It is therefore suggested that sediments associated with Unit 2 continue further west (Fig. 4.17).

Interpretation: The uppermost 200 m of Unit 2 were penetrated at ODP Site 968 (Fig. 4.6). Core studies have shown that these sediments consist of Cyprus-derived clastics with intercalations of gypsum. Such sediments were interpreted to represent Lago Mare deposits which accumulated under brackish water conditions in the final stage of the Messinian Salinity Crisis (Robertson, 1998d) and are now located on top of thick Messinian evaporites associated with Unit 3. Unfortunately, no reliable P-wave velocities were obtained for Unit 2 sediments at ODP Site 968 (Shipboard Scientific Party, 1996b). However, given the lithological composition of this unit, a P-wave velocity of averagely 2000 m/s presumably represents a good estimate, implying Unit 2 deposits to reach a maximum thickness of 700 m south of Cyprus. The frequently observed Unit 2 reflection pattern of parallel, high-

amplitude reflections separated by a package of low reflectivity (Fig. 4.16a) attests the heterogeneous nature of these sediments, pointing to at least three depositional sequences. Therefore only the uppermost 200 m of Unit 2 sampled at ODP Site 968 are regarded as Largo Mare deposits *sensu stricto*. This should be noted while usage is made of the term Largo Mare *sensu lato* with reference to the entire Unit 2 succession below.

4.4.2.5 Unit 1a

Unit 1a is composed of parallel, laterally continuous reflections of varying reflection intensity, identified in the Central and Northern Domains and within the easternmost Southern Domain (Figs. 4.5, 4.7-4.12, 4.13a,b,e,f, 4.14b,c, 4.15, 4.16). In the eastern part of the study area, Unit 1a is separated from Unit 3 by the Top Erosion Surface (TES) (e.g. Fig. 4.11) (according to the terminology of Messinian surfaces used by Lofi et al., 2011). Due to the absence of significant intra-Unit 3 reflectivity, the presence of erosion along the top of Unit 3 cannot be resolved by seismic profiles shown in this study. However, this reflection correlates to the TES widely observed in the Levant Basin (see Lofi et al., 2011 and references therein). Further west, Unit 1a is underlain by Unit 2. No erosional surface can be detected with certainty to separate these two units (e.g. Fig. 4.16). In the easternmost part of the study area, Unit 1a can be followed from the Central into the Southern Domain (Figs. 4.11, 4.13, 4.13a,b).

Due to significant structural complexity, the base of Unit 1a cannot be confidently followed into the Northern Domain (Fig. 4.11). While the uppermost few 100 ms (TWT) of strongly deformed sediments observable in the northernmost part of figure 4.11 (km 35-50) are likely to represent Unit 1a deposits, their base and thus thickness cannot be mapped with certainty. In the northernmost part of figure 4.10, Unit 1a-deposits occupy a small sub-basin, onlapping steeply dipping reflections of highly deformed strata below. The thickness distribution of Unit 1a could solely be mapped in the Central Domain, where thicknesses of up to 1100 ms (TWT) are reached (Fig. 4.18c).

Interpretation: Unit 1a can directly be correlated to ODP Site 968, where this unit was entirely drilled (Fig. 4.6). Based on core studies, these sediments consist of Pliocene-Quaternary nannofossil ooze, clay and silt turbidites which accumulated in a deep marine environment (Robertson, 1998a).

4.4.2.6 Unit 1b

Unit 1b is solely observed in the Southern Domain, internally characterized by wavy, parallel to sub-parallel, high-amplitude reflections (Figs. 4.5, 4.7-4.12, 4.13e,f, 4.15). The base of Unit 1b is defined by a distinct change in reflection characteristics, separating Unit 1b from a lower amplitude reflection package associated with Unit 1a/1c below. At its southern termination, Unit 1b onlaps a thin

layer of Unit 1a/1c deposits (Figs. 4.7a,b, 4.11). In the eastern part of the Southern Domain, Unit 1b onlaps faulted sediments associated with Unit 1a (Figs. 4.11, 4.12, 4.13e,f). Further west, Unit 1b appears to terminate near vertically against a prominent bathymetric escarpment, associated with the southward termination of Unit 3 (Figs. 4.7-4.10). The northernmost part of Unit 1b may be cut by thrust faults but a chaotic reflection pattern at the transition between the central and Southern Domains does not allow for a detailed interpretation (Figs. 4.7-4.10). Unit 1b shows a maximum thickness of 460 ms (TWT) in the easternmost study area, decreasing to less than 100 ms (TWT) towards the west (Fig. 4.18d).

Interpretation: As ODP Site 967 was drilled on top of an uplifted fault block near the interpreted southern termination of Unit 1b (Figs. 4.6, 4.7b), no direct correlation between Unit 1b and this ODP Site can be established. Along the seismic lines shown in figures 4.11, 4.12 and 4.13e,f, reflections associated with Unit 1b appear to onlap Unit 1a. Such observations imply a fairly recent, possibly Pleistocene or younger age for Unit 1b. High-amplitude, wavy internal reflections together with high backscatter reflection intensity (Fig. 4.4c) are indicative of an energetic depositional environment. Several seafloor channels extend towards/into the Southern Domain (Fig. 4.3b) and one of these channels was recently termed the Levant Turbidite Channel and shown to originate from the Levant slope (Gvirtzman et al., 2015). Therefore and based on the observed acoustic characteristics of Unit 1b, I suggest that this unit is dominantly composed of turbidites and channel-levee deposits.

4.4.2.7 Unit 1c

Unit 1c is composed of a set of horizontal, parallel to slightly divergent, low to medium amplitude reflections (Figs. 4.5, 4.7-4.10, 4.14b,c, 4.15). In the Southern Domain, Unit 1c shows onlap terminations against reflections associated with Unit 5 (Figs. 4.7-4.10, 4.15). The northward extent of these sediments is complicated by velocity effects associated with overlying evaporites. Zooming into the transition zone between the Central and Southern Domains, the lower part of Unit 1c appears to laterally continue from the Southern into the Central Domain (Figs. 4.7c,d). There, Unit 1c is separated from overlying evaporites by a prominent phase-reversed reflection, indicating a change from high-velocity evaporites to relatively lower velocity material below (Figs. 4.7, 4.14d-f). The apparent deformation at the transition zone, expressed by upward bending reflections, is attributed to velocity effects, mainly caused by overlying evaporites but also by adjacent deformed, possibly evaporite-bearing strata rather than indicating true structural deformation. This is essentially the same effect as already described for Unit 5. The thickness distribution of Unit 1c could only be mapped in the Southern Domain, as energy attenuation beneath evaporites of Unit 3 complicates interpretation of Unit 1c further north. The seismic profile shown in

figure 4.15 extends parallel to the bathymetric depression of the Southern Domain, revealing the thickness distribution of Unit 1c. In the western part of the Southern Domain, Unit 1c reaches a maximum thickness of 1040 ms (TWT) (Fig. 4.18e). Further east, reflections associated with Unit 1c onlap Unit 5, accompanied by a strong decrease in thickness (Figs. 4.15, 4.18e). Unit 1c nearly pinches out near a significant high of Unit 5, visible between km 50 and 60 in figure 4.15. However, the uppermost part of Unit 1c can be followed across this high, where it connects to sediments associated with Unit 1a. Note that the western part of figures 4.13e,f represents an enlarged version of the eastern edge of figure 4.15, showing Unit 1a to overlay Messinian evaporites. As figure 4.15 shows Unit 1c and Unit 1a to be partly connected and characterized by similar acoustic properties, I suggest that these two units essentially represent the same stratigraphic interval. However, as the observed local high within Unit 5 inhibits a direct correlation between Unit 1c and Unit 1a, these two Units were treated separately.

Interpretation: ODP Site 967 was drilled on top of an uplifted fault block near the pinchout of Unit 1c (Figs. 4.6, 4.7b). Sediments associated with Unit 1c are likely contained within the Pliocene-Quaternary succession drilled at ODP Site 967 even though a direct correlation cannot be established (see seismic data in figure 4.7b crossing ODP Site 967 in its southern part and extending to the vicinity of ODP Site 968 further north). In contrast, observing the lower part of Unit 1c to laterally continue beneath Messinian evaporites in the Central Domain may point towards a pre-Messinian age of these sediments. However, several lines of evidence contradict this assumption, rather suggesting a post-Messinian age for Unit 1c: i) in the easternmost part of figure 4.15, sediments associated with Unit 1c appear to correlate with Unit 1a which itself can be traced to ODP Site 968 and is clearly of Pliocene-Quaternary origin. ii) Furthermore, deposits associated with Unit 1c were also assigned to a post-Messinian age by Robertson et al. (1995b). Montadert et al. (2014) showed thick Pliocene-Quaternary sediments to be present within the western part of the collision zone as well as along the entire western flank of Eratosthenes Seamount and thus additionally support a post-Messinian age for Unit 1c (see also Fig. 9 by Peace et al., 2012). iii) Finally, if Unit 1c was of pre-Messinian age, these sediments should either be separated from Unit 1b by a Messinian erosion surface or by a layer of Messinian evaporites. Neither erosion nor evaporites appear to be present between Units 1b and 1c, pointing towards a post-Messinian age of these sediments.

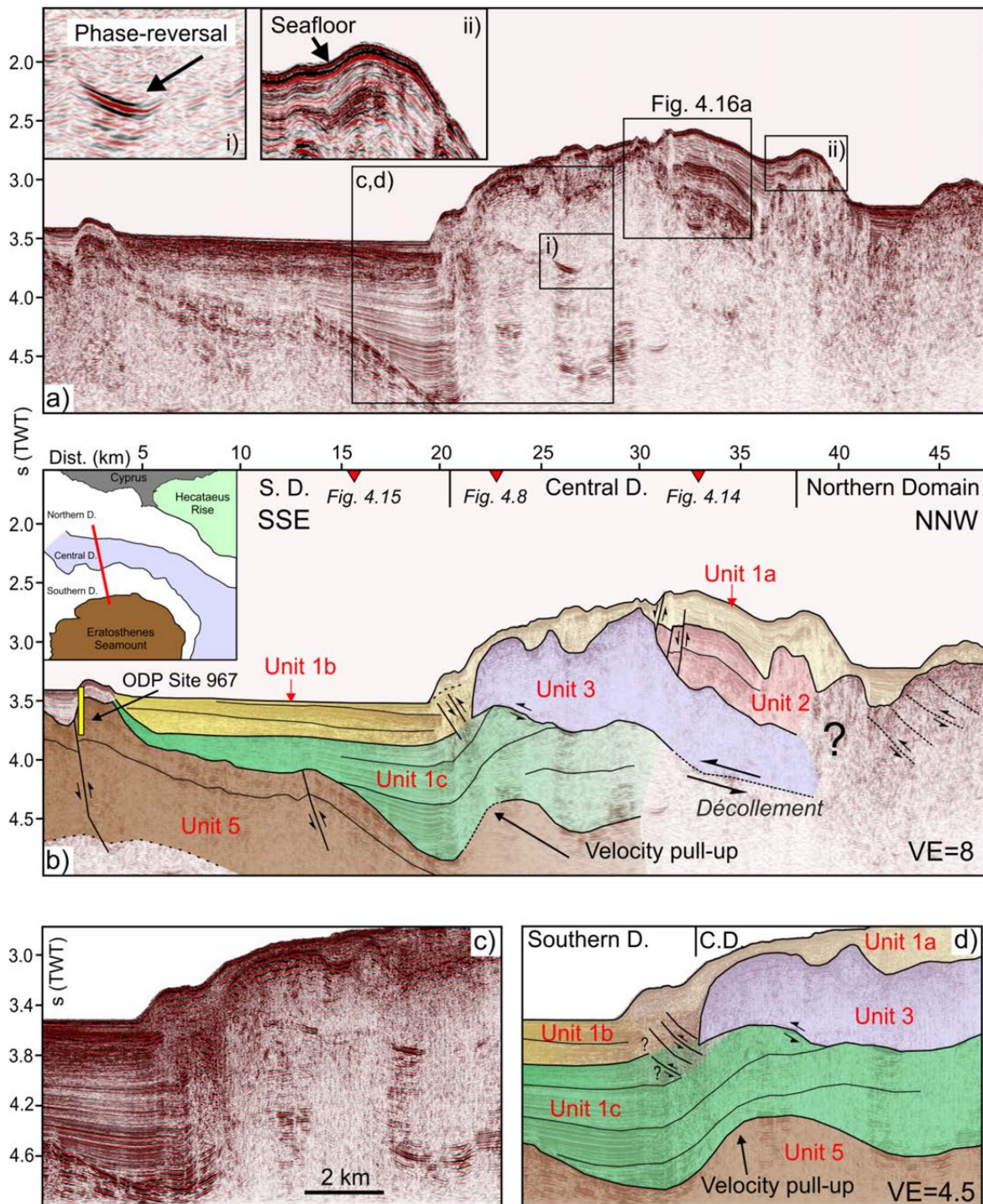


Figure 4.7 a) Seismic profile and b) the corresponding interpreted version from the westernmost part of the study area. Note the presence of Unit 3 above the southward continuation of Unit 1c. The base of Unit 3 follows a phase-reversed reflection event. Stippled lines are drawn where interpretations are rather uncertain. VE=vertical exaggeration. For location see figure 4.2. c) Enlarged seismic section and d) the corresponding interpretation from the profile shown above. The VE was reduced to 4.5. Reflections associated with Unit 1c can be followed from the Southern Domain into the Central Domain (C.D.) where this unit is overlain by Messinian evaporites (Unit 3). Upward-bending reflections at the transition from the Southern into the Central Domain are regarded as velocity-effects caused by overlying high-velocity evaporites.

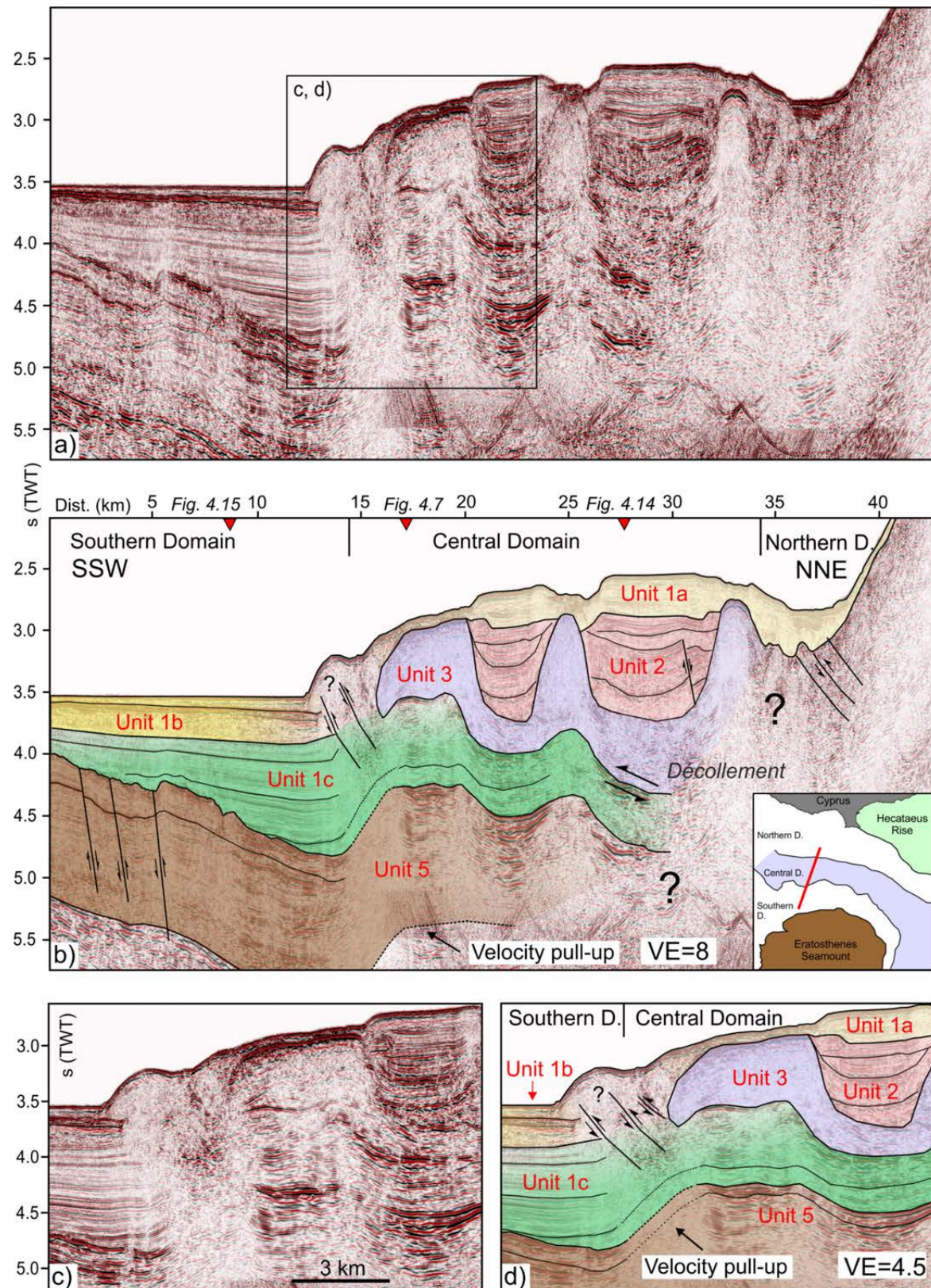


Figure 4.8 a) Seismic profile and b) interpreted version from the westernmost part of the study area. Thick packages of Unit 2 are separated by a prominent diapiric structure associated with Unit 3. For location see figure 4.2. c), d) Enlarged seismic section showing the transition from the Southern to the Central domain. VE=vertical exaggeration.

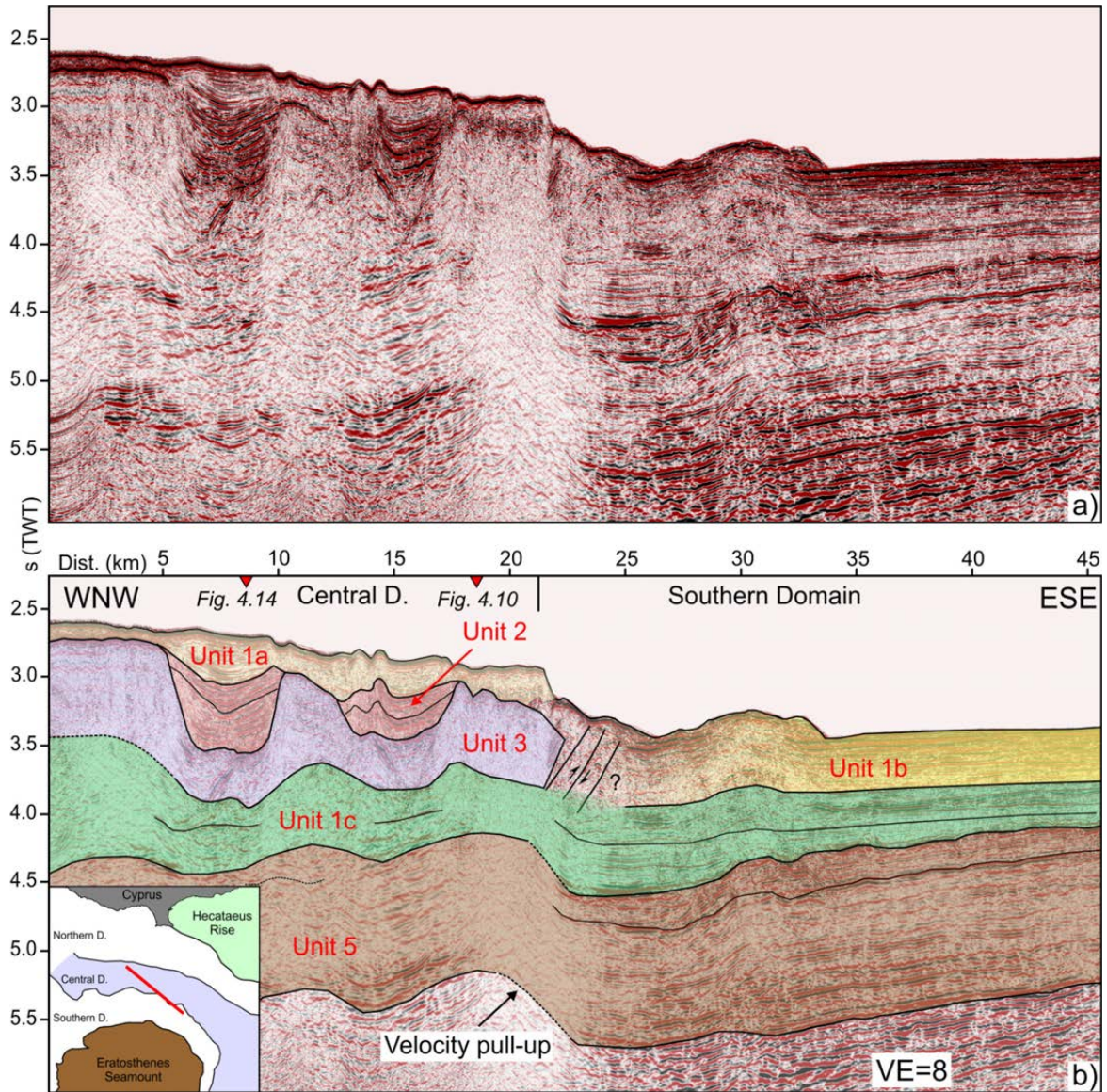


Figure 4.9 Uninterpreted **a)** and **b)** interpreted seismic profile showing the westward continuation of Unit 5 from the Southern into the Central Domain. The presence of high-velocity evaporites (Unit 3) creates velocity effects within sub-salt units near the southeastern termination of Unit 3. VE=vertical exaggeration. For location see figure 4.2.

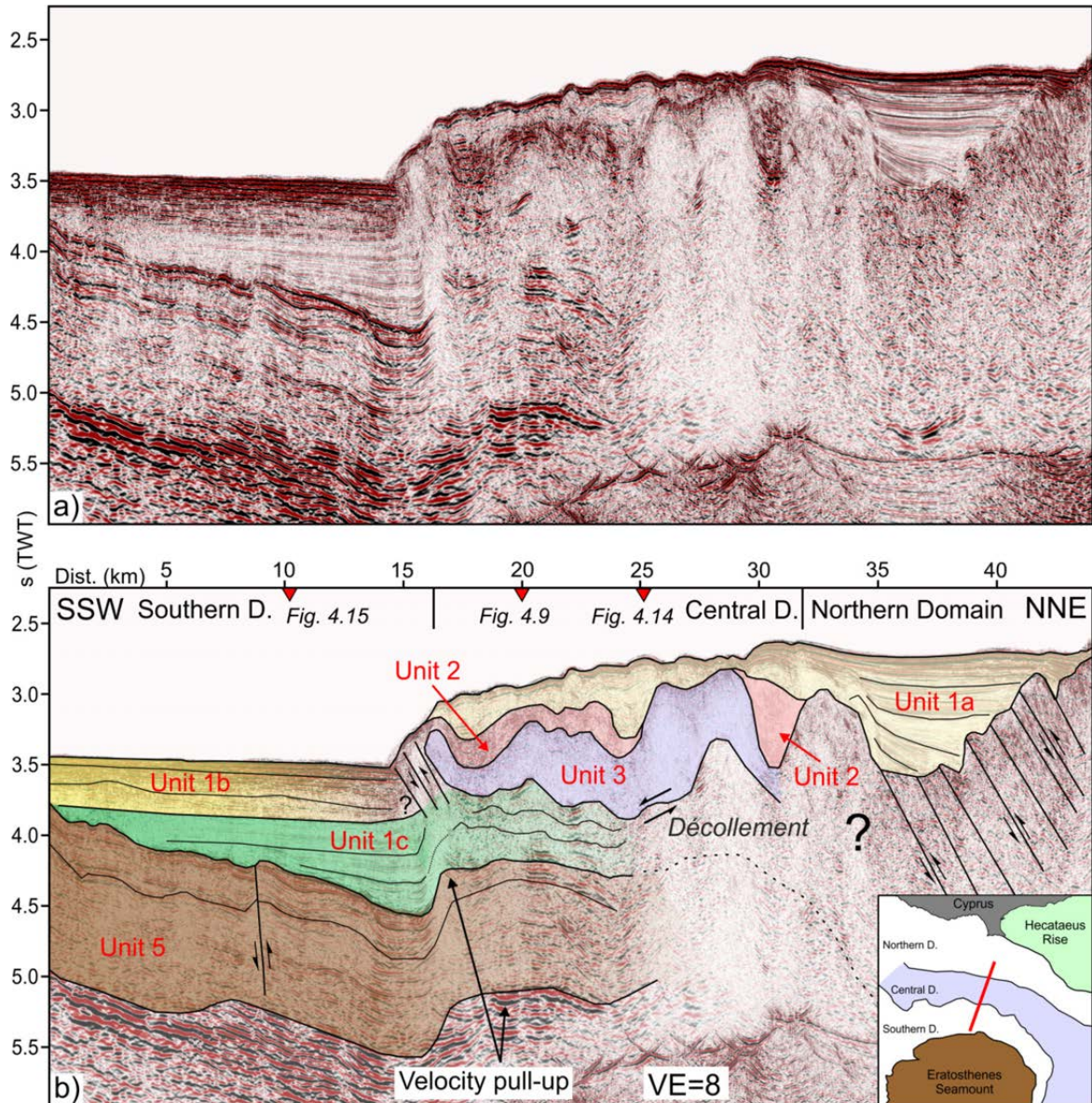


Figure 4.10 a) Seismic profile and **b)** its corresponding interpreted version from the central part of the study area. At the northern end of this profile, multiple, northward-dipping thrust faults are identified. These faults have apparently become inactive and are now buried by stratified sediments associated with Unit 1a. VE=vertical exaggeration. For location see figure 4.2.

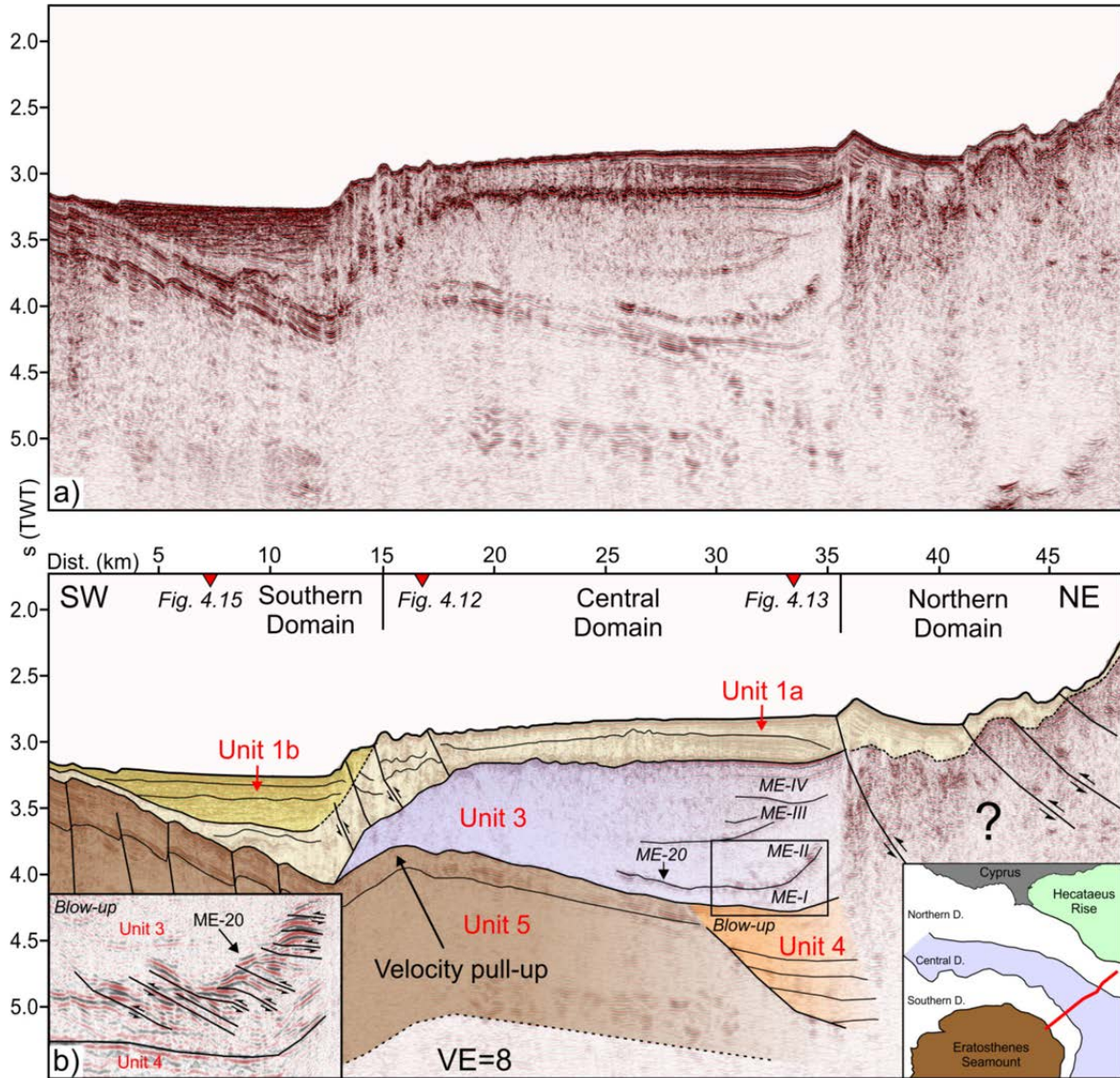


Figure 4.11 a) Seismic profile and b) its interpreted version from the eastern part of the study area. Unit 5 can easily be followed from the Southern into the Central Domain, being bent upwards at the transition zone due to overlying high-velocity evaporites (Unit 3). Intra-Unit 3 reflections are correlated to the intra-salt stratigraphy of the Levant Basin (Hübscher et al., 2007). Intra-Unit 3 reflection ME-20 is intensively shortened by multiple densely-stacked thrust faults at the northeastern end of Unit 3 (see blow-up section). VE=vertical exaggeration. For location see figure 4.2.

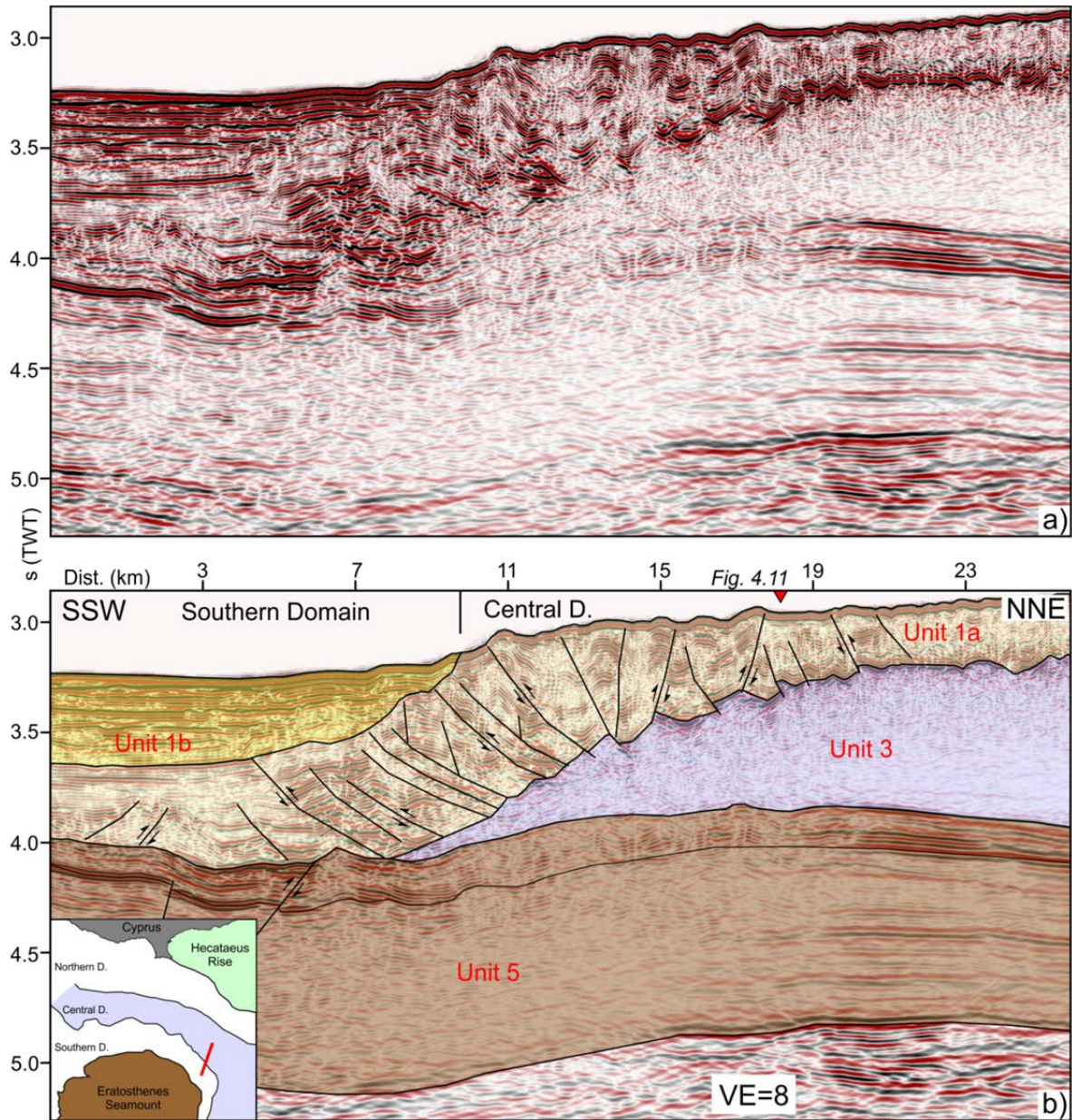


Figure 4.12 a) Uninterpreted and b) interpreted seismic profile showing the transition between the Central and Southern Domains in the eastern part of the study area. Unit 1a can be followed throughout the entire profile being intensively faulted on top of Unit 3. Reflections associated with Unit 1b on top of Unit 1a. VE=vertical exaggeration. For location see figure 4.2.

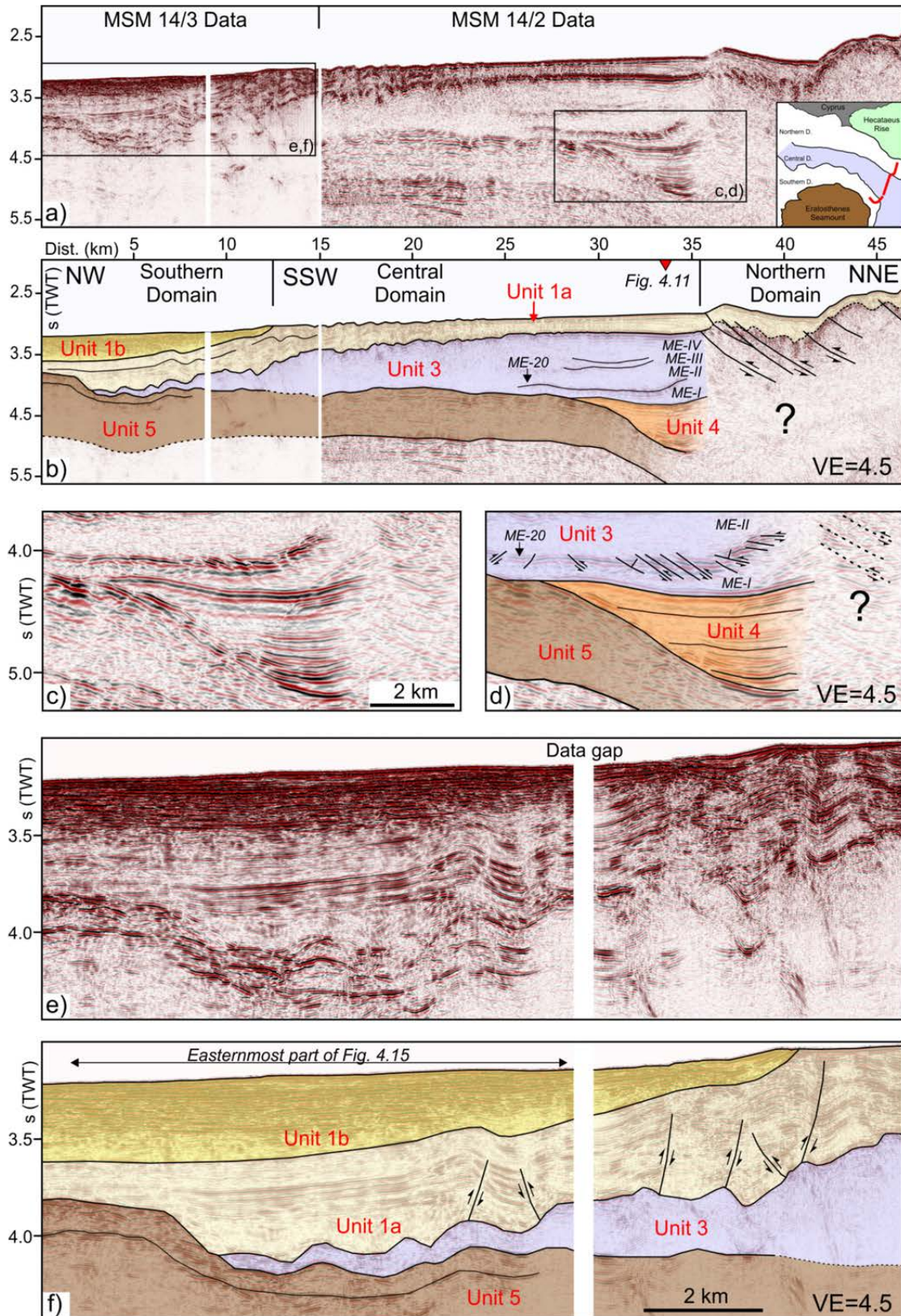


Figure 4.13 a) Composite seismic profile from the eastern part of the study area and b) its interpreted version. The enlarged raw and interpreted sections displayed in c), d) show the reflection character of Unit 4 which onlaps Unit 5. e), f) Enlarged section from the western part of the profile above. Note that the western part of this section also represents an enlarged version of the easternmost end of the profile shown in figure 4.15. Unit 1b pinches out at the transition between the Central and Southern Domains. VE=vertical exaggeration. For location see figure 4.2.

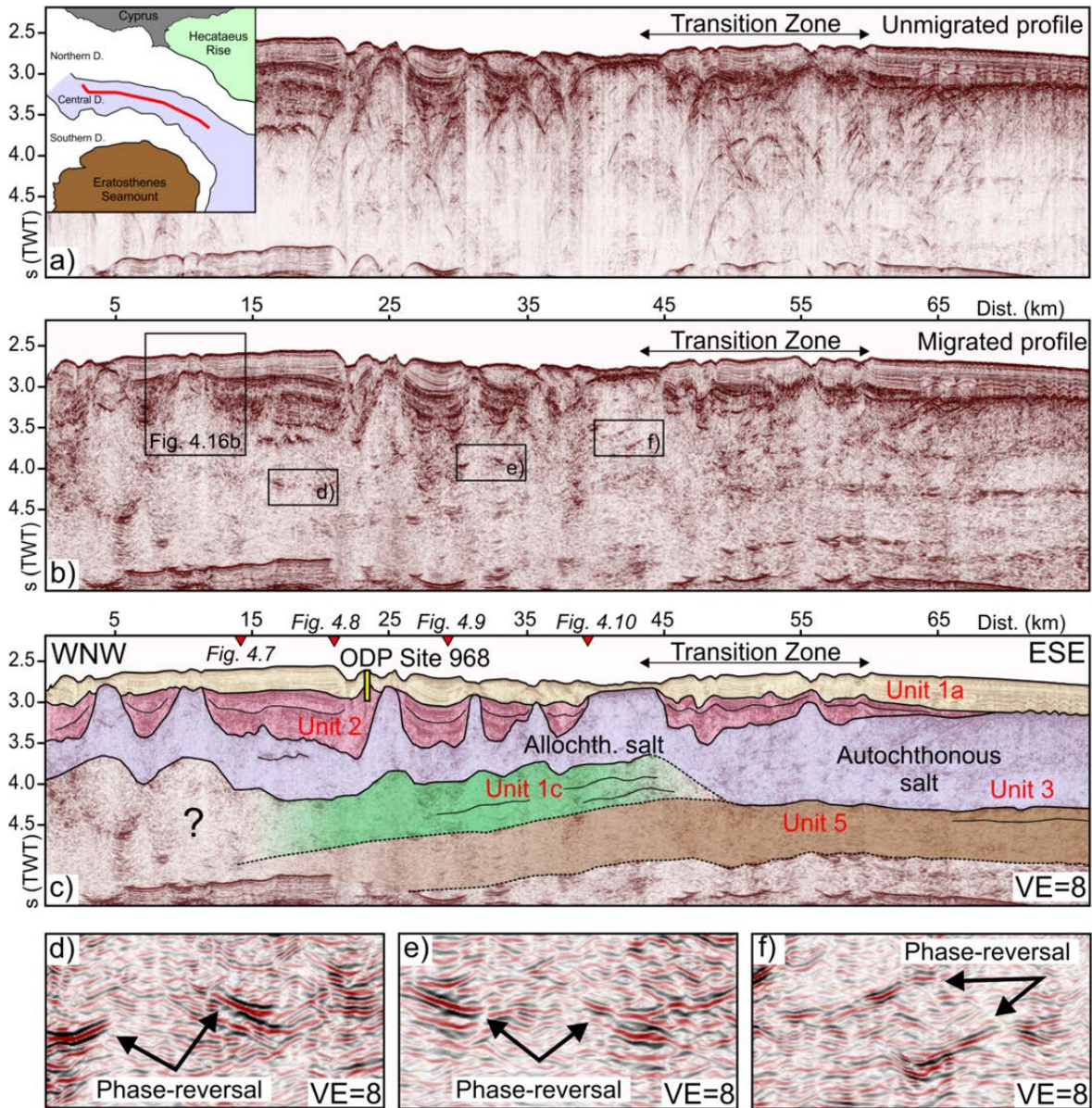


Figure 4.14 Seismic profile oriented parallel to the collision zone. **a)** Unmigrated seismic section showing the presence of several diffractions between profile km 45 and 60. **b)** Uninterpreted and **c)** interpreted seismic profile. Note the presence of thick Unit 2-packages adjacent to diapiric structures of Unit 3 in the western part of this profile. The presence of Unit 2 ceases towards the east, coinciding with a significant decrease in Unit 3-deformation. Sediments associated with Unit 1c are intercalated between Unit 3 and Unit 5 in the western part of the study area, separating the areas affected by allochthonous (west) and autochthonous (east) salt tectonics. **d), e), f)** Enlarged sections from figure 4.14b showing phase-reversed reflections which delineate the base of Unit 3 and the top of Unit 1c. VE=vertical exaggeration. For location see figure 4.2.

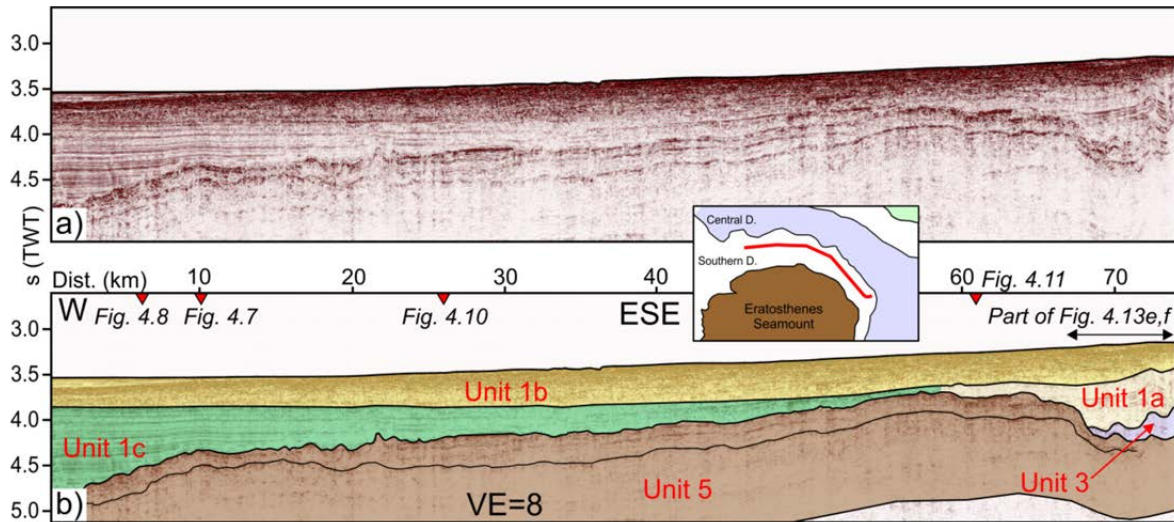


Figure 4.15 **a)** Approximately east-west oriented seismic profile across the Southern Domain and **b)** its corresponding interpreted version. Reflections associated with Unit 1c onlap Unit 5 towards the east until Unit 1c nearly pinches out at profile km 55. Further east, reflections below Unit 1b could clearly be correlated to Unit 1a (see figure 4.13e,f). Units 1c and 1a cannot directly be correlated due to separation by a Unit 5 positive structure. However, similarities in reflection characteristics between Unit 1c (west) and Unit 1a (east) suggest that these two units largely represent the same stratigraphic interval. VE=vertical exaggeration. For location see figure 4.2.

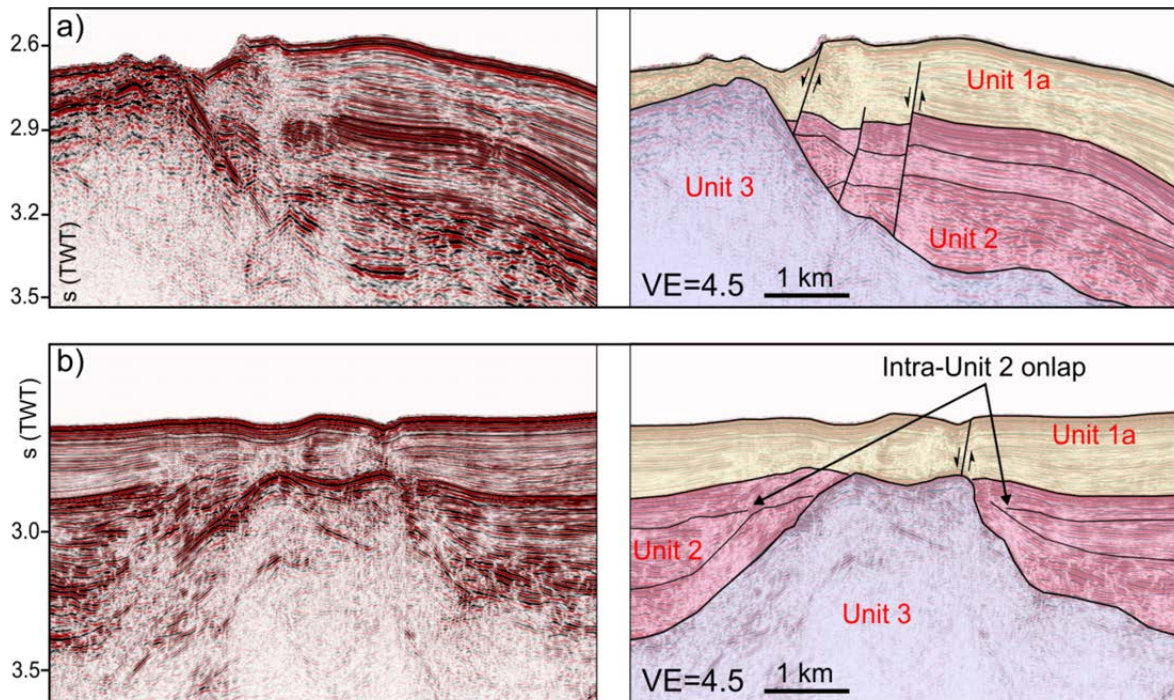


Figure 4.16 **a)** Uninterpreted and **b)** interpreted enlarged seismic sections showing Unit 2 deposits to terminate against salt diapirs associated with Unit 3. VE=vertical exaggeration. For location of **a)** see figure 4.7a and for **b)** see figure 4.14b.

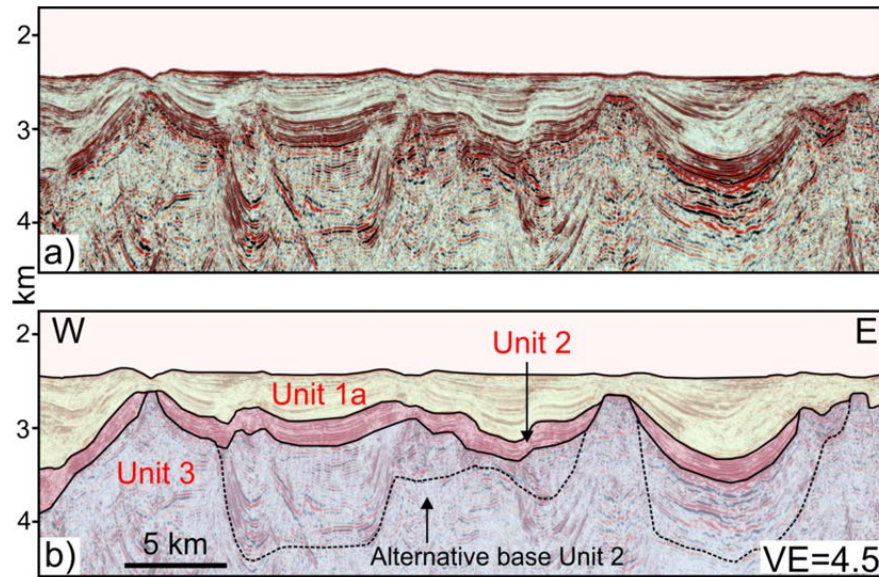


Figure 4.17 a) Industry seismic profile and b) its interpreted version located west of the Eratosthenes Seamount. For location see figure 4.1. Note the presence of a highly-reflective interval between Unit 1a and Unit 3 which is suggested to correlate with Unit 2 identified within the Cyprus collision zone. The stippled line below Unit 2 represents an alternative interpretation of its base. VE=vertical exaggeration.

4.4.3 Structural architecture

4.4.3.1 Southern Domain

The stratigraphic succession imaged in the Southern Domain is structurally characterized by largely undisturbed Pliocene-Quaternary sediments (Units 1a-1c) burying moderately to intensively faulted northwestward-dipping carbonates associated with Unit 5 (Figs. 4.7a,b, 4.8a,b, 4.9-4.11). One major west-southwest to east-northeast trending thrust fault clearly displaces sediments at the seafloor. This fault was targeted at ODP Site 967 (Shipboard Scientific Party, 1996a) and represents the northernmost active structure which extends into the Southern Domain (Figs. 4.3b, 4.7a,b). Additional structures observed in the Southern Domain represent northward dipping thrust faults which only offset reflections within Unit 5, being overlain by undisturbed sediments of Units 1b and 1c (e.g. km 0-5 in Figs. 4.8a,b). Deformation within the uppermost sedimentary succession is evident at the transition to the Central Domain. There, sediments adjacent to the salt body (Unit 3) in the western part of the study area exhibit chaotic reflections with local indications for the presence of northward-dipping thrusts. These structures are most clearly observed in figure 4.12, but can also be anticipated in figures 4.7-4.11. Further east, strongly southward thinning evaporites reach into the Southern Domain. Evaporites are overlain by deposits of Unit 1a which are offset by several, mainly northwestward dipping thrusts (Figs. 4.13e,f).

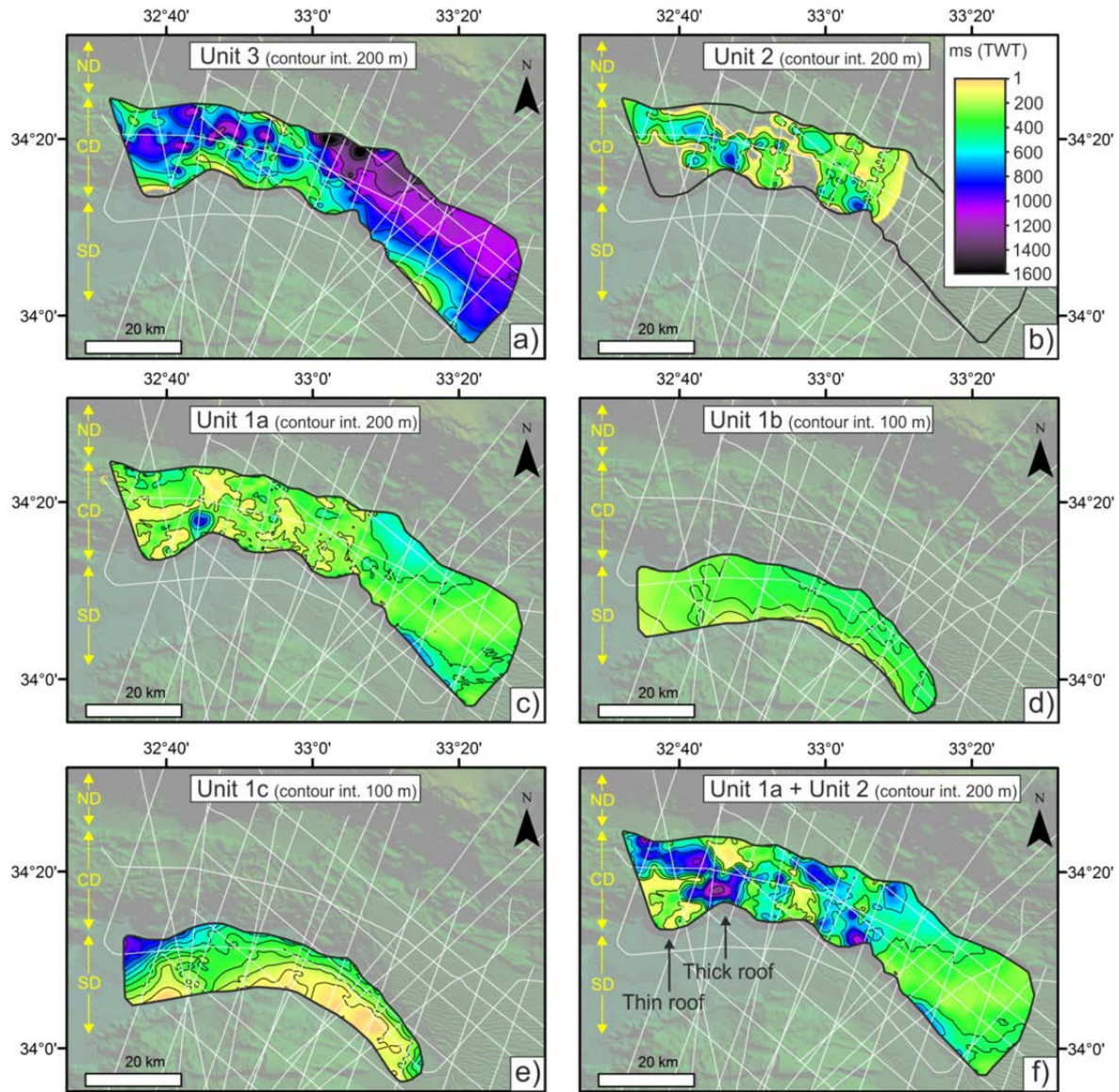


Figure 4.18 a) – f) Thickness maps of Units 3, 2, 1a, 1b, 1c and composite thickness of Units 1a and 2 in ms (TWT). The color scale shown in b) applies to all maps. Note that either a contour interval of 100 or 200 ms (TWT) was chosen, depending on the maximum thickness of the respective unit. White lines represent seismic profiles used for mapping the thickness distribution. ND=Northern Domain, CD=Central Domain, SD=Southern Domain.

4.4.3.2 Central Domain

Significant deformation has considerably altered the shape of the sedimentary succession in the western part of the Central Domain. Several diapiric structures are imaged within Unit 3 and are interpreted as salt diapirs (Figs. 4.8a,b, 4.9, 4.14b,c). Sediments within Unit 2 are frequently bent upwards adjacent to such diapirs (Figs. 4.8, 4.14b,c, 4.16). Observing growth strata and internal onlap terminations within Unit 2 which rarely oversteps the crests of adjacent diapiric structures is indicative for a phase of syn-depositional Unit 2 deformation coeval to salt diapir growth (Fig. 4.16). Upward bending or tilted reflections are also observed within Unit 1a (Figs. 4.14b,c, 4.16). Frequently, depressions within Unit

1a are observed above the crests of diapiric structures (Figs. 4.8a,b, 4.14b,c, 4.16). Within the area affected by salt diapirism, reflective sub-salt sediments (Unit 1c) are observed. Interpreting these sub-salt sediments to be of post-Messinian age (see Chapter 4.4.2.7) implies that evaporites of Unit 3 must have advanced across stratigraphically younger sediments. Salt in the western part of the Central Domain is thus regarded as allochthonous salt that has progressively advanced across post-Messinian strata along a base-salt detachment fault.

In contrast to intensive salt diapirism and significant supra-salt deformation in the western part of the collision zone, a clearly different deformation pattern is observed further east (Figs. 4.11-4.13). There, Unit 1a deformation is only observed at the transition between the Southern and Central Domains, ceasing towards the north where Unit 1a reflections turn into small-scale folds which are also expressed in the bathymetry (Figs. 4.3, 4.11). Compressional deformation is further observed within Unit 3, even though its upper termination is presently horizontal. At the southwestern flank of the Hecataeus Rise, intra-Unit 3 reflection ME-20 was shortened to a stack of 700-1500 m long thrust sheets (Figs. 4.11, 4.13c,d). No stratified sub-salt sediments of Unit 1c are observed beneath Unit 3 in the eastern part of the Central Domain, where evaporites of Unit 3 directly overly northward dipping reflections associated with Unit 5 (Figs. 4.11-4.12, 4.13a,b). Therefore salt in this part of the study area has generally remained in place and is thus regarded as autochthonous salt.

The boundary between allochthonous salt in the western part of the study area and autochthonous salt further east should correspond to the easternmost extent of stratified post-Messinian sub-salt sediments, associated with Unit 1c. While Unit 1c is poorly imaged in the trench-parallel profile displayed in figures 4.14b,c, it could locally be detected with the aid of cross-profiles. The presence of Unit 1c is believed to cease towards the east at approximately km 50 in figures 4.14b,c, even though its exact eastward extent is difficult to detect. The eastern end of this inferred transition zone between allochthonous and autochthonous salt is associated with a drastic eastward decrease in seafloor deformation (Fig. 4.4d). An unmigrated version of the seismic profile shown in figure 4.14 reveals the presence of several diffractions at the inferred location of this transition zone (between profile km 45 and 60 in Fig. 4.14a). As diffractions are frequently related to the presence of faults at depth, differential salt motion along this transition zone may have caused the development of intra-salt structures which efficiently scatter seismic energy.

4.4.3.3 Northern Domain

The Northern Domain directly borders on Cyprus in the west and terminates against the Hecataeus Rise further east. Directly south of Cyprus, no prominent faults offset the seafloor as clearly observed in the bathymetry (Figs. 4.3, 4.4a). At

depth a detailed interpretation is complicated by limited seismic penetration. At the north-northeastern end of figure 4.10, numerous stacked, landward dipping reverse faults are identified. The top of these steeply dipping reflections progressively deepens towards the south, forming the northern flank of a small basin-like depression (km 33-43 in Fig. 4.10). This basin is filled by up to 0.8 s (TWT) largely undisturbed sediments of post-Messinian age (Unit 1a).

In comparison to offshore southern Cyprus, significant seafloor deformation is observed along the southwestern flank of the Hecataeus Rise (Figs. 4.3, 4.4a). Again, interpretation of subsurface structures is inhibited by limited seismic penetration. In the northeastern part of figure 4.11 and in figures 4.13c,d, sediments associated with Unit 4 appear to terminate near vertically at the transition to the Northern Domain and cannot be followed any longer. Within the Northern Domain northeastward dipping reflections are interpreted to indicate the presence of faults (Fig. 4.11). In the easternmost part of the Northern Domain (km 35 in Fig. 4.11), a prominent reverse-fault offsets the seafloor by approximately 90 m (see also figures 4.13a,b). This structure can also be followed in the bathymetry, striking parallel to the southwestern flank of the Hecataeus Rise (Fig. 4.3).

4.5 Discussion

4.5.1 Convergence direction and location of the plate boundary

In accordance with previous studies on seismicity, the African-Anatolian plate boundary is generally inferred to run along the area bordered by Cyprus and Eratosthenes Seamount (Wdowinski et al., 2006; Imprescia et al., 2012). In the course of ODP Leg 160, this boundary was placed between ODP Sites 967 and 968, based on distinct differences in the sedimentary succession recovered at these two drilling locations (e.g. Robertson, 1998d). However, results of this study show that the flank of Eratosthenes Seamount (Unit 5) continues beneath the Southern and Central Domains, being overlain by Messinian and post-Messinian sediments (e.g. Fig. 4.9). The plate boundary is thus believed to be located within the Northern Domain, where the flank of Eratosthenes Seamount cannot be followed any longer (Figs. 4.8a,b, 4.10). There, Eratosthenes is presumably thrust underneath Cyprus and accreted material is evidently attached to the margin of the upper plate (Fig. 4.10) (see Chapter 4.5.4). This updated view on the location of the plate boundary considerably alters previous interpretations of stratigraphic differences encountered between ODP Sites 967 and 968 which were primarily influenced by Site 968 being located on top of mobile evaporites, while Site 967 was drilled into the flank of Eratosthenes Seamount.

The African-Anatolian plate boundary is suggested to continue southwest of the Hecataeus Rise as previously assumed by Ben-Avraham et al. (1995) and Vidal et

al. (2000b). This suggestion is based on the observation of significant compressional evaporite inflation within the area southwest of the Hecataeus Rise, accompanied by the formation of multiple thrust faults above the southern tip of the salt (Figs. 4.11, 4.12). The presence of densely-spaced intra-salt thrust sheets associated with reflection ME-20 can easily account for several km of shortening (Figs. 4.11, 4.13c,d). Furthermore, recently published refraction seismic velocity models reveal strong lateral heterogeneity along a transect stretching from Eratosthenes to the Hecataeus Rise together with significant differences in crustal composition between these two tectonic entities (Welford et al., 2015). The observation of Klimke and Ehrhardt (2014) that sub-salt strata south of the deformation front have remained undeformed is consistent with the structural characteristics observed within Unit 4, where undeformed sediments vertically terminate against the Northern Domain. This is also in accordance with results of previous reflection seismic studies across the Latakia Ridge, where shortening is entirely accommodated within the area north of the deformation front (Vidal et al., 2000a,b; Montadert et al., 2014).

GPS-based calculations of plate motions south of Cyprus show Africa and Anatolia to presently converge in northeast-southwest direction at a rate of $7\text{--}8\text{ mm yr}^{-1}$ (Wdowinski et al., 2006). Based on reflection seismic data across the eastern segment of the Cyprus Arc, Hall et al. (2005) reported that the present tectonic regime was initiated in Early Pliocene times. If such a change had also affected the plate boundary directly south of Cyprus, most of the shortening should have occurred between Eratosthenes and the Hecataeus Rise rather than between Cyprus and Eratosthenes Seamount. However, seismic profiles shown in this study indicate most significant lateral shortening and allochthonous salt advance directly south of Cyprus with comparably less compressional deformation within the area southwest of the Hecataeus Rise (Figs. 4.3, 4.14). While the plate tectonic puzzle along the Cyprus Arc has not been sufficiently understood and the presence of additional crustal-scale faults may cause segmentation of motion along the plate boundary (Schattner and Lazar, 2014), present results suggest that most of the post-Messinian convergence between Cyprus and Eratosthenes Seamount has occurred in north-south direction. This assumption corroborates recent structural work onshore Cyprus, suggesting north-northwest to south-southeast directed convergence to have lasted until Late Pliocene times with a later switch to the present, northeast-southwest convergence direction since the Pleistocene (Kinnaid and Robertson, 2012). As this assumption implies a later coupling of Cyprus to the westward motion of Anatolia than previously thought, I note the possibility that Pliocene transcurrent motion between Anatolia and Africa could have alternatively been accommodated along the Kyrenia Range (McCay and Robertson, 2013).

4.5.2 Structural evolution – previous models and new interpretation

Based on north-south trending seismic profiles across the Cyprus subduction zone, Montadert et al. (2014) forward a structural interpretation involving the presence of a large pop-up structure that has formed as a consequence of plate tectonic shortening at the location of the Central Domain. At the transition between the Southern and Central Domains, this structure is bordered by a large landward-dipping thrust which detaches along the top of the Eratosthenes Seamount flank (Unit 5) and forms a significant step at the seafloor (Montadert et al., 2014; see thrust fault at the southern edge of the frontal pop-up structure in Fig. 17a2). Based on reflection seismic data, the presence of a significant thrust fault at this location was also inferred by Robertson et al. (1995b) and interpreted to represent the boundary between the Cyprus margin and Eratosthenes Seamount.

However, the following findings of this study require an alternative interpretation: Undisturbed sediments within the Southern Domain (Unit 1c) appear to laterally continue beneath Messinian evaporites into the Central Domain (Figs. 4.7b,c). I relate apparent structural changes across this transition zone primarily to the southern limit of Messinian evaporites and associated sub-salt velocity effects than to the presence of a large frontal thrust. The interpreted leading thrust by Montadert et al. (2014) forms a step at the seafloor. This step coincides with the prominent bathymetric transition between the Central and Southern Domains. According to the interpretation of the present study, this step is related to the southern termination of the Messinian evaporites (Unit 3). Tracing this step in the bathymetry reveals its curved nature, rather resembling individual flow lobes of southward advancing salt than a thrust fault with strongly curved strike-direction (Figs. 4.3, 4.4). At a much larger scale a similarly curved geometry can also be observed at the near-surface salt pinchout along the Sigsbee Escarpment (e.g. Fig. 7 in Fort and Brun, 2012).

Based on results presented in this study, a different structural interpretation is proposed, where the main detachment level occurs at the base of the salt (Unit 3), efficiently carrying evaporites across post-Messinian strata as an allochthonous salt sheet. Sub-salt strata overflowed by progressively advancing evaporites have remained largely undisturbed as indicated by the continuation of Unit 1c from the Southern into the Central Domain (Figs. 4.7c,d). A base salt detachment was previously suggested and physically modeled for the Mediterranean Ridge, where Messinian evaporites have considerably influenced the structural evolution of this accretionary complex (Costa et al., 2004). South of Cyprus, the topographically elevated area of the Central Domain was interpreted as a pop-up structure by Montadert et al. (2014). I relate such observations to the presence of allochthonous and tectonically shortened Messinian evaporites, carrying roof

strata (Units 2 and 1a) across post-Messinian sediments (Unit 1c) and thereby creating a significant bathymetric step at their southern termination (Figs. 4.7-4.10). This concept of tectonically driven allochthonous salt advance can easily accommodate kilometer-scale shortening between Cyprus and Eratosthenes Seamount. A detailed discussion on salt tectonic mechanisms and the effect of salt on the structural evolution of the sedimentary cover within the Cyprus subduction is given below.

4.5.3 Salt tectonic concepts applied to evaporites in the Cyprus subduction zone

The most striking observation concerning the present-day shape of autochthonous salt in the eastern part of the collision zone is related to its steeply dipping southern termination (Fig. 4.11). Given evaporites have initially been deposited horizontally, salt in the collision zone is inferred to have experienced significant shortening as evident by numerous stacked intra-salt thrusts associated with reflection ME-20 (Figs. 4.11, 4.13c,d). Intercalated evaporite (e.g. gypsum/anhydrite) layers or clastics related to this reflection event were previously interpreted to deform brittlely and are thus believed to represent a good marker for intra-salt tectonic shortening (Reiche et al., 2014). In contrast, the bulk volume of evaporites comprised within Unit 3 is believed to have rather shortened plastically (Costa et al., 2004). From previous studies autochthonous salt is known to potentially respond by inflation to differential sediment loading, where salt laterally escapes the area of maximum sediment accumulation causing inflation within the distal part of the salt body (Hall, 2002; Albertz and Beaumont, 2010; Albertz and Ings, 2012; Rowan et al., 2012). Examples are known from the area south of Eratosthenes Seamount, where Nile-derived differential sediment loading has driven Eratosthenes-directed salt advance (Gaullier et al., 2000; Loncke et al., 2006; 2010). A similar mechanism with tectonic shortening as the main driving force may also apply to autochthonous salt between Eratosthenes and the Hecataeus Rise. While increasingly thickened evaporites are uplifted relative to surrounding strata, previously deposited roof strata (i.e. supra-salt sediments) are carried along. It is suggested that this differential vertical movement has caused the formation of the observed thrust faults at the boundary between the Central and the Southern Domains, separating progressively uplifted roof strata (Unit 1a) from peripheral sediments (Units 1a and 1b south of the salt body) (Figs. 4.11, 4.12, 4.13e,f). At the same time, newly deposited peripheral sediments, associated with Unit 1b, are increasingly trapped within the topographically lowered area of the Southern Domain (Figs. 4.11, 4.12). These sediments may have now acted as a backstop to salt advance and have thus hindered salt to flow further up the flank of Eratosthenes Seamount (Unit 5). Meanwhile, elevated roof strata of the Central Domain have rather experienced relative sediment starvation. Such differences in

thickness between topographically elevated roof deposits and peripheral sediments are also known from the Quaternary section along the Sigsbee Escarpment. There, sediments associated with the peripheral plain reach a thickness of 2.7 km while only 1.2 km of sediments have accumulated on top of the salt body (Hudec and Jackson, 2009).

Evaporites of distinctly different shape occupy the western part of the collision zone, interpreted as allochthonous salt which has advanced several kilometers across stratigraphically younger strata (Figs. 4.7-4.10). In order to understand the mechanisms involved in shaping evaporites in this part of the Cyprus subduction zone, insight may come from newly published salt tectonic concepts, focusing on the development and advance of allochthonous salt sheets (Hudec and Jackson, 2006; 2009; Jackson et al., 2010). According to Hudec and Jackson (2006) allochthonous salt sheets may advance in several ways, including extrusive, open-toed and thrust advance. Simplistically, these advance mechanisms represent salt either moving without any roof (extrusive), partly buried underneath a roof (open-toed), or salt which is completely covered by roof strata (thrust advance) (Hudec and Jackson, 2006). On most seismic lines, salt in the Central Domain is partly covered by Lago Mare deposits (adjacent to diapiric structures) and entirely covered by sediments of Pliocene to Quaternary age (Figs. 4.7a,b, 4.8-4.10). Hence evaporites have carried intact roof strata along, suggesting thrust advance to have most probably occurred. While examples of evaporites advancing by a basal thrust are best known from gravity-driven systems, the general style of salt advance may be quite similar to tectonically-driven settings (Hudec and Jackson, 2006). Therefore, concepts applied to allochthonous salt advance in the Gulf of Mexico and the Kwanza Basin, offshore Angola may also be applicable to evaporites in the Cyprus subduction zone. In the former case, salt along the Sigsbee Escarpment has mainly advanced by basal shear on a base-salt detachment that extends into a roof-edge thrust at the leading tip of the salt layer (Hudec and Jackson, 2009). The Angola salt nappe represents another example of allochthonous thrust advance (Hudec and Jackson, 2004), showing a remarkably similar geometry to evaporites imaged in the western part of the Cyprus subduction zone. More specifically, this salt nappe was classified as a source-fed thrust, where a thrust fault initially detaches at the base of autochthonous salt, carrying the salt sheet in its hanging wall across sediments which occupy the peripheral plain (see Fig. 18c by Hudec and Jackson, 2006). Such a case is also envisioned for the Cyprus evaporites, which have initially been deposited horizontally before tectonic shortening has initiated compressional thickening, similar to the present-day situation observed in the eastern part of the subduction zone. At this stage, roof deposits are already separated from peripheral sediments of the Southern Domain by several roof-edge-like thrusts (as shown along km 10-20 in Fig. 4.11, km 4-20 in 4.12). Subsequently, shortening of

greater magnitude is believed to have affected evaporites in the western part of the collision zone, ultimately initiating allochthonous salt advance. Salt may have now advanced by basal shear, with the base-salt detachment terminating into the roof edge thrust that represents the leading edge of a progressively advancing salt sheet. How effectively the base of salt may act as a *décollement* was recently shown at Calabria, where gravity-driven Messinian evaporites are presently moving downslope as a salt-detached megaslide, forcing the distal edge of the salt to advance across Pliocene-Pleistocene strata (Minelli et al., 2013).

In the westernmost part of the Central Domain, the leading edge of the salt sheet is sparsely covered by sediments (Figs. 4.7, 4.8). In this area, the toe domain of the salt sheet appears to have rather flown extrusively, suggesting the occurrence of open-toed advance at this part of the salt sheet. Along the Sigsbee Escarpment, Hudec and Jackson (2009) suggest a negative correlation between roof thickness and the distance of salt advance. Such a correlation may also apply to the offshore Cyprus salt, where the absence of thick roof strata is associated with the southernmost extent of Messinian evaporites (Fig. 4.18f). In contrast, adjacent to this southernmost salt lobe, supra-salt thickness greatly increases, suggesting thick roof strata to counteract salt translation until eventually pinning the salt sheet for a given period of time (Fig. 4.18f).

4.5.4 The impact of salt on the structural evolution of the Cyprus subduction zone

In the Southern Domain, horizontally stratified undeformed sediments (Units 1a, 1b, 1c) which onlap the northwestward-dipping partly faulted flank of Eratosthenes Seamount (Unit 5) are observed (Figs. 4.7-4.12). This setting largely resembles the structural configuration which is known from many subduction zones, where trench fill deposits onlap progressively deepening reflections of partly faulted subducting oceanic crust. At their landward side such sediments are often bordered by a prominent accretionary prism, separated from undisturbed trench fill deposits by a landward-dipping thrust (McCarthy and Scholl, 1985; Sick et al., 2006; Moeremans et al., 2014). However, in the Cyprus case this situation is complicated by Messinian evaporites, considerably altering the structural style encountered along the subduction zone.

Northeast of thickened autochthonous evaporites, at the flank of the Hecataeus Rise, northeastward dipping thrust faults may represent accreted material (Figs. 4.11, 4.13a,b). This is further supported by recently published refraction seismic velocity models showing this area to coincide with a large, approximately 10 km deep low-velocity trough, most likely of sedimentary origin (Welford et al., 2015). Miocene Unit 4-deposits, terminating near vertically against the southwestern flank of the Hecataeus Rise (Figs. 4.11, 4.13c,d), have likely been involved into

accretion and intensive deformation has possibly resulted in the observed chaotic reflection pattern of the Northern Domain. Close to the seafloor, Pliocene-Quaternary sediments are significantly faulted and appear to be presently within the stage of active accretion as also observed by a zone of highly irregular seafloor topography along the southwestern flank of the Hecataeus Rise (Figs. 4.3, 4.4a). In summary, active accretion evident by thrust faults and irregular seafloor topography is presently occurring north of inflated, autochthonous evaporites.

The structural situation observed along this segment of the subduction zone is termed „salt-inflation and active-accretion-compensated-shortening“ (Fig. 4.19a). Conceptually, this scenario involves plastically deforming, autochthonous evaporites which have compressionally been thickened and pushed south against a sedimentary backstop at the Southern Domain due to plate tectonic shortening. Unlike plastically deforming evaporites, sub-salt sediments associated with Unit 4 have entered the deformation front and were subject to accretion. At the same time as evaporites were driven south, supra-salt sediments previously resting on top of the salt body must have similarly been attached to the southwestern flank of the Hecataeus Rise, causing the presently observed irregular and faulted seafloor topography in this part of the convergence zone (Figs. 4.3, 4.4a).

Further west, at the southern limit of Cyprus and adjacent to allochthonous salt, the presence of highly faulted, accreted sediments is clearly evident in figure 4.10. However, unlike the area bordered by the Hecataeus Rise, none of these faults pierces the seafloor. To the contrary, accreted sediments are buried underneath thick Pliocene-Quaternary strata (Unit 1a), initially suggesting most of this accreted material to be of pre-Messinian age. However, if accretion, imaged in figure 4.10, has only involved pre-Messinian sediments and subsequently stopped, the presence of Lago Mare deposits between steeply faulted material and overlying undisturbed Pliocene-Quaternary strata would be expected. The apparent absence of Lago Mare deposits in such proximity to its anticipated source area (Robertson, 1998b) could be explained by a scenario where Miocene accreted material was located above late Messinian sea level and thus experienced erosion instead of sedimentation. However, given the present-day upper termination of accreted sediments to be at a water depth below 2.5 km and that this depth was likely much greater during Messinian times and later reduced by post-Messinian uplift of Cyprus, such a scenario can be excluded. Alternatively, most of the Lago Mare deposits previously occupying the Northern Domain may have later been accreted, implying accretion imaged in figure 4.10 to have lasted into post-Messinian times. In summary, north of allochthonous evaporites, accretion lasted until post Messinian times before becoming inactive.

Within the conceptual model, this stage is termed „allochthonous salt advance-compensated-shortening“ (Fig. 4.19b). In the western study area the magnitude of shortening was evidently greater compared to the eastern part of the subduction zone, suggesting the „salt-inflation and active-accretion-compensated-shortening“ scenario to have advanced to a later stage. I suggest that the area between Cyprus and Eratosthenes was already in a similar stage to the present-day situation of the eastern subduction zone by presumably Late Pliocene times. By the end of this stage, most of the observed accreted material was already attached to the Cyprus margin. Subsequently, inflated evaporites subject to continuous shortening must have begun to advance across sediments associated with Unit 1c of presumably Pliocene age. Now, shortening is believed to have entirely been accommodated at the leading edge of the salt sheet which was progressively rafted across stratigraphically younger strata along a base-salt detachment. Sediments deposited on top of the previously active accretionary prism have remained undisturbed. This scenario is consistent with the presently observed inactivity of accretion directly south of Cyprus, where previously accreted material is now covered by stratified sediments and no deformation is evident at the seafloor (Figs. 4.3, 4.4a, 4.10, 4.19). Sub-salt deposits associated with Unit 1c which may have (or will) reach the upper plate margin may subsequently become accreted, possibly at greater depths, eventually preventing faults from reaching the seafloor.

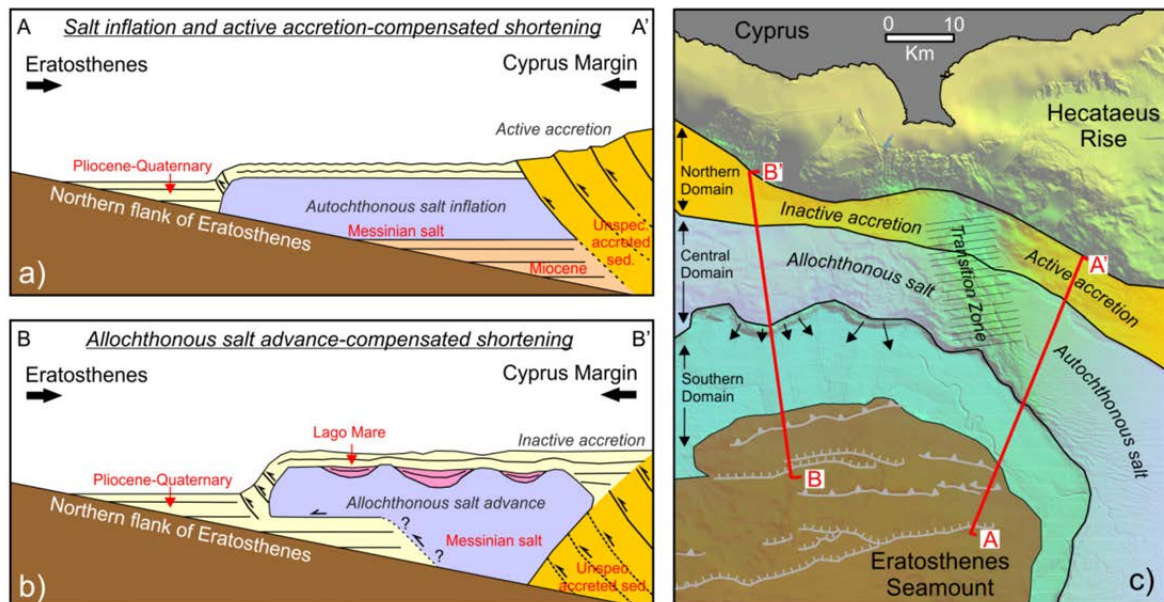


Figure 4.19 Conceptual sketch illustrating the structural differences between the eastern (A-A') and western (B-B') part of the study area. **a)** Tectonic shortening is believed to be accommodated by autochthonous salt inflation and active accretion of sub- and supra-salt deposits in the eastern part of the study area. **b)** Further west, shortening is compensated by allochthonous salt advance. In this case, shortening is entirely accommodated at the leading edge of the advancing salt sheet preventing sediments deposited on top of the previously active accretionary prism from compressional deformation. **c)** Map showing the distribution of allochthonous and autochthonous salt together with the approximate profile locations of the adjacent conceptual drawings.

4.5.5 The enigmatic circum-Eratosthenes depression – enigma solved?

Bathymetric data clearly show how the seafloor steps down into a semi-circular bathymetric low adjacent to the northern, eastern and southern flank of Eratosthenes Seamount (Fig. 4.3) (for the southern part of Eratosthenes Seamount see Mascle et al., 2001; 2006; Loncke et al., 2002; 2006; 2009; Klimke and Ehrhardt, 2014). This peculiar semi-circular depression was subject to significant scientific debate and various interpretations were proposed addressing this structure as a quadrilateral graben bordered by normal faults (Kempner, 1998), as a trough formed by evaporite dissolution (Major et al., 1998) or by evaporites sliding away from the seamount (Montadert et al., 2014). While interpretation of the Eratosthenes Seamount depression as a fault-bound graben was already excluded in the course of ODP Leg 160 (Robertson 1998a), the presence of compressional faults and the absence of extensional structures between evaporites and sediments occupying the semi-circular bathymetric low excludes a model related to salt dissolution and salt withdrawal away from the seamount (Figs. 4.11, 4.12, 4.13e,f).

Instead of previous explanations considering mechanisms which reduce topography around the seamount, I suggest that this semi-circular depression was essentially formed by relative uplift of the surrounding seafloor due to progressive Eratosthenes Seamount-directed salt advance. While this idea was previously proposed for the escarpment-like evaporite pinchout south and east of Eratosthenes Seamount (Gaullier et al., 2000; Mascle et al., 2001; 2006; Loncke et al., 2006), uncertainty remained for the northern part of this structure, where evaporites were long considered absent (Robertson, 1998d). In this study I have shown that the bathymetric step along the northern part of the Eratosthenes Seamount depression corresponds to the southern limit of Messinian evaporites (Fig. 4.3b). Due to shortening along the plate boundary, evaporites were progressively pushed towards Eratosthenes Seamount while sediments onlapping the seamount within the Southern Domain acted as a backstop to salt advance. Consequently, evaporites were compressionaly inflated, accompanied by thrusting above the southern limit of the salt body and the formation of topographic differences between the Central and the Southern Domains. This mechanism is also applicable to allochthonous salt within the subduction zone, as these evaporites are similarly pushed against a sedimentary backstop of the Southern Domain.

In accordance with previous studies (Gaullier et al., 2000; Mascle et al., 2001; 2006; Loncke et al., 2006), a similar scenario is believed to also account for the bathymetric step to the east and south of the seamount (Fig. 4.1), with the only difference being the mechanism driving salt advance. Compiling previous results

into a basin-wide scenario of salt tectonic deformation and its associated driving forces, Reiche et al. (2014) showed that evaporites within the Levant Basin were pushed basinward and thus also towards Eratosthenes Seamount by multiple driving mechanisms – the most important ones being differential sediment loading at marginal areas and westward tilt along the base of the salt (Reiche et al., 2014 and references therein). Evaporites removed from the margins were driven basinward towards the Eratosthenes Seamount, where sediments deposited on top of the lower flank of the seamount may counteract Eratosthenes-directed salt advance. In analogy to the scenario along the northern flank of the seamount, salt is compressionaly thickened while being pushed against Eratosthenes Seamount, creating elevation differences between evaporites and circum-Eratosthenes deposits.

4.5.6 Salt tectonic and sea level controlled Lago Mare deposition

Messinian: The presence of Messinian evaporites between Cyprus and Eratosthenes Seamount has long not been recognized in seismic profiles (Limonov et al., 1994; Robertson et al., 1995b). First seismic images of evaporites directly south of Cyprus were recently published by Klimke and Ehrhardt (2014) and Montadert et al. (2014). The presence of salt along this part of the Cyprus Arc considerably modifies previous interpretations. Instead of representing a lake-like setting (Robertson, 1998a), the area between Cyprus and Eratosthenes Seamount must have been a deep pre-Messinian basin, which was subsequently filled by evaporite precipitation while remaining connected to the adjacent Levant and Herodotus Basins. During the final stage of the Messinian Salinity Crisis, a Lago Mare unit (*sensu lato*) was deposited south of Cyprus. This unit was drilled at ODP Site 968, where the uppermost 200 m were recovered (Robertson, 1998a) (Fig. 4.6). However, seismic profiles presented in this study show that these deposits locally reach a thickness of up to 700 m (Fig. 4.18b). If all these sediments were deposited in the course of the Lago Mare stage (*sensu stricto*), this succession would belong to one of the thickest Lago Mare sections present within the Mediterranean realm (Cosentino et al., 2006). Seismic profiles show Lago Mare depocenters south of Cyprus to coincide with the area affected by salt diapirism (Figs. 4.8, 4.14). Within the limits of 2D seismic lines I speculate that these observations resemble a typical minibasin-like geometry (Hudec et al., 2009). Density inversion cannot account for the formation of sediment-filled minibasins as the thickness of Lago Mare deposits is not sufficient for such a scenario (Hudec and Jackson, 2006). Rowan et al. (2012) described how minibasins can form in the absence of density inversion, driven by lateral pressure differences that result from differential loading. However, it should be noted that internal onlap terminations within the lower part of Unit 2 indicate an early phase of diapir growth (Fig. 4.16b). At this time, supra-salt sediments associated with Unit 2 were of limited thickness (approximately 150 ms TWT) eventually insufficient to initiate

diapir growth. Instead, I interpret these observations to result from shortening, causing salt deformation and thereby creating local accommodation space to be filled with Cyprus-derived Lago Mare deposits. Following the concept by Hudec et al. (2009), sediment lenses resting on top of the salt now resist salt deformation which is rather accommodated by diapir growth resulting in the presently observed Lago Mare-filled minibasin-like geometry. A salt tectonic control on late Messinian supra-salt sediment deposition was previously reported from the Tyrrhenian Sea. There, early deformation of Messinian salt (Mobile Unit) has evidently controlled sediment distribution of supra-salt deposits (Upper Unit) (Gaullier et al., 2014).

The western limit of Lago Mare deposits is not recognized within the data of the present study. However, based on the seismic profile shown in figure 4.17, Lago Mare deposits appear to be present west of Eratosthenes Seamount. Even though this line is not crossed by the main seismic dataset of this study, I consider my interpretation quite robust given that inferred Lago Mare sediments west of Eratosthenes Seamount acoustically resemble those imaged directly south of Cyprus and similarly onlap and never overstep adjacent diapiric structures (Fig. 4.17). Furthermore, reflection seismic profiles acquired in the vicinity of the Florence Rise also reveal the presence of reflective supra-salt deposits, showing a similar onlap relation to evaporites as observed within the Cyprus subduction zone (Fig. 12.11 in Loncke et al., 2011). I therefore propose that Lago Mare deposits drilled at ODP Site 968 are not restricted to the Cyprus subduction zone but continue towards the west, implying their areal extent to be considerably larger than previously thought.

Given Lago Mare deposits to be mainly composed of Cyprus-derived material (Robertson, 1998a) and to continue several tens of kilometers into the Herodotus Basin, why do these deposits terminate abruptly towards the east – in such proximity to their anticipated source area? Apart from a local salt tectonic control on Lago Mare deposition, the most convincing answer to this question is related to sea level, controlling accommodation space available to be filled by Lago Mare sediments. Following the modelled sea level curve for the Eastern Mediterranean by Gargani and Rigollet (2007), I propose that the easternmost Mediterranean Sea was essentially desiccated during the final stage of the Messinian Salinity Crisis – a scenario supported by the formation of a wide-spread erosional unconformity on top of the Levant Basin evaporites (Netzeband et al., 2006b; Bertoni and Cartwright 2007a; Dümmong and Hübscher, 2011). Further west, along the Cyprus subduction zone, plate convergence may have caused northwestward tilting and subsidence of Eratosthenes Seamount together with incipient salt deformation. This may have locally provided accommodation space for Lago Mare deposition, resulting in the presently observed coincidence between Lago Mare deposits and salt diapirism (Figs. 4.8, 4.9, 4.14b,c). Similar to the present situation, the Herodotus Basin was presumably deeper than the Levant Basin at

that time and thus, at least locally, subject to accumulation of Lago Mare sediments.

In the light of sea level-controlled, locally 700 m thick Lago Mare deposition within the Eastern Mediterranean, one may speculate about a possible link of this unit to the Upper Evaporites widely evident and similarly thick within the Western Mediterranean (Lofi et al., 2011). Following this idea, the well-known absence of Upper Evaporites within the Levant Basin (e.g. Roveri et al., 2014) would simply be a result of desiccation while Lago Mare sediments near Cyprus and the Herodotus Basin may well correlate with Upper Evaporites within the Western Mediterranean Sea. Together with recent sedimentological work by Manzi et al. (2014), who correlated the previously termed “Lower Evaporites” onshore Cyprus with the second stage (5.6-5.5 Ma) of the Messinian Salinity Crisis and tentatively also with thick evaporites of the deep eastern Mediterranean basin, results of this study provide a possible further step towards a correlation between the deep evaporites widely present in the eastern and western Mediterranean basins.

4.5.7 Pliocene-Quaternary tectonostratigraphic evolution

Pliocene-Quaternary: In the western part of the study, area post-Messinian sediments associated with Unit 1c onlap Eocene carbonates of the northwestward dipping flank of Eratosthenes Seamount (Unit 5). As shown in figures 4.7 and 4.8, this depositional configuration extends to depths of up to 4.8 s (TWT) – as far as approximately 1.8 s (TWT) below the present-day top of Messinian salt in the Cyprus subduction zone (e.g. Figs. 4.14b,c). Strikingly, no seismically resolvable Messinian strata are intercalated between Eocene carbonates and Pliocene clastics at these depths (Figs. 4.7, 4.8). Despite logging results obtained at ODP Site 967 suggest the presence of a thin evaporite (Lago Mare) layer (Robertson, 1998b), such deposits are below seismic resolution and could not be imaged on top of Eocene carbonates within the entire Southern Domain. With Messinian strata thus largely being absent on top of Eratosthenes Seamount as far as throughout the Southern Domain, I follow previous ideas (e.g. Robertson and Shipboard Scientific Party, 1996) in suggesting that this part of the seamount was at a near sea level position or, more likely, subaerially exposed during Messinian times (subaerial exposure may have eventually extended even further north including the area now covered by allochthonous salt). In accordance with subsidence calculations at ODP Site 967, Eratosthenes Seamount experienced dramatic late Messinian/Early Pliocene subsidence in the order of 1.8 km, reaching bathyal depths by Early Pliocene times (Whiting, 1998). Given a Messinian sea level drop of 2 km (Gargani and Rigollet, 2007), followed by subsidence of Eratosthenes in the order of 1.8 km (Whiting, 1998), Eocene carbonates now overlapped by Pliocene strata at depths of 4.8 s (TWT) (approximates to 3.8 km given a water velocity of 1500 m/s and an average

sediment velocity of 1800 m/s) may have indeed been subaerially exposed, or very close to sea level, in the course of the Messinian Salinity Crisis.

After Eratosthenes has subsided to bathyal depths, Pliocene sediments (associated with Units 1c and 1a) were deposited between Cyprus and Eratosthenes Seamount, covering Messinian evaporites towards the north while accumulating on top of the seamounts' flank (Unit 5) south of the salt pinchout. The presence of slightly diverging reflections within Unit 1c (Fig. 4.7) is indicative for continuous Pliocene-Pleistocene northward tilting of the seamount.

During Pliocene-Pleistocene times, the area between Cyprus and Eratosthenes Seamount was subject to compression, accretion and salt tectonic deformation – processes described in Chapters 4.5.3 and 4.5.4. Given the lack of intra-Pliocene-Pleistocene stratigraphic markers, the timing of these individual events is difficult to constrain. The onset of allochthonous salt advance usually corresponds to the age of the lowermost thrust ramp which facilitated salt to move up section (Hudec and Jackson, 2006). As sub-salt imaging limitations prevent us from detecting the possible presence of such a thrust, the age of the uppermost Unit 1c reflection which is presently overflowed by allochthonous salt represents an upper limit for the onset of allochthonous salt advance. This event may have been coeval to a Late Pliocene Early Pleistocene phase of renewed significant subsidence of Eratosthenes Seamount (Whiting, 1998). At the same time, accretion directly north of Cyprus is believed to have stopped and previously accreted material became covered by undisturbed sediments (Figs. 4.10, 4.19).

Following the plate tectonic model forwarded by Kinnaird and Robertson (2012) and based on the discussion of convergence direction in Chapter 4.5.1, the Pliocene-Pleistocene transition may correspond to a 90° clockwise shift in convergence direction along the central segment of the Cyprus Arc, now converging in northeast-southwest direction.

Seismic data across the Southern Domain reveals a significant shift of acoustic properties between Units 1b and 1c (Figs. 4.7-4.10), indicating a change in depositional environment, tentatively correlated to Early Pleistocene or later times. In combination with high backscatter reflectivity within the Southern Domain (Fig. 4.4c), these highly reflective, wavy deposits are believed to be mainly composed of turbidites and stacked channel-levee deposits, representing a southern backstop to progressively inflating evaporites. As the observed seafloor channels east of Eratosthenes extend further into the Levant Basin and at least one of them all the way to the Israeli coast (Clark and Cartwright, 2009; Gvirtzman et al. 2015), such deposits may have originated from the Levant Margin which experienced significant uplift during Early Pleistocene times (Cartwright and Jackson, 2008).

4.6 Conclusions

This study has shown the large impact of Messinian salt on the Late Miocene-Quaternary evolution of the Cyprus subduction zone. Evaporites of up to 3.2 km thickness occupy the area between Cyprus/Hecataeus Rise and Eratosthenes Seamount and have significantly influenced the overall style of deformation, accretion and sediment deposition. Based on high-resolution bathymetric data and a dense grid of seismic reflection profiles, the following conclusions are drawn:

- Eocene-Cretaceous carbonates associated with the northwestward-dipping flank of Eratosthenes Seamount can be followed into the area previously believed to represent the Cyprus margin. The African-Anatolian plate boundary is thus located further north, presumably in close proximity to Cyprus.
- Up to 700 m thick late Messinian Lago Mare (*sensu lato*) deposits are identified in the western part of the study area, occupying small sub-basins which are flanked by salt diapirs. The observed stratal architecture indicates syn-depositional growth of salt diapirs, facilitating Lago Mare sediment delivery into small evaporite basins while no sediments were deposited on top of incipient diapiric structures. Late Messinian desiccation of the eastern part of the subduction zone and the entire Levant Basin may account for the presently observed absence of Lago Mare deposits further east.
- Post-Messinian tectonic shortening between Cyprus and Eratosthenes Seamount was accommodated along a base-salt detachment facilitating allochthonous salt advance across post-Messinian strata. Further east, between Eratosthenes and the Hecataeus Rise, autochthonous salt was significantly shortened and inflated.
- Densely stacked thrust faults near the Cyprus margin and the Hecataeus Rise indicate the presence of accreted sediments. In the vicinity of allochthonous evaporites, accretion has evidently become inactive, suggesting shortening to be entirely accommodated at the leading edge of the salt sheet. Northeast of autochthonous evaporites at the southwestern flank of the Hecataeus Rise, supra- and sub-salt deposits appear to be in the stage of active accretion. The observed relation between salt tectonics (autochthonous vs. allochthonous salt) and the style of sediment accretion (active vs. inactive) reveals the significant impact of evaporites on the structural evolution of the Cyprus subduction zone.
- Post-Messinian shortening of greater magnitude has affected the western part of the study area compared to the area between Eratosthenes and the Hecataeus Rise. I therefore suggest that post-Messinian convergence mainly

occurred in north-south direction, pointing towards a later coupling of Cyprus to the motion of Anatolia than previously thought.

- Near Eratosthenes Seamount, the seafloor steps down into a semi-circular depression. I relate the formation of the northern part of this bathymetric feature to compressional salt inflation and allochthonous Eratosthenes Seamount-directed salt advance.

Acknowledgements

I thank captain Friedhelm v. Staa and captain Matthias Günther, the officers and crew of RV MARIA S. MERIAN for their support during the survey campaigns. Spectrum is thanked for kindly providing the seismic data shown in figure 4.17. Claudia Vanelle, Sergius Dell and Benedikt Weiss are thanked for fruitful discussions throughout the preparation phase of this Chapter. I am grateful to Schlumberger for providing the Petrel software. This research was funded by Deutsche Forschungsgemeinschaft (DFG, Grant no. Hu698/20-1).

5 The Miocene-Quaternary tectonic evolution of the Hecataeus Rise

Abstract

The Hecataeus Rise represents a plateau-like structure, adjacent to the southern Cyprus margin and directly next to the Cyprus-Eratosthenes Seamount convergence zone, where incipient continent-continent-collision is believed to occur. Based on newly acquired reflection seismic and bathymetric data, I report on the Miocene to Quaternary structural evolution of this yet underexplored sector along the African-Anatolian plate boundary. A period of pre-Messinian compression has significantly deformed the western and southern part of the plateau area. Offshore continuation of onshore Cyprus lineaments attests the existence of a pre-Messinian structural link between Cyprus and the Hecataeus Rise. Owing to its relatively elevated position during the Messinian Salinity Crisis, the Hecataeus Rise experienced wide-spread Messinian erosion and only local deposition of evaporites which were precipitated within small, isolated sub-basins. Post-Messinian convergence was accommodated along the southeastern flank of the Hecataeus Rise, where northeast-southwest trending anticlinal structures experienced reactivation and significant growth. A prominent intra-Pliocene-Quaternary unconformity in the northwestern part of the plateau area may correlate with the Pliocene-Pleistocene transition and indicates the near synchronous occurrence of several tectonostratigraphic events. These events are suggested to represent a chain of structural and depositional changes initiated by incipient collision of Eratosthenes Seamount with Cyprus and the northwestern

corner of the Hecataeus Rise. Collision-derived uplift of Cyprus resulted in vertical separation between Cyprus and the Hecataeus Rise and the development of a prominent unconformity in the northwestern part of the plateau area. Increasing the slopes adjacent to Cyprus facilitated more energetic downslope sediment transport, expressed by the development of sediment waves and the evolution of a prominent canyon structure at the northeastern limit of the plateau area. Finally, a collision-derived coupling of Cyprus to westward moving Anatolia and an associated change from northwest to northeast directed convergence along the Cyprus Arc is consistent with observations of transcurrent deformation at the junction to the Levant Basin and the occurrence of northeast directed compression and uplift at the northwestern part of the plateau area.

5.1 Introduction

The Cyprus Arc, located in the easternmost Mediterranean Sea, represents a complex zone of tectonic convergence between the African and Anatolian plates (Vidal et al., 2000b; McClusky et al., 2003; Hall et al., 2005; Wdowinski et al., 2006; Le Pichon and Kreemer, 2010) (Fig. 5.1a). Major advances in understanding the evolution of the plate boundary were made in the course of scientific drilling at DSDP Leg 42a (Sites 375 and 376) (Shipboard Scientific Party, 1978) and ODP Leg 160 (Sites 965, 966, 967 and 968) (Robertson, 1998a,c) and by reflection seismic profiling at several locations along the Cyprus Arc (Ben-Avraham et al., 1995; Vidal et al., 2000a,b; Woodside et al., 2002; Hall et al., 2005; Kopf et al., 2005; Krashennnikov et al., 2005; Hübscher et al., 2009; Maillard et al., 2011; Sellier et al., 2013; Klimke and Ehrhardt, 2014; Montadert et al., 2014).

Yet, the existence of several underexplored sectors along this plate boundary complicates a consensus tectonic interpretation. One of such underexplored regions is represented by the Hecataeus Rise – an approximately 55 x 65 km sized rectangular, plateau-like structure (Fig. 5.1b). The Hecataeus Rise is bordered by Cyprus to the north, the Cyprus and Tartus Basins to the east, the Levant Basin to the southeast and the Eratosthenes Seamount to the southwest (Fig. 5.1b). With water depths between 250-1200 m, this structure is elevated by up to 1500 m above the surrounding seafloor.

Previous workers discussing the possible origin of the Hecataeus Rise have come to conflicting interpretations. While Robertson (1998c) raised the possibility that the Hecataeus Rise may represent an offshore extension of the Troodos ophiolite, other studies interpreted this structure as an accreted crustal unit (Rotstein and Ben-Avraham, 1985; Ben-Avraham et al., 1988). Yet, only few seismic lines were acquired across the Hecataeus Rise, making inferences on its structural evolution rather speculative. The only systematic reflection seismic study was published by McCallum et al. (1993), focussing on the northernmost part of this structure.

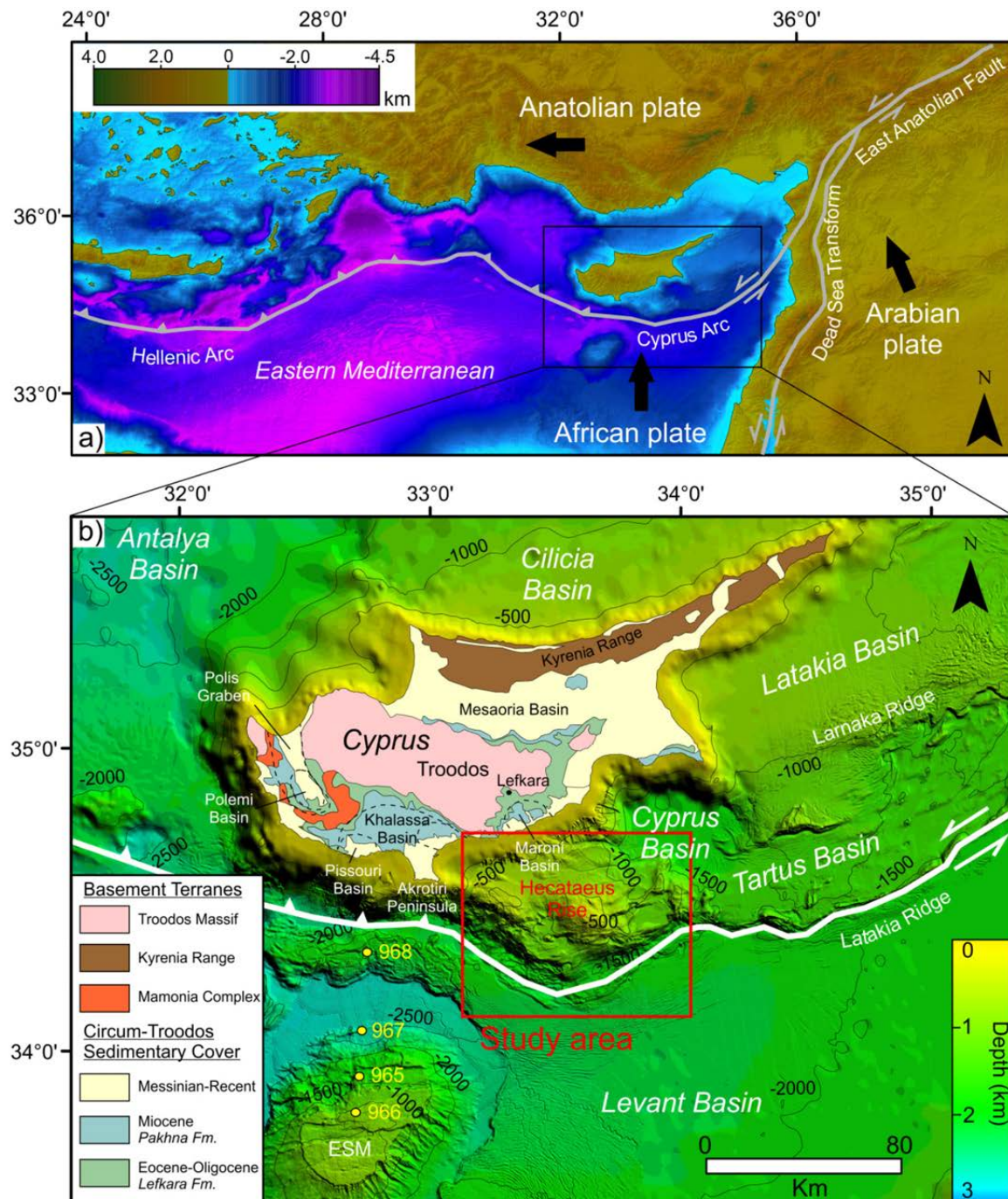


Figure 5.1 a) Overview and simplified tectonic map of the Eastern Mediterranean drawn with the aid of GeoMapApp® (<http://www.geomapapp.org>) comprising data published by Ryan et al. (2009). The large-scale tectonic configuration is based on Hall et al. (2014) and Schattner (2010). b) Enlarged map showing the bathymetry of the offshore-Cyprus-region, including data specified in Chapter 5.3.1. A simplified geological map of Cyprus was drawn after Kinnaird and Robertson (2012). Cyprus lineaments and sedimentary basins were delineated after Robertson et al. (1991). The bold white line represents the inferred location of the African-Anatolian plate boundary (see text in 5.2.1 for references). Yellow dots represent ODP Leg 160 drilling Sites. ESM=Erastosthenes Seamount.

In this study a comprehensive set of reflection seismic profiles is interpreted crossing the entire Hecataeus Rise plateau area combined with high-resolution bathymetric data (Fig. 5.2). Based on this newly acquired dataset, the following objectives are defined: i) to establish a seismostratigraphic framework for the Hecataeus Rise and provide a possible link to the onshore Cyprus stratigraphy ii) to present a first-order description and mapping of tectonic features across the Hecataeus Rise and iii) to discuss possible tectonic implications.

5.2 Geological background

5.2.1 Geodynamic setting and crustal composition

The present-day, large-scale tectonic configuration of the easternmost Mediterranean region is characterized by Arabia moving north with respect to Africa along the Dead Sea Transform while oblique northeast-southwest directed convergence between Africa and Anatolia is accommodated along the Cyprus Arc (Fig. 5.1a) (McClusky et al., 2003; Wdowinski et al., 2006; Le Pichon and Kreemer, 2010). The eastern segment of the Cyprus Arc extends from the junction with the East Anatolian Fault to the Hecataeus Rise. This part of the plate boundary is partly delineated by the Latakia Ridge, separating the Levant Basin to the south from the Cyprus and Tartus Basins further north (Fig. 5.1b) (Ben-Avraham et al., 1995). In the Levant Basin, seismic refraction and reflection surveys indicate the presence of stretched continental crust, overlain by 12-14 km of sedimentary basin fill deposits (Gardosh and Druckman, 2006; Netzeband et al., 2006a). In contrast, little knowledge exists on the crustal composition of the Anatolian side of the deformation front. Insight may come from reflection seismic profiles (Calon et al., 2005) and magnetic data (Rybakov et al., 1997) across the Larnaka Ridge – a prominent northeast-southwest trending bathymetric feature approximately 50 km north of the Latakia Ridge (Fig. 5.1b). This area was interpreted to represent a large, southward verging ramp anticline, underlain by the eastward continuation of the Troodos ophiolite (Robertson, 1998c; Calon et al., 2005).

Further west, along the central segment of the Cyprus Arc, the plate boundary follows the southern limit of the Hecataeus Rise (Fig. 5.1b) (Ben-Avraham et al., 1995; Vidal et al., 2000b). Recently published refraction seismic lines provide insight into the crustal composition of this structure (Welford et al., 2015). Velocity models along two profiles which cross the Hecataeus Rise in northeast-southwest direction did not reveal crustal velocities as high as measured for the onshore Cyprus Troodos ophiolite (Mackenzie et al., 2006; Welford et al., 2015). In contrast, velocities below 5 km/s are locally detected at depths down to 15 km, suggesting that the Hecataeus Rise is composed of a thick sedimentary cover on top of a thin continental crust (Welford et al., 2015). The plate boundary continues

along the southwestern edge of the Hecataeus Rise and directly south of Cyprus, delineating a zone of significant structural complexity where incipient continent-continent collision is inferred to occur between Cyprus/Hecataeus Rise and the Eratosthenes Seamount (Fig. 5.1b) (Kempner, 1998; Robertson, 1998a). This structural complexity is not only observed within the shallow sedimentary cover, where km-thick evaporites are actively shaped by ongoing collision/subduction (Reiche et al., 2015), but also by significant crustal heterogeneity along the southwestern flank of the Hecataeus Rise (Welford et al., 2015). There, refraction seismic velocity models indicate the presence of high-velocity basement blocks (approximately 7.0-7.2 km/s) oriented parallel to the margin of the Hecataeus Rise and followed by up to 10 km deep low-velocity troughs (below 5 km/s). Welford et al. (2015) interpreted this zone as a transform margin, where ancient Tethyan oceanic crust delineates the northern boundary of the Eratosthenes Seamount. Low velocity troughs may indicate the presence of accreted material as also imaged by reflection seismic lines directly south of Cyprus (Reiche et al., 2015). The seamount itself represents a carbonate platform of continental origin (Makris et al., 1983; Robertson, 1998c; Welford et al., 2015) and was recently interpreted as the elevated part of a larger continental block which was rifted from Arabia and may thus be regarded as the conjugate margin of the Levant Margin further east (Montadert et al., 2014).

5.2.2 Tectonostratigraphic evolution

From the Early Paleogene onwards pelagic carbonates of the Lefkara Formation covered the Upper Cretaceous Troodos ophiolite, reaching a maximum thickness of 700 m near Lefkara (Fig. 5.1b) (Robertson, 1998c and references therein). Subsequently, Miocene uplift of the Troodos Massif initiated a change to shallow water carbonate deposition (Robertson, 1977a). In southern Cyprus, uplift was associated with compressional tectonic activity along four east-southeast to west-northwest trending lineaments – the Akrotiri, Yerasa, Ayia Mavri and Petounda lineaments – presumably reflecting southward migration of the subduction zone to its present-day location (Fig. 5.3) (Robertson, 1977a; Robertson et al., 1991; Eaton and Robertson, 1993). The Yerasa lineament represents the most prominent of these structures. Pelagic carbonates of the Eocene-Oligocene Lefkara Formation are heavily deformed in its vicinity. Folded Lefkara deposits are covered by undeformed Tortonian transgressive limestones, indicating termination of tectonic activity by Late Miocene times (Robertson et al., 1991; Eaton and Robertson, 1993).

Based on shallow seismic profiles, the Akrotiri lineament was traced offshore from the southern tip of the Akrotiri Peninsula (Fig. 5.3) (McCallum et al., 1993). Compressional uplift of this structure is inferred from onshore borehole data,

showing Miocene sediments to be absent in this area (Robertson et al., 1991 and references therein). In southern Cyprus, Miocene carbonate deposition associated with the Pakhna Formation was concentrated in tectonically-controlled sub-basins, reaching a thickness of approximately 150 m within the Maroni Basin (Fig. 5.3) (Bagnall, 1960; Robertson et al., 1991; Eaton and Robertson, 1993).

Early Miocene compressional tectonic activity was further reported from the Cyprus Arc. Based on reflection seismic profiles across the Latakia Ridge, Hall et al. (2005) described a Miocene period of northwest directed compression, causing the formation of several northeast-southwest trending anticlines. Further west, Eratosthenes Seamount experienced significant Miocene tectonic uplift, possibly related to subduction initiation south of Cyprus (Robertson, 1998a). A phase of Miocene uplift was also reported for the Hecataeus Rise, based on thinning of Miocene deposits within the Levant Basin towards the Hecataeus Rise (Klimke and Ehrhardt, 2014).

With the onset of the Messinian Salinity Crisis, approximately 1.5 km thick, multi-layered evaporites were precipitated in the Levant Basin (e.g. Netzeband et al., 2006b; Hübscher et al., 2007; Reiche et al., 2014). No evaporites were drilled on top of the Eratosthenes Seamount, indicating an elevation above Messinian sea level (Robertson, 1998a). The Latakia Ridge had similarly existed as a prominent structure during that time as evaporites pinch out against its southern and northern limb (Hall et al., 2005; Maillard et al., 2011). Onshore Cyprus, evaporites consist of various gypsum facies and were precipitated in small, tectonically-controlled sub-basins coeval to evaporite precipitation within the entire Mediterranean realm (Robertson et al., 1995a; Krijgsman et al., 2002). Brackish water conditions prevailed during the terminal stage of the Messinian Salinity Crisis – the so called Lago Mare episode (Orszag-Sperber, 2006). Sediments associated with this period were sampled both onshore (Rouchy et al., 2001; Orszag-Sperber, 2006; Orszag-Sperber et al., 2009) and also directly offshore Cyprus (Robertson, 1998a). Offshore Cyprus, the uppermost 200 m of Lago Mare deposits were drilled at ODP Site 968 (Fig. 5.1b) being part of a horizontally layered succession that was recently imaged by reflection seismic profiles and shown to reach a total thickness of up to 700 m (Reiche et al., 2015). A period of Messinian compressional tectonic activity is evident by early evaporite deformation along the eastern segment of the Cyprus Arc and has also affected sediments within the Polemi Basin, onshore western Cyprus (Fig. 5.1b) (Orszag-Sperber et al., 2009; Maillard et al., 2011; Reiche et al., 2014).

After termination of the Messinian Salinity Crisis, the Eratosthenes Seamount subsided rapidly to bathyal depths and all Sites drilled in the course of ODP Leg 160 record a change to deep marine sedimentation by Early Pliocene times (Robertson, 1998a; Whiting, 1998). Subsidence of Eratosthenes was followed by

Late Pliocene to Quaternary uplift of Cyprus (Kinnaird et al., 2011; Harrison et al., 2013). Sedimentary evidence from the Mesaoria and the Pissouri basins suggest that the Troodos Massif was uplifted as a single tectonic entity (Kinnaird et al., 2011) with ongoing uplift throughout Holocene times at rates varying between 1.8 to 4.1 mm/yr during the last 40 ka (Harrison et al., 2013). Pliocene-Quaternary compressional tectonic activity is evident within the area between the Latakia and Larnaka Ridges, where Hall et al. (2005) report Pliocene transpressional reactivation of pre-existing anticlinal structures (Fig. 5.1b). Structural data from onshore Cyprus sedimentary Basins indicate the prevalence of strike-slip faulting since 3 Ma, letting Kinnaird and Robertson (2012) suggest that a collision-related coupling of Cyprus to the westward motion of Anatolia did not occur prior to that time. The idea of a later (than Early Pliocene) coupling between the motion of Cyprus and Anatolia is supported by reflection seismic investigations offshore southern Cyprus, where salt tectonic deformation suggests a predominately north-south oriented post-Messinian convergence direction between Cyprus and the Eratosthenes Seamount (Reiche et al., 2015).

5.3 Data acquisition and processing

5.3.1 Multibeam bathymetric data

The compilation of multibeam bathymetric data shown in this study includes data acquired in 2010 during RV MARIA S. MERIAN cruises MSM 14/2 (Ehrhardt, 2011) and MSM 14/3 (Hübscher, 2012) (Fig. 5.2). Additionally, data acquired in the course of the BLAC survey in 2003 were also included into the compilation (Benkhelil et al., 2005; Maillard et al., 2011). While the former datasets (MSM 14/2 and 14/3) were acquired with a SIMRAD EM120 multibeam echo sounder system, an EM300 system was operated during the BLAC survey. In order to obtain continuous bathymetric coverage, data gaps were locally filled with the ETOPO2 bathymetry (U.S. Department of Commerce, NOAA/DGDC, 2006). Data were gridded with a 50 m grid interval and exported to Petrel v. 2012 and ArcMap v. 10.0 for interpretation.

5.3.2 Multichannel seismic data

Multichannel seismic data used in this study were acquired during RV MARIA S. MERIAN cruise MSM 14/3 (Hübscher, 2012) (Fig. 5.2). Two GI-Guns with a total volume of 300 in³ were operated as a seismic source. Shots were fired at a constant time interval of 6-9 s, producing a seismic pulse with dominant frequencies centered around 100 Hz. A 24-channel analogue streamer with an active length of 600 m and a group spacing of 25 m recorded data at a sample

rate of 1 ms. For a general introduction to marine reflection seismics see Hübcher and Gohl (2014).

Seismic data processing included bandpass filtering, geometry-setup and CMP-binning with a CMP-distance of 12.5 m. As data were acquired at a constant ship's speed of 5 kn over ground, the resulting approximate shot distance of 20 m led to an average CMP-fold of around 15. In order to obtain high-quality seismic images, CRS stacks were produced for all available seismic profiles, following the approach described in Chapter 2.2. A post-stack time migration with a constant migration velocity of 1500 m/s was applied to all profiles. Profiles were exported to sgy-format and uploaded into Petrel v. 2012 for seismic interpretation.

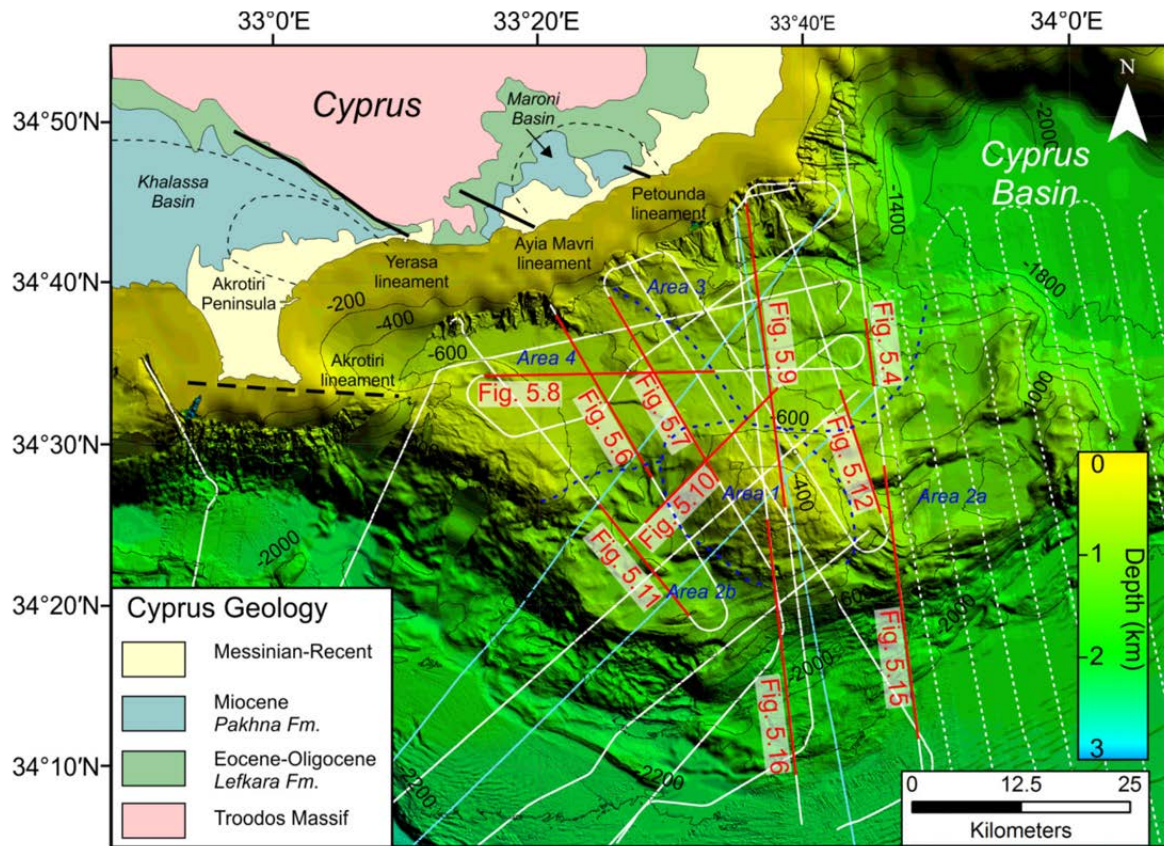


Figure 5.2 Seismic profile locations plotted on top of the Hecataeus Rise bathymetry. Solid white lines represent seismic reflection data acquired in the course of MSM 14/3. Light blue lines denote the locations of MSM 14/3 reflection seismic profiles acquired parallel to refraction seismic profiling (larger shot spacing, low frequency source, see Welford et al., 2015 for details). Seismic lines collected during the BLAC survey (Benkhelil et al., 2005; Maillard et al., 2011) are shown as stippled white lines. Figure locations are indicated as solid red lines. Cyprus lineaments and sedimentary basins were delineated after Robertson et al. (1991). A simplified geological map of Cyprus was drawn after Kinnaird and Robertson (2012).

In order to generate time structural as well as thickness maps and to map structural features across the entire Hecataeus Rise, additional seismic lines acquired in the course of the BLAC survey 2003 were utilized (Fig. 5.2). For details on the acquisition and processing history of these data, the reader is referred to Benkhelil et al. (2005) and Maillard et al. (2011). All seismic profiles are displayed

with a vertical exaggeration of approximately 6.5. This approximation is based on the (simplified) assumption of a constant velocity of 1500 m/s for all seismic sections. For aesthetical reasons, noise above the seafloor reflection was muted in all seismic profiles. Additionally, interpreted seismic sections were subject to a bottom mute, where arrivals below the seafloor multiple were eliminated (except of the southern end of figure 5.9).

5.4 Results

5.4.1 Physiography

Bathymetric data show the Hecataeus Rise as an elevated, plateau-like feature, rising along steep southeastern and southwestern flanks by up to 1500 m above the adjacent Levant Basin (Fig. 5.3). A highly irregular seafloor morphology is observed along the foot of the southwestern and to a lesser extent along the foot of the southeastern flank of the Hecataeus Rise. The northeastern edge of the Hecataeus Rise gently descends into the Cyprus Basin (Fig. 5.2). South of the Cyprus Basin, the Hecataeus Rise is separated by a prominent north-south trending ridge-like structure from the neighbouring Tartus Basin (Fig. 5.3a). The location of this ridge structure is associated with a significant kink in the shape of the Cyprus Arc and may be regarded as the junction between the Latakia Ridge and the Hecataeus Rise. Further north, the seafloor steeply ascends to a narrow shelf, connecting the Hecataeus Rise with the island of Cyprus (Fig. 5.3). The seafloor is heavily incised along this area and at the northeastern limit of the Hecataeus Rise several slope-parallel channels run into a large canyon-like structure which extends into the Cyprus Basin (Fig. 5.3a, inset I).

In order to ease geographic recognition of features mentioned below, the plateau area of the Hecataeus Rise was subdivided into five areas (Figs. 5.2, 5.3). Even though these areas were defined by morphotectonic criteria (structural characteristics of the subsurface and seabed morphology), they are primarily intended to ease geographic recognition of structures described below and should not strictly be regarded as individual structural entities.

The most prominent bathymetric feature shaping the morphology of the plateau area is a large circular high which occupies the central southern part of the Hecataeus Rise (Area 1) (Fig. 5.3). This structure has a diameter of approximately 17 km and rises to water depths as shallow as 250 m, being elevated by approximately 350-650 m above the surrounding plateau area. Seismic and bathymetric data allow for detection of several structures across this circular high with a predominantly east-west oriented strike-direction (Fig. 5.3b).

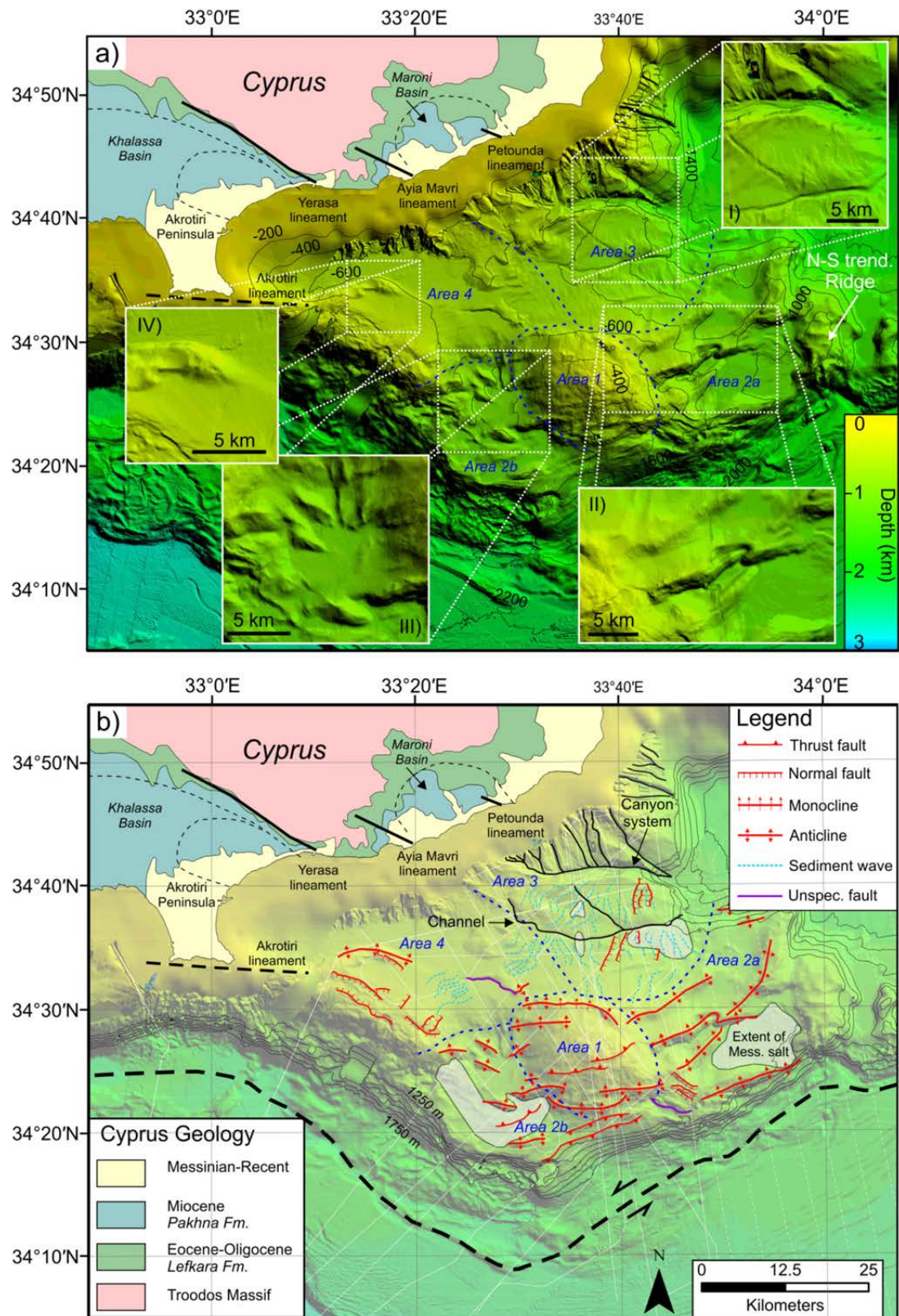


Figure 5.3 a) Bathymetric data from the study area with enlarged sections from selected locations. b) Morphotectonic map of the Hecataeus Rise. The study area was subdivided into five areas (Areas 1, 2a, 2b, 3 and 4) for geographic reference. Grey-shaded areas denote the areal extent of Messinian evaporite deposits. Onshore Cyprus lineaments and sedimentary basins were drawn according to Robertson et al. (1991). A simplified geological map of Cyprus was drawn after Kinnaird and Robertson (2012).

Four anticlines are mapped within the southeastern corner of the Hecataeus Rise (Area 2a) and show an east-northeast to west-southwest strike-direction. The central northern one of these anticlines reveals a significant kink at the intersection point with its neighbouring anticline (Fig. 5.3a, inset II). At the southwestern corner of the Hecataeus Rise anticlines appear to be segmented into several smaller, rather northwest-southeast oriented structures (Fig. 5.3a, inset III). A fairly smooth, locally wavy seafloor is observed in the northeastern part of the Hecataeus Rise (Area 3). The smooth-plateau area is locally cut by channel systems, where two branches merge into a single channel which runs into the Cyprus Basin (Fig. 5.3, inset I). Finally, the northwestern part of the Hecataeus Rise similarly exhibits a fairly smooth seafloor morphology. The seafloor ascends towards the western limit of the plateau area, where water depths shallower than 300 m are locally reached. The most prominent structure within this part of the Hecataeus Rise is represented by a slightly curved, mainly east-west oriented anticline near the northwestern termination of the plateau area (Fig. 5.3a, inset IV).

5.4.2 Seismic stratigraphy

5.4.2.1 Approach to stratigraphic interpretation

The well-known Messinian (erosion) surface can be followed across the entire Hecataeus plateau and subdivides the sedimentary succession of the study area into a pre-Messinian and a Messinian/post-Messinian interval, representing the only definite time marker available to gain age control on the stratigraphic subdivision suggested in this study (Fig. 5.4). Following the nomenclature for Messinian surfaces introduced by Lofi et al. (2011), this reflection is termed Margin Erosion Surface (MES) if no Messinian evaporites are present below (Fig. 5.4). In places where evaporites are locally present, the top evaporite reflection is termed Top Surface (TS), as the acoustically transparent character of evaporites on the Hecataeus Rise does not allow for identification of erosion on top of the evaporite unit. The base of the evaporite unit is termed Base Erosion Surface (BES) and is characterized by a phase-reversed reflection which locally truncates reflections below (Fig. 5.4). Sediments overlying the MES are assigned to Unit 1 and thus of Pliocene to Quaternary age. Sediments comprised between the BES and TS represent Messinian evaporites. In accordance with the offshore southern Cyprus stratigraphic framework developed in Chapter 4, these deposits are assigned to Unit 3 (for correlation purposes to Chapter 4, Unit 2 was chosen not to be defined in the present chapter).

Units 4 and 5 are identified below the Messinian surfaces and thus of pre-Messinian age. These units were exclusively distinguished on the basis of their acoustic characteristics and cannot simply be assigned to a certain time interval,

owing to the absence of well data. However, constraints on the sub-MES stratigraphy may, at least on a discussion basis, be obtained indirectly by correlating the acoustic and structural characteristics of the offshore seismic sequences to the onshore Cyprus stratigraphy. For the reader to follow the suggested onshore-offshore correlation such a discussion needs to be proceeded by a description of each unit's acoustic and structural properties.

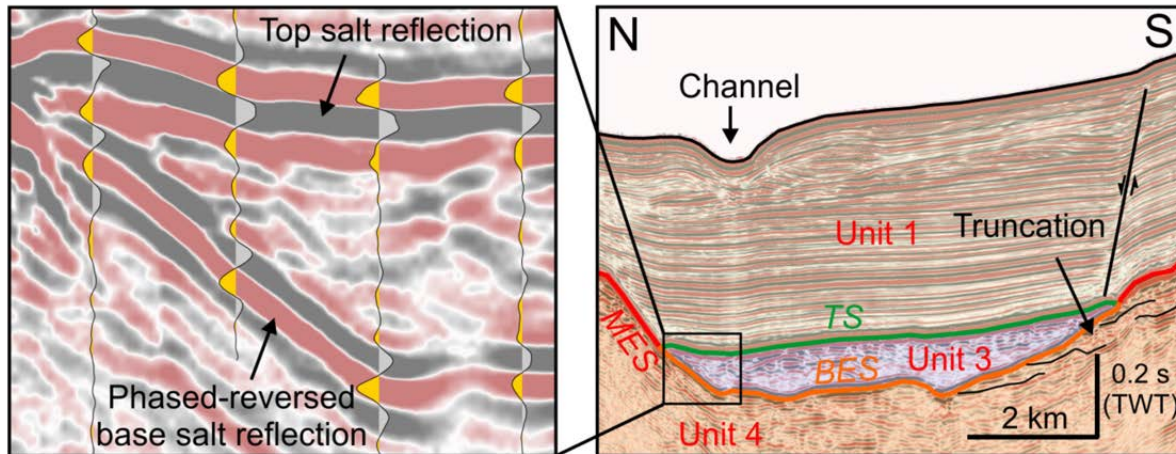

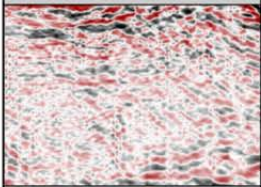
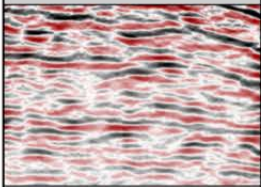
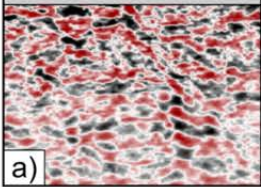


Figure 5.4 To the left, a seismic data example is shown, illustrating the geometry of the observed Messinian surfaces. For location see figure 5.2. To the right, an enlarged section of Unit 3 is overlain by seismic wiggle-traces. The base of Unit 3 follows a phase-reversed reflection event.

Figure 5.5a provides an overview of the defined seismostratigraphic units and their typical acoustic properties. The reflection characteristics of Units 1, 4 and 5 locally deviate from the examples shown in figure 5.5a owing to their acoustically heterogeneous nature. The suggested stratigraphic framework is summarized in figure 5.5b together with a correlation to the stratigraphy suggested by Hall et al. (2005) for the region north of the Latakia Ridge and a correlation to the onshore Cyprus stratigraphy. Note that the basis for the latter is treated in Chapter 5.5.1.

Additionally, a correlation to the offshore southern Cyprus stratigraphic framework, defined in Chapter 4, is shown (Fig. 5.5b). It should be noted that units identified across the Hecataeus Rise could not be followed to the offshore Cyprus region, inhibiting a direct correlation. Representing post-Messinian sediments and thus the same chronostratigraphic interval, Unit 1 can be correlated between offshore southern Cyprus and the Hecataeus Rise with certainty. Unit 3 similarly represents Messinian evaporites on the Hecataeus Rise and offshore southern Cyprus, even though evaporite deposition may have not necessarily been exactly coeval. Correlation of Units 4 and 5 between offshore southern Cyprus and the Hecataeus Rise is only based on the unit's (partial) coincidence in geologic time while reflection characteristics and lithologic composition may deviate. To ease recognition of similar chronostratigraphic units between the Hecataeus Rise and offshore southern Cyprus, the stratigraphic color code used in Chapter 4 is adopted.

<i>Seismic example</i>	<i>Seismic unit</i>	<i>Reflection character</i>
	Unit 1	Parallel, lateral continuous, locally wavy, low to high-amplitude reflections.
	Unit 3	Acoustic transparency.
	Unit 4	Parallel to sub-parallel, semi-continuous low to high-amplitude reflections.
	Unit 5	Mainly chaotic, occasionally transparent reflection character.

Age (Ma)	Epoch	Southern Cyprus	Latakia Basin (Hall et al., 2005)	Cyprus trench (Chapter 4)	Hecataeus Rise (this study)
0.0	Holocene - Pleistocene	Fanglomerate / Athalassa	Unit 1	Unit 1	Unit 1
2.6	Pliocene	Nicosia			
5.3	Miocene	Kalvasos	Unit 2	Unit 2	hiatus?
				Unit 3	Unit 3
7.2		Pakhna	Unit 3	Unit 4	BES
23.0	Oligocene	Lefkara	Unit 4	Unit 5	Unit 4
33.9	Eocene				Unit 4
56.0	Pre-Eocene	e.g. Moni Melange		Unit 5	Unit 5

Figure 5.5 a) Overview of seismostratigraphic units and their acoustic characteristics. While Unit 3 is characterized by a uniform reflection character, data examples shown for Units 1, 4 and 5 only represent a typical example and do not represent the acoustic characteristics of these units throughout the Hecataeus Rise (see text for details). Each seismic data example corresponds to a size of 1 km (horizontal) x 0.25 s TWT (vertical). **b)** Seismostratigraphic framework developed for the Hecataeus Rise and its suggested correlation to the onshore Cyprus stratigraphy (taken from Robertson et al., 1991), to the Larnaka-Latakia region stratigraphy (Hall et al., 2005) and to the offshore southern Cyprus stratigraphy developed in Chapter 4. Top and base of Unit 3 are labelled MES (Margin Erosion Surface)/TS (Top Surface) and BES (Base Erosion Surface), respectively.

5.4.2.2 Unit 5

Unit 5 represents the lowermost seismic unit identified within the study area and is internally characterized by a transparent to chaotic reflection character (Figs. 5.5a, 5.6, 5.7, 5.8a,b). This unit is exclusively observed in the northwestern part of the study area and deepens towards the south until it cannot be followed any longer due to masking by multiples (Figs. 5.6, 5.7). While the base of Unit 5 cannot be identified, its top is represented by a medium to high-amplitude reflection. Near Cyprus and the Akrotiri Peninsula, Unit 5 is directly overlain by sediments associated with Unit 1 (Figs. 5.6, 5.8a,b). Further east, Unit 5 is separated by a high-amplitude reflection from Unit 4 (Figs. 5.7, 5.8a,b).

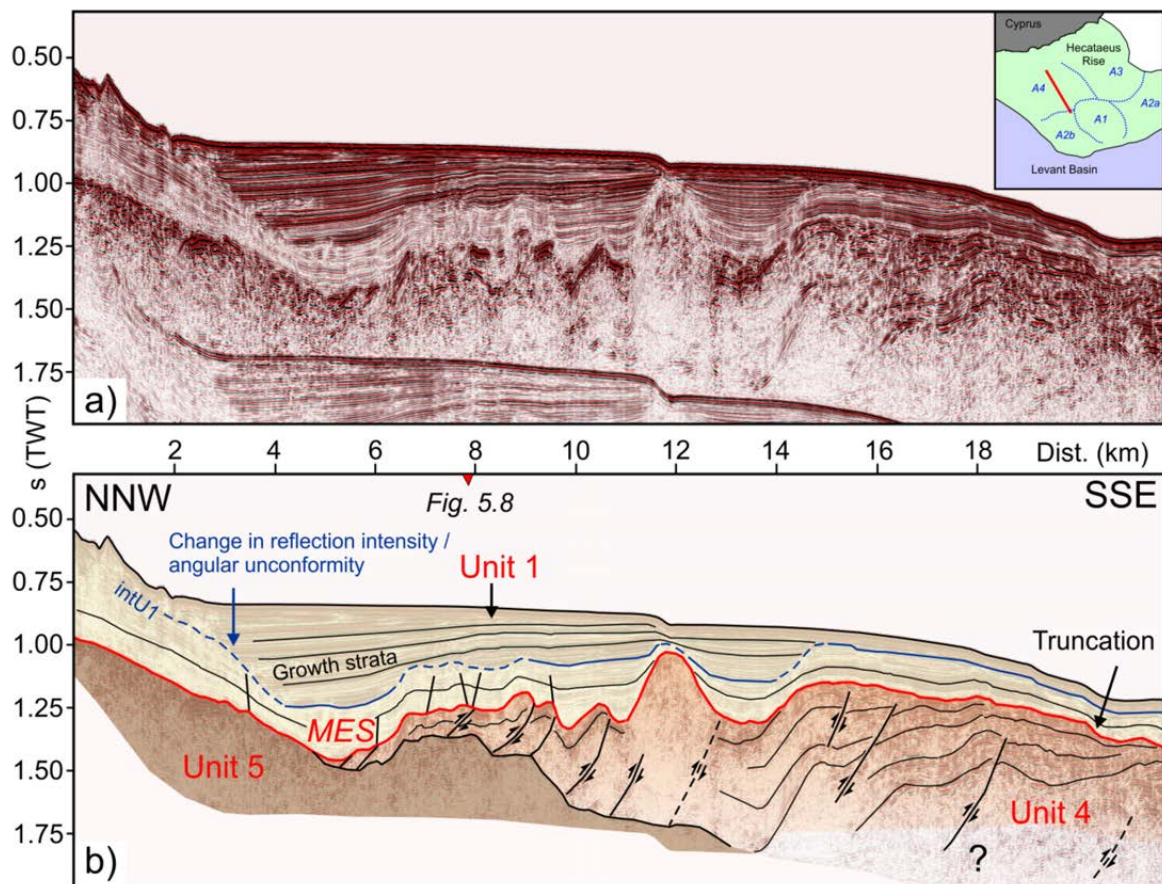


Figure 5.6 a) Uninterpreted and b) interpreted seismic profile from the northwestern part of the study area. Unit 4 is offset by several thrust faults which frequently terminate below the MES. A prominent intra-Unit 1 angular unconformity (intU1) is observed in the northern part of the profile. For detailed location see figure 5.2.

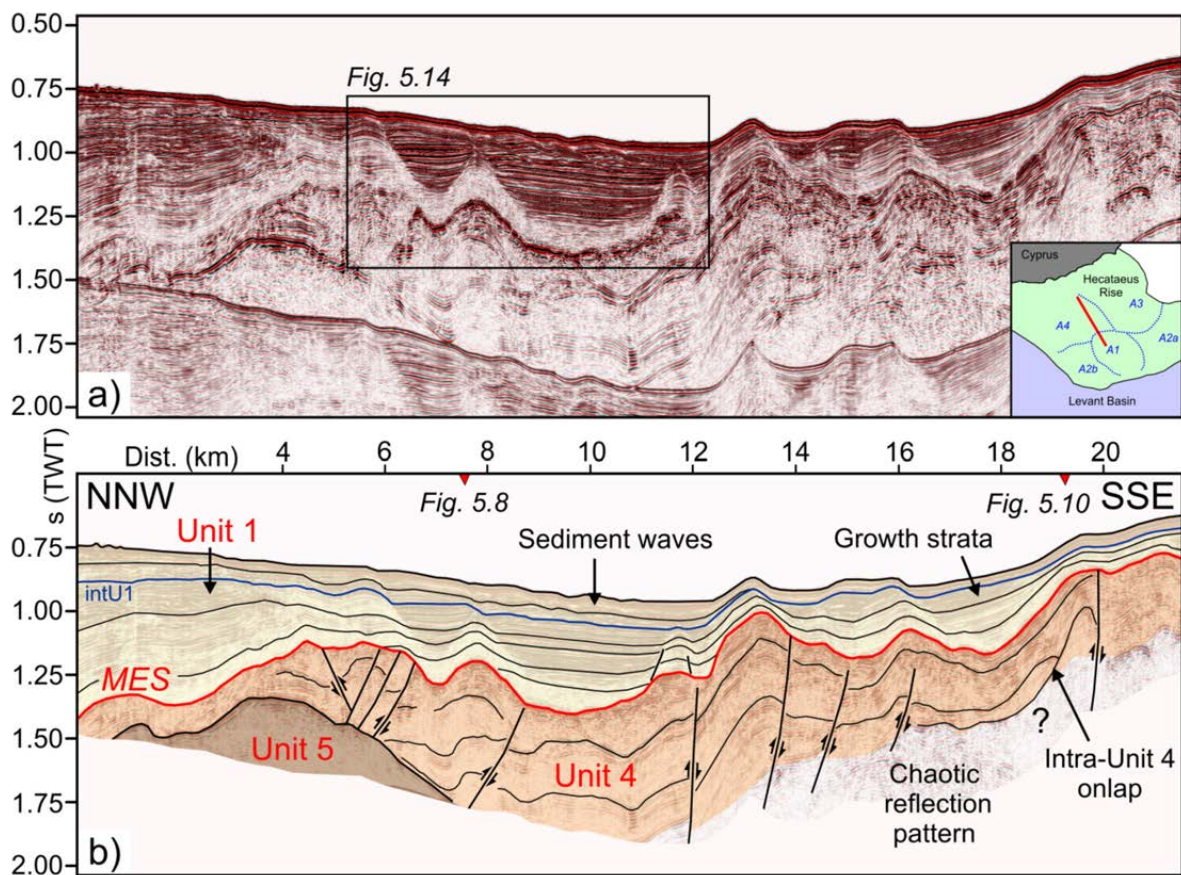


Figure 5.7 a) Seismic profile from the northwestern part of the Hecataeus Rise and b) its corresponding interpreted version. Reflections within Unit 4 converge towards the south and are offset by several thrust faults. Unit 1 exhibits a wavy reflection pattern above horizon intU1. For detailed location see figure 5.2.

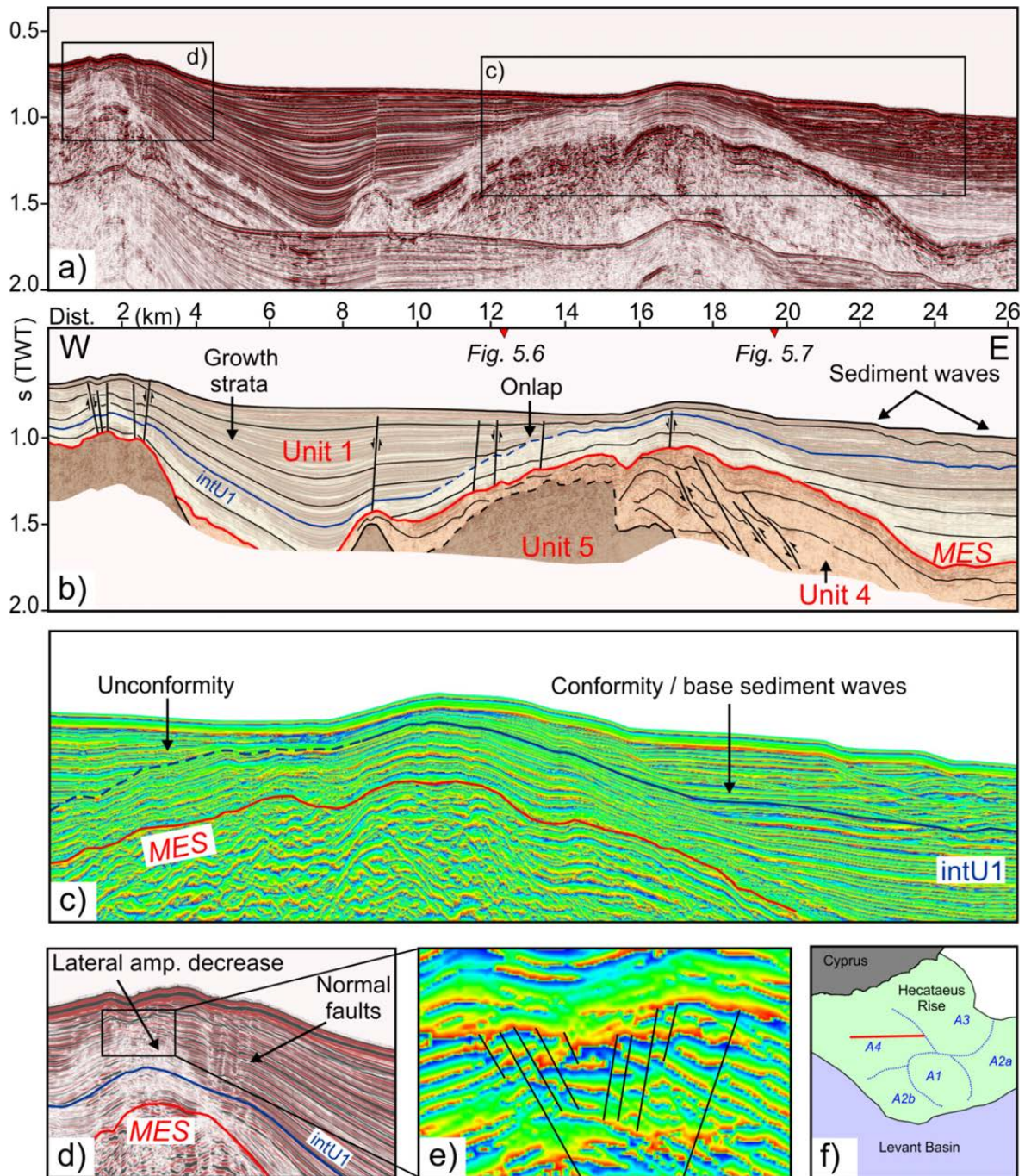


Figure 5.8 **a)** Seismic profile and **b)** its corresponding interpreted version crossing the northern part of the Hecataeus Rise in east-west direction. Note the presence of a significant high in the central part of the profile delineated by the MES-reflection. For detailed location see figure 5.2. **c)** Instantaneous phase plot highlighting the suggested eastward continuation of the intU1 chronostratigraphic horizon which corresponds to an angular unconformity further west. **d)** Enlarged section showing an abrupt lateral decrease in reflection amplitude together with the presence of several small-scale normal faults developed within Unit 1. **e)** Enlarged instantaneous phase plot from the region associated with a loss in reflection amplitude shown in d). Note the presence of densely spaced normal faults. **f)** Location map of the profile shown in a), b).

5.4.2.3 Unit 4

Except of areas where Unit 5 directly terminates against the MES (Figs. 5.6, 5.8a,b), Unit 4 is observed across the entire study area and mainly characterized by a package of parallel to sub-parallel, semi-continuous reflections of variable reflection intensity (Figs. 5.5a, 5.6, 5.7, 5.8a,b, 5.9a,b, 5.10-5.12, 5.15, 5.16). The top of Unit 4 is either defined by the MES or BES throughout the entire Hecataeus plateau. The base of Unit 4 is locally delineated by the top of Unit 5 in the northwestern part of the Hecataeus Rise (Figs. 5.6, 5.7, 5.8a,b). Across the remaining plateau area, the base of Unit 4 is locally inferred from detection of the lowermost parallel reflection package (Figs. 5.7, 5.10). However, the presence of multiples or strong acoustic attenuation with depth does often not allow for detecting the base and thus thickness of Unit 4 (Figs. 5.8a,b, 5.9a,b). A minimum thickness of 400-600 ms (TWT) is frequently observed (e.g. Figs. 5.7, 5.12).

In the southwestern part of the Hecataeus Rise (Area 4), Unit 4 is characterized by significant internal deformation. This deformation is particularly evident in the vicinity of Unit 5-highs, where Unit 4 deposits are offset by multiple faults (Figs. 5.6, 5.7, 5.8a,b). Further south, Unit 4 reflections slightly convergence and turn into a stack of densely spaced high-amplitude reflections (km 14-20 in Figs. 5.6 and 5.7). Near the southern edge of Area 4, intra-Unit 4 onlap terminations are locally observed (km 19 in Fig. 5.7).

Further east, throughout most of the plateau area defined by Area 3, Unit 4 is characterized by parallel, slightly wavy and moderately continuous, low to medium-amplitude reflections (Fig. 5.9a,b). The upper part of Unit 4 is heavily truncated parallel to the boundary between Area 3 and 1, where the MES delineates an approximately 3-4 km wide depression (km 18-22 in Fig. 5.9a,b, km 15-19 in Fig. 5.10).

The southwestern and southeastern edges of the Hecataeus Rise are defined by Areas 2a and 2b (Figs. 5.2, 5.3) where Unit 4 exhibits low to medium-amplitude sub-parallel reflections of limited lateral continuity which are broadly folded by several approximately east-northeast to west-southwest trending anticlinal structures (Figs. 5.11, 5.12). Locally, intra-Unit 4 reflections converge or show internal onlap terminations below these anticlines (km 14 in Fig. 5.11).

Unit 4 reflections observed across the large bathymetric high in the central southwestern part of the Hecataeus Rise (Area 1) are difficult to correlate to Unit 4 reflections described for the remaining plateau area. This is related to the fact that deformation or erosion along all edges of this circular structure interrupts lateral continuity of intra-Unit 4 reflections and thus complicates a direct correlation (km 20 in Fig. 5.7, km 24 in Fig. 5.9a,b, km 15 in Fig. 5.10).

Within Area 1 the top of Unit 4 is mainly delineated by a high-amplitude MES reflection. However, in some places – and frequently related to the presence of deformation – the MES reflection virtually disappears and the contact between Units 4 and 1 is only evident by its discordant nature (Fig. 5.9d). The base of Unit 4 is not observed within this part of the Hecataeus Rise owing to early arrival of multiple reflections. Internally, Unit 4 shows medium to high-amplitude, sub-parallel and largely discontinuous reflections (Fig. 5.10). One of the lowermost identifiable reflections of Unit 4 in this area shows a distinct wavy, sometimes near sinusoidal shape and appears to delineate locally truncated reflections below (Fig. 5.9d). This reflection could frequently be identified across the circular high and may indicate the presence of large channel-like structures.

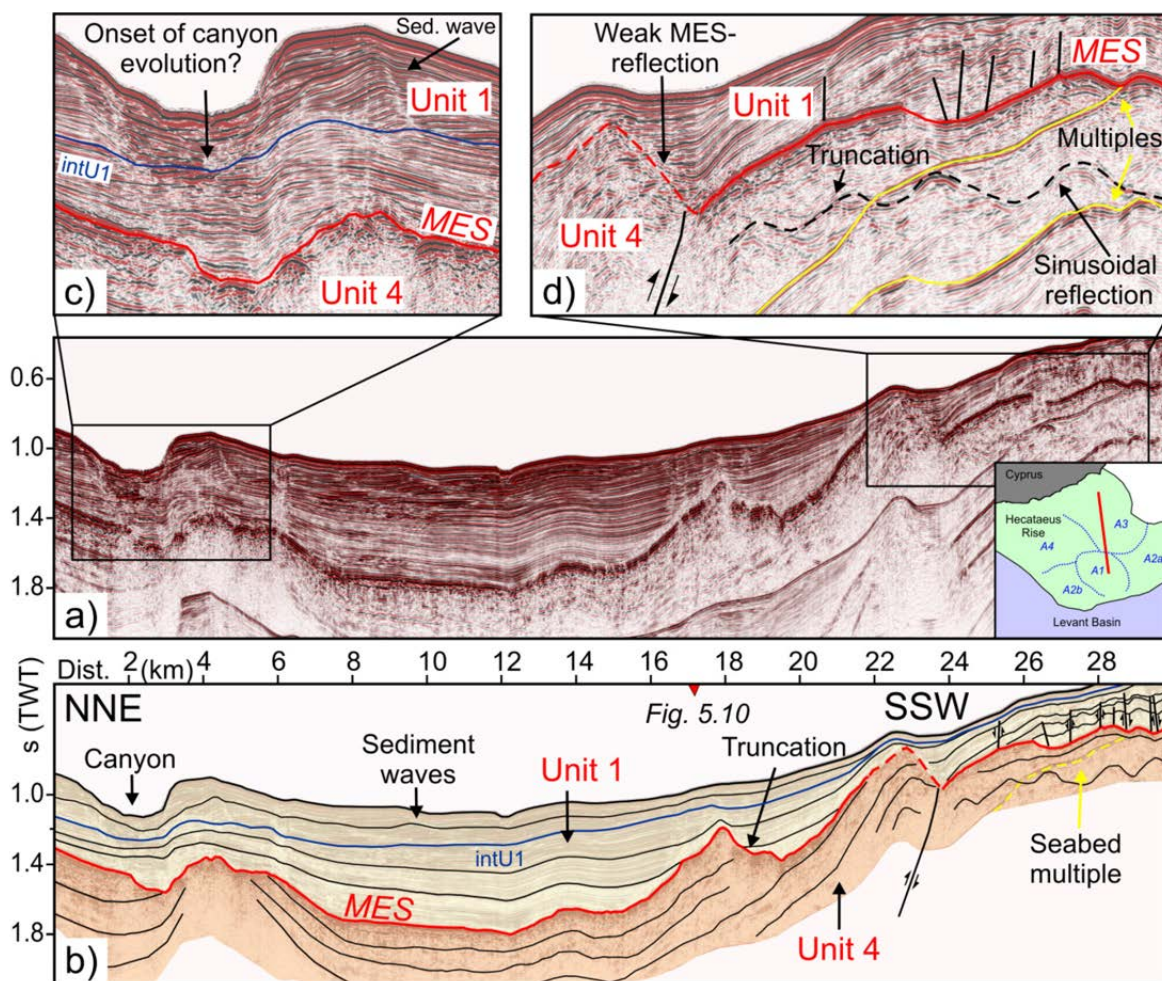


Figure 5.9 a) Uninterpreted and b) interpreted seismic profile from the eastern half of the Hecataeus Rise. For detailed location see figure 5.2. c) Enlarged section of a prominent canyon which incises the seabed at the northeastern corner of the Hecataeus Rise. While horizon intU1 defines the base of sediment waves adjacent to the canyon, it correlates to a high-amplitude reflection below the center of this structure. d) Enlarged section from the central part of the plateau area, where the seabed ascends to a prominent circular positive structure. Note the presence of an intra-Unit 4 sinusoidal reflection which truncates reflections below.

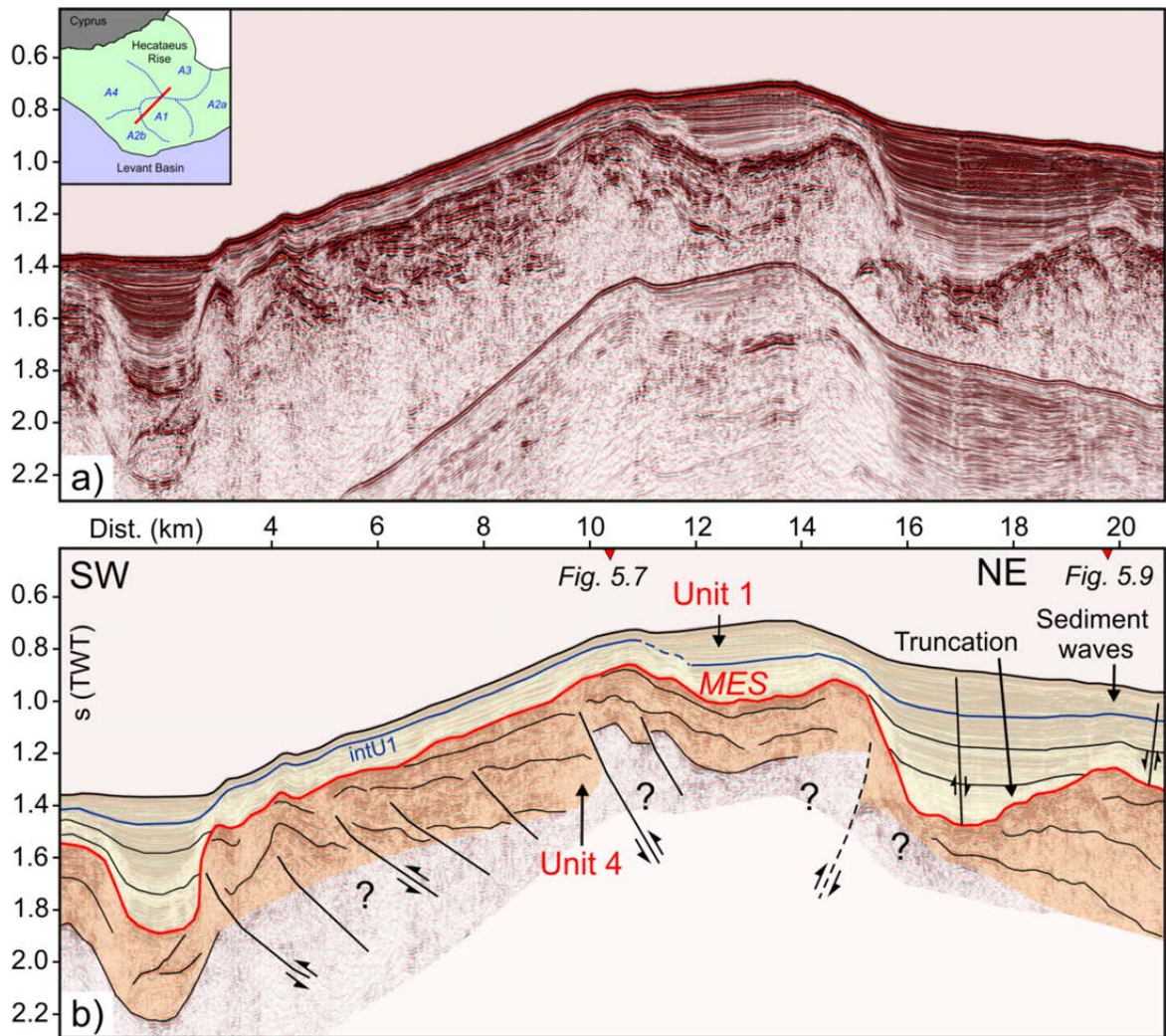


Figure 5.10 a) Seismic profile and **b)** its corresponding interpreted version crossing the northern edge of a prominent circular high, associated with Area 1. Two prominent thrust faults of opposite dip direction are inferred to have offset the most elevated part of this structure from the surrounding seafloor. For detailed location see figure 5.2.

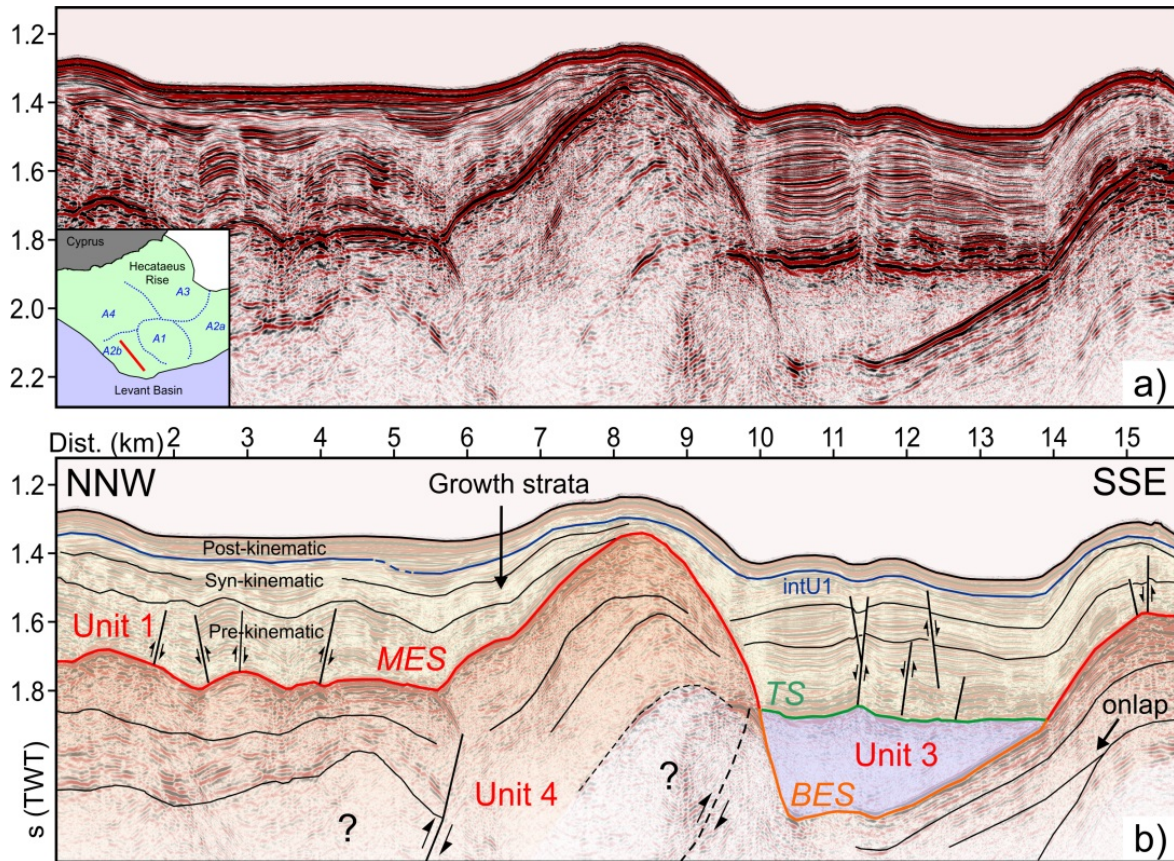


Figure 5.11 **a)** Seismic profile and **b)** its corresponding interpreted version from the southwestern part of the Hecataeus Rise. Two prominent anticlinal structures are developed within Unit 4 and flank a small evaporite basin in between. Deformation and growth strata developed within Unit 1 (syn-kinematic layer) indicate post-Messinian reactivation of anticlinal growth. For detailed location see figure 5.2.

5.4.2.4 Unit 3

Unit 3 is observed within small sub-basins at five locations across the Hecataeus Rise and reaches a maximum thickness of locally more than 300 ms (TWT) (Figs. 5.3b, 5.11). Acoustically, this unit is characterized by a near absence of internal reflectivity (Figs. 5.4, 5.5a, 5.11). The top of Unit 3 is delineated by a prominent reflection (TS) which onlaps the MES and always occurs at depths of 1.65-2.1 s (TWT) (Fig. 5.11). The base of Unit 3 is characterized by an equally prominent but phase-reversed reflection (Fig. 5.4). Considering that Unit 3 directly overlays the Messinian erosion surface (BES), the observed acoustic characteristics are indicative for the presence of Messinian evaporites and are very similar to previous reflection seismic observations north of the Latakia Ridge (Maillard et al., 2011).

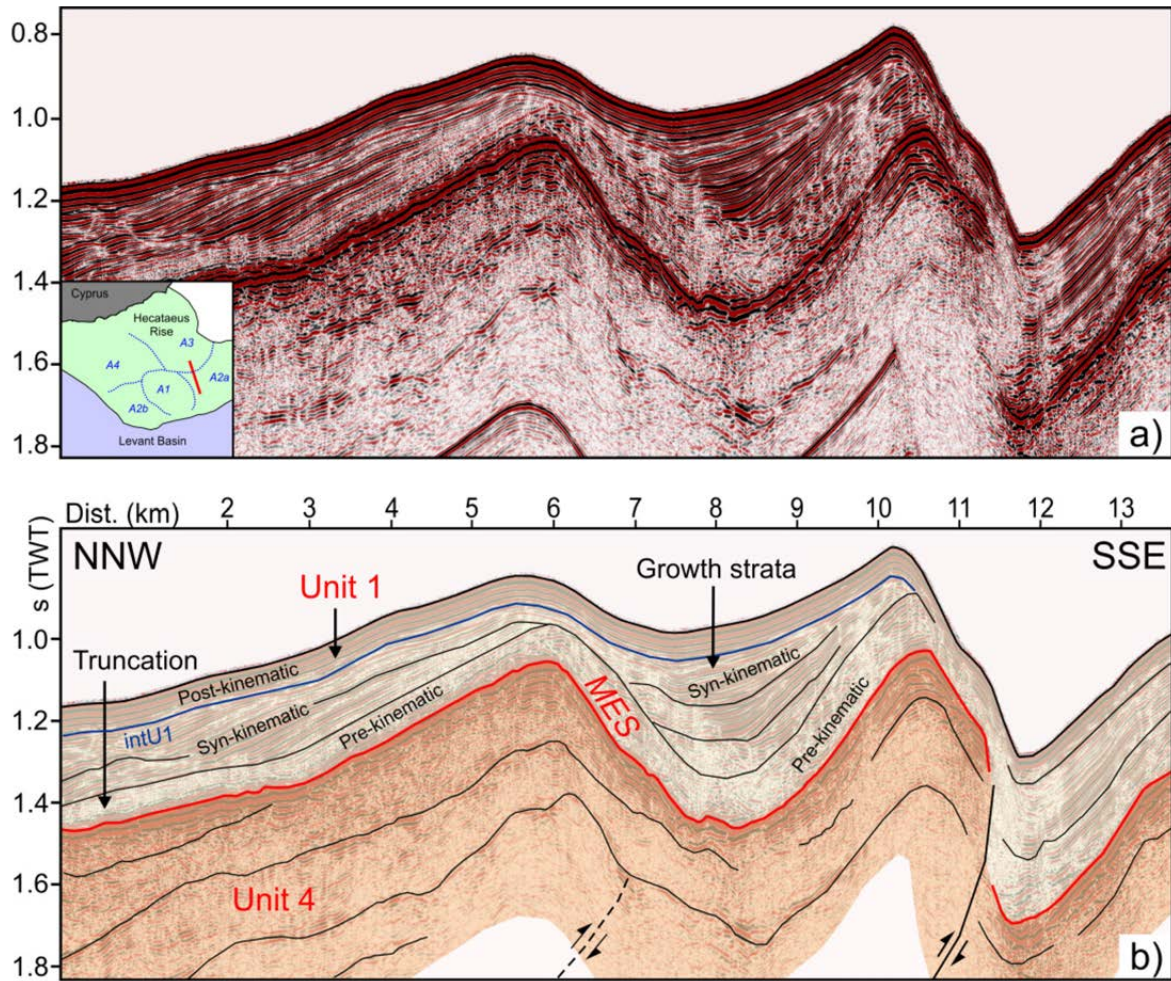


Figure 5.12 a) Seismic profile and **b)** its corresponding interpreted version from the southeastern part of the Hecataeus Rise. Three sub-units are identified within Unit 1 (pre-, syn- and post-kinematic). The central sub-unit exhibits divergent reflections, indicating a period of post-Messinian anticlinal growth. For detailed location see figure 5.2.

5.4.2.5 Unit 1

Unit 1 is observed within the entire study area and mainly separated from Unit 4 and locally from Units 3 and 5 by the MES and TS (Figs. 5.6, 5.7, 5.8a,b, 5.9-5.12, 5.15, 5.16). Acoustically, Unit 1 is characterized by parallel to divergent, locally wavy, lateral continuous reflections of variable reflection intensity (Fig. 5.5a). The thickness distribution of this unit reveals two isolated depocenters (Fig. 5.13a). A western, elongated depocenter is situated within the northwestern part of the plateau area and comprises up to 1000 ms (TWT) of post-Messinian sediments. Further west, up to 950 ms (TWT) thick Unit 1-deposits occupy two connected sub-basins. Both depocenters are separated by a north-northwest to south-southeast trending positive structure which extends from Cyprus to the structural high associated with Area 1 and is clearly visible within the base-Pliocene time structural surface (Fig. 5.13b). For the remaining plateau area, sediments

associated with Unit 1 reach only a limited thickness of mostly less than 300 ms (TWT) (Fig. 5.13a).

In the northwestern part of the Hecataeus Rise, Unit 1 is locally characterized by the discordant superposition of a low-reflectivity, stratified lower part and a high-reflectivity, stratified upper part. This is particularly well observed along the profile shown in figure 5.6, where MES-parallel, southward-dipping, low-amplitude reflections are onlapped by a package of high-amplitude, slightly northward-dipping, divergent reflections (km 0-6). A similar discordant reflection geometry is also observed between km 10 and 16 in figure 5.8, where the MES-parallel, westward-dipping lower part of Unit 1 is unconformably overlain by high-amplitude reflections associated with the upper part of Unit 1. While these two data examples clearly show the intra-Unit 1 low-reflectivity/high-reflectivity contact as an angular unconformity, this relation is only locally observed and does not apply to the entire plateau area.

For instance, tracing this apparent intra-Unit 1 unconformity from the western to the eastern Unit 1 depocenter in figures 5.8a,b is complicated by the presence of a north-south trending sub-Unit 1 high, expressed as a broad anticline delineated by the MES. Following the unconformity between low-amplitude and high-amplitude reflections across this anticline from west to east, suggests that this unconformity correlates with the base of wavy high-amplitude reflections within the upper part of Unit 1 further east. This assumption is supported by a seismogram emphasizing reflection continuity by displaying the attribute instantaneous phase, similarly showing the top of the low-reflectivity western sub-unit to correlate with the base of wavy deposits further east (Fig. 5.8c).

The ambiguous relation between high- and low-amplitude reflections within Unit 1 is further observed in figure 5.14a, where MES-positive structures correlate with several cone-shaped areas of low-amplitude reflections which show abrupt lateral transitions into adjacent areas of high reflectivity. These lateral changes in amplitude are evidently accompanied by frequency changes with low amplitude reflections being generally associated with a decrease in instantaneous frequency (Fig. 5.14c). The top of all low amplitude-highs was found to follow the same horizon, which also delineates the base of wavy reflections above. Again, looking at the attribute instantaneous phase suggests that reflections may laterally be followed from areas of low to areas of high-reflectivity (Fig. 5.14b).

In some profiles, a coincidence between sudden lateral/vertical changes in reflection strength and the presence of small-scale normal faults within Unit 1 is observed. This is most clearly seen in figures 5.8d,e, where a lateral decrease in reflection strength coincides with the presence of faults which are clearly traceable within an enlarged section showing the attribute instantaneous phase (Fig. 5.8e).

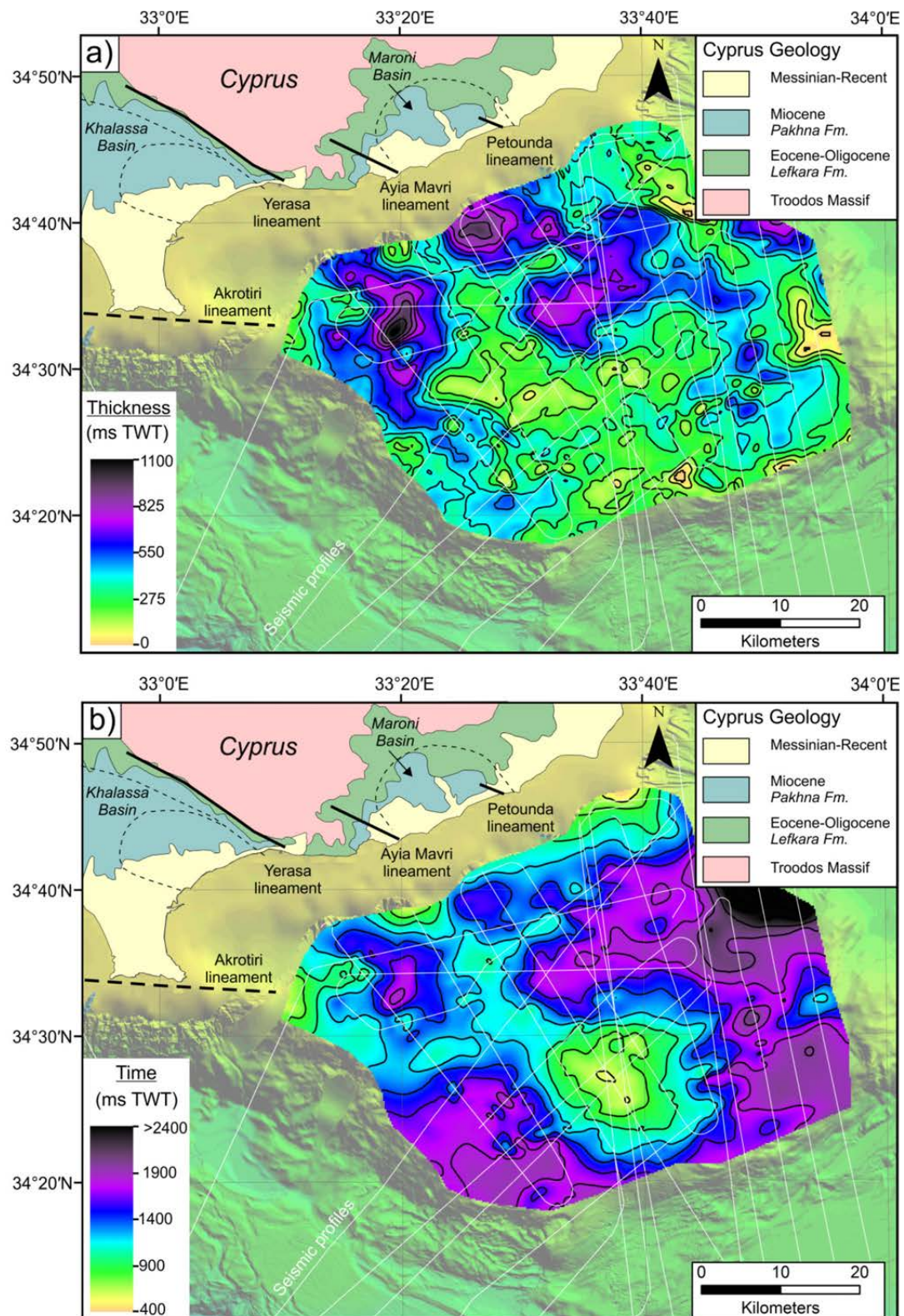


Figure 5.13 a) Map showing the thickness distribution of Pliocene-Quaternary sediments across the Hecataeus Rise in ms (TWT), with contour lines drawn every 100 ms (TWT). Note the presence of two depocenters separated by a northwest-southeast trending zone of limited sediment thickness. This zone can also be followed within the time structural map of the MES/TS reflection, shown in **b)** Contour lines correspond to 200 ms (TWT). Onshore Cyprus lineaments and sedimentary basins were drawn according to Robertson et al. (1991). A simplified geological map of Cyprus was drawn after Kinnaird and Robertson (2012).

Such small-scale faults can also be observed for the low-reflectivity Unit 1 package shown in figure 5.6 (km 0-12) and in the central part of the profile shown in figures 5.8a,b (km 10-16) even though faults are less frequently detected there, possibly as faults are often below the limit of seismic resolution. I suggest that, apart from a possible depositional control on reflection amplitude, small-scale faulting has influenced the acoustic characteristics of Unit 1 post-depositionally. A relation between shallow normal faults and amplitude loss in reflection seismograms was previously observed by Morley (2007). Amplitude loss due to small-scale faulting may also apply to low-reflectivity cones observed in figure 5.14a, where faults may simply not be seismically resolved. Concomitant decrease in frequency could be caused by faults acting as pathways for vertically migrating gaseous fluids (Fig. 5.14c). As an alternative view, the contact between low-amplitude and high-amplitude reflection packages could always be regarded as a chronostratigraphic boundary (e.g. in Fig. 5.14). However, an interpretation which allows for the occurrence of lateral amplitude changes within the same stratigraphic interval is locally more consistent with the observed lateral reflection continuity shown in instantaneous phase plots and with the relation between small-scale faults and changes in reflection strength.

I thus interpret the horizon delineating an angular unconformity in the northwestern part of the Hecataeus Rise and the base of a wavy high-amplitude package further east (Figs. 5.8a-c) as a chronostratigraphic marker which does not always represent the contact between low and highly reflective intervals. This horizon, termed IntU1, was followed across the entire Hecataeus plateau and marked in blue (as a solid line if conformable, as a stippled line if unconformable) within all interpreted seismic sections shown in figures 5.6-5.12 and 5.14.

Across the northeastern part of the Hecataeus Rise (Area 3), Unit 1 is characterized by continuous, parallel to slightly divergent reflections frequently onlapping against MES-topography below (km 15-22 in Figs. 5.9a,b, km 15-20 in Fig. 5.10). Reflection strength generally increases towards the seabed (Figs. 5.9a,b) but no distinct contrast between a low-reflectivity/high-reflectivity sub-unit is observed as for the northwestern Hecataeus Rise. Near the seabed in the eastern part of Area 4 and in Area 3, Unit-1 reflections frequently exhibit the presence of north-south trending sediment waves which are also reflected in the bathymetry (Figs. 5.3, 5.7, 5.8a-c, 5.9a-c, 5.14). The base of these wavy deposits correlates to the intU1 horizon introduced above. Following horizon intU1 below a prominent canyon system identified in the northeastern corner of the Hecataeus Rise suggests that this horizon correlates with a high-amplitude reflection beneath the center of the canyon (Fig. 5.9c).

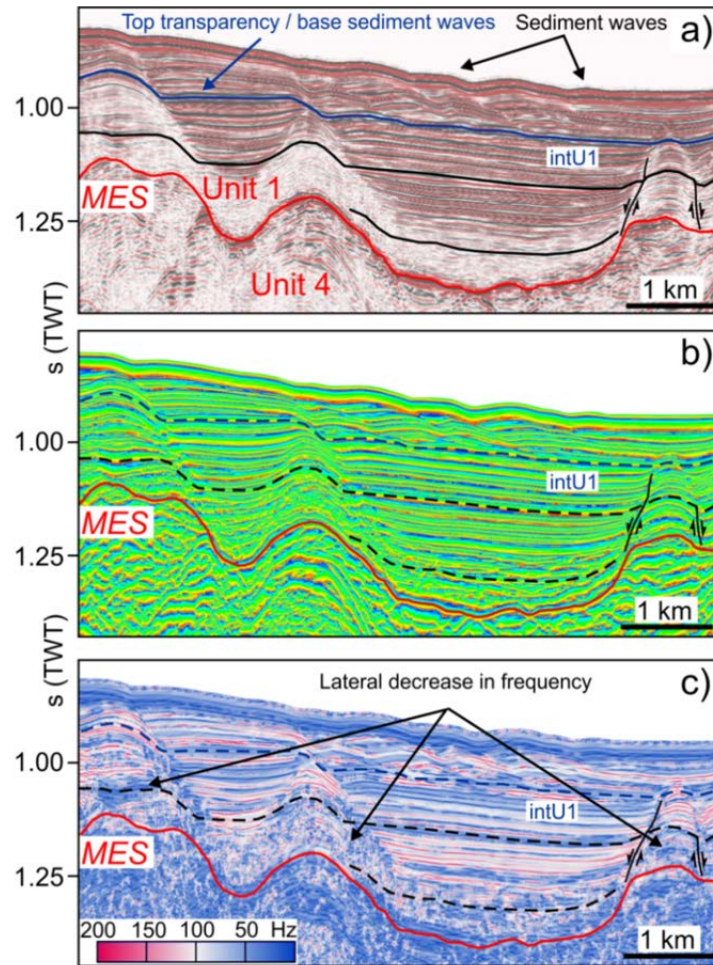


Figure 5.14 **a)** Enlarged seismic section from the profile shown in figure 5.7. Horizon intU1 delineates the base of sediment waves and the top of laterally confined transparent sections visible in the lower part of Unit 1. Below, reflections appear to laterally continue from areas of low to areas of high-amplitudes as also visible by following these events within the instantaneous phase plot shown in **b)**. **c)** The attribute instantaneous frequency shows relatively lower frequencies to correspond to areas of low-amplitude reflections while frequencies are generally higher within areas of greater reflectivity.

In the southwestern (Area 2b) and southeastern (Area 2a) parts of the Hecataeus Rise, Unit 1 deposits are deformed into several east-northeast to west-southwest trending anticlinal structures (Figs. 5.11, 5.12). There, Unit 1 deposits reach a thickness of up to 500 ms (TWT) being generally thicker on the backlimb than on the forelimb of the anticlines (Figs. 5.11, 5.12). Near anticlinal structures, Unit 1 may locally be subdivided into three sub-units, with the lowermost sub-unit being characterized by sub-parallel, irregular reflections of variable reflection strength which broadly follow the dip of the MES. This sub-unit is overlain by a package of locally divergent reflections, separated by the intU1-horizon from a thin layer or parallel, high-amplitude reflections above. In figures 5.11 and 5.12, these sub-units are labelled pre-kinematic, syn-kinematic and post-kinematic.

At the northern transition to the southern Hecataeus bathymetric high (Area 1), Unit 1 reflections onlap or converge towards a progressively ascending MES (km 17-19 in Fig. 5.7, km 18-22 in Figs. 5.9a,b). Across this significantly elevated part of the Hecataeus Rise, Unit 1 sediment thickness is generally less than 300 ms (TWT) (Fig. 5.13a). Throughout Area 1, the acoustic properties of Unit 1 are characterized by parallel to sub-parallel, locally discontinuous reflections of variable reflection intensity (Figs. 5.9d, 5.10).

5.4.3 Structural interpretation

The MES on the Hecataeus Rise represents a conclusive time marker, allowing to distinguish between a pre- and a post-Messinian phase of deformation. Pre-Messinian structures are frequently overprinted by subsequent, post-Messinian deformation events, making these structures generally more difficult to identify. Here, growth strata architecture of sub-MES reflections are used as an indication for pre-Messinian tectonic deformation as well as observations of sub-MES faults which terminate below/at the MES-reflection.

5.4.3.1 Pre-Messinian deformation

A pre-Messinian phase of compressional deformation is inferred to have significantly affected an elongated, several km wide transect extending from the southern tip of the onshore Yerasa lineament to the circular positive structure comprised within Area 1. This deformation corridor is approximately delineated by an elongated, north-northwest to south-southeast oriented MES-high shown in figure 5.13b. A seismic profile displayed in figure 5.6 is oriented along this strongly deformed area, showing a stack of steeply northward-dipping Unit 4-reflections, interpreted to represent an imbricate thrust system which was active in pre-Messinian times and became partly levelled by a Messinian phase of erosion. A peculiar high in the central part of figure 5.6 (km 12) may represent the hanging wall of such a thrust that withstood Messinian erosion. Moving towards the east, a neighboring, parallel seismic profile similarly displays pre-Messinian deformation (Fig. 5.7). There, Unit 4-reflections are similarly offset by several southward verging thrusts. Coincident folds developed in the lower part of Unit 1 attest that these structures have also experienced post-Messinian activity. However, a pre-Messinian phase of deformation is inferred from the presence of growth strata indicated by southward stratal thinning and intra-Unit 4 onlap terminations (Figs. 5.6, 5.7).

Moving even further towards the east, the structural characteristics of Unit 4 distinctly change. In the northern part of figures 5.9a,b, a broad anticline is developed within Unit 4. South of this structure no evidence of internal deformation is observed (km 8-20 in Figs. 5.9a,b). A significant eastward decrease in Unit 4

deformation is similarly recognized in figures 5.8a,b, where intra-Unit 5 thrusts appear to cease east of the MES-high (km 22-26).

Near the circular high associated with Area 1, intra-Unit 4 reflections are strongly tilted to the north and the MES is onlapped by Unit 1 (km 18-24 in Figs. 5.9a,b). Profiles crossing this circular high reveal significant intra-Unit 4 complexity at its edges. Reflections are generally offset by thrust faults adjacent to the bathymetric high, but such faults exhibit no consistent dip direction. While thrusts imaged at the transition to Area 1 in figures 5.7 (km 20) and 5.9a,b (km 24) clearly dip towards the north, this dip direction appears to be locally reversed as shown by the more southwestward dipping thrust at km 15 in figure 5.10.

Areas 2a and 2b are characterized by the presence of anticlinal structures which are developed within Units 1 and 4. Anticlines are generally characterized by short southward dipping forelimbs and relatively long northward dipping backlimbs (Figs. 5.11, 5.12). Thrust fault trajectories were drawn with the aid of intra-Unit 4 hanging wall cutoffs if observed or stippled if thrust trajectories could only be inferred. A large anticlinal structure shows 800 ms (TWT) vertical separation between the MES- and BES-horizons at profile km 6-10 in figure 5.11. The leading syncline to the south of this structure was filled by Unit 3 deposits. As Unit 3 never oversteps the crests of anticlines, these structures are suggested to have already been present in pre-Messinian times. This interpretation is supported by observing convergent Unit 4 reflections and interstratal onlap along the backlimbs of anticlines at km 9 and 14 in figure 5.11, suggesting a pre-Messinian phase of anticlinal growth.

Two seismic profiles crossing the southeastern slope of the Hecataeus Rise provide insight into the structural geometry near the transition to the Levant Basin (Figs. 5.15, 5.16). The eastern profile shows Unit 4-reflections to be bent upwards near the slope of the Hecataeus Rise, being unconformably overlain by a largely horizontal layer of Unit 1 deposits (km 12-17 in Fig. 5.15). Further south, where the seafloor steeply descends into the Levant Basin, Unit 4 can no longer be observed. The observed Unit 4 geometry might be related to the presence of a pre-Messinian large-scale thrust that has accommodated shortening and vertical separation between the Hecataeus Rise and the Levant Basin (Fig. 5.15). A different structural situation is encountered approximately 14 km further west, where another north-south oriented profile images the transition into the Levant Basin (Fig. 5.16). There, Unit 4 appears to largely dip parallel to the present-day slope of the seabed, showing the presence of thrusts and internal folds. Unit 4 is truncated by the MES at the foot of the slope and cannot be followed any further due to a change to chaotic reflections (km 18 in Fig. 5.16). As folds within Unit 4 are either of larger amplitude (km 6 in Fig. 5.16) or not reflected at all within Unit 1

(e.g. the syncline at km 12-15 in Fig. 5.16), I interpret these structures to reflect a pre-Messinian phase of compressional deformation.

5.4.3.2 Post-Messinian deformation

A second, post-Messinian phase of tectonic activity has particularly affected the southeastern half of the Hecataeus Rise, comprising Areas 1, 2a and 2b (Figs. 5.2, 5.3). Anticlinal structures developed within Unit 4 experienced post-Messinian reactivation after having initially been draped by a pre-kinematic lower Unit 1 sediment layer (Figs. 5.11, 5.12). The middle part of Unit 1 thins by interstratal onlap along the backlimb towards the crest of the anticlines (syn-kinematic layer) providing evidence for a phase of post-Messinian fold growth (Figs. 5.11, 5.12). The uppermost Unit 1 deposits, above horizon intU1, are again fairly isopacheous, suggesting limited recent anticlinal growth. Unit 1 growth strata is further observed near the northern slope of the Hecataeus bathymetric high (Area 1), where northward-dipping reflections strongly converge (km 17-19 in Fig. 5.7, km 18-22 in Figs. 5.9a,b). Such observations imply that Area 1 also experienced a phase of post-Messinian uplift relative to the plateau area further north.

While negligible Pliocene-Quaternary deformation has affected the entire northeastern part of the Hecataeus Rise (Area 3) (Figs. 5.9a,b), the northwestern plateau area (Area 4) exhibits some recently active structures. The seabed directly east of the onshore Cyprus Akrotiri Peninsula is folded by an approximately 4 km wide anticline (km 0-4 in Figs. 5.8a,b) which can also be traced in the bathymetry (Fig. 5.3a, inset IV). At the crest of this structure, Unit 1 is offset by numerous small, densely spaced normal faults which coincide with a dramatic loss in reflection amplitude (Figs. 5.8d,e). Recent anticlinal growth is evident by significant thinning of Unit 1 towards the crest of this structure (Figs. 5.8a,b). Further east, Unit 1 onlaps against low-amplitude reflections below the intU1 horizon (km 10-16 in Figs. 5.8a,b). The geometric relation of intra-Unit 1 growth strata onlapping a package of parallel, southeastward dipping reflections below horizon intU1, shows that anticlinal uplift post-dates the tectonic event that has initially caused the development of the observed intra-Unit 1 unconformity (see also Fig. 5.6).

Along the north-northwest to south-southeast trending corridor of previously described significant pre-Messinian deformation, local post-Messinian reactivation has led to the development of several smaller folds within Unit 1 (km 6-18 in Fig. 5.7).

Near the southeastern slope of the Hecataeus Rise, extensional faults offset reflections within Unit 1 along km 10-13 in figure 5.15 while steeply dipping thrust faults have deformed the seabed approximately 14 km further west (km 9-12 in Fig. 5.16). The seabed along the foot of the slope is slightly bulged and elevated relative to the adjacent Levant Basin (Figs. 5.2, 5.3, 5.15, 5.16). Several faults of

multiple dip directions offset the MES at the foot of the slope, revealing both normal and reverse displacement (Figs. 5.15, 5.16). These structures are interpreted to represent a slope-parallel positive flower structure where post-Messinian sinistral transpression was accommodated.

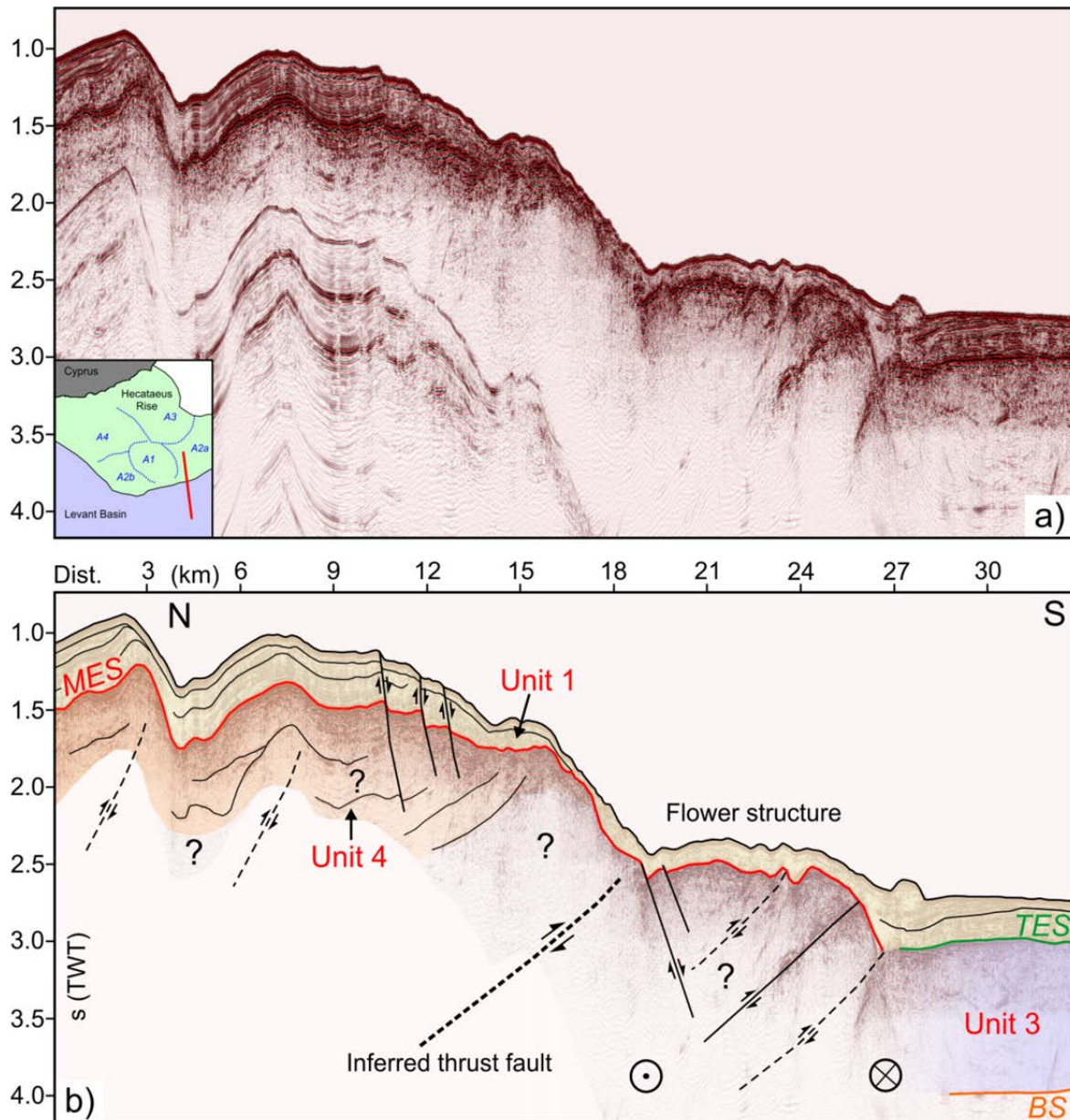


Figure 5.15 a) Seismic section and b) its corresponding interpreted version crossing the southeastern flank of the Hecataeus Rise and extending into the Levant Basin. Northward-dipping reflections developed within Unit 4 near the southern edge of the Hecataeus plateau may indicate the presence of a large-scale thrust at the junction between the Hecataeus Rise and the Levant Basin. Faults at the foot of the slope are interpreted to represent a positive flower structure. For detailed location see figure 5.2.

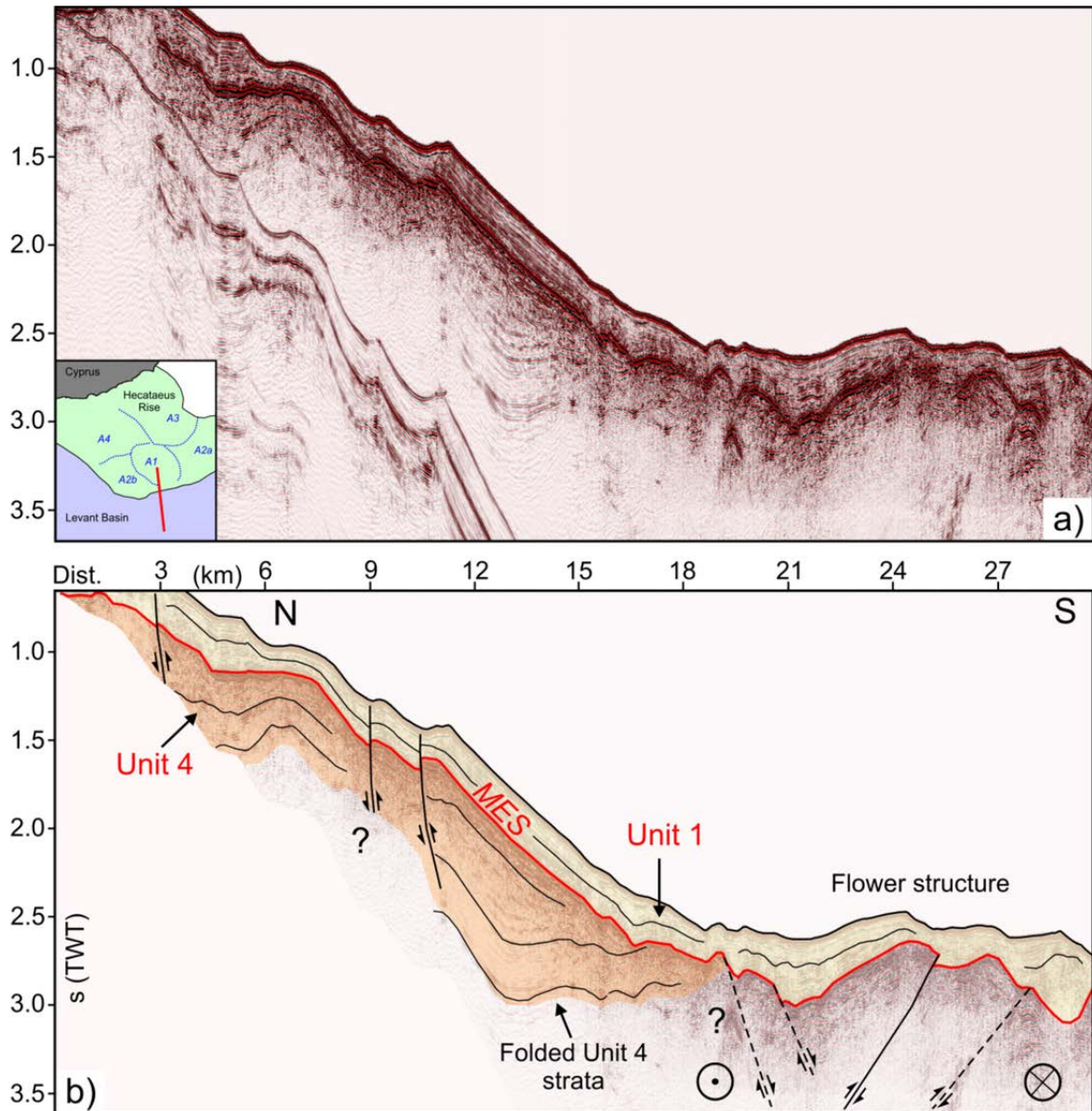


Figure 5.16 **a)** Uninterpreted and **b)** interpreted seismic profile crossing the southern flank of the Hecataeus Rise approximately 14 km west of the profile shown in figure 5.15. Units 1 and 4 exhibit the presence of folds and thrusts. Faults at the foot of the slope may correspond to a positive flower structure. For detailed location see figure 5.2.

5.5 Discussion

5.5.1 Structural and stratigraphic link to Cyprus

The continuation of onshore Cyprus structural features onto the Hecataeus Rise was initially proposed by McCallum et al. (1993) based on shallow seismic data. By observing folds within offshore deposits of inferred Miocene age, these authors suggested an offshore continuation of the Yerasa and Akrotiri lineaments that were evidently active during this time (Robertson et al., 1991; Eaton and Robertson, 1993). While the data by McCallum et al. (1993) were mainly restricted to the upper Cyprus margin, results of this study support an offshore continuation of

onshore lineaments even further into the offshore domain. Most intensive pre-Messinian deformation is observed in seismic profiles located in close vicinity to an inferred straight continuation of the Yerasa lineament (Figs. 5.2, 5.3, 5.6, 5.7). The onshore Yerasa lineament represented an elevated anticlinal structure during Miocene times, separating the Maroni Basin from the Khalassa Basin further west (Robertson et al., 1991; Eaton and Robertson, 1993) (Figs. 5.2, 5.3). Such a separation is also observed in the offshore domain, where Unit 4 deposits onlap a Unit 5 positive structure that is located near the inferred offshore continuation of the Yerasa lineament (Figs. 5.8a,b). This subdivision into two sub-basins has apparently lasted into post-Messinian times as Pliocene to Quaternary depocenters are presently separated by a north-northwest to south-southeast trending positive structure clearly appearing in the base Pliocene time structural surface and nicely lining up with the inferred offshore continuation of the Yerasa lineament (Fig. 5.13b).

Seismic data shown in this study further allow for speculating about an offshore continuation of the Akrotiri and Petounda lineaments. The former is closely located to a prominent anticlinal structure of similar orientation which clearly shows up in the base Pliocene time structural map (Fig. 5.13b) and in the present-day bathymetry (Fig. 5.3a, inset IV). Following the orientation of the Petounda lineament into the offshore domain coincides with the location of a prominent pre-Messinian fold (km 4 in Figs. 5.9a,b).

Given the existence of such an onshore-offshore structural link, deformation events of known temporal occurrence from the onshore Cyprus geology should also be reflected within the offshore domain and may thus allow for stratigraphic correlation. The structural configuration and timing of deformation near the onshore Yerasa lineament were investigated by Robertson et al. (1991) and Eaton and Robertson (1993). An Early Miocene-Tortonian phase of deformation has caused intensive deformation within Eocene-Oligocene pelagic carbonates of the Lefkara Formation which subsequently suffered significant erosion before being transgressed by the Tortonian Koronia Member of the Pakhna Formation at times of tectonic inactivity (Robertson et al., 1991; Follows, 1992; Eaton and Robertson, 1993). Near the inferred offshore continuation of the Yerasa lineament, Unit 4 is deformed throughout its entire thickness (Figs. 5.6, 5.7). Transferring the tectonostratigraphic situation of southern Cyprus directly to the offshore domain would therefore suggest that Unit 4 correlates with the onshore Eocene-Oligocene Lefkara Formation while Tortonian carbonates (present onshore Cyprus) are essentially absent on the Hecataeus Rise, given the lack of a corresponding intra-Unit 4 unconformity.

However, this correlation is contradicted by the presence of intra-Unit 4 growth strata (Figs. 5.6, 5.7). If growth within Unit 4 relates to the southern Cyprus Miocene compressional period, most of Unit 4 should essentially be Miocene in age. Observation of intra-Unit 4 channel-like structures across the southern Hecataeus bathymetric high may indicate subaerial or submarine erosion, eventually corresponding to a Miocene period of tectonic compression and uplift (Fig. 5.9d). Miocene offshore transport of material eroded from subaerially exposed parts of Cyprus may account for differences in thickness between the southern Cyprus Miocene Pakhna Formation (150 m near Ayios Theodoros, located within the Maroni Basin in Figs. 5.2, 5.3, according to Bagnall, 1960) and Unit 4 (approximately 450 ms (TWT) in Figs. 5.4 and 5.5 \approx 400-800 m, depending on the velocity used for conversion).

Finally, deformation events which affected southern Cyprus and the Hecataeus Rise may not have been entirely coeval. While compressional deformation was reported to have ceased by Tortonian (Yerasa lineament) to earliest Pliocene times (Akrotiri and Petounda lineaments), seismic data shown in this study indicate post-Messinian reactivation of structures located near these lineaments. The inferred continuation of the Akrotiri lineament represents one of the most recently active structures on the Hecataeus Rise, where growth strata is imaged directly below the present-day seabed (Figs. 5.8a,b). Folds located along the inferred offshore continuation of the Yerasa lineament were partly reactivated during Pliocene-Quaternary times (Fig. 5.7). It thus follows that a unique stratigraphic interpretation of Unit 4 is not possible based on the present dataset alone. I therefore correlate Unit 4 with the onshore Pakhna and Lefkara Formations without making any further discrimination (Fig. 5.5b).

Unit 5 underlies Unit 4 and is exclusively observed in the northwestern part of the Hecataeus Rise (Figs. 5.6, 5.7, 5.8a,b). I tentatively correlate this unit to the onshore southern Cyprus Moni Melange, composed of allochthonous rocks which were emplaced by gravity sliding within a Cretaceous subduction setting (Robertson, 1977b). Such a correlation is consistent with the internal transparent to chaotic reflection character of Unit 5 which would be expected for rocks with no internal stratigraphical order (Robertson, 1977b). Furthermore, rocks associated with the Moni Melange crop out at the southern cliffs of the Akrotiri Peninsula (Bear and Morel, 1960), in close vicinity to the inferred eastward continuation of the Akrotiri lineament, where the Moni Melange (Unit 5) is believed to directly underlay Unit 1 (km 0-4 in Figs. 5.8a,b). Finally, observation of most intensive compressional Unit 4 deformation near Unit 5 positive structures resembles the onshore Cyprus deformation pattern, where the Moni Melange was thrust over Eocene-Oligocene pelagic carbonates of the Lefkara Formation (Figs. 5.6, 5.7, 5.8a,b) (Robertson et al., 1991; Eaton and Robertson, 1993).

5.5.2 Pre-Messinian tectonostratigraphic evolution of the Hecataeus Rise

A pre-Messinian phase of deformation has affected the Hecataeus Rise, as evident by the presence of Unit 4 growth strata and sub-MES folds and thrusts generally observable in the southern and western parts of the Hecataeus Rise (Figs. 5.6, 5.7, 5.8a,b, 5.10, 5.11, 5.15, 5.16). A phase of Early Miocene-Tortonian compression was reported from onshore southern Cyprus (Eaton and Robertson, 1993) and from the Latakia Ridge, where Miocene deposits were folded into several northeast-southwest trending anticlinal structures (Hall et al., 2005). These anticlines resemble those identified along the southeastern flank of the Hecataeus Rise in orientation and geometry (i.e. short forelimbs and longer, gently dipping backlimbs, locally exhibiting sub-MES growth strata) (Figs. 5.11, 5.12). I therefore suggest that the Hecataeus Rise has experienced a Miocene phase of northwest directed African-Anatolian convergence that has also affected the Latakia Ridge further east, leading to the formation of anticlinal structures directly north of the inferred plate boundary (Fig. 5.3).

Apart from the southern Hecataeus-anticlines, seismic profiles of this study exhibit pre-Messinian compressional structures, which are predominantly detected within the western half of the study area (Figs. 5.6, 5.7, 5.8a,b, 5.10). Such geographic variations in the pre-Messinian intensity of compressional deformation raise the question about the underlying cause. Insight may come from seismic profiles across the transition zone between Hecataeus Rise and Levant Basin, where significant structural heterogeneity is observed (Figs. 5.15, 5.16). The eastern of these profiles bears indications for the presence of a large-scale thrust, believed to efficiently accommodate shortening along this segment of the Hecataeus-Levant Basin transition zone (Fig. 5.15). In contrast, no such fault is inferred further west, where folded sub-MES strata can be followed into the Levant Basin (Fig. 5.16). Based on this observation I suggest a more complex compressional regime along this western part of the plate boundary, where shortening may be accommodated less efficiently, facilitating stress transfer to the western plateau area. This concept is consistent with the observation of a dent within the western part of the southeastern Hecataeus flank compared to its eastern continuation (follow the contour lines along the slope from Area 2b to Area 2a in Fig. 5.3b).

The mechanism responsible for creating such structural differences along the southeastern flank of the Hecataeus Rise cannot be resolved by data of the present study. However, I note that recently published refraction seismic data revealed significant lateral velocity variations within the lower part of the crust at the western flank of the Hecataeus Rise (Welford et al., 2015). Based on these data, Welford et al. (2015) interpreted the plate boundary as a transform margin,

where strong lateral crustal heterogeneity is encountered. The possible arrival of rigid crustal blocks at the western part of the southeastern Hecataeus flank compared to its eastern continuation may provide an explanation for the observed structural differences.

Differences in the magnitude of Miocene shortening between the western and eastern half of the Hecataeus plateau may lead to the formation of a dextral strike-slip fault, accommodating shortening of the western plateau area with respect to its little deformed eastern continuation. The location of such a strike-slip fault would line up with the inferred offshore continuation of the Yerasa lineament, consistent with the presence of an elongated high within the base Pliocene surface (Fig. 5.13b). A seismic profile shown in figure 5.10 crosses this structure perpendicularly and indicates the presence of two significant thrusts of opposite dip direction (km 10 and 15 in Fig. 5.10). I interpret these faults to represent a positive flower structure separating strongly deformed Unit 4 deposits to the west from little deformed Unit 4 deposits further east. Finally, the processes suggested above would also provide a possible explanation for the formation of a circular high sitting at the southeastern flank of the Hecataeus Rise (Fig. 5.3). While few processes are generally conceivable to create such a structure (1. meteorite impact [Buchner and Kenkmann, 2008], 2. mud/serpentine volcanism [Kopf, 2002; Oakley et al., 2007], 3. salt tectonics [Jackson and Talbot, 1986], 4. magma emplacement [e.g. Howe et al., 2006]), none of these finds sufficient support in data of this study or in refraction seismic data published by Welford et al. (2015) (1. no rim syncline, 2. no evidence for mud flows or fluid migration 3. salt is not present in such quantities on the Hecataeus Rise, 4. too low crustal velocities). However, tectonic transpression represents a suitable mechanism to create positive structures of potentially near circular geometry (Dooley and Schreurs, 2012). Clearly, such a process requires fault-curvature to form a restraining bend, but the exact fault orientation cannot be followed below this structure in seismic profiles shown in this study. The development of antiformal popup structures was physically modelled by McClay and Bonora (2001) and in case of sufficiently large lateral displacements, domal pop-up structures with trans pop-up cross fault systems were generated. These structures bear geometrical similarities to the Hecataeus circular high and its associated east-west trending compressional faults and thus represent a suitable structural analogy (Fig. 5.3b).

5.5.3 Messinian-Quaternary tectonostratigraphic evolution of the Hecataeus Rise

In the course of the Messinian Salinity Crisis, evaporites were precipitated on the Hecataeus Rise within isolated sub-basins (Fig. 5.3b). The acoustic transparent character of evaporite deposits imaged within the study area is suggestive for halite (Figs. 5.4, 5.11). Truncation of sub-MES reflections indicates Messinian

erosion of the plateau area, clearly attesting that the Hecataeus Rise represented a topographically raised structure relative to the adjacent Levant Basin during Messinian times. Locally, several 100 ms (TWT) of Unit 4 deposits have been removed, as for instance observed by significant truncation of Unit 4-strata in figures 5.9a,b, and 5.10.

A period of post-Messinian compression has predominantly affected the southern half of the Hecataeus Rise, reflected in renewed uplift of the southern Hecataeus bathymetric high and significant growth of adjacent anticlinal structures (southern part of Figs. 5.9a,b and Figs. 5.11, 5.12). Observation of pre-, syn- and post-kinematic sediment packages at the backlimb of these anticlines resembles the situation north of the Latakia Ridge. In analogy to the Hecataeus Rise, three Pliocene-Quaternary sub-units were differentiated by Hall et al. (2005) with the middle sub-unit revealing significant growth (Figs. 5.11, 5.12). Hall et al. (2005) correlated the lower and middle sub-units with the lower and middle-upper Pliocene, respectively, while the upper sub-unit was correlated with Quaternary deposits of the Mesaoria Basin.

The boundary between the lower and upper sub-unit corresponds to the intU1 horizon, traced across most of the Hecataeus plateau area. Following the stratigraphic subdivision by Hall et al. (2005) and given my interpretation of this chronostratigraphic boundary to be valid, this horizon delineates the simultaneous onset/termination of several Late Pliocene/Early Pleistocene tectonostratigraphic events across the Hecataeus Rise: at the southern half of the plateau area (Areas 2a and 2b), intU1 corresponds to termination of growth strata deposition (Figs. 5.11, 5.12). Further southwest, near the Cyprus margin, intU1 delineates to top of southward-dipping transparent strata, indicating differential vertical motion and possibly Pleistocene uplift of Cyprus relative to the Hecataeus Rise (Fig. 5.6) (e.g. Kinnaird et al., 2011). Furthermore, intU1 defines an angular unconformity along the western flank of a prominent sub-Unit 1 positive structure shown in figures 5.8a-c. Development of this unconformity is related to down-folding at the time of intU1 and formation of the adjacent, western synclinal basin (km 2-10 in Fig. 5.8a,b). Finally, intU1 delineates the base of wavy deposits most widely observed in the northeastern part of the plateau area, indicating a change to more energetic sediment deposition (Figs. 5.7, 5.8a-c, 5.14). The base of sediment waves correlates with the base of a high-amplitude reflection package (HARP) below a prominent canyon structure near the northeastern corner of the Hecataeus Rise (Fig. 5.9c). Sediments below these high-amplitude reflections are moderately reflective and reveal good lateral continuity (Fig. 5.9c). I relate this change from low to high-amplitude reflections below the canyon, delineated by intU1, to the onset of post-Messinian canyon evolution. Similar observations were previously made at the Amazon Fan, where HARPs below a canyon system were shown to

correspond to sandy successions which mark the onset of canyon evolution (Pirmez et al., 1997).

The near simultaneous occurrence of tectonostratigraphic events described above is consistent with a model proposed by Kinnaird and Robertson (2012) of Late Pliocene-Early Pleistocene collision between Cyprus and Eratosthenes Seamount. Incipient collision was accompanied by rapid uplift of Cyprus, starting at around 2 Ma (Kinnaird et al., 2011). This is consistent with observation of northward dipping reflections below the intU1 unconformity at the northwestern corner of the Hecataeus Rise, where differential vertical motion between Cyprus and the Hecataeus Rise has evidently taken place (Fig. 5.6). It should be noted that this unconformity is not observed in Unit 1 deposits near the Cyprus margin further east but seismic profiles may not extent sufficiently far north in order to image associated structures.

The model proposed by Kinnaird and Robertson (2012) implies a change in convergence direction along the Cyprus Arc, owing to collision-derived tectonic coupling of Cyprus to westward moving Anatolia. Such a change in convergence direction would be accompanied by a transition from compressional to transpressional deformation between the Hecataeus Rise and the Levant basin, consistent with termination of growth strata deposition at the backlimb of anticlinal structures (Figs. 5.11, 5.12) and observation of transpressional faulting along the foot of the southeastern Hecataeus flank (Figs. 5.15, 5.16).

The western flank of the Hecataeus Rise has experienced a Pliocene-Pleistocene event of northeastward directed compression (Figs. 5.8a,b). Accordingly, incipient collision between Eratosthenes and the northwestern corner of the Hecataeus Rise has possibly occurred. This is consistent with the northward extent of the Eratosthenes Seamount carbonate platform, mapped by Reiche et al. (2015). While Eratosthenes has evidently not reached the southwestern limit of the Hecataeus Rise, it is likely in the stage of active collision with Cyprus and the Hecataeus Rise near the Akrotiri Peninsula and further west. Observation of approximately east-west directed folding and formation of a synclinal basin along this part of the Hecataeus Rise supports such assumptions (Figs. 5.8a,b). Recent uplift of an adjacent anticlinal structure is reflected by development of crestal normal faults that sporadically reach the seabed (Figs. 5.3a, inset IV, Fig. 5.8d,e). If collision with Eratosthenes Seamount was the primary cause for Pleistocene uplift of Cyprus (Robertson, 1998a,c) and if Eratosthenes has only locally collided with the Hecataeus Rise, it may be for this reason why these two structural entities have experienced the observed post-Messinian vertical separation.

Differential uplift between Cyprus and the Hecataeus Rise is further expected to have altered depositional processes on the Hecataeus Rise. The onset of wavy sediment deposition in the vicinity of a large canyon structure which has formed

during that time is consistent with the idea of increasing vertical separation between Cyprus and the Hecataeus Rise, resulting in more energetic downslope sediment transport (Figs. 5.7, 5.8a,b, 5.9a-c, 5.14).

Apart from being supported by the present dataset, the above described model is also consistent with recently published reflection seismic lines from the Cyprus-Eratosthenes collision zone (Reiche et al., 2015). Post-Messinian tectonic shortening of evidently greater magnitude occurred between Eratosthenes and Cyprus compared to shortening between Eratosthenes and the Hecataeus Rise. These observations suggest post-Messinian shortening to have mainly occurred in north-south (or possibly northwest-southeast) direction with a later switch (around the Pliocene-Pleistocene transition) to the presently observed northeast directed convergence regime (Reiche et al., 2015).

Finally, the occurrence of such a Pliocene-Pleistocene tectonic event triggered by incipient collision between Cyprus and Eratosthenes was previously suggested to have caused Eastern Mediterranean-wide tectonic changes (Schattner, 2010). The apparent time lag between initial subsidence of Eratosthenes Seamount at around 5 Ma (Robertson, 1998a; Whiting, 1998) and subsequent Late Pliocene/Early-Pleistocene tectonic events remains to be resolved.

5.5.4 On the origin of the Hecataeus Rise

Previous interpretations addressing the origin and crustal nature of the Hecataeus Rise have regarded this structure as an offshore extension of the Troodos ophiolite (Robertson, 1998c) or as an accreted crustal unit (Rotstein and Ben-Avraham, 1985; Ben-Avraham et al., 1988). While the former interpretation is contradicted by relatively low refraction seismic crustal velocities across the Hecataeus Rise (Welford et al., 2015), the latter model is not fully consistent with data shown in this study. Accretion of the Hecataeus Rise should be structurally reflected within the onshore Cyprus sedimentary record, where compression initiation is dated to Early Miocene times (Robertson et al., 1991; Eaton and Robertson, 1993). Seismic profiles shown in this study do not fully support the existence of such a post-Early Miocene Hecataeus-wide accretion event, owing to the relatively undisturbed nature of the sedimentary succession imaged in the northeastern part of the Hecataeus Rise (Figs. 5.9a,b). The observed continuation of onshore Cyprus structural lineaments onto the Hecataeus Rise is consistent with a model of pre-existing (pre-Miocene) proximity of these two tectonic entities. The basement of Hecataeus Rise may represent the offshore continuation of the Moni Melange known to be present onshore southernmost Cyprus (Robertson, 1977b) and presumably imaged below Unit 4 in the northwestern part of the study area (Figs. 5.6, 5.7, 5.8a,b).

Pre-Messinian anticlinal growth along the southeastern flank of the Hecataeus Rise favors African-Anatolian convergence to have predominantly been accommodated at the junction between the Hecataeus Rise and the Levant Basin. Similarly, most significant post-Messinian shortening is evident in this part of the study area, while little compressional deformation is observed near the Cyprus margin. A post-Messinian African-Anatolian plate boundary between Cyprus and the Hecataeus Rise can therefore be ruled out.

5.6 Conclusions

Based on interpretation of reflection seismic and bathymetric data across the Hecataeus Rise, the following conclusions are drawn:

- The sedimentary succession of the Hecataeus Rise is subdivided into four seismostratigraphic units. Observation of a Hecataeus-wide Messinian erosion surface allows for conclusive interpretation of seismic Units 1 and 3, representing Pliocene-Quaternary strata and Messinian evaporites, respectively. Unit 4 is tentatively correlated with Eocene-Miocene carbonates of the onshore Cyprus Lefkara and Pakhna Formations, while Unit 5 may represent the offshore continuation of the Cretaceous Moni Melange.
- Pre-Messinian structures identified in the northern part of the Hecataeus Rise line up with an inferred straight offshore continuation of onshore Cyprus structural lineaments. These observations are suggestive for a Miocene structural link between Cyprus and the Hecataeus Rise.
- Pre-Messinian compressional deformation is more widely observed in the western half of the Hecataeus Rise compared to its eastern continuation. I relate such observations to the presence of structural heterogeneities along the plate boundary, where lateral variations in shortening accommodation are observed.
- The Hecataeus Rise was elevated above the adjacent Levant Basin during the Messinian Salinity Crisis and widely subject to erosion. Messinian evaporites were precipitated within five isolated sub-basins, reaching a maximum thickness of locally more than 300 ms TWT (ca. 600 m).
- Pliocene-Quaternary deformation predominantly affected the southern half of the Hecataeus Rise, where pre-existing anticlinal structures experienced a phase of reactivation.
- A prominent unconformity is observed in the northwestern part of the Hecataeus Rise, tentatively interpreted to mark the Pliocene-Pleistocene

transition. This horizon indicates the near synchronous occurrence of several tectonostratigraphic events across the entire plateau area. These events are related to the Late Pliocene/Early Pleistocene collision between Cyprus and Eratosthenes Seamount, causing vertical separation between Cyprus and the Hecataeus Rise, where steepening of the slopes initiated the onset of submarine canyon evolution and wavy sediment deposition. The Collision triggered a change from northwest to northeast directed plate convergence and an associated switch from compressional to transpressional deformation along the southeastern flank of the Hecataeus Rise and the onset of east-west oriented compression in the northwestern part of the Hecataeus Rise.

- The fairly undisturbed nature of pre-Messinian and particularly post-Messinian strata near the junction to Cyprus suggests long-term proximity between Cyprus and the Hecataeus Rise. Consequently, African-Anatolian shortening was predominantly accommodated along the transition to the Levant Basin.

Acknowledgements

I thank captain Friedhelm v. Staa, the officers and crew of RV MARIA S. MERIAN for their support during the MSM 14/2 survey campaign. Alastair Robertson is thanked for discussions during the preparation phase of this Chapter. I am grateful to Schlumberger for providing the Petrel software used for seismic interpretation. This research was funded by Deutsche Forschungsgemeinschaft (DFG, Grant no. Hu698/20-1).

6 Conclusions and outlook

6.1 Conclusions

In this study, I interpret a comprehensive set of reflection seismic profiles and multibeam bathymetric data across the Levant Basin, the Hecataeus Rise and the Cyprus-Eratosthenes Seamount collision zone. Results shed new light on salt tectonic processes in the Levant Basin and lead to a significantly improved understanding of the Miocene-Quaternary structural evolution around the offshore Cyprus African-Anatolian plate boundary.

Deciphering the history of salt tectonics in salt-bearing sedimentary basins around the globe is not an easy task given the complexity salt structures may have. In contrast, evaporites in the Levant Basin are yet fairly undeformed, making this basin a prime example to study salt tectonics in its initial stage. Until now, early-stage deformation of Messinian evaporites in the Levant Basin was mainly explained by gravity-driven processes only. Interpretation of depth-migrated industry seismic profiles reveals a spatial coincidence between sub-salt extensional faults and intra-evaporite folds and faults in the northern part of the Levant Basin. Such observations indicate a sub-salt structural control on the internal shape of Messinian evaporites and add a new, fault-controlled evaporite deformation mechanism to the known mechanisms which drive salt tectonics in the Levant Basin. A conceptual model is presented to explain the observed intra-salt structural geometry: extensional faulting was initiated in Middle Miocene times and lasted until the late Messinian. Creation of extensional stresses within the sedimentary cover of the northernmost African plate is tentatively explained by subduction-related flexural bending. Extensional faulting led to development of syn-depositional fault-propagation folds within the salt layer. Subsequent tectonic shortening along the African-Anatolian plate boundary caused amplification of intra-salt folds and created the presently observed complex intra-evaporite structural geometry.

This newly considered mechanism of fault-controlled evaporite deformation in the Levant Basin is integrated into a basin-wide study of the temporal and spatial

occurrence of salt deformation mechanisms, combining previous results with findings of the present study. It is shown that syn-depositional, fault-controlled evaporite deformation predominantly affected the structural evolution of evaporites in the northern part of the Levant Basin. A phase of syn-depositional gravity-gliding has deformed evaporites near Eratosthenes Seamount while post-depositional gravity-spreading primarily drives evaporite deformation in the southern Levant Basin. This compilation shows that early-stage syn- and post-depositional evaporite deformation in the Levant Basin was driven by a set of principal salt tectonic deformation mechanism. These mechanisms may also be applicable to decipher the history of salt deformation in complex salt basins around the world.

While salt deformation in the central part of the Levant Basin is primarily expressed by the structural geometry of intra-salt tectonic markers, a case of tectonically-driven salt deformation along the Cyprus-Eratosthenes collision zone is investigated for the first time and clearly expressed in the present-day bathymetry. In the western part of the collision zone, bordered by Cyprus and Eratosthenes Seamount, strongly deformed salt is overlain by up to 700 m thick late Messinian supra-salt deposits, occupying small sub-basins flanked by salt diapirs. Their uppermost 200 m were drilled in the course of ODP Leg 160 (Site 968) and interpreted as Lago Mare sediments, deposited during the final stage of the Messinian Salinity Crisis (Robertson, 1998d). Rapid eastward thinning and pinchout of these deposits towards the Levant Basin is related to a sea level control on late Messinian sediment deposition, providing an explanation for the absence of Lago Mare deposits throughout the Levant Basin. Identification of a thick, late Messinian supra-salt unit offshore southern Cyprus and presumably also within the Herodotus Basin may represent another step towards a possible correlation between the Messinian successions occupying the deep Eastern and Western Mediterranean basins.

In this thesis, first evidence is presented on the structural evolution of the area enclosed by Cyprus, Eratosthenes Seamount and the Hecataeus Rise against the background that the collision zone is filled with km-thick Messinian salt. This area bears the unique opportunity to address the behavior of salt within an active collision and subduction setting. For imaging sub-salt structures, a processing workflow was applied which is normally used for seismic data with significantly greater offsets-to-target-ratios than the available MSM 14/3 dataset. This workflow involved pre-stack time migration and CRS-stacking (after Dell et al., 2012) by means of a velocity model which was derived by geological interpretation and lateral correlation of seismic velocity units from an available MSM 14/2 velocity model (Ehrhardt, 2013 personal commun.). Processing results showed significant improvements in data quality and allowed for a meaningful interpretation of sub-salt structures which would have otherwise been difficult to detect. Based on lateral differences in the style of salt deformation, the collision zone is subdivided

into two different salt tectonic domains. In the western part, Pliocene-Pleistocene sediments are shown to laterally continue from the northern flank of Eratosthenes Seamount beneath Messinian evaporites. Allochthonous salt has thus advanced across sediments of post-Messinian age, carrying a sequence of variably thick late Messinian-Quaternary roof strata along. In this domain, previously active sediment accretion at the Cyprus margin has now become inactive and shortening is largely accommodated at the leading edge of the allochthonous salt sheet. Further east, between Eratosthenes Seamount and the Hecataeus Rise, compressional thickening, autochthonous salt is observed. Sub- and supra-salt deposits within this area appear to be in the stage of active accretion inferred from observation of recently active faults at the southwestern margin of the Hecataeus Rise. Such a relation between the style of salt deformation (autochthonous vs. allochthonous) and sediment accretion (active vs. inactive) bears important implications for the interrelation between crustal tectonics and salt tectonics.

Observations of intensively deformed allochthonous salt between Cyprus and Eratosthenes Seamount and moderately deformed salt in the eastern part of the collision zone may reflect a predominately north-south or northwest-southeast oriented post-Messinian African-Anatolian convergence direction. A switch to the present northeast directed convergence regime could have been initiated later than previously thought, possibly around the Pliocene-Pleistocene transition. Observations across the Hecataeus Rise support the assumption of an intra-Pliocene-Pleistocene tectonic reorganization. A significant intra-Pliocene-Pleistocene unconformity is identified in the northwestern part of the Hecataeus Rise and temporarily correlated with a change from quiescent to more energetic, Cyprus-derived downslope sediment transport. These observations are consistent with a model initially proposed by Kinnaird and Robertson (2012), where collision between Cyprus and Eratosthenes Seamount near the Pliocene-Pleistocene transition initiated collision-derived coupling of Cyprus to the westward motion of the Anatolian plate. Associated changes in the plate tectonic convergence direction are expressed by northeast directed compression and salt inflation between Eratosthenes Seamount and the Hecataeus Rise. An eastward directed deformation event has also affected the northwestern part of the Hecataeus Rise and is now reflected by a prominent unconformity within Pliocene-Quaternary strata. Due to collision with Eratosthenes Seamount, Cyprus experienced rapid uplift and vertical separation from the Hecataeus Rise. Steepening of the slopes along the southern Cyprus margin is reflected by southward-dipping sediments and a concomitant change from quiescent to more energetic, Cyprus-derived downslope sediment transport. This interpretation draws the hitherto most comprehensive picture of the post-Messinian evolution within an area of great structural complexity. It further highlights the occurrence of a chain of structural

and depositional changes initiated when two continental blocks collide in an incipient stage.

6.2 Outlook

While results of this thesis have clearly improved our present-day understanding of salt deformation in the easternmost Mediterranean Sea and the structural evolution of the Cyprus-Eratosthenes collision zone, several open questions remain and may be subject to future research initiatives. Some of these open questions are briefly highlighted below.

Based on ODP leg 160 drilling results, rapid Early Pliocene subsidence of Eratosthenes Seamount was inferred. The cause of such rapid subsidence was related to tectonic collision and subsequent underthrusting of Eratosthenes beneath the island of Cyprus (Robertson, 1998d). In return, Cyprus experienced rapid Pleistocene uplift (Kinnaird et al., 2011). However, subsidence of Eratosthenes pre-dates uplift of Cyprus by approx. 2 Ma and the cause for such a time lag is poorly understood. While seismic data will probably not help to address such a question, hints may come from a numerical study. A yet to be constructed 3D structural model of Eratosthenes Seamount from gravity, seismic reflection and refraction data may serve as an input for subsequent numerical modelling studies.

Evaporites are only present within small, isolated sub-basins on the Hecataeus Rise. Such observations clearly indicate that this structure was elevated relative to the deep Levant Basin at the time of the Messinian Salinity Crisis. However, small evaporite basins are also present onshore Cyprus (Robertson, 1995a) and vertically separated from evaporites on the Hecataeus Rise by more than 1300 m. It is still unclear how much of this vertical separation can be explained by differential post-Messinian vertical motion between Cyprus and the Hecataeus Rise. On the other hand, how much of this elevation difference can be explained by sea level variations during the Messinian Salinity Crisis? Understanding these large elevation differences between evaporites onshore Cyprus, the Hecataeus Rise and the deep Levant Basin represents a challenging task for future considerations on vertical crustal motions and Messinian sea level variations in the easternmost Mediterranean Sea.

Identification of thick late Messinian sediments on top of mobile Messinian evaporites within the Cyprus-Eratosthenes collision zone and its tentative correlation to the Upper Evaporites of the deep Western Mediterranean basins may represent a first step towards an Eastern-Western Mediterranean correlation of Messinian depositional events. However, the presence of late Messinian supra-salt deposits offshore southern Cyprus is only a local observation and not suitable for a well-founded Mediterranean-wide correlation of Messinian sedimentary

successions. Additionally, absence of sub-salt Messinian sediments in the Eastern Mediterranean basins – which are termed Lower Evaporites in the Western Mediterranean basins (Lofi et al., 2011) – still needs to be understood. Only drilling of the deep basin evaporites bears the potential for a scientific breakthrough on these questions.

Finally, establishing a consensus tectonic model of the easternmost Mediterranean Sea is presently hindered by significant data gaps for the area north of the Latakia Ridge. Little is known about the crustal composition east of Cyprus, about the origin of the Cyprus Basin and even the crustal nature of the Hecataeus Rise could yet not be conclusively resolved. Additional seismic refraction and deep reflection profiling may help to answer some of these questions to eventually solve the Eastern Mediterranean puzzle.

Bibliography

- Adamuszek, M., Schmid, D.W., Dabrowski, M., 2013. Theoretical analysis of large amplitude folding of a single viscous layer. *Journal of Structural Geology* 48, 137-152.
- Aksu, A.E., Hall, J., Yalırak, C., 2005. Miocene to Recent tectonic evolution of the eastern Mediterranean: New pieces of the old Mediterranean puzzle. *Marine Geology* 221, 1-13.
- Albertz, M., Beaumont, C., 2010. An investigation of salt tectonic structural styles in the Scotian Basin, offshore Atlantic Canada: 2. Comparison of observations with geometrically complex numerical models. *Tectonics* 29, TC4017, doi:10.1029/2009TC002539.
- Albertz, M., Ings, S.J., 2012. Some consequences of mechanical stratification in basin-scale numerical models of passive-margin salt tectonics. In: Alsop, G.I., Archer, S.G., Hartley, A.J., Grant, N.T., Hodgkinson, R. (Eds.), *Salt Tectonics, Sediments and Prospectivity*. Geological Society, London, Special Publications 363, pp. 303-330.
- Allmendiger, R.W., 1998. Inverse and forward numerical modeling of trishear fault-propagation folds. *Tectonics* 17, 640-656.
- Almagor, G., 1984. Salt-controlled slumping on the Mediterranean slope of central Israel. *Marine Geophysical Researches* 6, 227-243.
- Bagnall, P.S., 1960. The Geology and Mineral Resources of the Pano Lefkara – Larnaca Area. *Cyprus Geological Survey Memoirs* 5, 1-116.
- Baykulov, M., Brink, H.-J., Gajewski, D., Yoon, M.-K., 2009. Revisiting the structural setting of the Glueckstadt Graben salt stock family, North German Basin. *Tectonophysics* 470, 162-172.
- Bear, L.M., Morel, S.W., 1960. The Geology and Mineral Resources of the Agros-Akrotiri Area. *Cyprus Geological Survey Memoirs* 7, 1-88.
- Ben-Avraham, Z., 1978. The structure and tectonic setting of the levant continental margin, Eastern Mediterranean. *Tectonophysics* 46, 313-331.
- Ben-Avraham, Z., Ginzburg, A., Makris, J., Eppelbaum, L., 2002. Crustal structure of the Levant Basin, eastern Mediterranean. *Tectonophysics* 346, 23-43.
- Ben-Avraham, Z., Kempler, D., Ginzburg, A., 1988. Plate convergence in the Cyprean Arc. *Tectonophysics* 146, 231-240.
- Ben-Avraham, Z., Tibor, G., Limonov, A.F., Leybov, M.B., Ivanov, M.K., Tokarev, M.Y., Woodside, J.M., 1995. Structure and tectonics of the eastern Cyprean Arc. *Marine and Petroleum Geology* 12, 263-271.

- Benkhelil, J., Bayerly, M., Branchoux, S., Courp, T., Gonthier, E., Hübscher, C., Maillard, A., Tahchi, E., 2005. La branche orientale de l'arc de Chypre. Morphostructure d'une frontière de plaques d'après les résultats de la campagne BLAC (2003). *Comptes Rendus Geoscience* 337, 1075-1083.
- Bertoni, C., Cartwright, J.A., 2005. 3D seismic analysis of circular evaporite dissolution structures, Eastern Mediterranean. *Journal of the Geological Society* 162, 909-926.
- Bertoni, C., Cartwright, J.A., 2006. Controls on the basinwide architecture of late Miocene (Messinian) evaporites on the Levant margin (Eastern Mediterranean). *Sedimentary Geology* 188-189, 93-114.
- Bertoni, C., Cartwright, J.A., 2007a. Major erosion at the end of the Messinian Salinity Crisis: evidence from the Levant Basin, Eastern Mediterranean. *Basin Research* 19, 1-18.
- Bertoni, C., Cartwright, J.A., 2007b. Clastic depositional systems at the base of the late Miocene evaporites of the Levant region, Eastern Mediterranean. In: Schreiber, B.C., Lugli, S., Babel, M. (Eds.), *Evaporites Through Space and Time*. Geological Society, London, Special Publications 285, pp. 37-52.
- Bertoni, C., Cartwright, J., Hermanrud, C., 2013. Evidence for large-scale methane venting due to rapid drawdown of sea level during the Messinian Salinity Crisis. *Geology* 41, 371-374.
- Biryol, C.B., Beck, S.L., Zandt, G., Özacar, A.A., 2011. Segmented African lithosphere beneath the Anatolian region inferred from teleseismic P-wave tomography. *Geophysical Journal International* 184, 1037-1057.
- Blanc-Valleron, M.-M., Rouchy, J.-M., Pierre, C., Badaut-Trauth, D., Schuler, M., 1998. Evidence of Messinian nonmarine deposition at Site 968 (Cyprus lower slope). In: Robertson, A.H.F., Emeis, K.-C., Richter, C., Camerlenghi, A. (Eds.), *Proceedings of the ODP, Scientific Results*, vol. 160. Ocean Drilling Program, College Station, TX, pp. 437-445.
- Bosworth, W., El-Hawat, A.S., Helgeson, D.E., Burke, K., 2008. Cyrenaican "shock absorber" and associated inversion strain shadow in the collision zone of northeast Africa. *Geology* 36, 695-698.
- Bosworth, W., Huchon, P., McClay, K., 2005. The Red Sea and Gulf of Aden Basins. *Journal of African Earth Sciences* 43, 334-378.
- Bozkurt, E., 2001. Neotectonics of Turkey – a synthesis. *Geodinamica Acta* 14, 3-30.
- Bradley, D.C., Kidd, W.S.F., 1991. Flexural extension of the upper continental crust in collisional foredeeps. *Geological Society of America Bulletin* 103, 1416-1438.
- Brun, J.-P., Fort, X., 2011. Salt tectonics at passive margins: Geology versus models. *Marine and Petroleum Geology* 28, 1123-1145.
- Buchner, E., Kenkmann, T., 2008. Upheaval Dome, Utah, USA: Impact origin confirmed. *Geology* 36, 227-230.
- Calon, T.J., Aksu, A.E., Hall, J., 2005. The Oligocene-Recent evolution of the Misaoria Basin (Cyprus) and its western marine extension, Eastern Mediterranean. *Marine Geology* 221, 95-120.
- Carton, H., Singh, S.C., Tapponnier, P., Elias, A., Briais, A., Sursock, A., Jomaa, R., King, G.C.P., Daëron, M., Jacques, E., Barrier, L., 2009. Seismic evidence for Neogene and active shortening offshore of Lebanon (Shalimar cruise). *Journal of Geophysical Research* 114, B07407, doi:10.1029/2007JB005391.
- Cartwright, J.A., Jackson, M.P.A., 2008. Initiation of gravitational collapse of an evaporite basin margin: The Messinian saline giant, Levant Basin, eastern Mediterranean. *Geological Society of America Bulletin* 120, 399-413.

- Cartwright, J., Jackson, M., Dooley, T., Higgins, S., 2012. Strain partitioning in gravity-driven shortening of a thick, multilayered evaporite sequence. In: Alsop, G.I., Archer, S.G., Hartley, A.J., Grant, N.T., Hodgkinson, R. (Eds.), *Salt Tectonics, Sediments and Prospectivity*. Geological Society, London, Special Publications 363, pp. 449-470.
- CIESM, 2008. The Messinian Salinity Crisis from mega-deposits to microbiology – A consensus report. In: Brian, F. (Ed.), *CIESM Workshop Monographs N°33*, Monaco, 168 pp.
- Clark, I.R., Cartwright, J.A., 2009. Interactions between submarine channel systems and deformation in deepwater fold belts: Examples from the Levant Basin, Eastern Mediterranean sea. *Marine and Petroleum Geology* 26, 1465-1482.
- Cosentino, D., Federici, I., Cipollari, P., Gliozzi, E., 2006. Environments and tectonic instability in central Italy (Garigliano Basin) during the late Messinian *Lago-Mare* episode: New data from the onshore Mondragone 1 well. *Sedimentary Geology* 188-189, 297-317.
- Costa, E., Camerlenghi, A., Polonia, A., Cooper, C., Fabretti, P., Mosconi, A., Murelli, P., Romanelli, M., Sormani, L., Wardell, N., 2004. Modeling deformation and salt tectonics in the eastern Mediterranean Ridge accretionary wedge. *Geological Society of America Bulletin* 116, 880-894.
- Daniels, J.J., Hite, R.J., Scott, J.H., U.S. Geological Survey, 1980. Geophysical Well-Log Measurements in Three Drill Holes at Salt Valley, Utah. U.S. Geological Survey, Open-File Report 81-36.
- de Lamotte, D.F., Raulin, C., Mouchot, N., Wrobel-Daveau, J.-C., Blanpied, C., Ringenbach, J.-C., 2011. The southernmost margin of the Tethys realm during the Mesozoic and Cenozoic: Initial geometry and timing of the inversion process. *Tectonics* 30, TC3002, doi:10.1029/2010TC002691.
- Dell, S., Gajewski, D., Vanelle, C., 2012. Prestack time migration by common-migrated-reflector-element stacking. *Geophysics* 77, 73-82.
- Dooley, T.P., Schreurs, G., 2012. Analogue modelling of intraplate strike-slip tectonics: A review and new experimental results. *Tectonophysics* 574-575, 1-71.
- Dümmong, S., Hübscher, C., 2011. Levant Basin – Central Basin. In: Lofi, J., Déverchère, J., Gaullier, V., Gillet, H., Gorini, C., Guennoc, P., Loncke, L., Maillard, A., Sage, F., Thion, I. (Eds.), *Seismic Atlas of the Messinian Salinity Crisis markers in the Mediterranean and Black Seas*. Mémoires de la Société Géologique de France, n.s., 179, and World Geological Map Commission, Paris, p. 55.
- Dümmong, S., Meier, K., Gajewski, D., Hübscher, C., 2008. Comparison of prestack stereotomography and NIP wave tomography for velocity model building: Instances from the Messinian evaporites. *Geophysics* 73, 291-302.
- Dupré, S., Woodside, J., Klauke, I., Mascle, J., Foucher, J.-P., 2010. Widespread active seepage activity on the Nile Deep Sea Fan (offshore Egypt) revealed by high-definition geophysical imagery. *Marine Geology* 275, 1-19.
- Eaton, S., Robertson, A., 1993. The Miocene Pakhna Formation, southern Cyprus and its relationship to the Neogene tectonic evolution of the Eastern Mediterranean. *Sedimentary Geology* 86, 273-296.
- Ehrhardt, A., 2011. RV MARIA S. MERIAN, Cruise Report MSM14/L2 Eratosthenes Seamount / Eastern Mediterranean Sea 2010. DFG Senatskommission für Ozeanographie, Bremen, 66 pp.
- Ergün, M., Okay, S., Sari, C., Oral, E.Z., Ash, M., Hall, J., Miller, H., 2005. Gravity anomalies of the Cyprus Arc and their tectonic implications. *Marine Geology* 221, 349-358.

- Faccenna, C., Bellier, O., Martinod, J., Piromallo, C., Regard, V., 2006. Slab detachment beneath eastern Anatolia: A possible cause for the formation of the North Anatolian fault. *Earth and Planetary Science Letters* 242, 85-97.
- Fagin, S., 1998. Model-Based Depth Imaging. Course Note Series, No. 10. Society of Exploration Geophysicists, Tulsa, Oklahoma.
- Follows, E.J., 1992. Patterns of reef sedimentation and diagenesis in the Miocene of Cyprus. *Sedimentary Geology* 79, 225-253.
- Fort, X., Brun, J.-P., 2012. Kinematics of regional salt flow in the northern Gulf of Mexico. In: Alsop, G.I., Archer, S.G., Hartley, A.J., Grant, N.T., Hodgkinson, R. (Eds.), *Salt Tectonics, Sediments and Prospectivity*. Geological Society, London, Special Publications 363, pp. 265-287.
- Galindo-Zaldívar, J., Nieto, L.M., Robertson, A.H.F., Woodside, J.M., 2001. Recent tectonics of Eratosthenes Seamount: an example of seamount deformation during incipient continental collision. *Geo-Marine Letters* 20, 233-242.
- Gardosh, M.A., Druckman, Y., 2006. Seismic stratigraphy, structure and tectonic evolution of the Levantine Basin, offshore Israel. In: Robertson, A.H.F., Mountrakis, D. (Eds.), *Tectonic Development of the Eastern Mediterranean Region*. Geological Society, London, Special Publications 260, pp. 201-227.
- Gardosh, M.A., Garfunkel, Z., Druckman, Y., Buchbinder, B., 2010. Tethyan rifting in the Levant Region and its role in Early Mesozoic crustal evolution. In: Homberg, C., Bachmann, M. (Eds.), *Evolution of the Levant Margin and Western Arabia Platform since the Mesozoic*. Geological Society, London, Special Publications 341, pp. 9-36.
- Garfunkel, Z., 1984. Large-scale submarine rotational slumps and growth faults in the Eastern Mediterranean. *Marine Geology* 55, 305-324.
- Garfunkel, Z., 1998. Constraints on the origin and history of the Eastern Mediterranean basin. *Tectonophysics* 298, 5-35.
- Garfunkel, Z., Almagor, G., 1985. Geology and structure of the continental margin off northern Israel and the adjacent part of the Levantine Basin. *Marine Geology* 62, 105-131.
- Gargani, J., Rigollet, C., 2007. Mediterranean Sea level variations during the Messinian salinity crisis. *Geophysical Research Letters* 34, L10405, doi:10.1029/2007GL029885.
- Gaullier, V., Chanier, F., Lymer, G., Vendeville, B.C., Maillard, A., Thinon, I., Lofi, J., Sage, F., Loncke, L., 2014. Salt tectonics and crustal tectonics along the Eastern Sardinian margin, Western Tyrrhenian: New insights from the "METYSS 1" cruise. *Tectonophysics* 615-616, 69-84.
- Gaullier, V., Mart, Y., Bellaiche, G., Mascle, J., Vendeville, B., Zitter, T., The Second Leg PRISMED II Scientific Party, 2000. Salt tectonics in and around the Nile deep-sea fan: insights from the PRISMED II cruise. In: Vendeville, B.C., Mart, Y., Vigneresse, J.-L. (Eds.), *Salt, Shale, and Igneous Diapirs in and around Europe*. Geological Society, London, Special Publications 174, pp. 111-129.
- Gradmann, S., Hübscher, C., Ben-Avraham, Z., Gajewski, D., Netzeband, G., 2005. Salt tectonics off northern Israel. *Marine and Petroleum Geology* 22, 597-611.
- Gvirtzman, Z., Garfunkel, Z., 1998. The transformation of southern Israel from a swell to a basin: stratigraphic and geodynamic implications for intracontinental tectonics. *Earth and Planetary Science Letters* 163, 275-290.
- Gvirtzman, Z., Reshef, M., Buch-Leviatan, O., Ben-Avraham, Z., 2013. Intense salt deformation in the Levant Basin in the middle of the Messinian Salinity Crisis. *Earth and Planetary Science Letters* 379, 108-119.

- Gvirtzman, Z., Reshef, M., Buch-Leviatan, O., Groves-Gidney, G., Karcz, Z., Makovsky, Y., Ben-Avraham, Z., 2015. Bathymetry of the Levant basin: interaction of salt-tectonics and surficial mass movements. *Marine Geology* 360, 25-39.
- Hall, S.H., 2002. The role of autochthonous salt inflation and deflation in the northern Gulf of Mexico. *Marine and Petroleum Geology* 19, 649-682.
- Hall, J., Aksu, A.E., King, H., Gogacz, A., Yaltırak, C., Çifçi, G., 2014. Miocene-Recent evolution of the western Antalya Basin and its linkage with the Isparta Angle, eastern Mediterranean. *Marine Geology* 349, 1-23.
- Hall, J., Calon, T.J., Aksu, A.E., Meade, S.R., 2005. Structural evolution of the Latakia Ridge and Cyprus Basin at the front of the Cyprus Arc, Eastern Mediterranean Sea. *Marine Geology* 221, 261-297.
- Hardy, S., McClay, K., 1999. Kinematic modelling of extensional fault-propagation folding. *Journal of Structural Geology* 21, 695-702.
- Harrison, R.W., Tsiolakis, E., Stone, B.D., Lord, A., McGeehin, J.P., Mahan, S.A., Chirico, P., 2013. Late Pleistocene and Holocene uplift history of Cyprus: implications for active tectonics along the southern margin of the Anatolian microplate. In: Robertson, A.H.F., Parlak, O., Ünlügenç, U.C. (Eds.), *Geological Development of Anatolia and the Easternmost Mediterranean Region*. Geological Society, London, Special Publications 372, pp. 561-584.
- Harrofield, M., Cunneen, J., Keep, M., Crow, W., 2003. Early-stage orogenesis in the Timor Sea region, NW Australia. *Journal of the Geological Society* 160, 991-1001.
- Harrofield, M., Keep, M., 2005. Tectonic modification of the Australian North-West Shelf: episodic rejuvenation of long-lived basin divisions. *Basin Research* 17, 225-239.
- Hawie, N., Gorini, C., Deschamps, R., Nader, F.H., Montadert, L., Granjeon, D., Baudin, F., 2013. Tectono-stratigraphic evolution of the northern Levant Basin (offshore Lebanon). *Marine and Petroleum Geology* 48, 392-410.
- Hertweck, T., Schleicher, J., Mann, J., 2007. Data stacking beyond CMP. *The Leading Edge* 26, 818-827.
- Hodgson, N., 2012. The Miocene hydrocarbon play in Southern Lebanon. *First Break* 30, 93-98.
- Howe, J.A., Stoker, M.S., Masson, D.G., Pudsey, C.J., Morris, P., Larter, R.D., Bulat, J., 2006. Seabed morphology and the bottom-current pathways around Rosemary Bank seamount, northern Rockall Trough, North Atlantic. *Marine and Petroleum Geology* 23, 165-181.
- Hsü, K.J., Cita, M.B., Ryan, W.B.F., 1973. The origin of the Mediterranean evaporites. In: Ryan, W.B.F., Hsü, K.J., et al. (Eds.), *Initial Reports of the DSDP*, vol. 13. U.S. Government Printing Office, Washington D.C., pp. 1203-1231.
- Hsü, K.J., Montadert, L., Bernoulli, D., Cita, M.B., Erickson, A., Garrison, R.E., Kidd, R.B., Mélières, F., Müller, C., Wright, R., 1978. History of the Mediterranean salinity crisis. In: Hsü, K.J., Montadert, L., et al. (Eds.), *Initial Reports of the DSDP*, vol. 42A. U.S. Government Printing Office, Washington D.C., pp. 1053-1078.
- Hübscher, C., 2012. RV MARIA S. MERIAN, Cruise Report MSM14/L3 Eratosthenes Seamount / Eastern Mediterranean Sea 2010. DFG Senatskommission für Ozeanographie, Bremen, 39 pp.
- Hübscher, C., Cartwright, J., Cypionka, H., De Lange, G.J., Robertson, A., Suc, J.-P., Urai, J.L., 2007. Global Look at Salt Giants. *Eos* 88, 177-179.

- Hübscher, C., Dümmong, S., 2011. Levant Basin – salt tectonics and fluid dynamics. In: Lofi, J., Déverchère, J., Gaullier, V., Gillet, H., Gorini, C., Guennoc, P., Loncke, L., Maillard, A., Sage, F., Thimon, I. (Eds.), *Seismic Atlas of the Messinian Salinity Crisis markers in the Mediterranean and Black Seas*. Mémoires de la Société Géologique de France, n.s., 179, and World Geological Map Commission, Paris, p. 58.
- Hübscher, C., Gohl, K., 2014. Reflection/Refraction seismology. *Encyclopedia of Marine Geosciences*, DOI 10.1007/978-94-007-6644-0_128-1.
- Hübscher, C., Netzeband, G.L., 2007. Evolution of a young salt giant: the example of the Messinian evaporites in the Levantine Basin. In: Wallner, M., Lux, K.-H., Minkley, W., Hardy, Jr., H.R. (Eds.), *The Mechanical Behavior of Salt – Understanding of THMC Processes in Salt*. Taylor & Francis Group, London, pp. 175-184.
- Hübscher, C., Tahchi, E., Klaucke, I., Maillard, A., Sahling, H., 2009. Salt tectonics and mud volcanism in the Latakia and Cyprus Basins, eastern Mediterranean. *Tectonophysics* 470, 173-182.
- Hudec, M.R., Jackson, M.P.A., 2004. Regional restoration across the Kwanza Basin, Angola: Salt tectonics triggered by repeated uplift of a metastable passive margin. *American Association of Petroleum Geologists Bulletin* 88, 971-990.
- Hudec, M.R., Jackson, M.P.A., 2006. Advance of allochthonous salt sheets in passive margins and orogens. *American Association of Petroleum Geologists Bulletin* 90, 1535-1564.
- Hudec, M.R., Jackson, M.P.A., 2007. Terra infirma: Understanding salt tectonics. *Earth-Science Reviews* 82, 1-28.
- Hudec, M.R., Jackson, M.P.A., 2009. Interaction between spreading salt canopies and their peripheral thrust systems. *Journal of Structural Geology* 31, 1114-1129.
- Hudec, M.R., Jackson, M.P.A., Schultz-Ela, D.D., 2009. The paradox of minibasin subsidence into salt: Clues to the evolution of crustal basins. *Geological Society of America Bulletin* 121, 201-221.
- Imprescia, P., Pondrelli, S., Vannucci, G., Gresta, S., 2012. Regional centroid moment tensor solutions in Cyprus from 1977 to the present and seismotectonic implications. *Journal of Seismology* 16, 147-167.
- Jackson, M.P.A., 1995. Retrospective salt tectonics. In: Jackson, M.P.A., Roberts, D.G., Snelson, S. (Eds.), *Salt tectonics: a global perspective*. American Association of Petroleum Geologists Memoir 65, pp. 1-28.
- Jackson, M.P.A., Hudec, M.R., Dooley, T.P., 2010. Some emerging concepts in salt tectonics in the deepwater Gulf of Mexico: intrusive plumes, canopy-margin thrusts, minibasin triggers and allochthonous fragments. In: Vining, B.A., Pickering, S.C. (Eds.), *Petroleum Geology: From Mature Basins to New Frontiers – Proceedings of the 7th Petroleum Geology Conference*. Petroleum Geology Conference series 7, pp. 889-912.
- Jackson, M.P.A., Talbot, C.J., 1986. External shapes, strain rates, and dynamics of salt structures. *Geological Society of America Bulletin* 97, 305-323.
- Jäger, R., Mann, J., Höcht, G., Hubral, P., 2001. Common-reflection-surface stack: Image and attributes. *Geophysics* 66, 97-109.
- Jin, G., Groshong, Jr., R.H., 2006. Trishear kinematic modeling of extensional fault-propagation folding. *Journal of Structural Geology* 28, 170-183.
- Kempler, D., 1998. Eratosthenes Seamount: The possible spearhead of incipient continental collision in the Eastern Mediterranean. In: Robertson, A.H.F., Emeis, K.-C., Richter, C., Camerlenghi, A. (Eds.), *Proceedings of the ODP, Scientific Results*, vol. 160. Ocean Drilling Program, College Station, TX, pp. 709-721.

- Kinnaird, T., Robertson, A., 2012. Tectonic and sedimentary response to subduction and incipient continental collision in southern Cyprus, easternmost Mediterranean region. In: Robertson, A.H.F., Parlak, O., Ünlügenç, U.C. (Eds.), *Geological Development of Anatolia and the Easternmost Mediterranean Region*. Geological Society, London, Special Publications 372, pp. 585-614.
- Kinnaird, T.C., Robertson, A.H.F., Morris, A., 2011. Timing of uplift of the Troodos Massif (Cyprus) constrained by sedimentary and magnetic polarity evidence. *Journal of the Geological Society* 168, 457-470.
- Klimke, J., Ehrhardt, A., 2014. Impact and implications of the Afro-Eurasian collision south of Cyprus from reflection seismic data. *Tectonophysics* 626, 105-119.
- Kopf, A.J., 2002. Significance of mud volcanism. *Reviews of Geophysics* 40, 1-52.
- Kopf, A., Vidal, N., Klaeschen, D., von Huene, R., Krasheninnikov, V.A., 2005. Multi-Channel Seismic Profiles across Eratosthenes Seamount and the Florence Rise Reflecting the Incipient Collision between Africa and Eurasia near the Island of Cyprus, Eastern Mediterranean. In: Hall, J.K., Krasheninnikov, V.A., Hirsch, F., Benjamini, C., Flexer, A. (Eds.), *Geological Framework of the Levant Volume II: The Levantine Basin and Israel*. Historical Productions-Hall, Jerusalem, pp. 57-71.
- Kosi, W., Tari, G., Nader, F.H., Skiple, C., Trudgill, B., Lazar, D., 2012. Structural analogy between the “piano key faults” of deep-water Lebanon and the extensional faults of the Canyonlands grabens, Utah, United States. *The Leading Edge* 31, 824-830.
- Krasheninnikov, V.A., Hall, J.K., Bragin, N., Klaeschen, D., Kopf, A., Silantyev, S., Vidal, N., von Huene, R., Zverev, S., 2005. From South-Western Cyprus to Eratosthenes. In: Hall, J.K., Krasheninnikov, V.A., Hirsch, F., Benjamini, C., Flexer, A. (Eds.), *Geological Framework of the Levant Volume II: The Levantine Basin and Israel*. Historical Productions-Hall, Jerusalem, pp. 701-732.
- Krijgsman, W., Blanc-Valleron, M.-M., Flecker, R., Hilgen, F.J., Kouwenhoven, T.J., Merle, D., Orszag-Sperber, F., Rouchy, J.-M., 2002. The onset of the Messinian salinity crisis in the Eastern Mediterranean (Pissouri Basin, Cyprus). *Earth and Planetary Science Letters* 194, 299-310.
- Krijgsman, W., Hilgen, F.J., Raffi, I., Sierro, F.J., Wilson, D.S., 1999. Chronology, causes and progression of the Messinian salinity crisis. *Nature* 400, 652-655.
- Lazar, M., Schattner, U., Reshef, M., 2012. The great escape: An intra-Messinian gas system in the eastern Mediterranean. *Geophysical Research Letters* 39, L20309, doi:10.1029/2012GL053484.
- Le Pichon, X., Kreemer, C., 2010. The Miocene-to-Present Kinematic Evolution of the Eastern Mediterranean and Middle East and Its Implications for Dynamics. *Annual Review of Earth and Planetary Sciences* 38, 323-351.
- Limonov, A.F., Woodside, J.M., Ivanov, M.K. (Eds.), 1994. Mud volcanism in the Mediterranean and Black Seas and shallow structure of the Eratosthenes Seamount. Initial results of the geological and geophysical investigations during the Third UNESCO-ESF “Training-through-Research” Cruise of RV *Gelendzhik* (June-July 1993). UNESCO reports in marine science 64, Paris, 173p.
- Lofi, J., Déverchère, J., Gaullier, V., Gillet, H., Gorini, C., Guennoc, P., Loncke, L., Maillard, A., Sage, F., Thion, I. (Eds.) 2011. *Seismic Atlas of the “Messinian Salinity Crisis” markers in the Mediterranean and Black Seas*. Mémoires de la Société Géologique de France, n.s., 179, and World Geological Map Commission, Paris, 72p.
- Loncke, L., Gaullier, V., Bellaiche, G., Mascle, J., 2002. Recent Depositional Patterns of the Nile Deep-Sea Fan from Echo-Character Mapping. *American Association of Petroleum Geologists Bulletin* 86, 1165-1186.

- Loncke, L., Gaullier, V., Droz, L., Ducassou, E., Migeon, S., Mascle, J., 2009. Multi-scale slope instabilities along the Nile deep-sea fan, Egyptian margin: A general overview. *Marine and Petroleum Geology* 26, 633-646.
- Loncke, L., Gaullier, V., Mascle, J., Vendeville, B., Camera, L., 2006. The Nile deep-sea fan: An example of interacting sedimentation, salt tectonics, and inherited subsalt paleotopographic features. *Marine and Petroleum Geology* 23, 297-315.
- Loncke, L., Mascle, J., Fanil Scientific Parties, 2004. Mud volcanoes, gas chimneys, pockmarks and mounds in the Nile deep-sea fan (Eastern Mediterranean): geophysical evidences. *Marine and Petroleum Geology* 21, 669-689.
- Loncke, L., Sellier, N., Mascle, J., 2011. Florence Ridge & South Antalya Basin. In: Lofi, J., Déverchère, J., Gaullier, V., Gillet, H., Gorini, C., Guennoc, P., Loncke, L., Maillard, A., Sage, F., Thimon, I. (Eds.), *Seismic Atlas of the "Messinian Salinity Crisis" markers in the Mediterranean and Black Seas*. Mémoires de la Société Géologique de France, n.s., 179, and World Geological Map Commission, Paris, p. 64.
- Loncke, L., Vendeville, B.C., Gaullier, V., Mascle, J., 2010. Respective contributions of tectonic and gravity-driven processes on the structural pattern in the Eastern Nile deep-sea fan: insight from physical experiments. *Basin Research* 22, 765-782.
- Longacre, M., Bentham, P., Hanbal, I., Cotton, J., Edwards, R., 2007. New Crustal Structure of the Eastern Mediterranean Basin: Detailed Integration and Modeling of Gravity, Magnetic, Seismic Refraction, and Seismic Reflection Data. EGM 2007 International Workshop, Innovation in EM, Grav and Mag Methods: a new Perspective for Exploration. 15-18 April, Capri, Italy. 4 pp.
- Løseth, H., Gading, M., Wensaas, L., 2009. Hydrocarbon leakage interpreted on seismic data. *Marine and Petroleum Geology* 26, 1304-1319.
- Mackenzie, G.D., Maguire, P.K.H., Coogan, L.A., Khan, M.A., Eaton, M., Petrides, G., 2006. Geophysical constraints on the crustal architecture of the Troodos ophiolite: results from the IANGASS project. *Geophysical Journal International* 167, 1385-1401.
- Maillard, A., Hübscher, C., Benkhelil, J., Tahchi, E., 2011. Deformed Messinian markers in the Cyprus Arc: tectonic and/or Messinian Salinity Crisis indicators. *Basin Research* 23, 146-170.
- Major, C.O., Ryan, W.B.F., Jurado-Rodríguez, M.J., 1998. Evolution of paleoenvironments of Eratosthenes Seamount based on downhole logging integrated with carbonate petrology and reflection profiles. In: Robertson, A.H.F., Emeis, K.-C., Richter, C., Camerlenghi, A. (Eds.), *Proceedings of the ODP, Scientific Results*, vol. 160. Ocean Drilling Program, College Station, TX, pp. 483-508.
- Makris, J., Ben-Avraham, Z., Behle, A., Ginzburg, A., Giese, P., Steinmetz, L., Whitmarsh, R.B., Eleftheriou, S., 1983. Seismic refraction profiles between Cyprus and Israel and their interpretation. *Geophysical Journal International* 75, 575-591.
- Mann, J., Jäger, R., Müller, T., Höcht, G., Hubral, P., 1999. Common-reflection-surface stack – a real data example. *Journal of Applied Geophysics* 42, 301-318.
- Manzi, V., Lugli, S., Roveri, M., Pierre, F.D., Gennari, R., Lozar, F., Natalicchio, M., Schreiber, B.C., Taviani, M., Turco, E., 2014. The Messinian salinity crisis in Cyprus: a further step towards a new stratigraphic framework for Eastern Mediterranean. *Accepted in Basin Research*.
- Mart, Y., Ben Gai, Y., 1982. Some depositional patterns at continental margin of southeastern Mediterranean Sea. *American Association of Petroleum Geologists Bulletin* 66, 460-470.
- Mascle, J., Sardou, O., Loncke, L., Migeon, S., Caméra, L., Gaullier, V., 2006. Morphostructure of the Egyptian continental margin: Insights from swath bathymetry surveys. *Marine Geophysical Researches* 27, 49-59.

- Mascle, J., Zitter, T., Bellaiche, G., Droz, L., Gaullier, V., Loncke, L., Prismed Scientific Party 2001. The Nile deep sea fan: preliminary results from a swath bathymetry survey. *Marine and Petroleum Geology* 18, 471-477.
- McCallum, J.E., Scrutton, R.A., Robertson, A.H.F., Ferrari, W., 1993. Seismostratigraphy and Neogene – Recent depositional history of the south central continental margin of Cyprus. *Marine and Petroleum Geology* 10, 426-438.
- McCarthy, J., Scholl, D.W., 1985. Mechanisms of subduction accretion along the central Aleutian Trench. *Geological Society of America Bulletin* 96, 691-701.
- McCay, G.A., Robertson, A.H.F., 2013. Upper Miocene-Pleistocene deformation of the Girne (Kyrenia) Range and Dar Dere (Ovgos) lineaments, northern Cyprus: role in collision and tectonic escape in the easternmost Mediterranean region. In: Robertson, A.H.F., Parlak, O., Ünlügenç, U.C. (Eds.), *Geological Development of Anatolia and the Easternmost Mediterranean Region*. Geological Society, London, Special Publications 372, pp. 421-445.
- McClay, K., Bonora, M., 2001. Analog Models of Restraining Stepovers in Strike-Slip Fault Systems. *American Association of Petroleum Geologists Bulletin* 85, 233-260.
- McClusky, S., Reilinger, R., Mahmoud, S., Ben Sari, D., Tealeb, A., 2003. GPS constraints on Africa (Nubia) and Arabia plate motions. *Geophysical Journal International* 155, 126-138.
- Menyoli, E., Gajewski, D., Hübscher, C., 2004. Imaging of complex basin structures with the common reflection surface (CRS) stack method. *Geophysical Journal International* 157, 1206-1216.
- Minelli, L., Billi, A., Faccenna, C., Gervasi, A., Guerra, I., Orecchio, B., Speranza, G., 2013. Discovery of a gliding salt-detached megaslide, Calabria, Ionian Sea, Italy. *Geophysical Research Letters* 40, 4220-4224.
- Moeremans, R., Singh, S.C., Mukti, M., McArdle, J., Johansen, K., 2014. Seismic images of structural variations along the deformation front of the Andaman-Sumatra subduction zone: Implications for rupture propagation and tsunamigenesis. *Earth and Planetary Science Letters* 386, 75-85.
- Mohr, M., Kukla, P.A., Urai, J.L., Bresser, G., 2005. Multiphase salt tectonic evolution in NW Germany: seismic interpretation and retro-deformation. *International Journal of Earth Sciences* 94, 917-940.
- Montadert, L., Nicolaides, S., Semb, P.H., Lie, Ø., 2014. Petroleum Systems Offshore Cyprus. In: Marlow, L., Kendall, C.C.G., Yose, L.A. (Eds.), *Petroleum Systems of the Tethyan Region*. American Association of Petroleum Geologists Memoir 106, pp. 301-334.
- Moores, E.M., Robinson, P.T., Malpas, J., Xenophonotos, C., 1984. Model for the origin of the Troodos massif, Cyprus, and other mideast ophiolites. *Geology* 12, 500-503.
- Morley, C.K., 2007. Development of crestal normal faults associated with deepwater fold growth. *Journal of Structural Geology* 29, 1148-1163.
- Netzeband, G.L., Gohl, K., Hübscher, C.P., Ben-Avraham, Z., Dehghani, G.A., Gajewski, D., Liersch, P., 2006a. The Levantine Basin – crustal structure and origin. *Tectonophysics* 418, 167-188.
- Netzeband, G.L., Hübscher, C.P., Gajewski, D., 2006b. The structural evolution of the Messinian evaporites in the Levantine Basin. *Marine Geology* 230, 249-273.
- Oakley, A.J., Taylor, B., Fryer, P., Moore, G.F., Goodliffe, A.M., Morgan, J.K., 2007. Emplacement, growth, and gravitational deformation of serpentinite seamounts on the Mariana forearc. *Geophysical Journal International* 170, 615-634.

- Orszag-Sperber, F., 2006. Changing perspectives in the concept of "Lago-Mare" in Mediterranean Late Miocene evolution. *Sedimentary Geology* 188-189, 259-277.
- Orszag-Sperber, F., Caruso, A., Blanc-Valleron, M.-M., Merle, D., Rouchy, J.M., 2009. The onset of the Messinian salinity crisis: Insights from Cyprus sections. *Sedimentary Geology* 217, 52-64.
- Peace, D.G., Stieglitz, T., Spoors, R., 2012. Imaging new opportunities and play concepts in the Adriatic Sea and Levantine Basin. *Petroleum Geoscience* 18, 405-416.
- Pirmez, C., Hiscott, R.N., Kronen Jr., J.D., 1997. Sandy turbidite successions at the base of channel-levee systems of the Amazon Fan revealed by FMS logs and cores: Unraveling the facies architecture of large submarine fans. In: Flood, R.D., Piper, D.J.W., Klaus, A., Peterson, L.C. (Eds.), *Proceedings of the ODP, Scientific Results*, vol. 155. Ocean Drilling Program, College Station, TX, pp. 7-33.
- Quirk, D.G., Schødt, N., Lassen, B., Ings, S.J., Hsu, D., Hirsch, K.K., Von Nicolai, C., 2012. Salt tectonics on passive margins: examples from Santos, Campos and Kwanza basins. In: Alsop, G.I., Archer, S.G., Hartley, A.J., Grant, N.T., Hodgkinson, R. (Eds.), *Salt Tectonics, Sediments and Prospectivity*. Geological Society, London, Special Publications 363, pp. 207-244.
- Reiche, S., Hübscher, C., Beitz, M., 2014. Fault-controlled evaporite deformation in the Levant Basin, Eastern Mediterranean. *Marine Geology* 354, 53-68.
- Reiche, S., Hübscher, C., Ehrhardt, A., 2015. The impact of salt on the late Messinian to recent tectonostratigraphic evolution of the Cyprus subduction zone. *Submitted to Basin Research*.
- Reilinger, R.E., McClusky, S.C., Oral, M.B., King, R.W., Toksoz, M.N., Barka, A.A., Kinik, I., Lenk, O., Sanli, I., 1997. Global Positioning System measurements of present-day crustal movements in the Arabia–Africa–Eurasia plate collision zone. *Journal of Geophysical Research* 102, 9983-9999.
- Robertson, A.H.F., 1977a. Tertiary uplift history of the Troodos massif, Cyprus. *Geological Society of America Bulletin* 88, 1763-1772.
- Robertson, A.H.F., 1977b. The Moni Mélangé, Cyprus: an olistostrome formed at a destructive plate margin. *Journal of the Geological Society* 133, 447-466.
- Robertson, A.H.F., 1998a. Formation and destruction of the Eratosthenes Seamount, Eastern Mediterranean Sea, and implications for collisional processes. In: Robertson, A.H.F., Emeis, K.-C., Richter, C., Camerlenghi, A. (Eds.), *Proceedings of the ODP, Scientific Results*, vol. 160. Ocean Drilling Program, College Station, TX, pp. 681-699.
- Robertson, A.H.F., 1998b. Late Miocene paleoenvironments and tectonic setting of the southern margin of Cyprus and the Eratosthenes Seamount. In: Robertson, A.H.F., Emeis, K.-C., Richter, C., Camerlenghi, A. (Eds.), *Proceedings of the ODP, Scientific Results*, vol. 160. Ocean Drilling Program, College Station, TX, pp. 453-463.
- Robertson, A.H.F., 1998c. Mesozoic–Tertiary tectonic evolution of the easternmost Mediterranean area: Integration of marine and land evidence. In: Robertson, A.H.F., Emeis, K.-C., Richter, C., Camerlenghi, A. (Eds.), *Proceedings of the ODP, Scientific Results*, vol. 160. Ocean Drilling Program, College Station, TX, pp. 723-782.
- Robertson, A.H.F., 1998d. Tectonic significance of the Eratosthenes Seamount: a continental fragment in the process of collision with a subduction zone in the eastern Mediterranean (Ocean Drilling Program Leg 160). *Tectonophysics* 298, 63-82.
- Robertson, A.H.F., Eaton, S., Follows, E.J., McCallum, J.E., 1991. The role of local tectonics versus global sea-level change in the Neogene evolution of the Cyprus active margin. In: Macdonald, D.I.M. (Ed.), *Sedimentation, Tectonics and Eustasy*. International Association of Sedimentologists, Special Publication 12, pp. 331-372.

- Robertson, A.H.F., Eaton, S., Follows, E.J., Payne, A.S., 1995a. Depositional processes and basin analysis of Messinian evaporites in Cyprus. *Terra Nova* 7, 233-253.
- Robertson, A.H.F., Kidd, R.B., Ivanov, M.K., Limonov, A.F., Woodside, J.M., Galindo-Zaldivar, J., Nieto, L., Scientific Party of the 1993 TTR-3 Cruise 1995b. Eratosthenes Seamount: collisional processes in the easternmost Mediterranean in relation to the Plio-Quaternary uplift of southern Cyprus. *Terra Nova* 7, 254-264.
- Robertson, A.H.F., Shipboard Scientific Party, 1996. Role of the Eratosthenes Seamount in collisional processes in the Eastern Mediterranean. In: Emeis, K.-C., Robertson, A.H.F., Richter, C., et al. (Eds.), *Proceedings of the ODP, Initial Reports*, vol. 160. Ocean Drilling Program, College Station, TX, pp. 513-520.
- Rotstein, Y., Ben-Avraham, Z., 1985. Accretionary processes at subduction zones in the eastern mediterranean. *Tectonophysics* 112, 551-561.
- Rouchy, J.M., Orszag-Sperber, F., Blanc-Valleron, M.-M., Pierre, C., Rivière, M., Combourieu-Nebout, N., Panayides, I., 2001. Paleoenvironmental changes at the Messinian-Pliocene boundary in the eastern Mediterranean (southern Cyprus basins): significance of the Messinian Lago-Mare. *Sedimentary Geology* 145, 93-117.
- Roveri, M., Flecker, R., Krijgsman, W., Lofi, J., Lugli, S., Manzi, V., Sierro, F.J., Bertini, A., Camerlenghi, A., De Lange, G., Govers, R., Hilgen, F.J., Hübscher, C., Meijer, P.Th., Stoica, M., 2014. The Messinian Salinity Crisis: Past and future of a great challenge for marine sciences. *Marine Geology* 352, 25-58.
- Rowan, M.G., Peel, F.J., Vendeville, B.C., 2004. Gravity-driven Fold Belts on Passive Margins. In: McClay, K.R. (Ed.), *Thrust tectonics and hydrocarbon systems*. American Association of Petroleum Geologists Memoir 82, pp. 157-182.
- Rowan, M.G., Peel, F.J., Vendeville, B.C., Gaullier, V., 2012. Salt tectonics at passive margins: Geology versus models – Discussion. *Marine and Petroleum Geology* 37, 184-194.
- Ryan, W.B.F., Carbotte, S.M., Coplan, J.O., O'Hara, S., Melkonian, A., Arko, R., Weissel, R.A., Ferrini, V., Goodwillie, A., Nitsche, F., Bonczkowski, J., Zemsky, R., 2009. Global Multi-Resolution Topography synthesis. *Geochemistry Geophysics Geosystems* 10, Q03014, doi:10.1029/2008GC002332
- Rybakov, M., Goldshmidt, V., Rotstein, Y., 1997. New regional gravity and magnetic maps of the Levant. *Geophysical Research Letters* 24, 33-36.
- Schattner, U., 2010. What triggered the early-to-mid Pleistocene tectonic transition across the entire eastern Mediterranean? *Earth and Planetary Science Letters* 289, 539-548.
- Schattner, U., Ben-Avraham, Z., Lazar, M., Hübscher, C., 2006. Tectonic isolation of the Levant basin offshore Galilee–Lebanon – effects of the Dead Sea fault plate boundary on the Levant continental margin, eastern Mediterranean. *Journal of Structural Geology* 28, 2049-2066.
- Schattner, U., Lazar, M., 2014. Flip convergence across the Phoenician basin through nucleation of subduction. *Gondwana Research* 25, 729-735.
- Schreiber, E., Fox, P.J., Peterson, J.J., 1973. Compressional wave velocities in selected samples of gabbro, schist, limestone, anhydrite, gypsum and halite. In: Ryan, W.B.F., Hsü, K.J., et al. (Eds.), *Initial Reports of the DSDP*, vol. 13. U.S. Government Printing Office, Washington D.C., pp. 595–598.
- Sellier, N.C., Loncke, L., Vendeville, B.C., Mascle, J., Zitter, T., Woodside, J., Loubrieu, B., 2013. Post-Messinian evolution of the Florence Ridge area (Western Cyprus Arc), Part I: Morphostructural analysis. *Tectonophysics* 591, 131-142.

- Shipboard Scientific Party, 1978. Sites 375 and 376: Florence Rise. In: Hsü, K.J., Montadert, L., Bernoulli, D., et al. (Eds.), Initial Reports of the DSDP, vol. 42, Part I. US Government Printing Office, Washington, DC, pp. 219-304.
- Shipboard Scientific Party, 1996a. Site 967. In: Emeis, K.-C., Robertson, A.H.F., Richter, C., et al. (Eds.), Proceedings of the ODP, Initial Reports, vol. 160. Ocean Drilling Program, College Station, TX, pp. 251-287.
- Shipboard Scientific Party, 1996b. Site 968. In: Emeis, K.-C., Robertson, A.H.F., Richter, C., et al. (Eds.), Proceedings of the ODP, Initial Reports, vol. 160. Ocean Drilling Program, College Station, TX, pp. 289-333.
- Sick, C., Yoon, M.-K., Rauch, K., Buske, S., Lüth, S., Araneda, M., Bataille, K., Chong, G., Giese, P., Krawczyk, C., Mechie, J., Meyer, H., Oncken, O., Reichert, C., Schmitz, M., Shapiro, S., Stiller, M., Wigger, P., 2006. Seismic Images of Accretive and Erosive Subduction Zones from the Chilean Margin. In: Oncken, O., Chong, G., Franz, G., Giese, P., Götze, H.-J., Ramos, V.A., Strecker, M.R., Wigger, P. (Eds.), The Andes. Springer, Berlin, Heidelberg, pp. 147-169.
- Skiple, C., Anderson, E., Fürstenau, J., 2012. Seismic interpretation and attribute analysis of the Herodotus and the Levantine Basin, offshore Cyprus and Lebanon. *Petroleum Geoscience* 18, 433-442.
- Steinberg, J., Gvirtzman, Z., Folkman, Y., 2010. New age constraints on the evolution of the Mt Carmel structure and its implications on a Late Miocene extensional phase of the Levant continental margin. *Journal of the Geological Society* 167, 203-216.
- Steinberg, J., Gvirtzman, Z., Folkman, Y., Garfunkel, Z., 2011. Origin and nature of the rapid late Tertiary filling of the Levant Basin. *Geology* 39, 355-358.
- Steinberg, J., Gvirtzman, Z., Garfunkel, Z., 2014. Flexural response of a continental margin to sedimentary loading and lithospheric rupturing: The mountain ridge between the Levant Basin and the Dead Sea Transform. *Tectonics* 33, 166-186.
- Strozyk, F., Van Gent, H., Urai, J.L., Kukla, P.A., 2012. 3D seismic study of complex intra-salt deformation: An example from the Upper Permian Zechstein 3 stringer, western Dutch offshore. In: Alsop, G.I., Archer, S.G., Hartley, A.J., Grant, N.T., Hodgkinson, R. (Eds.), Salt Tectonics, Sediments and Prospectivity. Geological Society, London, Special Publications 363, pp. 489-501.
- Tibor, G., Ben-Avraham, Z., 1992. Late Tertiary seismic facies and structures of the Levant passive margin off central Israel, eastern Mediterranean. *Marine Geology* 105, 253-274.
- Trippetta, F., Collettini, C., Vinciguerra, S., Meredith, P.G., 2010. Laboratory measurements of the physical properties of Triassic Evaporites from Central Italy and correlation with geophysical data. *Tectonophysics* 492, 121-132.
- U.S. Department of Commerce, National Oceanic and Atmospheric Administration, National Geophysical Data Center, 2006. *2-minute Gridded Global Relief Data (ETOPO2v2)* <http://www.ngdc.noaa.gov/mgg/fliers/06mgg01.html>
- Urai, J.L., Schlöder, Z., Spiers, C.J., Kukla, P.A., 2008. Flow and Transport Properties of Salt Rocks. In: Littke, R., Bayer, U., Gajewski, D., Nelskamp, S. (Eds.), Dynamics of Complex Intracontinental Basins: The Central European Basin System. Springer-Verlag, Berlin, Heidelberg, pp. 277-290.
- Van Gent, H., Urai, J.L., de Keijzer, M., 2011. The internal geometry of salt structures – A first look using 3D seismic data from the Zechstein of the Netherlands. *Journal of Structural Geology* 33, 292-311.
- Vidal, N., Alvarez-Marrón, J., Klaeschen, D., 2000a. Internal configuration of the Levantine Basin from seismic reflection data (eastern Mediterranean). *Earth and Planetary Science Letters* 180, 77-89.

- Vidal, N., Klaeschen, D., Kopf, A., Docherty, C., Von Huene, R., Krasheninnikov, V.A., 2000b. Seismic images at the convergence zone from south of Cyprus to the Syrian coast, eastern Mediterranean. *Tectonophysics* 329, 157-170.
- Walley, C.D., 1998. Some outstanding issues in the geology of Lebanon and their importance in the tectonic evolution of the Levantine region. *Tectonophysics* 298, 37-62.
- Warren, J.K., 2010. Evaporites through time: Tectonic, climatic and eustatic controls in marine and nonmarine deposits. *Earth-Science Reviews* 98, 217-268.
- Wdowinski, S., Ben-Avraham, Z., Arvidsson, R., Ekström, G., 2006. Seismotectonics of the Cyprian Arc. *Geophysical Journal International* 164, 176-181.
- Welford, J.K., Hall, J., Hübscher, C., Reiche, S., Loudon, K., 2015. Crustal seismic velocity structure from Eratosthenes Seamount to Hecataeus Rise across the Cyprus Arc, eastern Mediterranean. *Geophysical Journal International* 200, 935-953.
- Whiting, B.M., 1998. Subsidence record of early-stage continental collision, Eratosthenes platform (Sites 966 and 967). In: Robertson, A.H.F., Emeis, K.-C., Richter, C., Camerlenghi, A. (Eds.), *Proceedings of the ODP, Scientific Results*, vol. 160. Ocean Drilling Program, College Station, TX, pp. 509-515.
- Withjack, M.O., Callaway, S., 2000. Active Normal Faulting Beneath a Salt Layer: An Experimental Study of Deformation Patterns in the Cover Sequence. *American Association of Petroleum Geologists Bulletin* 84, 627-651.
- Withjack, M.O., Olson, J., Peterson, E., 1990. Experimental models of extensional forced folds. *American Association of Petroleum Geologists Bulletin* 74, 1038-1054.
- Woodside, J.M., Mascle, J., Zitter, T.A.C., Limonov, A.F., Ergün, M., Volkonskaia, A., shipboard scientists of the PRISMED II Expedition, 2002. The Florence Rise, the Western Bend of the Cyprus Arc. *Marine Geology* 185, 177-194.
- Yoon, M.-K., Baykulov, M., Dümmong, S., Brink, H.-J., Gajewski, D., 2008. New insights into the crustal structure of the North German Basin from reprocessing of seismic reflection data using the Common Reflection Surface stack. *International Journal of Earth Sciences* 97, 887-898.

Acknowledgements

First of all I would like to thank my supervisor Christian Hübscher. Thank you for the possibility to work on this interesting topic, for your continuous support and guidance throughout my time in Hamburg, for several insightful discussions, for sharing your passion and enthusiasm on all earth science related aspects and for sending me on different cruises to really learn the practical aspects of reflection seismics.

I would further like to thank Benedikt Weiß whom I had the pleasure to share an office with. Bene, thank you for countless discussions on all science-related aspects, your continuous willingness to help whenever you could, for sharing your experience in seismic data acquisition and for telling me all tricks to eventually avoid getting sea sick.

Claudia Vanelle, Sergius Dell and Benjamin Schwarz are thanked for introducing me to the mysterious world of multi-parameter stacking. Claudia, thank you for always taking the time to answer my questions and for proof-reading my data chapter.

I thank Axel Ehrhardt for letting me work on the great reflection seismic data acquired during MSM 14/2. Furthermore I thank the CoCoCo working group, in particular Jeremy Hall, for insightful discussion during our annual project meetings.

I truly enjoyed the company of very nice colleagues: Muayyad Al Hseinat, Daniela Wolf, Janina Kammann, Kristina Meier and Claudia Kalvelage – be it for a cup of coffee after lunch or while making a joint effort during seismic cruises and the onshore field work that we did.

Sven Winter is thanked for his patience whenever an airgun-screw was not as quickly tightened as if he would have done it himself and for sharing a beer in times of limited availability.

I thank the DFG for supporting this project (DFG, Grant no. Hu698/20-1).

I thank my family for many wonderful breaks whenever I had the pleasure to come for a visit to Norway. Finally and most deeply I thank my fiancée Daria. Thank you for your patience and your endless support.

Hiermit erkläre ich an Eides statt, dass ich die vorliegende Dissertationsschrift selbst verfasst und keine anderen als die angegebenen Quellen und Hilfsmittel benutzt habe.

Aachen, den 28. Januar 2015

Sönke Reiche

